UNCERTAINTY RELATIONS AND THEIR APPLICATIONS

EDITED BY: Dong Wang, Ming-Liang Hu, Jun Feng and Yao-Zhong Zhang
PUBLISHED IN: Frontiers in Physics

frontiers Research Topics

ISSN 1664-8714
ISBN 978-2-83250-137-5
DOI 10.3389/978-2-83250-137-5

About Frontiers

Frontiers is more than just an open-access publisher of scholarly articles: it is a pioneering approach to the world of academia, radically improving the way scholarly research is managed. The grand vision of Frontiers is a world where all people have an equal opportunity to seek, share and generate knowledge. Frontiers provides immediate and permanent online open access to all its publications, but this alone is not enough to realize our grand goals.

Frontiers Journal Series

The Frontiers Journal Series is a multi-tier and interdisciplinary set of open-access, online journals, promising a paradigm shift from the current review, selection and dissemination processes in academic publishing. All Frontiers journals are driven by researchers for researchers; therefore, they constitute a service to the scholarly community. At the same time, the Frontiers Journal Series operates on a revolutionary invention, the tiered publishing system, initially addressing specific communities of scholars, and gradually climbing up to broader public understanding, thus serving the interests of the lay society, too.

Dedication to Quality

Each Frontiers article is a landmark of the highest quality, thanks to genuinely collaborative interactions between authors and review editors, who include some of the world's best academicians. Research must be certified by peers before entering a stream of knowledge that may eventually reach the public - and shape society; therefore, Frontiers only applies the most rigorous and unbiased reviews.
Frontiers revolutionizes research publishing by freely delivering the most outstanding research, evaluated with no bias from both the academic and social point of view. By applying the most advanced information technologies, Frontiers is catapulting scholarly publishing into a new generation.

What are Frontiers Research Topics?

Frontiers Research Topics are very popular trademarks of the Frontiers Journals Series: they are collections of at least ten articles, all centered on a particular subject. With their unique mix of varied contributions from Original Research to Review Articles, Frontiers Research Topics unify the most influential researchers, the latest key findings and historical advances in a hot research area! Find out more on how to host your own Frontiers Research Topic or contribute to one as an author by contacting the Frontiers Editorial Office: frontiersin.org/about/contact

UNCERTAINTY RELATIONS AND THEIR APPLICATIONS

Topic Editors:
Dong Wang, Anhui University, China
Ming-Liang Hu, Xi'an University of Posts and Telecommunications, China
Jun Feng, Xi'an Jiaotong University, China
Yao-Zhong Zhang, The University of Queensland, Australia

Citation: Wang, D., Hu, M.-L., Feng, J., Zhang, Y.-Z., eds. (2022). Uncertainty Relations and Their Applications. Lausanne: Frontiers Media SA.
doi: 10.3389/978-2-83250-137-5

Table of Contents

04 ***Editorial: Uncertainty Relations and Their Applications***
Dong Wang, Ming-Liang Hu, Jun Feng and Yao-Zhong Zhang

06 ***Studying Heisenberg-like Uncertainty Relation with Weak Values in One-dimensional Harmonic Oscillator***
Xing-Yan Fan, Wei-Min Shang, Jie Zhou, Hui-Xian Meng and Jing-Ling Chen

13 ***Uncertainty Relation and Quantum Phase Transition in the Two-Dimensional Ising Model***
Yu-Yan Fang, Tian-Yi Jiang, Xin-Ye Xu and Jin-Ming Liu

22 ***Near-Optimal Variance-Based Uncertainty Relations***
Yunlong Xiao, Naihuan Jing, Bing Yu, Shao-Ming Fei and Xianqing Li-Jost

29 ***Experimental Investigation of Quantum Uncertainty Relations With Classical Shadows***
Lu Liu, Ting Zhang, Xiao Yuan and He Lu

36 ***Uncertainty Relations of Non-Hermitian Operators: Theory and Experimental Scheme***
Xinzhi Zhao and Chengjie Zhang

42 ***Finite-Size Scaling on a Digital Quantum Simulator Using Quantum Restricted Boltzmann Machine***
Bilal Khalid, Shree Hari Sureshbabu, Arnab Banerjee and Sabre Kais

53 ***Unextendible Entangled Bases With a Fixed Schmidt Number Based on Generalized Weighing Matrices***
Yuan-Hong Tao, Xin-Lei Yong, Ya-Ru Bai, Dan-Ni Xu and Shu-Hui Wu

61 ***On Non-Convexity of the Nonclassicality Measure* via *Operator Ordering Sensitivity***
Shuangshuang Fu, Shunlong Luo and Yue Zhang

67 ***Probing Genuine Multipartite Einstein–Podolsky–Rosen Steering and Entanglement Under an Open Tripartite System***
Wen-Yang Sun, Amin Ding, Haitao Gao, Le Wang, Juan He and Liu Ye

frontiers | Frontiers in Physics

TYPE Editorial
PUBLISHED 23 August 2022
DOI 10.3389/fphy.2022.997835

OPEN ACCESS

EDITED AND REVIEWED BY
Alexandre M. Zagoskin,
Loughborough University,
United Kingdom

*CORRESPONDENCE
Dong Wang,
dwang@ahu.edu.cn
Ming-Liang Hu,
mingliang0301@163.com
Jun Feng,
j.feng@xjtu.edu.cn
Yao-Zhong Zhang,
yzz@maths.uq.edu.au

SPECIALTY SECTION
This article was submitted to Quantum Engineering and Technology, a section of the journal Frontiers in Physics

RECEIVED 19 July 2022
ACCEPTED 29 July 2022
PUBLISHED 23 August 2022

CITATION
Wang D, Hu M-L, Feng J and Zhang Y-Z (2022), Editorial: Uncertainty relations and their applications.
Front. Phys. 10:997835.
doi: 10.3389/fphy.2022.997835

Editorial: Uncertainty relations and their applications

Dong Wang[1]*, Ming-Liang Hu[2]*, Jun Feng[3,4]* and Yao-Zhong Zhang[5]*

[1]School of Physics and Optoelectronic Engineering, Anhui University, Hefei, China, [2]School of Science, Xi'an University of Posts and Telecommunications, Xi'an, China, [3]School of Physics, Xi'an Jiaotong University, Xi'an, China, [4]Institute of Theoretical Physics, Xi'an Jiaotong University, Xi'an, China, [5]School of Mathematics and Physics, The University of Queensland, Brisbane, QLD, Australia

KEYWORDS

uncertainty relation, one-dimensional harmonic oscillator, non-Hermitian operators, quantum entanglement, Boltzmann machine, quantum Rabi model, nonclassicality, Schmidt number

Editorial on the Research Topic
Uncertainty relations and their applications

Quantum mechanics is regarded as a significant achievement in our exploration of the microscopic world. It helps us understand the initial seeds of the whole Universe, explore the formation of the matter world with elementary particles, and manipulate the quantum materials composed of a huge number of atoms. Quantum mechanics plays a vital role in revealing the intrinsic nature laws and forms the basis of modern science and technology. Therefore, increasing focus on quantum physics is of great significance to any possible breakthrough in quantum engineering and technology. As one of the most fundamental and vital concepts of quantum theory, the uncertainty relation is at the heart of quantum physics, yielding various versatile applications. In this regard, we organized the Research Topic "*uncertainty relations and their applications*" in Frontiers in Physics. Currently, nine contributed articles have been collected on this topic. The first part of contributions has been made on the theoretical exploration on the various form of quantum uncertainty relations. By introducing the uncertainty interval, a concept derived by combining lower and upper bounds together, Xiao et al. use the entropic uncertainty relations to formulate lower bounds of variance-based uncertainty relations, which successfully establishes the connections between different forms of uncertainty relations. Concerning the Heisenberg uncertainty, Fan et al. raise an interesting question: what will happen if the mean values are replaced by weak values in the Heisenberg uncertainty relation? To answer this question, they delve into the case of position and momentum measurements in a simple harmonic oscillator, with pre-selected states as eigenstates and the post-selections as the superposition states. Their results show that the original Heisenberg limit can be improved in this case, replaced by a weak value canonical uncertainty relation holding for simple harmonic oscillators in coherent states. Thus, the work of Fan et al. provides an important supplement to the field of uncertainty relations with weak measurement and go beyond the standard Heisenberg limit.

Second part of contributions focus on the applications of the uncertainty relations for the manipulatable quantum systems in lab. In particular, Fang et al. investigate both linear-entropy-based uncertainty relation and quantum entanglement in a two-dimensional (2D) Ising model. By the derived effective Hamiltonian and quantum renormalization group (QRG) equations of the model, they have found by numerical analysis that both the uncertainty relation and the quantum entanglement can be used to detect quantum phase transition (QPT), while the linear-entropy-based uncertainty relation can be a more powerful indicator for the detection of the QPT. This result may pave a promising pathway to observe QPTs of the solid-state system by means of the uncertainty relation. Additionally, for a finite size system, it would be difficult to find critical points and critical exponents through the standard Finite-Size Scaling (FSS) approach, Khalid et al. propose an alternative FSS method in which the truncation of the system is made in the Hilbert space instead of the physical space and apply this approach to calculate the critical point for the QPT of Quantum Rabi Model. They also provide a protocol for the implementation of this method on a digital quantum simulator using the Quantum Restricted Boltzmann Machine algorithm. On the experimental side, based on their generalized unitary uncertainty relation theory and proposed uncertainty relations of non-Hermitian operators, Zhao and Zhang design an experimental implementation which can test the uncertainty relation for two non-Hermitian operators through the Mach-Zehnder interferometer. Also, Liu et al. report an experimental test on the coherence uncertainty relations based on the classical shadow algorithm. They examine the tightness of various lower bounds and draw a novel conclusion that tightness of quantum coherence lower bounds depends on the reference bases and the purity of the quantum state. This may deeply reveal the relationship between uncertainty relation and characteristics of quantum system.

Associated with uncertainty relations, quantum resources are also of great significance in quantum engineering and technology. The third part of contributions concerns on the various quantum resources related to uncertainty relations. Amongst these, nonclassicality is one of the valuable quantum resources related to the quantum aspect of photons. Fu et al. argue that the requirement for nonclassicality measurement in the sense of Glauber-Sudarshan is convex. Based on the non-convexity of nonclassicality measure in Ref. [1], they find that this measure is intrinsically connected with the Wigner-Yanase skew information, a measure of quantum uncertainties. Inspired by this, Fu et al. propose a faithful measure of nonclassicality, which is convex. Entanglement is another essential resource of quantum information processing. In order to characterize quantum entanglement, the analysis of various bases in the state space is in demand. Tao et al. systematically investigate the constructions of unextendible entangled bases with a fixed Schmidt number k (UEB*k*) in a bipartite system by using generalized weighing matrices and propose three ways to construct different members of UEB*k*s.

In conclusion, this editorial is created to present the latest progress of the Research Topic: *Uncertainty relations and their applications*. Our special thanks to all authors of the articles published on this Research Topic for their valuable contributions and the Frontiers in Physics team for the technical assistance with publishing.

Author contributions

All authors listed have made a substantial, direct, and intellectual contribution to the work and approved it for publication.

Funding

DW was supported by the National Natural Science Foundation of China (Grant Nos. 12075001 and 61601002), Anhui Provincial Key Research and Development Plan (Grant No. 2022b13020004), and the Fund of CAS Key Laboratory of Quantum Information (Grant No. KQI201701). M-LH was supported by the National Natural Science Foundation of China (Grant No. 11675129). JF was supported by the National Natural Science Foundation of China (Grant No. 12075178) and the Natural Science Basic Research Plan in Shaanxi Province of China (Grant No. 2018JM1049). Y-ZZ was supported by the Discovery Project from the Australian Research Council (Grant No. DP190101529).

Conflict of interest

The authors declare that the research was conducted in the absence of any commercial or financial relationships that could be construed as a potential conflict of interest.

Publisher's note

Reference

1. De Bièvre S, Horoshko DB, Patera G, Kolobov MI. Measuring nonclassicality of bosonic field quantum states via operator ordering sensitivity. *Phys Rev Lett* (2019) 122:080402. doi:10.1103/PhysRevLett.122.080402

frontiers in Physics

ORIGINAL RESEARCH
published: 10 January 2022
doi: 10.3389/fphy.2021.803494

Studying Heisenberg-like Uncertainty Relation with Weak Values in One-dimensional Harmonic Oscillator

*Xing-Yan Fan[1], Wei-Min Shang[1], Jie Zhou[1], Hui-Xian Meng[2] and Jing-Ling Chen[1,2]**

[1]Theoretical Physics Division, Chern Institute of Mathematics, Nankai University, Tianjin, China, [2]School of Mathematics and Physics, North China Electric Power University, Beijing, China

As one of the fundamental traits governing the operation of quantum world, the uncertainty relation, from the perspective of Heisenberg, rules the minimum deviation of two incompatible observations for arbitrary quantum states. Notwithstanding, the original measurements appeared in Heisenberg's principle are strong such that they may disturb the quantum system itself. Hence an intriguing question is raised: What will happen if the mean values are replaced by weak values in Heisenberg's uncertainty relation? In this work, we investigate the question in the case of measuring position and momentum in a simple harmonic oscillator via designating one of the eigenkets thereof to the pre-selected state. Astonishingly, the original Heisenberg limit is broken for some post-selected states, designed as a superposition of the pre-selected state and another eigenkets of harmonic oscillator. Moreover, if two distinct coherent states reside in the pre- and post-selected states respectively, the variance reaches the lower bound in common uncertainty principle all the while, which is in accord with the circumstance in Heisenberg's primitive framework.

Keywords: Heisenberg-like uncertainty relation, weak values, selected states, one-dimensional harmonic oscillator, coherent states

OPEN ACCESS

Edited by:
Ming-Liang Hu,
Xi'an University of Posts and Telecommunications, China

Reviewed by:
Kai Chen,
University of Science and Technology of China, China
Dianmin Tong,
School of Physics, Shandong University, China
Saeed Haddadi,
Semnan University, Iran
Jin-Ming Liu,
East China Normal University, China

****Correspondence:***
Jing-Ling Chen
chenjl@nankai.edu.cn

Specialty section:
This article was submitted to Quantum Engineering and Technology, a section of the journal Frontiers in Physics

Received: *28 October 2021*
Accepted: *19 November 2021*
Published: *10 January 2022*

Citation:
Fan X-Y, Shang W-M, Zhou J, Meng H-X and Chen J-L (2022) Studying Heisenberg-like Uncertainty Relation with Weak Values in One-dimensional Harmonic Oscillator. Front. Phys. 9:803494. doi: 10.3389/fphy.2021.803494

1 INTRODUCTION

The non-commutativity in quantum mechanics leads to the essential contradistinction between itself and classical mechanics. Among diverse quantum phenomena, the uncertainty relation is representative, which was first uncovered by Heisenberg [1], then generalized via Robertson [2] to any two observables A and B for arbitrary kets of the following form,

$$\langle(\Delta A)^2\rangle\langle(\Delta B)^2\rangle \geq \frac{1}{4}|\langle[A,\ B]\rangle|^2, \tag{1}$$

where $\langle(\Delta A)^2\rangle \coloneqq \langle A^2\rangle - (\langle A\rangle)^2$, represents the variance of measuring a quantum system via A, so does $\langle(\Delta B)^2\rangle$.

However, there exist some shortcomings for standard Heisenberg uncertainty principle (**Eq. 1**). On the one hand, for instance, the derivation of the z components of angular momentum increases in the case of a three-level problem [3], though the information we have gathered therein increases, which is discordant with classical information theory. Thus the concept of entropy was imported into the field of uncertainty relation [4, 5].

On the other hand, initial uncertainty relation only involves strong measurement, and it may destroy the measured system inevitably in most cases, which leads to another way of exploring

Heisenberg uncertainty principle relying on the heritage of weak measurement. In 1988, Y. Aharonov et al. [6] proposed the concept of "weak value" to overcome the blemish of measurement collapse in quantum mechanics. The weak value of an observable O is denoted as

$$\langle O\rangle_{\mathrm{w}} \coloneqq \frac{\langle\psi_{\mathrm{f}}|O|\psi_{\mathrm{i}}\rangle}{\langle\psi_{\mathrm{f}}|\psi_{\mathrm{i}}\rangle}, \tag{2}$$

with $|\psi_{\mathrm{i}}\rangle$ and $|\psi_{\mathrm{f}}\rangle$ representing the states of pre- and post-selections respectively.

In recent illuminating works, Song and Qiao [7] constructed a new type of uncertainty relation in weak measurement with the help of a non-Hermitian operator defined in [8]. Additionally, Hall et al. [9] generalized the representation theorem given by Shikano and Hosoya [10] and studied the uncertainty relation *via* weak values. Afterwards, Šindelka, and Moiseyev [11] considered a Heisenberg-like situation that measuring a quantum system "weakly" *via* an observable A without imposing postselection, following a strong measurement by another observable B subsequently. But there is hardly any work involving researching Heisenberg-like uncertainty principle via replacing mean value by weak value merely, which is the simplest case in this field.

In this work, we study the Heisenberg-like uncertainty relation in the case of measuring position and momentum in a one-dimensional (1D) simple harmonic oscillator with the pre-selected state appointed as one of its eigenstates. We found that if post-selected states are specified as a superposition of the pre-selected state and another eigenstates of harmonic oscillator, primitive Heisenberg relation fails. Furthermore, providing the pre- and post-selected states are designed as two distinct coherent states, the variance in the sense of weak values will arrive at the lower bound in usual Heisenberg principle all through, which is in agreement with Heisenberg's original argument.

This paper is organized as follows: In **Section 2** we show our main results about Heisenberg-like uncertainty principle through replacing expectation values by weak values in rudimental Heisenberg's idea. Four major parts are included in this section. In **Section 2.1**, we retrospect some basic knowledge about 1D simple harmonic oscillator in occupation number representation. And then in **Section 2.2**, we study two non-orthonormal cases of selected states by considering $|\psi_{\mathrm{i}}\rangle = |0\rangle$ and $|\psi_{\mathrm{i}}\rangle = |n\rangle$ ($n \in \mathbb{N}^*$, i.e., n is a positive integer), respectively. Next in **Section 2.3**, we explore the orthogonal selected states as the limitation of non-orthogonal circumstances. And in **Section 2.4**, the pre- and post-selected states are designed as two coherent states. Finally in **Section 3**, we make a summary and bring up some open questions.

2 REPLACING MEAN VALUES BY WEAK VALUES

2.1 Simple Harmonic Oscillator in Occupation Number Representation

Set $n \in \mathbb{N}$ the quantum number referring to energy levels of given 1D simple harmonic oscillator with Hamiltonian H. Let $|n\rangle$ ($n \in \mathbb{N}$) the eigenkets thereof, then via Schrödinger equation $H|n\rangle = E_n|n\rangle$, we obtain $E_n = (n + 1/2)\hbar\omega$ as the formula of energy, with $\hbar$ the Plank constant up to a factor $1/(2\pi)$, and ω the vibration frequency of corresponding oscillator. Especially when $n = 0$, $E_0 = (1/2)\hbar\omega$ implies the ground state energy.

Define the annihilation operator a and the creation operator $a^\dagger$, which satisfy

$$\begin{aligned} a|n\rangle &= \sqrt{n}|n-1\rangle, \\ a^\dagger|n\rangle &= \sqrt{n+1}|n+1\rangle, \end{aligned} \tag{3}$$

where $a|0\rangle = 0$.

Postulate that $\alpha \equiv \sqrt{m\omega/\hbar}$, $X \equiv \alpha x$, and $P \equiv [\alpha/(m\omega)]p$, with m expressing the mass of aforementioned harmonic oscillator. Note that X and P are Hermitian. After that, from the canonical commutative relation $(x, p) = \mathrm{i}\hbar$, we have $(X, P) = \mathrm{i}$, together with

$$\begin{aligned} X &= \frac{1}{\sqrt{2}}\left(a + a^\dagger\right), \\ P &= \frac{1}{\mathrm{i}\sqrt{2}}\left(a - a^\dagger\right). \end{aligned} \tag{4}$$

Next we will compute the Heisenberg-like uncertainty principle with weak values by combining **Eqs 1**, **2** and some properties of 1D harmonic oscillator.

2.2 Non-orthonormal Selected States

This subsection includes the situations of non-orthonormal pre- and post-selections. When the pre-selected state is initialized as $|n\rangle$, its post-selected partner is set as $\cos\theta|n\rangle + \sin\theta\, e^{\mathrm{i}\varphi}|m\rangle$, where $\theta \in (0, \pi/2) \cup (\pi/2, \pi)$, $\varphi \in [0, 2\pi)$ and $n \neq m$.

Case 1.—$n = 0$, $|\psi_{\mathrm{i}}\rangle = |0\rangle$.

In this case, we set $|\psi_{\mathrm{f}}\rangle = \cos\theta|0\rangle + \sin\theta\, e^{\mathrm{i}\varphi}|m\rangle$, where $\theta \in (0, \pi/2) \cup (\pi/2, \pi)$, $\varphi \in [0, 2\pi)$ and $m \in \mathbb{N}^*$. Thereby, $\langle\psi_{\mathrm{f}}|\psi_{\mathrm{i}}\rangle = \cos\theta$, and

$$\begin{aligned} \langle X\rangle_{\mathrm{w}} &= \frac{\langle\psi_{\mathrm{f}}|X|\psi_{\mathrm{i}}\rangle}{\langle\psi_{\mathrm{f}}|\psi_{\mathrm{i}}\rangle} \\ &= \frac{\left[\cos\theta\langle 0| + \sin\theta\, e^{-\mathrm{i}\varphi}\langle m|\right]\left(a + a^\dagger\right)|0\rangle}{\sqrt{2}\cos\theta} \\ &= \frac{\tan\theta\, e^{-\mathrm{i}\varphi}\langle m|1\rangle}{\sqrt{2}} \\ &= \frac{\tan\theta\, e^{-\mathrm{i}\varphi}\,\delta_{m,1}}{\sqrt{2}}, \end{aligned}$$

where $\delta_{m,n}$ implies the Kronecker delta symbol.

Thereafter, we arrive at

$$\left(\langle X\rangle_{\mathrm{w}}\right)^2 = \frac{\tan^2\theta\, e^{-\mathrm{i}2\varphi}\,\delta_{m,1}^2}{2}, \tag{5}$$

and

$$\begin{aligned} \langle X^2\rangle_{\mathrm{w}} &= \frac{\langle\psi_{\mathrm{f}}|\left[a^2 + aa^\dagger + a^\dagger a + \left(a^\dagger\right)^2\right]|\psi_{\mathrm{i}}\rangle}{2\langle\psi_{\mathrm{f}}|\psi_{\mathrm{i}}\rangle} \\ &= \frac{1 + \sqrt{2}\tan\theta\, e^{-\mathrm{i}\varphi}\,\delta_{m,2}}{2}. \end{aligned} \tag{6}$$

Combine **Eq. 6** with **Eq. 5** together, then we attain the variance of X in the form of weak value as follows

$$\begin{aligned}\langle \Delta X\rangle_{\mathrm{w}}^{2} &\equiv \langle X^{2}\rangle_{\mathrm{w}} - (\langle X\rangle_{\mathrm{w}})^{2}\\ &= \frac{1+\sqrt{2}\tan\theta\, e^{-\mathrm{i}\varphi}\,\delta_{m,2} - \tan^{2}\theta\, e^{-\mathrm{i}2\varphi}\,\delta_{m,1}^{2}}{2}.\end{aligned} \tag{7}$$

On the other hand,

$$\begin{aligned}\langle P\rangle_{\mathrm{w}} &= \frac{\langle \psi_{\mathrm{f}}|P|\psi_{\mathrm{i}}\rangle}{\langle \psi_{\mathrm{f}}|\psi_{\mathrm{i}}\rangle}\\ &= \frac{\left[\cos\theta\langle 0| + \sin\theta\, e^{-\mathrm{i}\varphi}\langle m|\right](a-a^{\dagger})|0\rangle}{\mathrm{i}\sqrt{2}\cos\theta}\\ &= \frac{\mathrm{i}\tan\theta\, e^{-\mathrm{i}\varphi}\,\delta_{m,1}}{\sqrt{2}},\end{aligned}$$

which indicates that

$$(\langle P\rangle_{\mathrm{w}})^{2} = -\frac{\tan^{2}\theta\, e^{-\mathrm{i}2\varphi}\,\delta_{m,1}^{2}}{2}, \tag{8}$$

and

$$\begin{aligned}\langle P^{2}\rangle_{\mathrm{w}} &= \frac{\langle \psi_{\mathrm{f}}|\left[aa^{\dagger} + a^{\dagger}a - a^{2} - (a^{\dagger})^{2}\right]|\psi_{\mathrm{i}}\rangle}{2\langle \psi_{\mathrm{f}}|\psi_{\mathrm{i}}\rangle}\\ &= \frac{1-\sqrt{2}\tan\theta\, e^{-\mathrm{i}\varphi}\,\delta_{m,2}}{2}.\end{aligned} \tag{9}$$

Therefore,

$$\begin{aligned}\langle \Delta P\rangle_{\mathrm{w}}^{2} &\equiv \langle P^{2}\rangle_{\mathrm{w}} - (\langle P\rangle_{\mathrm{w}})^{2}\\ &= \frac{1-\sqrt{2}\tan\theta\, e^{-\mathrm{i}\varphi}\,\delta_{m,2} + \tan^{2}\theta\, e^{-\mathrm{i}2\varphi}\,\delta_{m,1}^{2}}{2},\end{aligned} \tag{10}$$

then we can calculate the uncertainty relation in terms of weak values, namely.

$$\begin{aligned}\langle \Delta X\rangle_{\mathrm{w}}^{2}\langle \Delta P\rangle_{\mathrm{w}}^{2} &= \frac{1-\tan^{2}\theta\left[\sqrt{2}\ e^{-\mathrm{i}\varphi}\,\delta_{m,2} - \tan\theta\, e^{-\mathrm{i}2\varphi}\,\delta_{m,1}^{2}\right]^{2}}{4}\\ &= \frac{1-\tan^{2}\theta\left[2\, e^{-\mathrm{i}2\varphi}\,\delta_{m,2}^{2} + \tan^{2}\theta\, e^{-\mathrm{i}4\varphi}\,\delta_{m,1}^{4}\right]}{4},\end{aligned} \tag{11}$$

which means that

$$\begin{aligned}\left|\langle \Delta X\rangle_{\mathrm{w}}^{2}\langle \Delta P\rangle_{\mathrm{w}}^{2}\right| &= \left|\frac{1-\tan^{2}\theta\left[2\, e^{-\mathrm{i}2\varphi}\,\delta_{m,2}^{2} + \tan^{2}\theta\, e^{-\mathrm{i}4\varphi}\,\delta_{m,1}^{4}\right]}{4}\right|\\ &= \frac{1}{4}\Big|\Big\{1-\tan^{2}\theta\left[2\,\delta_{m,2}^{2}\cos(2\varphi) + \tan^{2}\theta\,\delta_{m,1}^{4}\cos(4\varphi)\right]\Big\}\\ &\quad +\mathrm{i}\tan^{2}\theta\left[2\,\delta_{m,2}^{2}\sin(2\varphi) + \tan^{2}\theta\,\delta_{m,1}^{4}\sin(4\varphi)\right]\Big|\\ &= \frac{1}{4}\sqrt{\begin{array}{c}\Big\{1-\tan^{2}\theta\left[2\,\delta_{m,2}^{2}\cos(2\varphi) + \tan^{2}\theta\,\delta_{m,1}^{4}\cos(4\varphi)\right]\Big\}^{2}\\ +\tan^{4}\theta\left[2\,\delta_{m,2}^{2}\sin(2\varphi) + \tan^{2}\theta\,\delta_{m,1}^{4}\sin(4\varphi)\right]^{2}\end{array}}\\ &= \frac{1}{4}\sqrt{\begin{array}{c}1+\tan^{4}\theta\left(4\,\delta_{m,2}^{4} + \tan^{4}\theta\,\delta_{m,1}^{8}\right)\\ -2\tan^{2}\theta\left[2\,\delta_{m,2}^{2}\cos(2\varphi) + \tan^{2}\theta\,\delta_{m,1}^{4}\cos(4\varphi)\right]\end{array}}\\ &\geq \frac{1}{4}\sqrt{1+\tan^{4}\theta\left(4\,\delta_{m,2}^{4} + \tan^{4}\theta\,\delta_{m,1}^{8}\right) - 2\tan^{2}\theta\left(2\,\delta_{m,2}^{2} + \tan^{2}\theta\,\delta_{m,1}^{4}\right)}\\ &= \frac{1}{4}\left|1-\tan^{2}\theta\left(2\,\delta_{m,2}^{2} + \tan^{2}\theta\,\delta_{m,1}^{4}\right)\right|.\end{aligned} \tag{12}$$

Analysis—For $A = X$, $B = P$, the Heisenberg uncertainty relation is given by

$$\langle \Delta X\rangle^{2}\langle \Delta P\rangle^{2} = \left|\langle \Delta X\rangle^{2}\langle \Delta P\rangle^{2}\right| \geq \frac{1}{4}. \tag{13}$$

In this work, the Heisenberg-like uncertainty relation with weak values is modified as

$$\left|\langle \Delta X\rangle_{\mathrm{w}}^{2}\langle \Delta P\rangle_{\mathrm{w}}^{2}\right| \geq \frac{1}{4}. \tag{14}$$

We now compare **Eq. 12** with Heisenberg-like uncertainty relation (**Eq. 14**) in virtue of different m.

1) If $m \neq 1$ and $m \neq 2$, $|\langle \Delta X\rangle_{\mathrm{w}}^{2}\langle \Delta P\rangle_{\mathrm{w}}^{2}| = 1/4$, the relation (**Eq. 14**) holds, and it is in coincidence with the usual Heisenberg uncertainty relation (**Eq. 13**).
2) If $m = 1$,

$$\left|\langle \Delta X\rangle_{\mathrm{w}}^{2}\langle \Delta P\rangle_{\mathrm{w}}^{2}\right| = \frac{1}{4}\sqrt{1+\tan^{8}\theta - 2\cos(4\varphi)\tan^{4}\theta}.$$

Then we have $(1/4)|1-\tan^{4}\theta| \leq |\langle \Delta X\rangle_{\mathrm{w}}^{2}\langle \Delta P\rangle_{\mathrm{w}}^{2}| \leq (1/4)(1+\tan^{4}\theta)$, and the left equality sign holds once $\varphi = 0$, $\pi/2$ or π; While $\varphi = \pi/4$ or $3\pi/4$, the right equality sign is obtained. In the interval of $\theta \in (0, \arctan(\sqrt[4]{2})) \cup (\pi - \arctan(\sqrt[4]{2}), \pi)$, it is possible for $|\langle \Delta X\rangle_{\mathrm{w}}^{2}\langle \Delta P\rangle_{\mathrm{w}}^{2}|$ to arrive at some values less than 1/4. While for other legal θ, the uncertainty relation (**Eq. 14**) holds. See **Figure 1** for more details. It is worth mentioning that once $|\langle \Delta X\rangle_{\mathrm{w}}^{2}\langle \Delta P\rangle_{\mathrm{w}}^{2}|$ reaches the lower bound, and $\theta = \pi/4$ or $3\pi/4$, the variance $|\langle \Delta X\rangle_{\mathrm{w}}^{2}\langle \Delta P\rangle_{\mathrm{w}}^{2}|$ vanishes, and further study shows that $\langle \Delta X\rangle_{\mathrm{w}}^{2} = \langle \Delta P\rangle_{\mathrm{w}}^{2} = 0$, which implies the product of weak values corresponding to two incompatible observables X and P can be measured precisely. The result is reasonable, since strong measurement is substituted by weak measurement, then the disturbance for quantum system weaken, and two incompatible observations may be assured simultaneously.

3) If $m = 2$,

$$\left|\langle \Delta X\rangle_{\mathrm{w}}^{2}\langle \Delta P\rangle_{\mathrm{w}}^{2}\right| = \frac{1}{4}\sqrt{1+4\tan^{4}\theta - 4\cos(2\varphi)\tan^{2}\theta}.$$

After that, $(1/4)|1-2\tan^{2}\theta| \leq |\langle \Delta X\rangle_{\mathrm{w}}^{2}\langle \Delta P\rangle_{\mathrm{w}}^{2}| \leq (1/4)(1+2\tan^{2}\theta)$, and the left equality sign holds once $\varphi = 0$ or π; While $\varphi = \pi/2$, the right equality sign is obtained. In the case of $\theta \in (0, \pi/4) \cup (3\pi/4, \pi)$, it is possible for $|\langle \Delta X\rangle_{\mathrm{w}}^{2}\langle \Delta P\rangle_{\mathrm{w}}^{2}|$ to arrive at some values less than 1/4. And in other cases, the uncertainty relation (**Eq. 14**) holds. In like manner, there exist two ideal $\theta = \arctan(1/\sqrt{2})$ or $\pi - \arctan(1/\sqrt{2})$ when $\varphi = 0$ or $\pi/2$, such that the product of the weak values of X and P is affirmatory.

In one word, the Heisenberg uncertainty principle can be broken in the sense of weak values when we fix the pre-selected state as $|\psi_{\mathrm{i}}\rangle = |0\rangle$, then set the post-selections to the superposition of $|0\rangle$ and $|1\rangle$ or $|2\rangle$. More general cases will be discussed similarly.

Case 2.—$|\psi_{\mathrm{i}}\rangle = |n\rangle$, $n \in \mathbb{N}^{*}$.

Let $|\psi_{\mathrm{i}}\rangle = |n\rangle$, and $|\psi_{\mathrm{f}}\rangle = \cos\theta|n\rangle + \sin\theta\, e^{\mathrm{i}\varphi}|m\rangle$, where $\theta \in (0, \pi/2) \cup (\pi/2, \pi)$, $\varphi \in [0, 2\pi)$, $n, m \in \mathbb{N}^{*}$, and $n \neq m$. Likewise, $\langle \psi_{\mathrm{f}}|\psi_{\mathrm{i}}\rangle = \cos\theta$, then

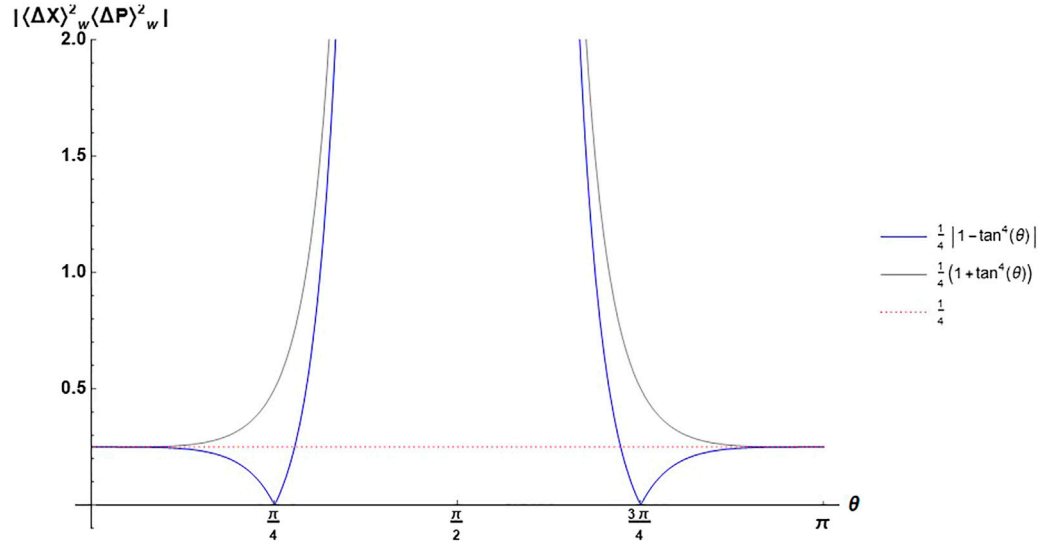

FIGURE 1 | The variation diagram of $|\langle\Delta X\rangle_w^2\langle\Delta P\rangle_w^2|$ with respect to the superposition parameter $\theta \in (0, \pi/2) \cup (\pi/2, \pi)$ in the case of $|\psi_i\rangle = |0\rangle$ and $m = 1$. The blue line represents the lower bound of $|\langle\Delta X\rangle_w^2\langle\Delta P\rangle_w^2|$, so does the grey line connecting the upper bound of $|\langle\Delta X\rangle_w^2\langle\Delta P\rangle_w^2|$, which is greater than 1/4 all the time.

$$\begin{aligned}\langle X\rangle_w &= \frac{\langle\psi_f|X|\psi_i\rangle}{\langle\psi_f|\psi_i\rangle}\\ &= \frac{\left[\cos\theta\langle n| + \sin\theta\, e^{-i\varphi}\langle m|\right](a+a^\dagger)|n\rangle}{\sqrt{2}\cos\theta}\\ &= \frac{\tan\theta\, e^{-i\varphi}\left(\sqrt{n}\,\langle m|n-1\rangle + \sqrt{n+1}\,\langle m|n+1\rangle\right)}{\sqrt{2}}\\ &= \frac{\tan\theta\, e^{-i\varphi}\left(\sqrt{n}\,\delta_{m,n-1} + \sqrt{n+1}\,\delta_{m,n+1}\right)}{\sqrt{2}}.\end{aligned}$$

In this case,

$$\begin{aligned}(\langle X\rangle_w)^2 &= \frac{\tan^2\theta\, e^{-i2\varphi}\left(\sqrt{n}\,\delta_{m,n-1} + \sqrt{n+1}\,\delta_{m,n+1}\right)^2}{2}\\ &= \frac{\tan^2\theta\, e^{-i2\varphi}\left[n\,\delta_{m,n-1}^2 + (n+1)\,\delta_{m,n+1}^2\right]}{2}.\end{aligned} \tag{15}$$

Similarly, we can compute that

$$\begin{aligned}\langle X^2\rangle_w &= \frac{\langle\psi_f|\left[a^2 + aa^\dagger + a^\dagger a + (a^\dagger)^2\right]|\psi_i\rangle}{2\langle\psi_f|\psi_i\rangle}\\ &= \frac{\left[\cos\theta\langle n| + \sin\theta\, e^{-i\varphi}\langle m|\right]\left[a^2 + aa^\dagger + a^\dagger a + (a^\dagger)^2\right]|n\rangle}{2\cos\theta}\\ &= \frac{\left[\cos\theta\langle n| + \sin\theta\, e^{-i\varphi}\langle m|\right]}{2\cos\theta}\\ &\quad\frac{\left[\sqrt{n(n-1)}\,|n-2\rangle + (2n+1)|n\rangle + \sqrt{(n+1)(n+2)}\,|n+2\rangle\right]}{2\cos\theta}\\ &= n + \frac{1}{2} + \frac{\tan\theta\, e^{-i\varphi}}{2}\left[\sqrt{n(n-1)}\,\delta_{m,n-2} + \sqrt{(n+1)(n+2)}\,\delta_{m,n+2}\right].\end{aligned} \tag{16}$$

Then

$$\begin{aligned}\langle\Delta X\rangle_w^2 &\equiv \langle X^2\rangle_w - (\langle X\rangle_w)^2\\ &= n + \frac{1}{2} + \frac{-\tan^2\theta\, e^{-i2\varphi}\left[n\,\delta_{m,n-1}^2 + (n+1)\,\delta_{m,n+1}^2\right]}{2}\\ &\quad\tan\theta\, e^{-i\varphi}\left[\sqrt{n(n-1)}\,\delta_{m,n-2} + \sqrt{(n+1)(n+2)}\,\delta_{m,n+2}\right].\end{aligned} \tag{17}$$

Similarly, we have

$$\begin{aligned}\langle P\rangle_w &= \frac{\langle\psi_f|P|\psi_i\rangle}{\langle\psi_f|\psi_i\rangle}\\ &= \frac{\left[\cos\theta\langle n| + \sin\theta\, e^{-i\varphi}\langle m|\right](a-a^\dagger)|n\rangle}{i\sqrt{2}\cos\theta}\\ &= \frac{i\tan\theta\, e^{-i\varphi}\left(\sqrt{n+1}\,\delta_{m,n+1} - \sqrt{n}\,\delta_{m,n-1}\right)}{\sqrt{2}},\end{aligned}$$

which indicates that

$$(\langle P\rangle_w)^2 = -\frac{\tan^2\theta\, e^{-i2\varphi}\left[(n+1)\,\delta_{m,n+1}^2 + n\,\delta_{m,n-1}^2\right]}{2}, \tag{18}$$

and

$$\begin{aligned}\langle P^2\rangle_w &= \frac{\langle\psi_f|\left[aa^\dagger + a^\dagger a - a^2 - (a^\dagger)^2\right]|\psi_i\rangle}{2\langle\psi_f|\psi_i\rangle}\\ &= \frac{\left[\cos\theta\langle n| + \sin\theta\, e^{-i\varphi}\langle m|\right]\left[aa^\dagger + a^\dagger a - a^2 - (a^\dagger)^2\right]|n\rangle}{2\cos\theta}\\ &= \frac{\left[\cos\theta\langle n| + \sin\theta\, e^{-i\varphi}\langle m|\right]}{2\cos\theta}\\ &\quad\frac{\left[(2n+1)|n\rangle - \sqrt{n(n-1)}\,|n-2\rangle - \sqrt{(n+1)(n+2)}\,|n+2\rangle\right]}{2\cos\theta}\\ &= n + \frac{1}{2} - \frac{\tan\theta\, e^{-i\varphi}}{2}\left[\sqrt{n(n-1)}\,\delta_{m,n-2} + \sqrt{(n+1)(n+2)}\,\delta_{m,n+2}\right].\end{aligned} \tag{19}$$

Hence,

$$\begin{aligned}\langle\Delta P\rangle_{\mathrm{w}}^{2} &\equiv \langle P^{2}\rangle_{\mathrm{w}} - (\langle P\rangle_{\mathrm{w}})^{2} \\ &= n+\frac{1}{2}-\frac{\begin{matrix}\tan\theta\, e^{-\mathrm{i}\varphi}\left[\sqrt{n(n-1)}\ \delta_{m,n-2}+\sqrt{(n+1)(n+2)}\ \delta_{m,n+2}\right] \\ -\tan^{2}\theta\, e^{-\mathrm{i}2\varphi}\left[(n+1)\,\delta_{m,n+1}^{2}+n\,\delta_{m,n-1}^{2}\right]\end{matrix}}{2}.\end{aligned} \tag{20}$$

which means that

$$\begin{aligned}&\langle\Delta X\rangle_{\mathrm{w}}^{2}\langle\Delta P\rangle_{\mathrm{w}}^{2} \\ &=\left(n+\frac{1}{2}\right)^{2} \\ &\quad-\frac{\begin{Bmatrix}\tan\theta\, e^{-\mathrm{i}\varphi}\left[\sqrt{n(n-1)}\ \delta_{m,n-2}+\sqrt{(n+1)(n+2)}\ \delta_{m,n+2}\right] \\ -\tan^{2}\theta\, e^{-\mathrm{i}2\varphi}\left[(n+1)\,\delta_{m,n+1}^{2}+n\,\delta_{m,n-1}^{2}\right]\end{Bmatrix}^{2}}{4} \\ &=\left(n+\frac{1}{2}\right)^{2}-\frac{\tan^{2}\theta\, e^{-\mathrm{i}2\varphi}}{4}\left[n(n-1)\,\delta_{m,n-2}^{2}+(n+1)(n+2)\,\delta_{m,n+2}^{2}\right] \\ &\quad-\frac{\tan^{4}\theta\, e^{-\mathrm{i}4\varphi}}{4}\left[(n+1)^{2}\,\delta_{m,n+1}^{4}+n^{2}\,\delta_{m,n-1}^{4}\right] \\ &=\frac{1}{4}\{(2n+1)^{2}-\tan^{2}\theta\, e^{-\mathrm{i}2\varphi}\left[n(n-1)\,\delta_{m,n-2}^{2}+(n+1)(n+2)\,\delta_{m,n+2}^{2}\right] \\ &\quad-\tan^{4}\theta\, e^{-\mathrm{i}4\varphi}\left[(n+1)^{2}\,\delta_{m,n+1}^{4}+n^{2}\,\delta_{m,n-1}^{4}\right]\}.\end{aligned} \tag{21}$$

After that, we can calculate the absolute value of **Eq. 21**, namely

$$\begin{aligned}&\left|\langle\Delta X\rangle_{\mathrm{w}}^{2}\langle\Delta P\rangle_{\mathrm{w}}^{2}\right| \\ &=\frac{1}{4}\Big|(2n+1)^{2}-\tan^{2}\theta\, e^{-\mathrm{i}2\varphi}\left[n(n-1)\,\delta_{m,n-2}^{2}+(n+1)(n+2)\,\delta_{m,n+2}^{2}\right] \\ &\quad-\tan^{4}\theta\, e^{-\mathrm{i}4\varphi}\left[(n+1)^{2}\,\delta_{m,n+1}^{4}+n^{2}\,\delta_{m,n-1}^{4}\right]\Big| \\ &\geq\frac{1}{4}\Big|(2n+1)^{2}-\tan^{2}\theta\left[n(n-1)\,\delta_{m,n-2}^{2}+(n+1)(n+2)\,\delta_{m,n+2}^{2}\right] \\ &\quad-\tan^{4}\theta\left[(n+1)^{2}\,\delta_{m,n+1}^{4}+n^{2}\,\delta_{m,n-1}^{4}\right]\Big|.\end{aligned} \tag{22}$$

Analysis—Analogously, we will analyze the value of m in the following way:

1) If $m \neq n-2$, $m \neq n-1$, $m \neq n+1$ and $m \neq n+2$, $|\langle\Delta X\rangle_{\mathrm{w}}^{2}\langle\Delta P\rangle_{\mathrm{w}}^{2}| = (1/4)(2n+1)^{2} > 1/4$, because $n > 0$, thus it coincides with the Heisenberg uncertainty relation.
2) If $m = n-2$,

$$\frac{1}{4}\left|(2n+1)^{2}-n(n-1)\tan^{2}\theta\right| \leq \left|\langle\Delta X\rangle_{\mathrm{w}}^{2}\langle\Delta P\rangle_{\mathrm{w}}^{2}\right| \leq \left|(2n+1)^{2}+n(n-1)\tan^{2}\theta\right|.$$

Once $n = 1$, then $|\langle\Delta X\rangle_{\mathrm{w}}^{2}\langle\Delta P\rangle_{\mathrm{w}}^{2}| = 9/4 > 1/4$, nevertheless, $m = n-2 = -1$ is illegal. Hence we focus on the situation of $n > 1$. By $|(2n+1)^{2}-n(n-1)\tan^{2}\theta| \geq 1$, we have $\tan^{2}\theta \geq [(2n+1)^{2}+1]/[n(n-1)]$, or $\tan^{2}\theta \leq [(2n+1)^{2}-1]/[n(n-1)]$, and the uncertainty relation always holds. Otherwise, there exist unviolated situations if $[(2n+1)^{2}-1]/[n(n-1)] \leq \tan^{2}\theta \leq [(2n+1)^{2}+1]/[n(n-1)]$.

3) If $m = n-1$,

$$\frac{1}{4}\left|(2n+1)^{2}-n^{2}\tan^{4}\theta\right| \leq \left|\langle\Delta X\rangle_{\mathrm{w}}^{2}\langle\Delta P\rangle_{\mathrm{w}}^{2}\right| \leq \left|(2n+1)^{2}+n^{2}\tan^{4}\theta\right|,$$

which implies that when $\tan^{4}\theta \geq [(2n+1)^{2}+1]/n^{2}$ or $\tan^{4}\theta \leq [(2n+1)^{2}-1]/n^{2}$, $|\langle\Delta X\rangle_{\mathrm{w}}^{2}\langle\Delta P\rangle_{\mathrm{w}}^{2}| \geq 1/4$ forever, while for $[(2n+1)^{2}-1]/n^{2} \leq \tan^{4}\theta \leq [(2n+1)^{2}+1]/n^{2}$, the limitation 1/4 may be broken.

4) If $m = n+1$,

$$\frac{1}{4}\left|(2n+1)^{2}-(n+1)^{2}\tan^{4}\theta\right| \leq \left|\langle\Delta X\rangle_{\mathrm{w}}^{2}\langle\Delta P\rangle_{\mathrm{w}}^{2}\right| \leq \left|(2n+1)^{2}+(n+1)^{2}\tan^{4}\theta\right|.$$

Therefore when $\tan^{4}\theta \geq [(2n+1)^{2}+1]/(n+1)^{2}$ or $\tan^{4}\theta \leq [(2n+1)^{2}-1]/(n+1)^{2}$, $|\langle\Delta X\rangle_{\mathrm{w}}^{2}\langle\Delta P\rangle_{\mathrm{w}}^{2}| \geq 1/4$ all the while, but for $[(2n+1)^{2}-1]/(n+1)^{2} \leq \tan^{4}\theta \leq [(2n+1)^{2}+1]/(n+1)^{2}$, counterexamples could be found.

5) If $m = n+2$,

$$\frac{1}{4}\left|(2n+1)^{2}-(n+1)(n+2)\tan^{2}\theta\right| \leq \left|\langle\Delta X\rangle_{\mathrm{w}}^{2}\langle\Delta P\rangle_{\mathrm{w}}^{2}\right| \leq \left|(2n+1)^{2}+(n+1)(n+2)\tan^{2}\theta\right|.$$

After that, via $|(2n+1)^{2}-(n+1)(n+2)\tan^{2}\theta| \geq 1$, we attain $\tan^{2}\theta \geq [(2n+1)^{2}+1]/[(n+1)(n+2)]$, or $\tan^{2}\theta \leq [(2n+1)^{2}-1]/[(n+1)(n+2)]$, and the uncertainty relation is not violated all through. However, in the case of $[(2n+1)^{2}-1]/[(n+1)(n+2)] \leq \tan^{2}\theta \leq [(2n+1)^{2}+1]/[(n+1)(n+2)]$, violations might appear.

2.3 Orthonormal Pre- and Post- Selected States

Following the above deduction, when $\theta \to \pi/2$, $\langle\psi_{\mathrm{f}}|\psi_{\mathrm{i}}\rangle \to 0$, or the pre- and post-selected states tend to be mutual orthogonal phase differently. For instance, assume that $n = 0$ and $m = 1$, in so doing,

$$\frac{1}{4}\left|1-\tan^{4}\theta\right| \leq \left|\langle\Delta X\rangle_{\mathrm{w}}^{2}\langle\Delta P\rangle_{\mathrm{w}}^{2}\right| \leq \frac{1}{4}\left|1+\tan^{4}\theta\right|, \tag{23}$$

and we can see from **Figure 1** that once $\langle\psi_{\mathrm{f}}|\psi_{\mathrm{i}}\rangle \to 0$, the product of two deviations in the form of weak values is tending towards infinity, which agrees with Heisenberg's statement.

2.4 Coherent States of the Simple Harmonic Oscillator

The coherent state of the simple harmonic oscillator is devised to simulate the classical oscillator [12], which can be represented as

$$|z\rangle = \mathrm{e}^{za^{\dagger}-z^{*}a}|0\rangle = \mathrm{e}^{-|z|^{2}}\sum_{n=0}\frac{z^{n}}{\sqrt{n!}}|n\rangle, \quad z \in \mathbb{C}, \tag{24}$$

with the following traits:

$$a|z\rangle = z|z\rangle, \quad (a|z\rangle)^{\dagger} = \langle z|a^{\dagger} = z^{*}\langle z|. \tag{25}$$

After that, label the pre- and post-selected states as $|z_{\mathrm{i}}\rangle$ and $|z_{\mathrm{f}}\rangle$ respectively, then the weak value of X reads

$$\langle X\rangle_{\mathrm{w}}=\frac{\langle z_{\mathrm{f}}|X|z_{\mathrm{i}}\rangle}{\langle z_{\mathrm{f}}|z_{\mathrm{i}}\rangle}=\frac{\langle z_{\mathrm{f}}|\left(a+a^{\dagger}\right)|z_{\mathrm{i}}\rangle}{\sqrt{2}\langle z_{\mathrm{f}}|z_{\mathrm{i}}\rangle}=\frac{z_{\mathrm{f}}^{*}+z_{\mathrm{i}}}{\sqrt{2}}, \tag{26}$$

which implies that

$$\langle X\rangle_{\mathrm{w}}^{2}=\left[\frac{z_{\mathrm{f}}^{*}+z_{\mathrm{i}}}{\sqrt{2}}\right]^{2}=\frac{\left(z_{\mathrm{f}}^{*}\right)^{2}+z_{\mathrm{i}}^{2}+2z_{\mathrm{f}}^{*}z_{\mathrm{i}}}{2}. \tag{27}$$

For that matter,

$$\begin{aligned}\langle X^{2}\rangle_{\mathrm{w}}&=\frac{\langle z_{\mathrm{f}}|X^{2}|z_{\mathrm{i}}\rangle}{\langle z_{\mathrm{f}}|z_{\mathrm{i}}\rangle}=\frac{\langle z_{\mathrm{f}}|\left[a^{2}+aa^{\dagger}+a^{\dagger}a+\left(a^{\dagger}\right)^{2}\right]|z_{\mathrm{i}}\rangle}{2\langle z_{\mathrm{f}}|z_{\mathrm{i}}\rangle}\\&=\frac{\langle z_{\mathrm{f}}|\left[a^{2}+2a^{\dagger}a+1+\left(a^{\dagger}\right)^{2}\right]|z_{\mathrm{i}}\rangle}{2\langle z_{\mathrm{f}}|z_{\mathrm{i}}\rangle}\\&=\frac{z_{\mathrm{i}}^{2}+2z_{\mathrm{f}}^{*}z_{\mathrm{i}}+\left(z_{\mathrm{f}}^{*}\right)^{2}+1}{2}.\end{aligned} \tag{28}$$

Thus,

$$\langle\Delta X\rangle_{\mathrm{w}}^{2}\equiv\langle X^{2}\rangle_{\mathrm{w}}-\left(\langle X\rangle_{\mathrm{w}}\right)^{2}=\frac{1}{2}. \tag{29}$$

With the same argument, the weak value of P can be expressed as

$$\langle P\rangle_{\mathrm{w}}=\frac{\langle z_{\mathrm{f}}|P|z_{\mathrm{i}}\rangle}{\langle z_{\mathrm{f}}|z_{\mathrm{i}}\rangle}=\frac{\mathrm{i}\langle z_{\mathrm{f}}|\left(a^{\dagger}-a\right)|z_{\mathrm{i}}\rangle}{\sqrt{2}\langle z_{\mathrm{f}}|z_{\mathrm{i}}\rangle}=\frac{\mathrm{i}\left(z_{\mathrm{f}}^{*}-z_{\mathrm{i}}\right)}{\sqrt{2}}, \tag{30}$$

then

$$\langle P\rangle_{\mathrm{w}}^{2}=\left[\frac{\mathrm{i}\left(z_{\mathrm{f}}^{*}-z_{\mathrm{i}}\right)}{\sqrt{2}}\right]^{2}=\frac{2z_{\mathrm{f}}^{*}z_{\mathrm{i}}-\left(z_{\mathrm{f}}^{*}\right)^{2}-z_{\mathrm{i}}^{2}}{2}. \tag{31}$$

Thus,

$$\begin{aligned}\langle P^{2}\rangle_{\mathrm{w}}&=\frac{\langle z_{\mathrm{f}}|P^{2}|z_{\mathrm{i}}\rangle}{\langle z_{\mathrm{f}}|z_{\mathrm{i}}\rangle}=\frac{\langle z_{\mathrm{f}}|\left[aa^{\dagger}+a^{\dagger}a-a^{2}-\left(a^{\dagger}\right)^{2}\right]|z_{\mathrm{i}}\rangle}{2\langle z_{\mathrm{f}}|z_{\mathrm{i}}\rangle}\\&=\frac{\langle z_{\mathrm{f}}|\left[2a^{\dagger}a+1-a^{2}-\left(a^{\dagger}\right)^{2}\right]|z_{\mathrm{i}}\rangle}{2\langle z_{\mathrm{f}}|z_{\mathrm{i}}\rangle}\\&=\frac{2z_{\mathrm{f}}^{*}z_{\mathrm{i}}-z_{\mathrm{i}}^{2}-\left(z_{\mathrm{f}}^{*}\right)^{2}+1}{2}.\end{aligned} \tag{32}$$

which means that,

$$\langle\Delta P\rangle_{\mathrm{w}}^{2}\equiv\langle P^{2}\rangle_{\mathrm{w}}-\left(\langle P\rangle_{\mathrm{w}}\right)^{2}=\frac{1}{2}, \tag{33}$$

namely

$$\langle\Delta X\rangle_{\mathrm{w}}^{2}\langle\Delta P\rangle_{\mathrm{w}}^{2}=\frac{1}{4}. \tag{34}$$

Obviously, the uncertainty relation for the coherent state of the simple harmonic oscillator in the sense of weak value reaches the lower bound of Heisenberg uncertainty relation (**Eq. 13**) all the while, which is in accord with the traditional case using expectation value.

3 SUMMARY

We delve into the case of measuring position and momentum in a simple harmonic oscillator with pre-selected states as eigenstates and the post-selections as the superposition states. Remarkably, we find out that Heisenberg's claim for two incompatible observables fails in the situation of weak values for typical selections listed previously. But the weak value canonical uncertainty relation holds for the simple harmonic oscillator in coherent states.

Our work may offer a beneficial supplement in the field of uncertainty relation with weak measurement, and beat the standard Heisenberg limit. Of course, we do not consider complete process of weak measurement, as none interaction Hamiltonian of quantum system with environment appear, hence the present work is not appropriate for experimental test, which we are struggling for.

In fact, although Heisenberg's principle is sufficiently elegant and classical in current textbooks, it cannot undergo the test relating to weak measurement [13]. Nevertheless, two generalizations, the one is presented via M. Ozawa [14] and the other is dedicated by C. Branciard [15], about Heisenberg's work, were successfully verified in the same experiment [13]. Then can we discover a more general and concise uncertainty formula to unify all current results? And why is the nature of quantum world uncertainty (see[1] as one of the 125 open questions in *Science*)? We may understand these questions more thoroughly by dint of geometry. Some papers have appeared, e.g., [16, 17]. We anticipate more progress on the relation between the uncertainty relations and the weak measurements in the near future.

DATA AVAILABILITY STATEMENT

The original contributions presented in the study are included in the article/Supplementary Material, further inquiries can be directed to the corresponding author.

AUTHOR CONTRIBUTIONS

X-YF and J-LC contributed to conception and design of the study. X-YF organized the database. X-YF and J-LC performed the statistical analysis. X-YF wrote the first draft of the manuscript. W-MS, JZ, H-XM, and J-LC wrote sections of the manuscript. All authors contributed to manuscript revision, read, and approved the submitted version.

FUNDING

J-LC was supported by the National Natural Science Foundations of China (Grant Nos 11875167 and 12075001). X-YF, W-MS, and JZ were supported by the Nankai Zhide Foundation. H-XM was supported by the National Natural Science Foundations of China (Grant No. 11901317).

[1]https://www.science.org/content/resource/125-questions-exploration-and-discovery

REFERENCES

1. Heisenberg W Über den anschaulichen Inhalt der quantentheoretischen Kinematik und Mechanik. *Z Phys* (1927) 43:172–98.
2. Robertson HP The Uncertainty Principle. *Phys Rev* (1929) 34:163–4. doi:10.1103/physrev.34.163
3. Coles PJ, Berta M, Tomamichel M, Wehner S Entropic Uncertainty Relations and Their Applications. *Rev Mod Phys* (2017) 89:015002. doi:10.1103/revmodphys.89.015002
4. Everett H "Relative State" Formulation of Quantum Mechanics. *Rev Mod Phys* (1957) 29:454–62. doi:10.1103/revmodphys.29.454
5. Hirschman II, Jr. A Note on Entropy. *Am J Math* (1957) 79:152–6. doi:10.2307/2372390
6. Aharonov Y, Albert DZ, Vaidman L How the Result of a Measurement of a Component of the Spin of a Spin-1/2particle Can Turn Out to Be 100. *Phys Rev Lett* (1988) 60:1351–4. doi:10.1103/physrevlett.60.1351
7. Song Q, Qiao C Uncertainty Equalities and Uncertainty Relation in Weak Measurement. *J Univ Chin Acad Sci* (2016) 33(1):37. doi:10.7523/j.issn.2095-6134.2016.01.006
8. Pati AK, Wu J *Uncertainty and Complementarity Relations in Weak Measurement*. New York: Cornell University at Ithaca (2014). arXiv:quant-ph/1411.7218v1.
9. Hall MJW, Pati AK, Wu J Products of Weak Values: Uncertainty Relations, Complementarity, and Incompatibility. *Phys Rev A* (2016) 93:052118. doi:10.1103/physreva.93.052118
10. Shikano Y, Hosoya A Weak Values with Decoherence. *J Phys A: Math Theor* (2009) 43:025304. doi:10.1088/1751-8113/43/2/025304
11. Šindelka1 M, Moiseyev N Quantum Uncertainties and Heisenberg-like Uncertainty Relations for a Weak Measurement Scheme Involving Two Arbitrary Noncommuting Observables. *Phys Rev A* (2018) 97:012122. doi:10.1103/physreva.97.012122
12. Sakurai JJ, Napolitano J *Modern Quantum Mechanics*. 2nd ed. Cambridge, UK: Cambridge University Press (2017).
13. Kaneda F, Baek SY, Ozawa M, Edamatsu K Experimental Test of Error-Disturbance Uncertainty Relations by Weak Measurement. *Phys Rev Lett* (2014) 112:020402. doi:10.1103/physrevlett.112.020402
14. Ozawa M Universally Valid Reformulation of the Heisenberg Uncertainty Principle on Noise and Disturbance in Measurement. *Phys Rev A* (2003) 67:042105. doi:10.1103/physreva.67.042105
15. Branciard C Error-tradeoff and Error-Disturbance Relations for Incompatible Quantum Measurements. *Proc Natl Acad Sci* (2013) 110:6742–7. doi:10.1073/pnas.1219331110
16. Lobo AC, Ribeiro Cd. A *The Geometry of Von-Neumann's Pre-measurement and Weak Values* New York: Cornell University at Ithaca (2011). arXiv:quant-ph/1111.4205v2.
17. Kechrimparis S, Weigert S Geometry of Uncertainty Relations for Linear Combinations of Position and Momentum. *J Phys A: Math Theor* (2018) 51:025303. doi:10.1088/1751-8121/aa9cfc

Conflict of Interest: The authors declare that the research was conducted in the absence of any commercial or financial relationships that could be construed as a potential conflict of interest.

frontiers in Physics

ORIGINAL RESEARCH
published: 21 March 2022
doi: 10.3389/fphy.2022.874802

Uncertainty Relation and Quantum Phase Transition in the Two-Dimensional Ising Model

Yu-Yan Fang[1], *Tian-Yi Jiang*[1], *Xin-Ye Xu*[1,2]* and *Jin-Ming Liu*[1]*

[1]State Key Laboratory of Precision Spectroscopy, School of Physics and Electronic Science, East China Normal University, Shanghai, China, [2]Shanghai Research Center for Quantum Sciences, Shanghai, China

By using quantum renormalization group (QRG) approach, we first derive the effective Hamiltonian and QRG equations of the two-dimensional (2D) Ising models with two different time-dependent transverse magnetic fields analytically. Then we examine the nonanalytic and scaling behaviors of the linear-entropy-based uncertainty relation and quantum entanglement of the models near the critical point through numerical analysis. Moreover, we investigate the relation between the quantum critical point and the external magnetic field. Our results show that both the uncertainty relation and the quantum entanglement are feasible to detect the quantum phase transition (QPT), and the uncertainty relation may be a better indicator of QPT than quantum entanglement. Our findings could shed new light on the observable of the QPTs of the solid-state system with the uncertainty relation.

Keywords: uncertainty relation, quantum phase transition, quantum renormalization group, quantum entanglement, Ising model

OPEN ACCESS

Edited by:
Dong Wang,
Anhui University, China

Reviewed by:
Liu Ye,
Anhui University, China
Chengjie Zhang,
Ningbo University, China

***Correspondence:**
Xin-Ye Xu
xyxu@phy.ecnu.edu.cn
Jin-Ming Liu
jmliu@phy.ecnu.edu.cn

Specialty section:
This article was submitted to Quantum Engineering and Technology, a section of the journal Frontiers in Physics

Received: *13 February 2022*
Accepted: *23 February 2022*
Published: *21 March 2022*

Citation:
Fang Y-Y, Jiang T-Y, Xu X-Y and Liu J-M (2022) Uncertainty Relation and Quantum Phase Transition in the Two-Dimensional Ising Model. Front. Phys. 10:874802. doi: 10.3389/fphy.2022.874802

1 INTRODUCTION

Quantum entanglement is one of the most astonishing notions of quantum mechanics [1, 2] and is at the centre of the large amount of applications in quantum sciences and technologies, such as quantum cryptography [3], quantum teleportation [4], superdense coding [5], and telecloning [6]. Negativity as the witness of the bipartite entanglement was introduced by Życzkowski et al [7] and then proven by Vidal and Werner [8] to be a monotone under the local operation and classical communication.

As we know, the relation between quantum entanglement and quantum phase transition (QPT) [9] is of considerable interest [10]. QPT is induced by the change of external parameters or interaction coupling constants. The divergence of the correlation length in the vicinity of the quantum critical points (QCP) indicates that the different components of the quantum system are strongly correlated. Quantum entanglement can be used as a way to measure quantum correlations and to indicate the behavior of QPT such as discontinuity close to the QCP [11, 12]. In the past few years the behavior of entanglement near QCP in different spin systems [13–15] was considered as a subject of profound significance [16–19]. Recently, A lot of work was devoted to the study of Heisenberg spin chains, particularly the one-dimensional (1D) spin chains, which can be given quantitative results and be exactly solvable [20–25]. The QPT of Heisenberg spin chains is caused by quantum fluctuations, which is essentially induced by quantum uncertainty relation of the system. Up to now, quantum uncertainty relation has gone through considerable development. Nevertheless, to our knowledge there are few studies on the relation between the uncertainty and QPT [26–29].

The quantum uncertainty relation is deemed one of the most unique and fundamental features in quantum mechanics, which states that it is impossible to simultaneously determine the definite measurement outcomes of noncommutative observables. Based on the distributions of measurement results, the uncertainty relation can be depicted in different ways [30–33]. Historically, the uncertainty principle was originally formulated by Heisenberg [34] for the coordinate and the momentum in an infinite dimensional Hilbert space. Later, Robertson generalized Heisenberg uncertainty inequality to arbitrary pairs of observables [30]. Instead of the standard deviation, the uncertainty relation can also be delicately given in terms of Shannon entropies associated with the measurement bases [35]. By considering the quantum entanglement with a memory system [36], an entropic uncertainty relation in the presence of quantum memory was proposed and attracted wide attentions [37, 38]. Taking the entangled quantum memory into account, these uncertainty relations have potential applications in quantum key distributions and entanglement witnessing [37, 39, 40]. However, all the uncertainty relations proposed above involve the measurement between only two observations and are expressed in the form of inequality. Very recently, Wang et al. [41] put forward a novel entropic uncertainty relation for bipartite systems composed of a measured subsystem A and a quantum memory B, in which projection measurements is based on a complete set of mutually unbiased bases (MUBs). By means of the complete set of MUBs, an uncertainty equality based on conditional linear entropy was derived [42, 43]. The uncertainty equality implies that the sum of uncertainties is exactly equal to the fixed quantity related to the initial bipartite state which was confirmed experimentally with optical systems [41, 44]. This uncertainty relation can be applied to quantum random number generation and quantum guessing games. On the other hand, quantum renormalization group (QRG) is one of the conceptual pillars of quantum field theory and statistical mechanics, which revolves around the idea of rescaling transformations and coarse-graining of a large-scale system [45].

The QRG method is widely used to solve exactly the 1D Ising, XXZ, XYZ and XY models [20, 46, 47]. At zero temperature, the QRG method provides insights into how the block uncertainty and entanglement change as the size of the system becomes large in 1D spin chains. On the basis of the 1D case, some further contributions on two-dimensional (2D) and higher-dimensional systems have been recently made [48–53]. In this work, we introduce two different types of the time-dependent magnetic fields into the 2D Ising models, and obtain the effective Hamiltonian of the models by employing the QRG method. Moreover, we investigate the evolution of the uncertainty in contrast to the quantum entanglement in terms of the magnetic field to characterize the QPT.

This paper is structured as follows. In **Section 2**, we first derive the QRG equations for the 2D models with the time-dependent magnetic fields. And in **Section 3**, the evolutions of the uncertainty and quantum entanglement are discussed in the 2D model. A conclusion is given in **Section 4**.

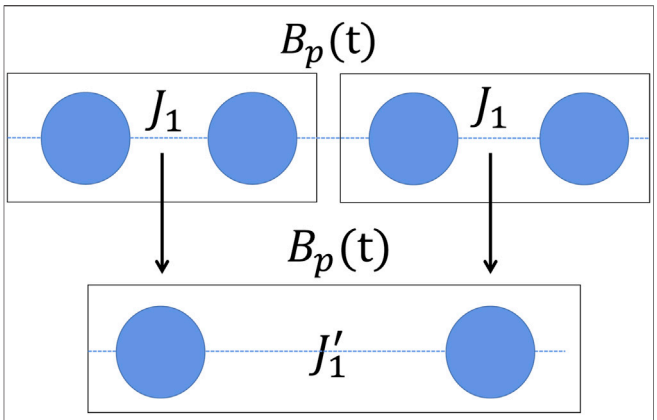

FIGURE 1 | The procedure of the 1D model partitioning.

2 QRG FOR THE TRANSVERSE-FIELD ISING MODELS

The QRG method can effectively process large-scale quantum spin systems [45]. The key of the QRG method is the mode thinning of the degrees of freedom followed by iterations which reduces the number of parameters step by step until reaching a fixed point. In this section, we derive the QRG equation for 2D Ising models with time-dependent magnetic fields following the method of 1D QRG.

The Hamiltonian of the 1D Ising model with N sites can be expressed as

$$H_1(t) = -J_1 \sum_{i=1}^{N} \sigma_i^z \sigma_{i+1}^z - B_p(t) \sum_{i}^{N} \sigma_i^x, \tag{1}$$

where $J_1 > 0$ is the exchange coupling constant, σ_i^α $(\alpha = x, y, z)$ are the Pauli matrices at site i, $B_p(t)$ $(p = 1, 2)$ denote the time-dependent magnetic field strengths. Here, we define

$$B_1(t) = kt, \tag{2}$$

$$B_2(t) = \sqrt{2}\sin(\omega t). \tag{3}$$

Clearly, $B_1(t)$ denotes the magnetic field strength with the linear coefficient k, while $B_2(t)$ is the sinusoidal magnetic field strength with the frequency of ω.

Similarly, the Hamiltonian of a spin-1/2 2D Ising model with the transverse magnetic field is given by:

$$H_2(t) = -J_2 \sum_{\langle i,j \rangle}^{N} \sigma_i^z \sigma_j^z - B_q(t) \sum_{i}^{N} \sigma_i^x, \tag{4}$$

where the coupling constant $J_2 > 0$, the first sum contains all the nearest-neighbor interactions, and $B_q(t)$ $(q = 3, 4)$ are the time-dependent linear and sinusoidal magnetic field strengths defined by

$$B_3(t) = kt, \tag{5}$$

$$B_4(t) = 1.835\,4\sqrt{2}\sin(\omega t), \tag{6}$$

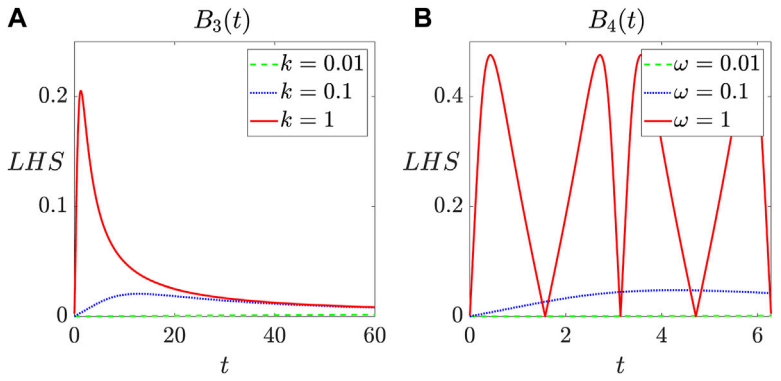

FIGURE 2 | *LHS* of the adiabatic approximation condition versus time t for different magnetic fields: **(A)**$B_3(t)$ and **(B)**$B_4(t)$.

respectively. Here the coefficient $1.835\,4\sqrt{2}$ is chosen for easier analysis of numerical results, as 1.8354 is the critical point of the 2D Ising model described in the following text.

The QRG procedure of the 1D Ising model is started by decomposing the system into isolated blocks (**Figure 1**) and accordingly the Hamiltonian $H_1(t)$ is divided into two parts.

$$H_1(t) = H_k(t) + H_{kk}(t). \tag{7}$$

Here $H_k(t)$ and $H_{kk}(t)$ are the block and interblock Hamiltonian, respectively, which are given by

$$\begin{aligned} H_k(t) &= \sum_I^{N/2} h_k^I(t), \\ h_k^I(t) &= -J_1\sigma_{I,1}^z\sigma_{I,2}^z - B_p(t)\sigma_{I,1}^x, \\ H_{kk}(t) &= \sum_I^{N/2} h_{kk}^{I,I+1}(t), \\ h_{kk}^{I,I+1}(t) &= -J_1\sigma_{I,2}^z\sigma_{I+1,1}^z - B_p(t)\sigma_{I,2}^x, \end{aligned} \tag{8}$$

where $h_k^I(t)$ and $h_{kk}^{I,I+1}(t)$ are respectively the Ith block Hamiltonian and the interblock Hamiltonian between the blocks I and $I + 1$.

Next we focus on the effect of magnetic field strength on QPT and do not care about the specific details of the evolution of the system. Therefore, we can make the magnetic field strength change very slowly over time, where the process coincides with the idea of quantum adiabatic approximation. The strict derivation of the quantum adiabatic theorem was first mentioned by [54]. Later, quantum adiabatic approach was extended to the degenerate case, and the quantum adiabatic condition for the degenerate case was obtained [55, 56]. The theorem states that when the time-varying rate of the Hamiltonian approaches to zero, the probability of the system leaving the instantaneous eigenstates of the Hamiltonian can be considered to be zero. In the degenerate case, the Hamiltonian $h_k^I(t)$ of the system depending on parameter $t = [t_1, t_2, t_3, \ldots, t_N]$ have degenerate eigenstates $|n, \alpha\rangle \equiv |n, \alpha(t)\rangle (\alpha = 1, 2, \ldots, d_n)$, corresponding to the eigenvalues $E_n(t)$ with d_n being degeneracy. The adiabatic approximation condition can be written as

$$\left|\frac{\langle n, \alpha|\frac{d}{dt}|n', \alpha'\rangle}{E_n - E_{n'}}\right| \ll 1\,(n \neq n'). \tag{9}$$

A detailed analysis are further performed on the left hand side (LHS) of **Eq. 9** with different magnetic field parameters as shown in **Figure 2**. From **Figure 2A**, we can see that for different values of k, the LHS of the adiabatic approximation condition versus time t in linear magnetic fields $B_3(t)$ have the similar trend, *i.e.*, it first increases to the maximum value and then gradually decreases to 0. However, the maximum value of *LHS* diminishes rapidly from 0.2052 to approximately 0 (much less than 1) as k decreases from 1 to 0.01. **Figure 2B** shows that the maximum values of *LHS* appear periodically over time for the sinusoidal magnetic fields $B_4(t)$. Our primary concern is that when the value of ω decreases to 0.01, the value of *LHS* is approximate to 0. As discussed above, we can set the values of magnetic field parameters k and ω as 0.01 to satisfy the adiabatic approximation condition. On the basis of the approximation condition, the transitions between energy levels of the systems can be ignored, so we can complete the subsequent QRG process by solving the stationary Schrodinger equation $h_k^I(t)|\psi_j\rangle = E_j|\psi_j\rangle\ (j = 1, 2)$.

After solving the Schrodinger equation at a certain time t, we obtain two degenerate ground states $|\psi_1\rangle$ and $|\psi_2\rangle$, which can be used to construct the projection operator as follows

$$P = \otimes_{I=1}^{N/2} P_I,\ \ P_I = |\psi_1\rangle\langle\uparrow| + |\psi_2\rangle\langle\downarrow|, \tag{10}$$

where $|\uparrow\rangle$ and $|\downarrow\rangle$ are the eigenstates of σ_z, and P_I is the projection operator of $h_k^I(t)$. Using the above formulas, we can obtain the following effective Hamiltonian H_{eff} given by

$$\begin{aligned} H_{eff1} &= P^\dagger H P = P^\dagger (H_k + H_{kk}) P \\ &= J_1' \sum_I^{N/2} \sigma_I^z \sigma_{I+1}^z - B_q'(t) \sum_I^{N/2} \sigma_I^x. \end{aligned} \tag{11}$$

where

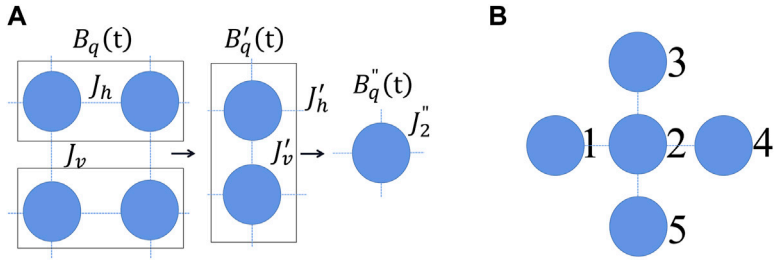

FIGURE 3 | (A) The process of the 2D model partitioning, with first horizontal transformation and then vertical transformation. **(B)** The basic cluster with the nearest neighbor interaction in the 2D model.

$$J_1' = \frac{J_1^2}{\sqrt{J_1^2 + B_q^2(t)}},$$
$$B'(t) = \frac{B_q^2(t)}{\sqrt{J_1^2 + B_q^2(t)}}, \tag{12}$$

which are called QRG equation. Notably, we define the effective magnetic field $h_1 = B_q(t)/J_1$. Then QRG equation can be written as

$$h_1' = h_1^2, \tag{13}$$

where h_1 becomes h_1' after one QRG iteration. The stable and unstable fixed points $h_1 = (0, 1, \infty)$ of the QRG equations are obtained by solving $h_1 = h_1' = h_1^*$, where $h_1 = 1$ is an unstable fixed point and the QCP of the 1D system.

Using the similar QRG method of 1D model [48, 49, 51, 52], now we turn to investigate the related properties of the 2D square lattice. As previously discussed, the values of k and ω are theoretically set to be 0.01 in the rest of this paper. To study the ground state phases of the Hamiltonian in **Eq. 4**, we partition the square lattice into blocks of two sites in horizontal and vertical directions as depicted in **Figure 3A**.

In **Figure 3A**, J_h and J_v represent the ferromagnetic exchange coupling constants in the horizontal and vertical directions respectively, and $J_h = J_v = J_2$. Similar to the 1D case, we first perform the horizontal transformation

$$J_h' = \frac{J_h^2}{\sqrt{J_h^2 + B_q^2(t)}},$$
$$B_q'(t) = \frac{B_q^2(t)}{\sqrt{J_h^2 + B_q^2(t)}}, \tag{14}$$
$$J_v' = J_v\left(1 + \frac{J_h^2}{J_h^2 + B_q^2(t)}\right),$$

and then the vertical transformation as follows,

$$J_h'' = J_h'\left(1 + \frac{J_v'^2}{J_v'^2 + B_q'^2(t)}\right),$$
$$B_q''(t) = \frac{B_q'^2(t)}{\sqrt{J_v'^2 + B_q'^2(t)}}, \tag{15}$$
$$J_v'' = \frac{J_v'^2}{\sqrt{J_v'^2 + B_q'^2(t)}}.$$

To preserve the symmetry of the system, the geometric mean idea [57] is applied to the entire transformation process $J_2'' = \sqrt{J_h'' J_v''}$. Then the effective Hamiltonian H_{eff2} of the 2D model can be expressed as follows

$$H_{eff2}(t) = -J_2'' \sum_{\langle i,j\rangle}^{N} \sigma_i^z \sigma_j^z - B_q''(t) \sum_{i}^{N} \sigma_i^x. \tag{16}$$

The effective magnetic field is set to $h_2 = B_2(t)/J_2$. After the horizontal and vertical transformations, the QRG equation for the 2D model can be obtained as

$$h_2' = \frac{h_2^4\left(\left(1+h_2^2\right)^3\left(4+4h_2^2+2h_2^4+h_2^6\right)\right)^{1/4}}{\left(2+h_2^2\right)\left(8+8h_2^2+3h_2^4+h_2^6\right)^{1/2}}, \tag{17}$$

where h_2 becomes h_2' after one QRG iteration. By solving $h_2 = h_2' = h_2^*$, we can get three fixed points $h_2 = (0, 1.835\ 4, \infty)$, where $h_2 = 1.835\ 4$ is QCP of the ferromagnetic paramagnetic phase transition of the 2D system. Considering the symmetry of the 2D system, we select a basic cluster as the research object shown in **Figure 3B**, and the corresponding Hamiltonian H_c is given by

$$H_c = -J_2''\left(\sigma_2^z\sigma_1^z + \sigma_2^z\sigma_3^z + \sigma_2^z\sigma_4^z + \sigma_2^z\sigma_5^z\right)$$
$$-B_q''(t)\left(\sigma_1^x + \sigma_2^x + \sigma_3^x + \sigma_4^x + \sigma_5^x\right).$$

From the ground state $|\psi_g\rangle$ of H_c, we can construct the density operator $\rho = |\psi_g\rangle\langle\psi_g|$. Then by tracing the density matrix of the subsystems 3, 4 and 5, the reduced density matrix between the sites 1 and 2 is written as

$$\rho_{12} = Tr_{345}\rho. \tag{18}$$

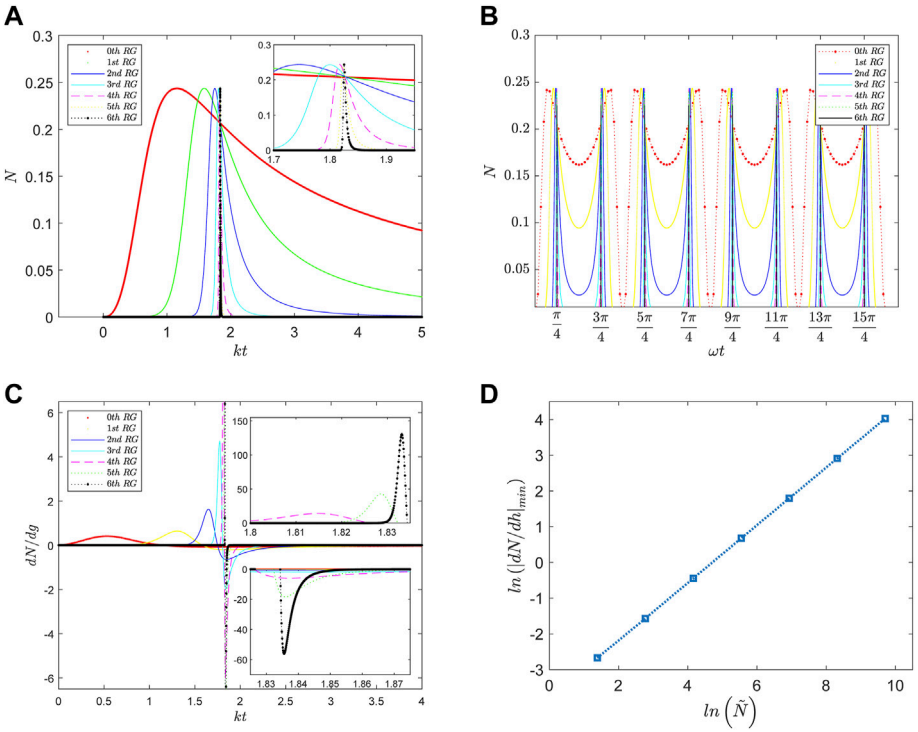

FIGURE 4 | (A) The evolution of negativity of the 2D model *versus kt* with $B_3(t)$, and **(B)** that versus ωt with $B_4(t)$ in terms of QRG iterations. **(C)** The evolution of first derivative of N in terms of QRG iterations with $B_3(t)$. The upper and lower insets show the maximum and minimum of dN/dg at the critical point respectively. **(D)** The scaling behavior of $\ln(|dN/dg|_{\min})$ with respect to the system size $\ln(\tilde{N})$.

As a result, after the QRG iterative process, the relation between the local and global properties of the 2D system is built. By means of the reduced density matrix ρ_{12}, we can analyze the quantum property of the 2D Ising models by calculating uncertainty relation, quantum entanglement, and so on.

3 UNCERTAINTY RELATION AND QUANTUM ENTANGLEMENT OF THE 2D ISING MODELS

In this section, we first use the quantum entanglement to gain a preliminary understanding of the long-range properties and the critical behavior in the 2D Ising model. We adopt the negativity proposed by Vidal and Werner [8] to measure quantum entanglement, which is described by

$$N(\rho_{12}) = \sum_i \left|\lambda_i(\rho_{12}^{T_1})\right| - 1, \tag{19}$$

where ρ_{12} is the reduced density matrix of subsystems 1 and 2, $\rho_{12}^{T_1}$ is the partial transpose matrix about particle 1, and λ_i denotes the ith eigenvalue of $\rho_{12}^{T_1}$. The subsystem 1 and 2 are maximally entangled for $N(\rho_{12}) = 1$, and partially entangled for $N(\rho_{12}) < 1$.

In **Figure 4**, we plot the properties of negativity and its first derivative for the 2D transverse-field Ising model. As seen from **Figure 4A**, as kt increases, N first increases gradually from zero to the maximum $N_{\max} = 0.243\ 7$ for each QRG iteration, then decreases to zero monotonically. When $kt = 1.835\ 4$, the effective magnetic field h_2 is equal to 1.8354, which is the QPT point of the 2D system. For higher QRG iterations, the space in which N can exist gradually becomes smaller and the maximum occurring of N is closer to the QCP at $kt = 1.835\ 4$.

As shown in **Figure 4B**, the negativity maximums $N_{\max} = 0.243\ 7$ display periodicity versus ωt with the magnetic field $B_4(t)$. As the size of the system increases, $N_{\max}$ appears approximately at $\omega t = \frac{\pi}{4}, \frac{3\pi}{4}, \frac{5\pi}{4} \ldots$, and herein the corresponding effective magnetic field strength satisfies $h_2 = 1.835\ 4$, which is the QCP of 2D models.

As we know, the divergence of the first derivative of N means that the system has nonanalytic behavior. From **Figure 4C** we can see that maxima and minima of N are almost symmetric. The maxima exhibit at the critical point of $kt = 1.835\ 4$ and become larger under the system size increasing.

We also note that the entanglement in the vicinity of the QCP shows scaling behavior [58]. **Figure 4D** plots the logarithm of the absolute value of minimum of dN/dh versus the system scale $\ln(\tilde{N})$, displaying a standard linear relation, where $\tilde{N}$ represents the size of the system. From the linear relation, a formula between $|dN/dg|_{\min}$ and $\tilde{N}$ can be obtained as $|dN/dg|_{\min} = \tilde{N}^{0.796\,0}$, which reflects the scaling behavior of entanglement.

In general the quantum entanglement of a system is closely related to its uncertainty. To compare with quantum entanglement, in the following we investigate the uncertainty equality and inequality based on linear entropy [41]. Suppose that

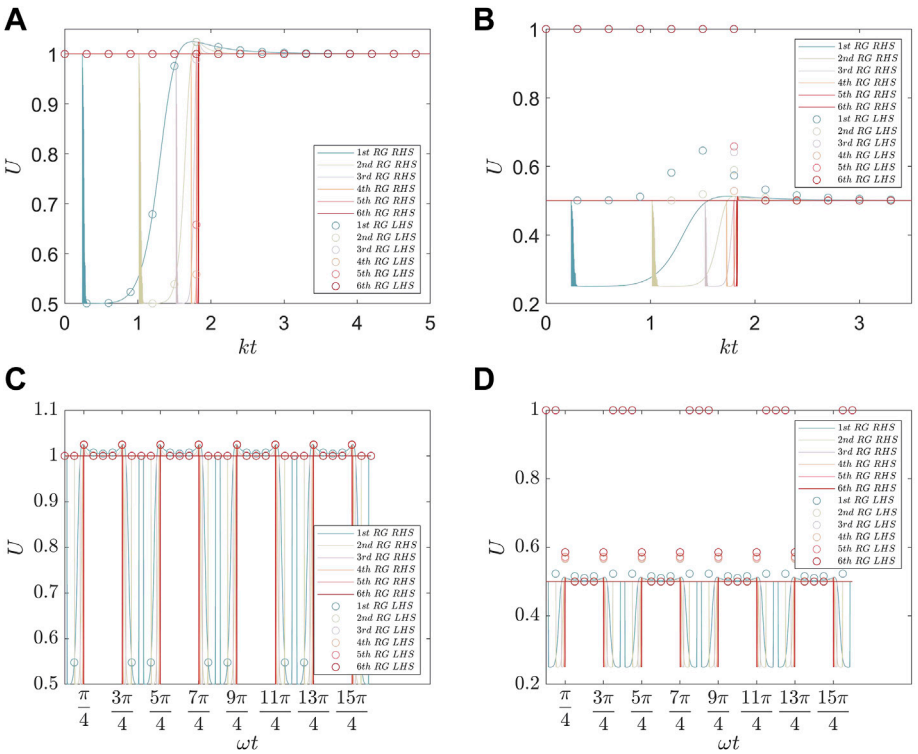

FIGURE 5 | The evolution of the uncertainty of the 2D Ising model. The uncertainty equality **(A)** and inequality **(B)** *versus kt* with the magnetic field $B_3(t)$, the uncertainty equality **(C)** and inequality **(D)** *versus* ωt with the magnetic field $B_4(t)$.

there is a bipartite quantum state ρ_{12} consisting of subsystems 1 and 2 in a $d_1 \times d_2$ ($d_1 < d_2$) dimensional Hilbert space. First, subsystem 1 is performed a local projection measurement with the eigenstates $\{|m\rangle\}$. Then, the bipartite state can be expressed as $\rho_{12}^m = (|m\rangle_1\langle m|\otimes \mathbb{I}_2)\rho_{12}(|m\rangle_1\langle m|\otimes \mathbb{I}_2)/p_m$, where $\mathbb{I}_2$ represents the identity operator of subsystem 2 and $p_m = \mathrm{Tr}[(|m\rangle_1\langle m|\otimes \mathbb{I}_2)\rho_{12}]$ is the measurement probability. As a result, the overall state of the system after the local measurement on subsystem 1 is given by

$$\rho_{M2} = \sum_{m=1}^{d_1} p_m\rho_m = \sum_{m=1}^{d_1} |m\rangle_1\langle m|\otimes \langle m|\rho_{12}|m\rangle_1. \tag{20}$$

To quantify the uncertainty of the composite system, we introduce conditional linear entropy $S_L(M|2)$ as follows,

$$S_L(M \mid 2) = S_L\left(\rho_{M|2}\right) - S_L(\rho_2) = \mathrm{Tr}\left(\rho_2^2\right) - \mathrm{Tr}\left(\rho_{M2}^2\right), \tag{21}$$

where $\rho_2 = \mathrm{Tr}_1(\rho_{12})$ is the reduced density matrix of subsystem 2 and $S_L(\rho) = 1 - \mathrm{Tr}(\rho^2)$ is the linear entropy. For the density matrix ρ_{12}, if a complete set of MUBs $\{M_\theta(\theta = 1, 2, \ldots, d_1 + 1)\}$ are performed, the uncertainty equality is

$$\sum_{i=1}^{d_1+1} S_L(M_\theta \mid 2) = d_1\left(\mathrm{Tr}\left(\rho_2^2\right) - \frac{1}{d_1}\mathrm{Tr}\left(\rho_{12}^2\right)\right). \tag{22}$$

For a two-dimensional subsystem 1, the simplest complete set of MUBs is

$$M_1 = \{|\uparrow\rangle, |\downarrow\rangle\}, M_2 = \left\{\frac{|\uparrow\rangle + |\downarrow\rangle}{\sqrt{2}}, \frac{|\uparrow\rangle - |\downarrow\rangle}{\sqrt{2}}\right\},$$
$$M_3 = \left\{\frac{|\uparrow\rangle + i|\downarrow\rangle}{\sqrt{2}}, \frac{|\uparrow\rangle - i|\downarrow\rangle}{\sqrt{2}}\right\}, \tag{23}$$

where M_1, M_2, M_3 are the eigenvectors of $\sigma_x, \sigma_y, \sigma_z$ respectively. If an incomplete set of d ($d < d_1 + 1$) MUBs (for example, M_2 and M_3) are performed on the $d_1 \times d_2$ dimensional Hilbert space, the uncertainty satisfies the uncertainty inequality

$$\sum_{i=1}^{d} S_L(M_i \mid 2) \geqslant (d-1)\left[\mathrm{Tr}\left(\rho_2^2\right) - \frac{1}{d}\mathrm{Tr}\left(\rho_{12}^2\right)\right]. \tag{24}$$

For the 2D Ising system, the uncertainty equality and inequality are plotted in **Figure 5** under different magnetic fields. For each QRG iteration, the uncertainty first decreases to the minimum of 0.5 and then increases to the maximum of 1.0 with the growth of kt in **Figure 5A**. The change tendency of uncertainty is opposite to that of entanglement in **Figure 4A**, which indicates that quantum entanglement might suppress the uncertainty of the system. As the size of the system becomes larger, the uncertainty minimum occurs at $kt = 1.835\ 4$ near QCP, where the decay from maximum to minimum is very rapid and accompanied by intensive oscillations, which means that this uncertainty can precisely describe the critical behavior of the system due to the

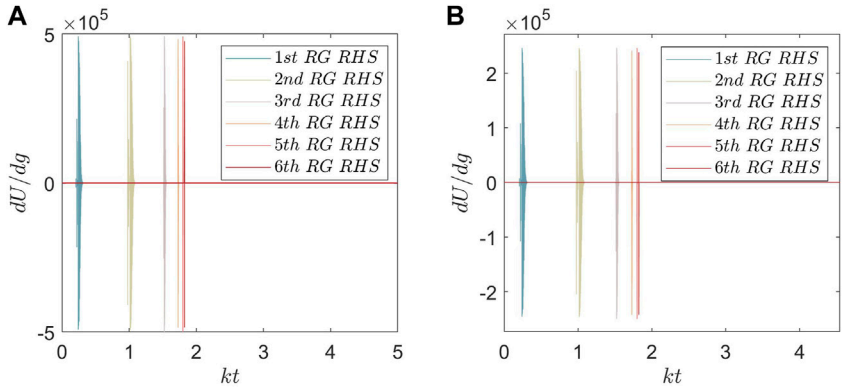

FIGURE 6 | First derivative of the uncertainty equality **(A)** and inequality **(B)** *versus kt* with the increasing number of QRG iterations.

sensitivity of this uncertainty. The uncertainties shown in **Figure 5B** and **Figure 5A** have the similar evolution trend, implying that the uncertainty can characterize the QPT even without choosing the complete set of MUBs.

From **Figure 5C** and **Figure 5D**, we can see that the behaviors of uncertainty against ωt in each half cycle are almost consistent with those against kt in **Figure 5A** and **Figure 5B**, respectively. With the system size increasing, the uncertainty minima appear nearly at $\omega t = \frac{\pi}{4}, \frac{3\pi}{4}, \frac{5\pi}{4}\ldots$, and the corresponding effective magnetic field $h_2 = 1.835\,4$ is the QCP of the 2D model. Thus the application of the periodic magnetic field $B_4(t)$ reveals the close relation between QPT and the effective magnetic field, *i.e.*, QPT depends on the magnetic field strength rather than how the magnetic field evolves.

Through the first derivative of the uncertainty dU/dg, we can analyze its nonanalytic behavior at the QCP. For simplicity, in **Figure 6** we only plot the first derivative of the uncertainty of the 2D Ising model under $B_3(t)$ versus kt, where dU/dg denotes the first derivative of the right hand side of **Eq. 22** and **Eq. 24**. Surprisingly, the extreme values of the first derivative of the uncertainty can reach up to about 10^5 for each iteration, which are almost three order of magnitude larger than those of negativity. This shows that the linear-entropy-based uncertainty relation might be a better indicator of QPT than quantum entanglement. Clearly, we can see from **Figure 6** that dU/dg oscillates at a high frequency between the maximum and the minimum in a very narrow range near the critical point $kt = 1.835\,4$, which can illustrate the rapidly oscillating behavior of the uncertainty in **Figure 5A** and **Figure 5B**. Moreover, with the increase of QRG iterations, the range where the maxima and minima of dU/dg can exist becomes smaller and is approximate to the critical point. Thus, the QPT occurs very fast near the QCP for the large QRG iterations, which can also be exhibited from the rapid variation tendency of the uncertainty with respect to the magnetic field strength. These results indicate that the QRG implementation of uncertainty really captures the QPT behavior of the 2D Ising model.

4 CONCLUSIONS

To summarize, we have analytically derived the effective Hamiltonian and QRG equations by employing the QRG approach. Then the behaviors of the linear-entropy-based uncertainty relation and the quantum entanglement for 2D Ising models with linear and sinusoidal transverse fields are investigated through numerical analysis. Under the linear magnetic field $B_3(t)$, we found that the range where the maxima of entanglement and the minima of the uncertainty can exist becomes smaller and appears near the critical point as the size of the system increases. The entanglement shows an opposite evolution trend to that of the uncertainty. The evolutions of the first derivatives of the uncertainty and the entanglement in terms of QRG iterations indicate a nonanalytic behavior at the QCP. Furthermore, the absolute value of the minimum derivative of negativity against the size of the system exhibits a nice linear relationship. The uncertainty given by **Eqs 22**, **24** and its first derivative are more sensitive to changes of the magnetic field, resulting in oscillations at high frequency and the uncertainty derivative maxima up to 10^5, compared with the negativity derivative maxima ($\sim 10^2$), in the vicinity of QCP. Therefore, the uncertainty may be used as a better indicator to characterize QPT than quantum entanglement. Under the sinusoidal magnetic field $B_4(t)$, the maxima of the entanglement and the minima of the uncertainty appear periodically versus the magnetic field, but as the system size increases, they can still gradually approach the QCP. The strong dependence of QPT on the magnetic field strength is clearly illustrated in the case of the sinusoidal magnetic field.

Our findings might be helpful to use the linear-entropy-based uncertainty relation as the indicator for the detection of the QPT, and to reveal the nature of uncertainty relation and quantum entanglement in the 2D Ising model with time-dependent transverse magnetic fields. We expect our results to be of interest for a wide range of applications in other

meaningful high-dimensional spin models with the QRG method.

DATA AVAILABILITY STATEMENT

The original contributions presented in the study are included in the article/Supplementary Material, further inquiries can be directed to the corresponding authors.

AUTHOR CONTRIBUTIONS

Y-YF and J-ML contributed to conception and design of the study. Y-YF wrote the first draft of the manuscript. T-YJ, X-YX, and J-ML wrote sections of the manuscript. All authors contributed to manuscript revision, read, and approved the submitted version.

FUNDING

This work was supported by the National Natural Science Foundation of China under Grant Nos. 91950112, 11174081, and 11134003, the National Key Research and Development Program of China under Grant Nos. 2016YFB0501601, 2016YFA0302103, and 2017YFF0212003, the Shanghai Municipal Science and Technology Major Project under No. 2019SHZDZX01, and the Shanghai Excellent Academic Leaders Program under No. 12XD1402400.

REFERENCES

1. Einstein A, Podolsky B, Rosen N. Can Quantum-Mechanical Description of Physical Reality Be Considered Complete? *Phys Rev* (1935) 47:777–80. doi:10.1103/physrev.47.777
2. Schrödinger E. Discussion of Probability Relations between Separated Systems. *Math Proc Camb Phil Soc* (1935) 31:555–63. doi:10.1017/s0305004100013554
3. Ekert AK. Quantum Cryptography Based on Bell's Theorem. *Phys Rev Lett* (1991) 67:661–3. doi:10.1103/physrevlett.67.661
4. Bennett CH, Brassard G, Crépeau C, Jozsa R, Peres A, Wootters WK. Teleporting an Unknown Quantum State via Dual Classical and Einstein-Podolsky-Rosen Channels. *Phys Rev Lett* (1993) 70:1895–9. doi:10.1103/physrevlett.70.1895
5. Bennett CH, Wiesner SJ. Communication via One- and Two-Particle Operators on Einstein-Podolsky-Rosen States. *Phys Rev Lett* (1992) 69:2881–4. doi:10.1103/physrevlett.69.2881
6. Scarani V, Iblisdir S, Gisin N, Acín A. Quantum Cloning. *Rev Mod Phys* (2005) 77:1225–56. doi:10.1103/revmodphys.77.1225
7. Życzkowski K, Horodecki P, Sanpera A, Lewenstein M. Volume of the Set of Separable States. *Phys Rev A* (1998) 58:883–92. doi:10.1103/physreva.58.883
8. Vidal G, Werner RF. Computable Measure of Entanglement. *Phys Rev A* (2002) 65:032314. doi:10.1103/physreva.65.032314
9. Sachdev S. Quantum Phase Transitions. *Phys World* (1999) 12:33–8. doi:10.1088/2058-7058/12/4/23
10. Osterloh A, Amico L, Falci G, Fazio R. Scaling of Entanglement Close to a Quantum Phase Transition. *Nature* (2002) 416:608–10. doi:10.1038/416608a
11. Wu L-A, Sarandy MS, Lidar DA. Quantum Phase Transitions and Bipartite Entanglement. *Phys Rev Lett* (2004) 93:250404. doi:10.1103/physrevlett.93.250404
12. Latorre JI, Lütken CA, Rico E, Vidal G. Entanglement Entropy in the Lipkin-Meshkov-Glick Model. *Phys Rev A* (2005) 71:034301. doi:10.1103/physreva.71.064101
13. Gu S-J, Deng S-S, Li Y-Q, Lin H-Q. Entanglement and Quantum Phase Transition in the Extended Hubbard Model. *Phys Rev Lett* (2004) 93:086402. doi:10.1103/physrevlett.93.086402
14. Anfossi A, Giorda P, Montorsi A. Entanglement in Extended Hubbard Models and Quantum Phase Transitions. *Phys Rev B* (2007) 75:165106. doi:10.1103/physrevb.75.165106
15. Ren J, You W-L, Wang X. Entanglement and Correlations in a One-Dimensional Quantum Spin-1/2 Chain with Anisotropic Power-Law Long-Range Interactions. *Phys Rev B* (2020) 101:094410. doi:10.1103/physrevb.101.094410
16. Vidal J, Palacios G, Mosseri R. Entanglement in a Second-Order Quantum Phase Transition. *Phys Rev A* (2004) 69:022107. doi:10.1103/physreva.69.022107
17. Verstraete F, Popp M, Cirac JI. Entanglement versus Correlations in Spin Systems. *Phys Rev Lett* (2004) 92:027901. doi:10.1103/physrevlett.92.027901
18. Biswas G, Biswas A. Entanglement in First Excited States of Some many-body Quantum Spin Systems: Indication of Quantum Phase Transition in Finite Size Systems. *Phys Scr* (2020) 96:025003. doi:10.1088/1402-4896/abce33
19. Souza F, Veríssimo LM, Strečka J, Lyra ML, Pereira MS. Interplay between Charge and Spin thermal Entanglement in Hubbard Dimers. *Phys Rev B* (2020) 102:064414. doi:10.1103/physreva.102.032421
20. Ma F-W, Liu S-X, Kong X-M. Entanglement and Quantum Phase Transition in the One-Dimensional Anisotropic XY Model. *Phys Rev A* (2011) 83:062309. doi:10.1103/physreva.83.062309
21. Amico L, Fazio R, Osterloh A, Vedral V. Entanglement in many-body Systems. *Rev Mod Phys* (2008) 80:517–76. doi:10.1103/revmodphys.80.517
22. Wu X, Ivanchenko MV, Jandal HA, Cicconet M, Indzhykulian AA, Corey DP. PKHD1L1 Is a Coat Protein of Hair-Cell Stereocilia and Is Required for normal Hearing. *Nat Commun* (2019) 10:3801. doi:10.1038/s41467-019-11712-w
23. Taylor SR, Scardicchio A. Subdiffusion in a One-Dimensional Anderson Insulator with Random Dephasing: Finite-Size Scaling, Griffiths Effects, and Possible Implications for many-body Localization. *Phys Rev B* (2021) 103:184202. doi:10.1103/physrevb.103.184202
24. Tutsch U, Tsyplyatyev O, Kuhnt M, Postulka L, Wolf B, Cong PT, et al. Specific Heat Study of 1D and 2D Excitations in the Layered Frustrated Quantum Antiferromagnets Cs_2CuCl_{4-x} Br_x. *Phys Rev Lett* (2019) 123:147202. doi:10.1103/PhysRevLett.123.147202
25. Liu Y, Ma Y. One-Dimensional Plasmonic Sensors. *Front Phys* (2020) 8:260. doi:10.3389/fphy.2020.00312
26. Coulamy IB, Warnes JH, Sarandy MS, Saguia A. Scaling of the Local Quantum Uncertainty at Quantum Phase Transitions. *Phys Lett A* (2016) 380:1724–8. doi:10.1016/j.physleta.2016.03.026
27. Liu C-C, Ye L. Probing Quantum Coherence, Uncertainty, Steerability of Quantum Coherence and Quantum Phase Transition in the Spin Model. *Quan Inf. Process* (2017) 16:138. doi:10.1007/s11128-017-1588-9
28. Xiong S-J, Sun Z, Liu J-M. Entropic Uncertainty Relation and Quantum Phase Transition in Spin-1/2 Heisenberg Chain. *Laser Phys Lett* (2020) 17:095203. doi:10.1088/1612-202x/aba2ef
29. Karpat G, Çakmak B, Fanchini FF. Quantum Coherence and Uncertainty in the Anisotropic XY Chain. *Phys Rev B* (2014) 90:104431. doi:10.1103/physrevb.90.104431
30. Robertson HP. The Uncertainty Principle. *Phys Rev* (1929) 34:163–4. doi:10.1103/physrev.34.163
31. Maccone L, Pati AK. Stronger Uncertainty Relations for All Incompatible Observables. *Phys Rev Lett* (2014) 113:260401. doi:10.1103/physrevlett.113.260401
32. Busch P, Lahti P, Werner RF. Colloquium: Quantum Root-Mean-Square Error and Measurement Uncertainty Relations. *Rev Mod Phys* (2014) 86:1261–81. doi:10.1103/revmodphys.86.1261
33. Fan X-Y, Shang W-M, Zhou J, Meng H-X, Chen J-L. Studying Heisenberg-like Uncertainty Relation with Weak Values in One-Dimensional Harmonic Oscillator. *Front Phys* (2022) 9:803494. doi:10.3389/fphy.2021.803494
34. Heisenberg W. Über den anschaulichen Inhalt der quantentheoretischen Kinematik und Mechanik. In: *Original Scientific Papers Wissenschaftliche Originalarbeiten*. Springer: Springer (1985). p. 478–504. doi:10.1007/978-3-642-61659-4_30

35. Maassen H, Uffink JBM. Generalized Entropic Uncertainty Relations. *Phys Rev Lett* (1988) 60:1103–6. doi:10.1103/physrevlett.60.1103
36. Horodecki R, Horodecki P, Horodecki M, Horodecki K. Quantum Entanglement. *Rev Mod Phys* (2009) 81:865–942. doi:10.1103/revmodphys.81.865
37. Berta M, Christandl M, Colbeck R, Renes JM, Renner R. The Uncertainty Principle in the Presence of Quantum Memory. *Nat Phys* (2010) 6:659–62. doi:10.1038/nphys1734
38. Wang D, Ming F, Hu ML, Ye L. Quantum-Memory-Assisted Entropic Uncertainty Relations. *Annalen Der Physik* (2019) 531:1900124. doi:10.1002/andp.201900124
39. Tomamichel M, Lim CCW, Gisin N, Renner R. Tight Finite-Key Analysis for Quantum Cryptography. *Nat Commun* (2012) 3:1. doi:10.1038/ncomms1631
40. Gehring T, Händchen V, Duhme J, Furrer F, Franz T, Pacher C, et al. Implementation of Continuous-Variable Quantum Key Distribution with Composable and One-sided-device-independent Security against Coherent Attacks. *Nat Commun* (2015) 6:1. doi:10.1038/ncomms9795
41. Wang H, Ma Z, Wu S, Zheng W, Cao Z, Chen Z, et al. Uncertainty equality with Quantum Memory and its Experimental Verification. *Npj Quan Inf* (2019) 5:1. doi:10.1038/s41534-019-0153-z
42. Wootters WK, Fields BD. Optimal State-Determination by Mutually Unbiased Measurements. *Ann Phys* (1989) 191:363–81. doi:10.1016/0003-4916(89)90322-9
43. Yuan H, Zhou Z-W, Guo G-C. Quantum State Tomography via Mutually Unbiased Measurements in Driven Cavity QED Systems. *New J Phys* (2016) 18:043013. doi:10.1088/1367-2630/18/4/043013
44. Ding Z-Y, Yang H, Yuan H, Wang D, Yang J, Ye L. Experimental Investigation of Entropic Uncertainty Relations and Coherence Uncertainty Relations. *Phys Rev A* (2020) 101:022116. doi:10.1103/physreva.101.032101
45. Fisher ME. Renormalization Group Theory: Its Basis and Formulation in Statistical Physics. *Rev Mod Phys* (1998) 70:653–81. doi:10.1103/revmodphys.70.653
46. Langari A. Quantum Renormalization Group ofXYZmodel in a Transverse Magnetic Field. *Phys Rev B* (2004) 69:100402. doi:10.1103/physrevb.69.100402
47. Balazadeh L, Najarbashi G, Tavana A. Quantum Renormalization of L1-Norm and Relative Entropy of Coherence in Quantum Spin Chains Share on. *Quan Inf. Process.* (2020) 19:1. doi:10.1007/s11128-020-02677-7
48. Sadiek G, Xu Q, Kais S. Tuning Entanglement and Ergodicity in Two-Dimensional Spin Systems Using Impurities and Anisotropy. *Phys Rev A* (2012) 85:042313. doi:10.1103/physreva.85.042313
49. Kallin AB, Hyatt K, Singh RRP, Melko RG. Entanglement at a Two-Dimensional Quantum Critical Point: A Numerical Linked-Cluster Expansion Study. *Phys Rev Lett* (2013) 110:135702. doi:10.1103/physrevlett.110.135702
50. Ju H, Kallin AB, Fendley P, Hastings MB, Melko RG. Entanglement Scaling in Two-Dimensional Gapless Systems. *Phys Rev B* (2012) 85:165121. doi:10.1103/physrevb.85.165121
51. Gao K, Xu Y-L, Kong X-M, Liu Z-Q. Thermal Quantum Correlations and Quantum Phase Transitions in Ising-XXZ diamond Chain. *Physica A: Stat Mech its Appl* (2015) 429:10–6. doi:10.1016/j.physa.2015.02.007
52. Xu Y-L, Kong X-M, Liu Z-Q, Wang C-Y. Quantum Entanglement and Quantum Phase Transition for the Ising Model on a Two-Dimension Square Lattice. *Physica A: Stat Mech its Appl* (2016) 446:217–23. doi:10.1016/j.physa.2015.12.002
53. Ambjorn J, Gizbert-Studnicki J, Görlich A, Jurkiewicz J, Loll R. Renormalization in Quantum Theories of Geometry. *Front Phys* (2020) 8:247. doi:10.3389/fphy.2020.00247
54. Kato T. On the Adiabatic Theorem of Quantum Mechanics. *J Phys Soc Jpn* (1950) 5:435–9. doi:10.1143/jpsj.5.435
55. Wilczek F, Zee A. Appearance of Gauge Structure in Simple Dynamical Systems. *Phys Rev Lett* (1984) 52:2111–4. doi:10.1103/physrevlett.52.2111
56. Sun C-P, Ge M-L. Generalizing Born-Oppenheimer Approximations and Observable Effects of an Induced Gauge Field. *Phys Rev D* (1990) 41:1349–52. doi:10.1103/physrevd.41.1349
57. Kubica A, Yoshida B. Precise Estimation of Critical Exponents from Real-Space Renormalization Group Analysis. preprint arXiv:1402.0619. https://arxiv.53yu.com/abs/1402.0619 (2014).
58. Osborne TJ, Nielsen MA. Entanglement in a Simple Quantum Phase Transition. *Phys Rev A* (2002) 66:032110. doi:10.1103/physreva.66.032110

Conflict of Interest: The authors declare that the research was conducted in the absence of any commercial or financial relationships that could be construed as a potential conflict of interest.

Publisher's Note: All claims expressed in this article are solely those of the authors and do not necessarily represent those of their affiliated organizations, or those of the publisher, the editors and the reviewers. Any product that may be evaluated in this article, or claim that may be made by its manufacturer, is not guaranteed or endorsed by the publisher.

frontiers | Frontiers in Physics

ORIGINAL RESEARCH
published: 01 April 2022
doi: 10.3389/fphy.2022.846330

Near-Optimal Variance-Based Uncertainty Relations

Yunlong Xiao[1,2], *Naihuan Jing*[3,4]*, *Bing Yu*[5], *Shao-Ming Fei*[6,2] *and Xianqing Li-Jost*[2]

[1]Nanyang Quantum Hub, School of Physical and Mathematical Sciences, Nanyang Technological University, Singapore, Singapore, [2]Max Planck Institute for Mathematics in the Sciences, Leipzig, Germany, [3]Department of Mathematics, North Carolina State University, Raleigh, NC, United States, [4]School of Mathematics, South China University of Technology, Guangzhou, China, [5]School of Mathematics and Systems Science, Guangdong Polytechnic Normal University, Guangzhou, China, [6]School of Mathematical Sciences, Capital Normal University, Beijing, China

Learning physical properties of a quantum system is essential for the developments of quantum technologies. However, Heisenberg's uncertainty principle constrains the potential knowledge one can simultaneously have about a system in quantum theory. Aside from its fundamental significance, the mathematical characterization of this restriction, known as 'uncertainty relation', plays important roles in a wide range of applications, stimulating the formation of tighter uncertainty relations. In this work, we investigate the fundamental limitations of variance-based uncertainty relations, and introduce several 'near optimal' bounds for incompatible observables. Our results consist of two morphologically distinct phases: lower bounds that illustrate the uncertainties about measurement outcomes, and the upper bound that indicates the potential knowledge we can gain. Combining them together leads to an *uncertainty interval*, which captures the essence of uncertainties in quantum theory. Finally, we have detailed how to formulate lower bounds for product-form variance-based uncertainty relations by employing entropic uncertainty relations, and hence built a link between different forms of uncertainty relations.

Keywords: numbers: 03.65.ta, 03.67.a, 42.50.lc, uncertainty relation, variance-based, uncertainty interval

OPEN ACCESS

Edited by:
Dong Wang,
Anhui University, China

Reviewed by:
Zheng-Yuan Xue,
South China Normal University, China
Yu Guo,
Shanxi Datong University, China
Jun Zhang,
Taiyuan University of Technology, China

***Correspondence:**
Naihuan Jing
jing@ncsu.edu

Specialty section:
This article was submitted to Quantum Engineering and Technology, a section of the journal Frontiers in Physics

Received: *31 December 2021*
Accepted: *02 March 2022*
Published: *01 April 2022*

Citation:
Xiao Y, Jing N, Yu B, Fei S-M and Li-Jost X (2022) Near-Optimal Variance-Based Uncertainty Relations. Front. Phys. 10:846330. doi: 10.3389/fphy.2022.846330

1 INTRODUCTION

Uncertainty principle, originally introduced by Heisenberg [1], clearly sets quantum theory apart from our classical world. Formally, it states that it is impossible to predict the outcomes of incompatible measurements simultaneously, such as the position and momentum of a particle. The corresponding mathematical formulation for position and momentum are given by Kennard in Ref. [2] (see also Ref. [3]). Later, a general form of uncertainty relation has been established by Robertson [4], and has been further improved by Schrödinger in Ref. [5], which is expressed in terms of commutator and anticommutator of obserables:

$$V(A)V(B) \geq |\frac{1}{2}\langle [A,B]\rangle|^2 + |\frac{1}{2}\langle \{\bar{A},\bar{B}\}\rangle|^2, \tag{1}$$

where the quantity $V(A) = \langle \bar{A}^2 \rangle$ (resp. $V(B)$) stands for the variance of observable A (resp. B), the operator $\bar{A}$ is defined as $A - \langle A \rangle$, and the expectation value $\langle\ \rangle$ is over the quantum state $|\Psi\rangle$. Another way to demonstrate the joint uncertainty associated with incompatible observables is through the summation, namely $V(A) + V(B)$ [6–9], which highlights an advantage in the parameter estimation of quantum system [10–13].

Riding the waves of information theory, entropies have been used to quantify the uncertainties associated with quantum measurements [14]. For instance, the entropies of probability distributions of

canonically conjugate variables obey Białynicki-Birula-Mycielski uncertainty relation [15]. It is noteworthy that Heisenberg's uncertainty relation follows from Ref. [15] as a special case. The entropic uncertainty relation for any pair of bounded observables is established by Deutsch in Ref. [16]. An improved expression was subsequently conjectured by Kraus [17] and then had been proved by Maassen and Uffink [18]. With access to a memory system, the conventional entropic uncertainty relations have been further generalized to entanglement-assisted formalism [19]. Soon afterwards, several improvements and extensions, including the cases of multiple measurements, universal uncertainty regions and quantum processes, have been proposed in Refs. [20–25]. Recently, beyond inertial frames, the uncertainty trade-off occurred near the event horizon of a Schwarzschild black hole [26] and the relativistic protocol of an uncertainty game in the presence of localized fermionic quantum fields inside cavities [27] have also been demonstrated.

Aside from their theoretical significance [28], these uncertainty relations support a variety of applications and have been widely used in current quantum technologies, such as analyzing the security of quantum key distribution protocols [19], witnessing quantum correlations [29–32], and even inferring causality from quantum dynamics [33]. Thus, pushing the boundary of uncertainty relation will not only deepen our understanding of quantum foundations, but also has impact on practical applications.

In this work, we focus on the case of variance-based uncertainty relations, with the forms of both product and summation, and introduce the concept of uncertainty interval. The formulation of such an interval can of course be subdivided into two, namely finding the lower bound and upper bounds for joint uncertainties. To do so, we establish the *partial Cauchy-Schwarz inequality*, which generalizes the standard Cauchy-Schwarz inequality, and use this toolkit to construct near-optimal bounds for variance-based uncertainty relations. Numerical results highlight the advantages of our framework.

2 PRODUCT-FORM VARIANCE-BASED UNCERTAINTY RELATIONS

Throughout this paper, we consider quantum systems acting on finite-dimensional Hilbert space. Let us start with a pair of incompatible observables A and B, and denote their spectral decompositions as $A = \sum_i a_i|a_i\rangle\langle a_i|$ and $B = \sum_i b_i|b_i\rangle\langle b_i|$ respectively. On the other hand, assume the alternative observable $\bar{A}$ and $\bar{B}$ have the following spectral decompositions; that are $\bar{A} = \sum_i a_i'|a_i\rangle\langle a_i|$ and $\bar{B} = \sum_i b_i'|b_i\rangle\langle b_i|$. Remark that, here all the eigenvalues are real numbers, i.e. $a_i, a_i', b_i, b_i' \in \mathbb{R}$. Now for any given orthonormal basis $\{|\psi_i\rangle\}$, we can re-express $\bar{A}|\Psi\rangle$ and $\bar{B}|\Psi\rangle$ as $\sum_i \alpha_i|\psi_i\rangle$ and $\sum_i \beta_i|\psi_i\rangle$ respectively. It is worth mentioning that in general both $\bar{A}|\Psi\rangle$ and $\bar{B}|\Psi\rangle$ are unnormalized, and hence the vectors (α_i) and (β_i) do not forms probability distributions. Then, by defining the absolute value of α_i and β_i as x_i and y_i respectively, the variance of observables A and B can be rewritten as

$$V(A) = |\vec{x}|^2, \quad V(B) = |\vec{y}|^2, \tag{2}$$

and thus we have

$$V(A)V(B) = |\vec{x}|^2 \cdot |\vec{y}|^2. \tag{3}$$

It now follows from Cauchy-Schwarz inequality immediately that

$$V(A)V(B) \geq \left(\sum_i x_i y_i\right)^2. \tag{4}$$

We note that such a choice of x_i and y_i leads directly to the main results presented in a recent formulation of strong uncertainty relation [34]. Clearly, this is not the only choice of x_i and y_i. By setting x_i as $|a_i'|\sqrt{\langle\Psi|a_i\rangle\langle a_i|\Psi\rangle}$ and y_i as $|b_i'|\sqrt{\langle\Psi|b_i\rangle\langle b_i|\Psi\rangle}$, we re-obtain another part of results constructed in Ref. [34]. Here, for simplicity, we further denote the Uhlmann's fidelity between $|\Psi\rangle$ and $|a_i\rangle$ ($|b_i\rangle$) as F_i^a (F_i^b), which are

$$F_i^a = \langle\Psi|a_i\rangle\langle a_i|\Psi\rangle, \quad F_i^b = \langle\Psi|b_i\rangle\langle b_i|\Psi\rangle. \tag{5}$$

A key observation in this work is that any improvement over the well-known Cauchy-Schwarz inequality will give us a better bound of variance-based uncertainty relation, with the same amount of information required in **Eq. (4)**. To this end, we investigate the intrinsic connection between the arithmetic-geometric mean (AM-GM) inequality and the Cauchy-Schwarz inequality. We start by writing down the product of $|\vec{\alpha}|^2$ and $|\vec{\beta}|^2$,

$$\begin{aligned} |\vec{\alpha}|^2|\vec{\beta}|^2 = \sum_{ij} x_i^2 y_j^2 &= \sum_{i<j}\left(x_i^2 y_j^2 + x_j^2 y_i^2\right) + \sum_i x_i^2 y_i^2 \\ &\geq \sum_{i<j}\left(2x_i x_j y_j y_i\right) + \sum_i x_i^2 y_i^2 \\ &= \left(\sum_i x_i y_i\right)^2. \end{aligned} \tag{6}$$

Above inequality is a result of $n(n-1)/2$ rounds of AM-GM inequalities for $x_i^2 y_j^2 + x_j^2 y_i^2 \geq 2x_i y_j x_j y_i$ with different indexes. Therefore, the equality condition holds if and only if $x_i y_j = x_j y_i$ for all $i \neq j$. By defining the quantity I_k as

$$\sum_{1\leq i<j\leq k}\left(2x_i x_j y_j y_i\right) + \sum_{\substack{1\leq i<j\leq n \\ k<j}}\left(x_i^2 y_j^2 + x_j^2 y_i^2\right) + \sum_{1\leq i\leq n} x_i^2 y_i^2, \tag{7}$$

we can write the left-hand-side of **Eq. 4** as

$$I_0 = |\vec{x}|^2|\vec{y}|^2 = V(A)V(B), \tag{8}$$

which is precisely the product-form joint uncertainty. On the other hand, the previous known bound in Ref. [34], i.e. right-hand-side quantity of **Eq. 4**, can be reformatted as

$$I_n = \left(\sum_i x_i y_i\right)^2. \tag{9}$$

Now we introduce a chain of inequalities that outperform Cauchy-Schwarz inequality. More precisely, we have.

Theorem 1. *For any n-dimensional real vectors $\vec{x}$, $\vec{y}$ with non-negative components, and I_k defined in* **Eq. 7**, *we have*

$$I_0 \geq I_2 \geq \ldots, \geq I_{n-1} \geq I_n. \tag{10}$$

Actually, for any index k it follow from the AM-GM inequality that

$$I_{k+1} = I_k + \sum_{i=1}^{k} \left(2x_i x_{k+1} y_i y_{k+1} - x_i^2 y_{k+1}^2 - x_{k+1}^2 y_i^2\right) \leq I_k, \tag{11}$$

as required. Algebraically, the inequality $|\vec{x}|^2|\vec{y}|^2 \geq I_k$ is obtained by applying AM-GM inequality to the first k components of both $\vec{x}$ and $\vec{y}$, and hence can be viewed as a partial Cauchy-Schwarz inequality. More importantly, such a partial Cauchy-Schwarz inequality, see **Eq. 10**, provides $n-2$ tighter lower bounds for $V(A)V(B)$ compared with the main result of [34], namely $I_0 = V(A)V(B) \geq I_n$. In particular, we can insert more terms in the above descending chain by selecting arbitrary $x_i^2 y_j^2 + x_j^2 y_i^2$ $(i < j)$. For example, the inequality $I_0 \geq I_{n-1}$ obtained from our Thm. One immediately leads to a tighter bound. More precisely, **Eq. 4** can be improved to

$$\begin{aligned} V(A)V(B) \geq \frac{1}{4}\Bigg(\sum_{i=1}^{n-1}\left|\langle[\bar{A},\bar{B}_n]\rangle + \langle\{\bar{A},\bar{B}_n\}\rangle\right| \Bigg)^2 \\ + \left|\langle\Psi|\bar{A}|\psi_n\rangle\right|^2\left(\sum_{i=1}^{n}\left|\langle\Psi|\bar{B}|\psi_n\rangle\right|^2\right) \\ + \left|\langle\Psi|\bar{B}|\psi_n\rangle\right|^2\left(\sum_{i=1}^{n}\left|\langle\Psi|\bar{A}|\psi_n\rangle\right|^2\right) \\ - \left|\langle\Psi|\bar{A}|\psi_n\rangle\right|^2\left|\langle\Psi|\bar{B}|\psi_n\rangle\right|^2 \coloneqq \mathcal{L}_1, \end{aligned} \tag{12}$$

which offers a stronger bound than that of

$$\mathcal{L}_1 \geq \frac{1}{4}\Bigg(\sum_{i=1}^{n}\left|\langle[\bar{A},\bar{B}_n]\rangle + \langle\{\bar{A},\bar{B}_n\}\rangle\right| \Bigg)^2 \geq \left|\langle\bar{A}\bar{B}\rangle\right|^2. \tag{13}$$

Note that the method of constructing bounds presented here for variance-based uncertainty relations requires the same amount of information, i.e. the fidelity between quantum state and the eigenvector of observables, needed in previous works, such as the one considered in Ref. [34], but provable tighter.

We now move on to further strengthening the bounds of uncertainty relations by considering the action of symmetric group $\mathfrak{S}_n$. For any two permutations $\pi_1, \pi_2 \in \mathfrak{S}_n$, we define

$$\begin{aligned} (\pi_1,\pi_2)I_k = \sum_{1\leq\pi_1(i)<\pi_2(j)\leq k}\left(2x_{\pi_1(i)}x_{\pi_2(j)}y_{\pi_2(j)}y_{\pi_1(i)}\right) \\ + \sum_{\substack{1\leq\pi_1(i)<\pi_2(j)\leq n \\ k<\pi_2(j)}}\left(x_{\pi_1(i)}^2 y_{\pi_2(j)}^2 + x_{\pi_2(j)}^2 y_{\pi_1(i)}^2\right) \\ + \sum_{\pi_1(i)=\pi_2(j)} x_{\pi_1(i)}^2 y_{\pi_2(j)}^2. \end{aligned} \tag{14}$$

It is straightforward to check that the quantity I_0 is stable under the action of $\mathfrak{S}_n \times \mathfrak{S}_n$. Writing everything out explicitly, we have.

Theorem 2. *For any permutations $\pi_1, \pi_2 \in \mathfrak{S}_n$, we have*

$$I_0 \geq (\pi_1,\pi_2)I_2 \geq \ldots, \geq (\pi_1,\pi_2)I_{n-1} \geq (\pi_1,\pi_2)I_n. \tag{15}$$

Optimizing over the symmetric group $\mathfrak{S}_n$, a stronger version of the variance-based uncertainty relations is obtained.

Theorem 3. *For any permutations $\pi_1, \pi_2 \in \mathfrak{S}_n$, we have*

$$I_0 \geq \max_{\pi_1,\pi_2\in\mathfrak{S}_n}(\pi_1,\pi_2)I_2 \geq \ldots, \geq \max_{\pi_1,\pi_2\in\mathfrak{S}_n}(\pi_1,\pi_2)I_n. \tag{16}$$

Mathematically, above inequalities are tighter than the result in Thm. 1, since $\max_{\pi_1,\pi_2\in\mathfrak{S}_n}(\pi_1,\pi_2)I_k \geq I_k$ holds for any permutations. Physically, the action of symmetric group works well since the overlaps between quantum state and the eigenvectors of observables are not uniformly distributed.

3 SUM-FORM VARIANCE-BASED UNCERTAINTY RELATIONS

In this section we turn our attention to the sum-form variance-based uncertainty relations. Before doing so, let us recall the *rearrangement inequality* first. Let (x_i) and (y_i) be two n-tuple of real positive numbers arranged in non-increasing order, namely $x_i \geq x_{i+1}$ and $y_i \geq y_{i+1}$, with their *direct sum*, *random sum* and *reverse sum* between x_i and y_i being defined as

$$\begin{aligned} Di &\coloneqq x_1y_1 + x_2y_2 + \cdots + x_ny_n, \\ Ra &\coloneqq x_1y_{\pi(1)} + x_2y_{\pi(2)} + \cdots + x_ny_{\pi(n)}, \quad \pi \in \mathfrak{S}_n \\ Re &\coloneqq x_1y_n + x_2y_{n-1} + \cdots + x_ny_1. \end{aligned} \tag{17}$$

Then the following lemma characterizes the relationship among these quantities; that is.

Lemma. (Rearrangement inequality) *For any two non-increasing n-tuples x and y of nonnegative numbers, we have*

$$Di \geq Ra \geq \mathrm{Re}. \tag{18}$$

From the parallelogram law, the summation of variances can be re-expressed as

$$V(A) + V(B) = \frac{1}{2}\sum_i \left(x_i + y_i\right)^2 + \frac{1}{2}\sum_i \left(x_i - y_i\right)^2. \tag{19}$$

Combining with the rearrangement inequality we obtain the following result.

Theorem 4. *For any two permutations $\pi_1, \pi_2 \in \mathfrak{S}_n$, we have*

$$\begin{aligned} V(A) + V(B) \geq \frac{1}{2}\sum_i \left(x_i + y_i\right)\left(x_{\pi_1(i)} + y_{\pi_1(i)}\right) \\ + \frac{1}{2}\sum_i \left|x_i - y_i\right|\left|x_{\pi_2(i)} - y_{\pi_2(i)}\right|. \end{aligned} \tag{20}$$

Remark that, by setting $\pi_1 = (1)$, our newly constructed uncertainty relation outperforms similar results of sum-form variance-based uncertainty relation considered in Ref. [34]. We denote by $\mathcal{L}_2$ the bound of Thm. Four corresponding to the choice of $\pi_1 = (1)$, $\pi_2 = (1\ 2\ \ldots\ n)$, $x_i = |\alpha_i|$, $y_i = |\beta_i|$, which will be used in Sec. V.

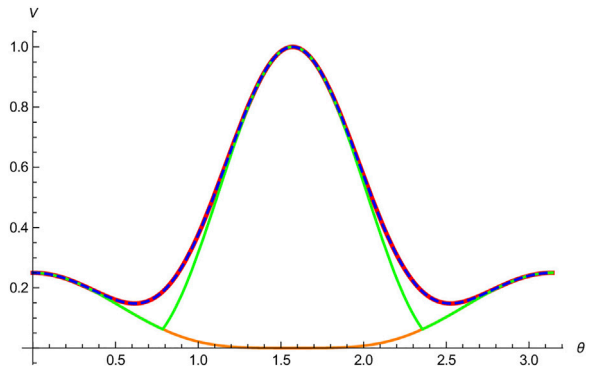

FIGURE 1 | Lower bounds of $V(A)V(B)$ for a family of spin-1 particles $|\Psi(\theta)\rangle$: the product-form uncertainty relation $V(A)V(B)$, the bound $\mathcal{L}_1$ of **Eq. 12**, the bound of Ref. [34], and the bound of Schrödinger uncertainty relation [5] are depicted in red, blue, green, and orange respectively.

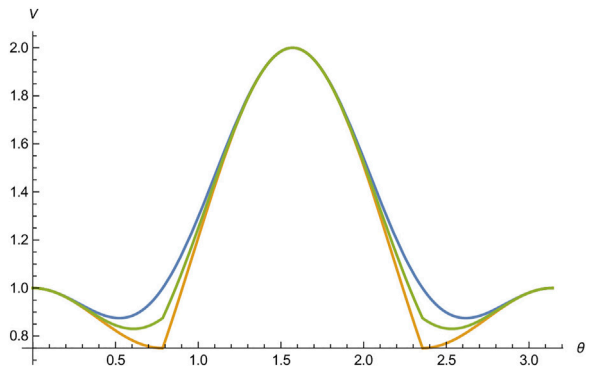

FIGURE 2 | Lower bounds of $V(A) + V(B)$ for a family of spin-1 particles $|\Psi(\theta)\rangle$: the sum-form uncertainty relation $V(A) + V(B)$, our bound $\mathcal{L}_2$ of **Eq. 20**, and the bound of Ref. [34] are depicted in blue, green, and yellow respectively.

4 UNCERTAINTY INTERVALS

Quantum theory does not only impose restrictions on the lower bounds of uncertainties, but also sets limitations on the upper bounds of uncertainties [34], which are known as reverse uncertainty relations in the literature. In this section, we investigate the reverse uncertainty relations for both the product-form and sum-form uncertainty relations, and introduce several tighter bounds. Consequently, our lower bounds presented in previous sections together with the results obtained in this section lead to intervals for joint uncertainty, which are referred as uncertainty intervals.

For index $1 \le i \le n$, we define

$$\begin{aligned} X &= \max_i\{x_i\}, \quad x = \min_i\{x_i\}, \\ Y &= \max_i\{y_i\}, \quad y = \min_i\{y_i\}. \end{aligned} \tag{21}$$

Using the rearrangement inequality, we thus see that

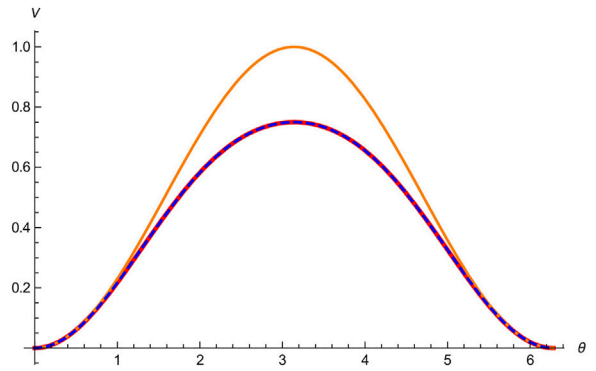

FIGURE 3 | Upper bounds of $V(A)V(B)$ for a family of spin-1/2 particles $\rho(\theta)$: the product-form uncertainty relation $V(A)V(B)$, our bound $\mathcal{U}_1$ of **Eq. 23**, and the bound of Ref. [34] are depicted in red, blue, and orange respectively.

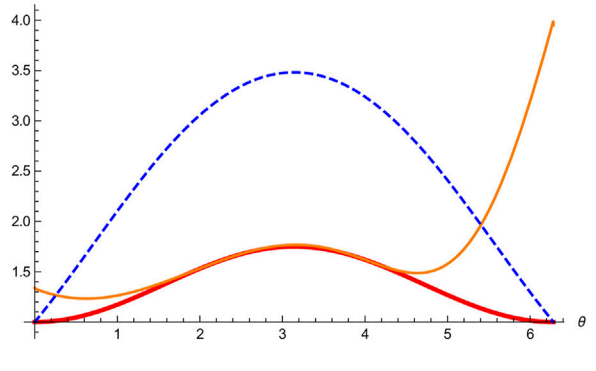

FIGURE 4 | Upper bounds of $V(A) + V(B)$ for a family of spin-1/2 particles $\rho(\theta)$: the sum-form uncertainty relation $V(A)V(B)$, our bound $\mathcal{U}_2$ of **Eq. 25**, and the bound of Ref. [34] are depicted in red, blue, and orange respectively.

$$\begin{aligned} \frac{(xy+XY)^2}{4xyXY}\left(\sum_i x_i y_i\right)^2 &\ge \frac{(xy+XY)^2}{4xyXY}\left(\sum_i x_i y_{\pi(i)}\right)^2 \\ &\ge V(A)V(B). \end{aligned} \tag{22}$$

By taking minimum over all permutations $\pi \in \mathfrak{S}_n$, we obtain a tighter upper bound for $V(A)V(B)$:

$$V(A)V(B) \le \min_{\pi\in\mathcal{S}_n} \frac{(xy+XY)^2}{4xyXY}\left(\sum_i x_i y_{\pi(i)}\right)^2 := \mathcal{U}_1, \tag{23}$$

which proves that the joint uncertainty of incompatible observables A and B (for the product-form) is restricted within the interval $[\mathcal{L}_1, \mathcal{U}_1]$, i.e. $V(A)V(B) \in [\mathcal{L}_1, \mathcal{U}_1]$. In other words, $[\mathcal{L}_1, \mathcal{U}_1]$ is an *uncertainty interval* for $V(A)V(B)$.

On the other hand, using the fact $V(A) = |\vec{\alpha}|^2$ and $V(B) = |\vec{\beta}|^2$, one derive an upper bound on the sum of variances of incompatible observables A and B as

$$V(A)+V(B)=\sum_i\left(x_i^2+y_i^2\right)\leq\sum_i\left(x_i+y_i\right)^2. \tag{24}$$

Recalling the definitions $x_i=|\alpha_i|$ and $y_i=|\beta_i|$, we have that

$$V(A)+V(B)\leq\sum_i\left(\left|\langle\psi_n|\bar{A}|\Psi\rangle\right|+\left|\langle\psi_n|\bar{B}|\Psi\rangle\right|\right)^2. \tag{25}$$

Denote the right-hand (RHS) of **(25)** by $\mathcal{U}_2$. Thus we have obtained a uncertainty interval for $V(A)+V(B)$: $[\mathcal{L}_2,\mathcal{U}_2]$. We remark that $\mathcal{U}_2$ is not always better than the bound obtained by [34], but it provides a complementary one. The comparison will be discussed by examples in the next section.

5 NUMERICAL EXAMPLES AND CONCLUSION

In this section we provide numerical examples to show how the bounds obtained in this work outperform previous strong results [34]. First of all, let us consider the spin-1 particle with the state $|\Psi(\theta)\rangle=\cos\theta|1\rangle-\sin\theta|0\rangle$, where the state $|0\rangle$ and $|1\rangle$ are eigenstates of the angular momentum L_z. We investigate the uncertainty associated with angular momentum operators for spin-1 particle, namely $A=L_x$ and $B=L_y$. To formulate bounds for uncertainty relations, we choose $x_i=|\alpha_i|$ and $y_i=|\beta_i|$ (similar for $x_i=|a_i'|\sqrt{\langle\Psi(\theta)|a_i\rangle\langle a_i|\Psi(\theta)\rangle}$ and $y_i=|b_i'|\sqrt{\langle\Psi(\theta)|b_i\rangle\langle b_i|\Psi(\theta)\rangle}$).

In **Figure 1**, our bound $\mathcal{L}_1$ has been compared with that of [34] in the product-form for the family of spin-1 particles $|\Psi(\theta)\rangle$. As shown in our numerical results, the bound $\mathcal{L}_1$ (in blue) provides the best estimation and is almost optimal. As a supplement, we also compare our result with Schrödinger's uncertainty relation (in orange). In **Figure 2**, we plot lower bounds for the sum-form variance-based uncertainty relation for the family of the spin-1 particles $|\Psi(\theta)\rangle$, which highlights the advantage of our method.

Let us move on to considering the spin-$\frac{1}{2}$ particle with the following density matrix

$$\rho(\theta)=\frac{1}{2}\left(Id+\cos\frac{\theta}{2}\sigma_x+\frac{\sqrt{3}}{2}\sin\frac{\theta}{2}\sigma_y+\frac{1}{2}\sin\frac{\theta}{2}\sigma_z\right), \tag{26}$$

where the two incompatible observables are taken as $A=\sigma_x$ and $B=\sigma_z$. In **Figure 3**, it has been shown that our upper bound $\mathcal{U}_1$ provides the best estimation for the product of two variances and typically outperforms the upper bound from Ref. [34]. Note that our bound is almost optimal, as it is almost identical to the optimal value. However, our upper bound $\mathcal{U}_2$ for the sum of variances $V(A)+V(B)$ for states $\rho(\theta)$ is not always tighter than that of Ref. [34]. Nevertheless, it still provides an improvements for most of the time. See **Figure 4** for an illustration.

Apart from constructing stronger uncertainty relations, our method introduced in Sec. II also helps to fill up the gap between product-form variance-based uncertainty relations and entropic uncertainty relations. Following Ref. [35], we have

$$V(A)+V(B)\geq H(A)+H(B)+c, \tag{27}$$

where $H(\cdot)$ stands for the Shannon entropy and c is a state-independent constant. Using Thm. 1, it is straightforward to check that

$$V(A)V(B)\geq\frac{1}{4}\left(\sum_{i=1}^{n-1}x_iy_i\right)^2+x_n^2V(B)+y_n^2V(A)-x_n^2y_n^2. \tag{28}$$

On the one hand, the term $x_n^2V(B)+y_n^2V(A)$ appeared above forms a so-called *weighted uncertainty relation* [7]. Notice that we can always assume $x_n^2=y_n^2$ in the numerical calculation, since $V(rA)V(B)=r^2V(A)V(B)$. Thus, **Eq. 28** can be bounded as

$$V(A)V(B)\geq\frac{1}{4}\left(\sum_{i=1}^{n-1}x_iy_i\right)^2+x_n^2\left(H(A)+H(B)+c\right)-x_n^4. \tag{29}$$

Therefore both the incompatibility between observables and mixness of the quantum state will affect the variance-based uncertainty relations. Moreover, any entropic uncertainty relation can be employed to construct a lower bound for product-form variance-based uncertainty relation.

To summarize, we have introduced several variance-based uncertainty relations both in the sum and product forms. Our results contain both the lower bounds and the upper bounds, which leads to the concept of uncertainty intervals. Numerical experiments illustrate the advantages of our bounds, and in some cases our bounds are near optimal. Quite remarkable, our method in deriving stronger variance-based uncertainty relations also fills the gap between the product-form variance-based uncertainty relations and the entropic uncertainty relations. Beside the results present here, our framework can also be used in formulating unitary uncertainty relations. For more details, see our follow-up work [36].

DATA AVAILABILITY STATEMENT

The raw data supporting the conclusion of this article will be made available by the authors, without undue reservation.

AUTHOR CONTRIBUTIONS

YX and NJ conceived the original idea and developed the theory. YX designed the numerical experiments and performed the numerical calculations. YX and NJ wrote the first draft of the paper and YX contributed to the final version. All authors analysed the results and reviewed the manuscript.

FUNDING

YX is supported by the Natural Sciences, the National Research Foundation (NRF). Singapore, under its NRFF Fellow programme (Grant No. NRF-NRFF2016-02), Singapore

Ministry of Education Tier 1 Grants RG162/19 (S), the Quantum Engineering Program QEP-SF3, and No FQXi-RFP-1809 (The Role of Quantum Effects in Simplifying Quantum Agents) from the Foundational Questions Institute and Fetzer Franklin Fund (a donor-advised fund of Silicon Valley Community Foundation). BY acknowledges the support of Startup Funding of Guangdong Polytechnic Normal University No. 2021SDKYA178, and Guangdong Basic and Applied Basic Research Foundation No. 2020A1515111007. S-MF acknowledges the support of National Natural Science Foundation of China (NSFC) under Grant Nos. 12075159 and 12171044; Beijing Natural Science Foundation (Grant No. Z190005); the Academician Innovation Platform of Hainan Province. The work is supported by National Natural Science Foundation of China (grant Nos. 12126351, 12126314 and 11531004), Natural Science Foundation of Hubei Province grant No. 2020CFB538, China Scholarship Council and Simons Foundation grant No. 523868. Any opinions, findings and conclusions or recommendations expressed in this material are those of the author(s) and do not reflect the views of National Research Foundation or Ministry of Education, Singapore.

REFERENCES

1. Heisenberg W. Über den anschaulichen Inhalt der quantentheoretischen Kinematik und Mechanik. *Z Physik* (1927) 43:172–98. doi:10.1007/BF01397280
2. Kennard EH. Zur Quantenmechanik Einfacher Bewegungstypen. *Z Physik* (1927) 44:326–52. doi:10.1007/BF01391200
3. Weyl H. Quantenmechanik und Gruppentheorie. *Z Physik* (1927) 46:1–46. doi:10.1007/BF02055756
4. Robertson HP. The Uncertainty Principle. *Phys Rev* (1929) 34:163–4. URL https://link.aps.org/doi/10.1103/PhysRev.34.163. doi:10.1103/physrev.34.163
5. Schrödinger E. About Heisenberg Uncertainty Relation. *Ber Kgl Akad Wiss Berlin* (1930) 24:296.
6. Pati AK, Sahu PK. Sum Uncertainty Relation in Quantum Theory. *Phys Lett A* (2007) 367:177–81. ISSN 0375-9601, URL https://www.sciencedirect.com/science/article/pii/S0375960107003696. doi:10.1016/j.physleta.2007.03.005
7. Xiao Y, Jing N, Li-Jost X, Fei S-M. Weighted Uncertainty Relations. *Sci Rep* (2016) 6:23201. doi:10.1038/srep23201
8. Xiao Y. *A Framework for Uncertainty Relations*. Leipzig, Germany: Leipzig University (2017). Ph.D. thesis. URL https://ul.qucosa.de/landing-page/?tx_dlf[id]=https%3A%2F%2Ful.qucosa.de%2Fapi%2Fqucosa%253A15366%2Fmets
9. Xiao Y, Guo C, Meng F, Jing N, Yung M-H. Incompatibility of Observables as State-independent Bound of Uncertainty Relations. *Phys Rev A* (2019) 100:032118. URL https://link.aps.org/doi/10.1103/PhysRevA.100.032118. doi:10.1103/physreva.100.032118
10. Giovannetti V, Lloyd S, Maccone L. Quantum-Enhanced Measurements: Beating the Standard Quantum Limit. *Science* (2004) 306:1330–6. URL https://www.science.org/doi/abs/10.1126/science.1104149.doi:10.1126/science.1104149
11. Giovannetti V, Lloyd S, Maccone L. Quantum Metrology. *Phys Rev Lett* (2006) 96:010401. URL https://link.aps.org/doi/10.1103/PhysRevLett.96.010401. doi:10.1103/PhysRevLett.96.010401
12. Roy SM, Braunstein SL. Exponentially Enhanced Quantum Metrology. *Phys Rev Lett* (2008) 100:220501. URL https://link.aps.org/doi/10.1103/PhysRevLett.100.220501. doi:10.1103/physrevlett.100.220501
13. Giovannetti V, Lloyd S, Maccone L. Advances in Quantum Metrology. *Nat Photon* (2011) 5:222–9. doi:10.1038/nphoton.2011.35
14. Wehner S, Winter A. Entropic Uncertainty Relations-A Survey. *New J Phys* (2010) 12:025009. doi:10.1088/1367-2630/12/2/025009
15. Białynicki-Birula I, Mycielski J. Uncertainty Relations for Information Entropy in Wave Mechanics. *Commun.Math Phys* (1975) 44:129–32. doi:10.1007/BF01608825
16. Deutsch D. Uncertainty in Quantum Measurements. *Phys Rev Lett* (1983) 50:631–3. URL https://link.aps.org/doi/10.1103/PhysRevLett.50.631. doi:10.1103/physrevlett.50.631
17. Kraus K. Complementary Observables and Uncertainty Relations. *Phys Rev D* (1987) 35:3070–5. URL https://link.aps.org/doi/10.1103/PhysRevD.35.3070. doi:10.1103/physrevd.35.3070
18. Maassen H, Uffink JBM. Generalized Entropic Uncertainty Relations. *Phys Rev Lett* (1988) 60:1103–6. URL https://link.aps.org/doi/10.1103/PhysRevLett.60.1103. doi:10.1103/physrevlett.60.1103
19. Berta M, Christandl M, Colbeck R, Renes JM, Renner R. The Uncertainty Principle in the Presence of Quantum Memory. *Nat Phys* (2010) 6:659–62. doi:10.1038/nphys1734
20. Coles PJ, Piani M. Improved Entropic Uncertainty Relations and Information Exclusion Relations. *Phys Rev A* (2014) 89:022112. URL https://link.aps.org/doi/10.1103/PhysRevA.89.022112.doi:10.1103/PhysRevA.89.022112
21. Xiao Y, Jing N, Fei S-M, Li T, Li-Jost X, Ma T, et al. Strong Entropic Uncertainty Relations for Multiple Measurements. *Phys Rev A* (2016) 93:042125. URL https://link.aps.org/doi/10.1103/PhysRevA.93.042125. doi:10.1103/PhysRevA.93.042125
22. Xiao Y, Jing N, Fei S-M, Li-Jost X. Improved Uncertainty Relation in the Presence of Quantum Memory. *J Phys A: Math Theor* (2016) 49:49LT01. doi:10.1088/1751-8113/49/49/49lt01
23. Xiao Y, Jing N, Li-Jost X. Uncertainty under Quantum Measures and Quantum Memory. *Quan Inf Process* (2017) 16:104. doi:10.1007/s11128-017-1554-6
24. Xiao Y, Fang K, Gour G. *The Complementary Information Principle of Quantum Mechanics* (2019). 1908.07694. URL https://arxiv.org/abs/1908.07694.
25. Xiao Y, Sengupta K, Yang S, Gour G. Uncertainty Principle of Quantum Processes. *Phys Rev Res* (2021) 3:023077. URL https://link.aps.org/doi/10.1103/PhysRevResearch.3.023077. doi:10.1103/physrevresearch.3.023077
26. Huang J-L, Gan W-C, Xiao Y, Shu F-W, Yung M-H. Holevo Bound of Entropic Uncertainty in Schwarzschild Spacetime. *Eur Phys J C* (2018) 78:545. doi:10.1140/epjc/s10052-018-6026-3
27. Qian C, Wu Y-D, Ji J-W, Xiao Y, Sanders BC. Multiple Uncertainty Relation for Accelerated Quantum Information. *Phys Rev D* (2020) 102:096009. URL https://link.aps.org/doi/10.1103/PhysRevD.102.096009. doi:10.1103/PhysRevD.102.096009
28. Candes EJ, Romberg J, Tao T. Robust Uncertainty Principles: Exact Signal Reconstruction from Highly Incomplete Frequency Information. *IEEE Trans Inform Theor* (2006) 52:489–509. doi:10.1109/tit.2005.862083
29. Hofmann HF, Takeuchi S. Violation of Local Uncertainty Relations as a Signature of Entanglement. *Phys Rev A* (2003) 68:032103. URL https://link.aps.org/doi/10.1103/PhysRevA.68.032103. doi:10.1103/PhysRevA.68.032103
30. Rutkowski A, Buraczewski A, Horodecki P, Stobińska M. Quantum Steering Inequality with Tolerance for Measurement-Setting Errors: Experimentally Feasible Signature of Unbounded Violation. *Phys Rev Lett* (2017) 118:020402. URL https://link.aps.org/doi/10.1103/PhysRevLett.118.020402. doi:10.1103/PhysRevLett.118.020402
31. Xiao Y, Xiang Y, He Q, Sanders BC. Quasi-fine-grained Uncertainty Relations. *New J Phys* (2020) 22:073063. doi:10.1088/1367-2630/ab9d57
32. Coles PJ, Berta M, Tomamichel M, Wehner S. Entropic Uncertainty Relations and Their Applications. *Rev Mod Phys* (2017) 89:015002. URL https://link.aps.org/doi/10.1103/RevModPhys.89.015002. doi:10.1103/RevModPhys.89.015002
33. Xiao Y, Yang Y, Wang X, Liu Q, Gu M. Under preparation (2022).
34. Mondal D, Bagchi S, Pati AK. Tighter Uncertainty and Reverse Uncertainty Relations. *Phys Rev A* (2017) 95:052117. URL https://link.

aps.org/doi/10.1103/PhysRevA.95.052117. doi:10.1103/PhysRevA.95.052117
35. Huang Y. Variance-based Uncertainty Relations. *Phys Rev A* (2012) 86:024101. URL https://link.aps.org/doi/10.1103/PhysRevA.86.024101. doi:10.1103/PhysRevA.86.024101
36. Yu B, Jing N, Li-Jost X. Strong Unitary Uncertainty Relations. *Phys Rev A* (2019) 100:022116. URL https://link.aps.org/doi/10.1103/PhysRevA.100.022116. doi:10.1103/PhysRevA.100.022116

Conflict of Interest: The authors declare that the research was conducted in the absence of any commercial or financial relationships that could be construed as a potential conflict of interest.

Publisher's Note: All claims expressed in this article are solely those of the authors and do not necessarily represent those of their affiliated organizations, or those of the publisher, the editors and the reviewers. Any product that may be evaluated in this article, or claim that may be made by its manufacturer, is not guaranteed or endorsed by the publisher.

frontiers | Frontiers in Physics

ORIGINAL RESEARCH
published: 13 April 2022
doi: 10.3389/fphy.2022.873810

Experimental Investigation of Quantum Uncertainty Relations With Classical Shadows

Lu Liu[1], *Ting Zhang*[1], *Xiao Yuan*[2]* and *He Lu*[1]*

[1]School of Physics, State Key Laboratory of Crystal Materials, Shandong University, Jinan, China, [2]Center on Frontiers of Computing Studies, Peking University, Beijing, China

The quantum component in uncertainty relation can be naturally characterized by the quantum coherence of a quantum state, which is of paramount importance in quantum information science. Here, we experimentally investigate quantum uncertainty relations construed with relative entropy of coherence, l_1 norm of coherence, and coherence of formation. Instead of quantum state tomographic technology, we employ the classical shadow algorithm for the detection of lower bounds in quantum uncertainty relations. With an all-optical setup, we prepare a family of quantum states whose purity can be fully controlled. We experimentally explore the tightness of various lower bounds in different reference bases on the prepared states. Our results indicate that the tightness of quantum coherence lower bounds depends on the reference bases and the purity of the quantum state.

Keywords: quantum uncertainty relation, quantum coherence measures, classical shadow, purity of quantum states, photonic quantum information processing

OPEN ACCESS

Edited by:
Dong Wang,
Anhui University, China

Reviewed by:
Shao-Ming Fei,
Capital Normal University, China
Xiongfeng Ma,
Tsinghua University, China

***Correspondence:**
Xiao Yuan
xiaoyuan@pku.edu.cn
He Lu
luhe@sdu.edu.cn

Specialty section:
This article was submitted to Quantum Engineering and Technology, a section of the journal Frontiers in Physics

Received: *11 February 2022*
Accepted: *11 March 2022*
Published: *13 April 2022*

Citation:
Liu L, Zhang T, Yuan X and Lu H (2022) Experimental Investigation of Quantum Uncertainty Relations With Classical Shadows. Front. Phys. 10:873810. doi: 10.3389/fphy.2022.873810

1 INTRODUCTION

The uncertainty principle lies at the heart of quantum mechanics, which makes it different from classical theories of the physical world. It behaves as a fundamental limitation describing the precise outcomes of incompatible observables, and plays a significant role in quantum information science from quantum key distribution [1–4] to quantum random number generation [5, 6], and from quantum entanglement witness [7–9] to quantum steering [10, 11] and quantum metrology [12, 13] (also see Ref. [14] for the review of uncertainty relation and applications).

The seminal concept of uncertainty relation was proposed by Heisenberg in 1927 [15], in which he observed that the measurement of position x of an electron with error $\Delta(x)$ causes the disturbance $\Delta(p)$ on its momentum p. In particular, their product has a lower bound set by Planck constant, that is, $\Delta(x)\Delta(p) \sim \hbar$. Later, Robertson generalized the Heisenberg's uncertainty relation to two arbitrary observables by $\Delta A\Delta B \geq \frac{1}{2}|\langle [A, B]\rangle|$, with ΔA (ΔB) being the standard deviation of observable A (B), $[A, B] = AB - BA$ being the commutator of A and B, and $\langle\cdot\rangle$ being the expected value in a given state ρ [16]. Indeed, such an uncertainty relation has a state-dependent lower bound so that it fails to reveal the intrinsic incompatibility when A and B are noncommuting.

To address the issue of state-independence of Robertson's uncertainty relation, the entropic uncertainty relation has been developed by Deutsch [17], Kraus [18], and Maassen and Uiffink [19]: Consider a quantum state ρ and two observables A and B; the eigenstates $|a_i\rangle$ and $|b_i\rangle$ of observable A and B constitute measurement bases $\mathbb{A} = \{|a_i\rangle\}$ and $\mathbb{B} = \{|b_i\rangle\}$. The probability of measuring A on

state ρ with ith outcome is $p_i = \mathrm{Tr}[\rho|a_i\rangle\langle a_i|]$, and the corresponding Shannon entropy of measurement outcomes is $H(A) = -\sum_i p_i \log_2 p_i$. Then, $H(A) + H(B)$ is lower bounded by $H(A) + H(B) \geq -\log_2 c$ with $c = \max_{i,j}|\langle a_i|b_j\rangle|^2$ the maximal overlap between $|a_i\rangle$ and $|b_j\rangle$. According to the definition of Shannon entropy, $H(A)$ quantifies the uncertainty or lack of information associated to a random variable, but does not indicate whether the uncertainty comes from classical or quantum parts. For instance, the measurement of Pauli observable Z on states $|+\rangle = (|0\rangle + |1\rangle)/\sqrt{2}$ and $I/2 = (|0\rangle\langle 0| + |1\rangle\langle 1|)/2$ both lead to $H(Z) = 1$.

It is natural to consider quantum coherence, which is one of the defining features of quantum mechanics, to quantify the quantum component in uncertainty [20–22]. Along with this, rigorous connections between quantum coherence and entropic uncertainty have been established [23, 24] based on the framework of coherence quantification [25], and the quantum uncertainty relations (QURs) have been theoretically constructed with various coherence measures [26]. On the experimental side, the QURs using relative entropy of coherence have been demonstrated to investigate the trade-off relation [27] and connection between entropic uncertainty and coherence uncertainty [28]. Still, there are several unexplored matters along the line of experimental investigations. First, although various QURs have been theoretically constructed with relative entropy of coherence, the experimental feasibility and comparison have not been tested. Second, the experimental realizations of QURs using other coherence measures beyond relative entropy of coherence are still lacking. Finally, the lower bounds in QURs are generally obtained with quantum state tomography (QST) [27, 28], which becomes a challenge when the dimension of quantum state increases.

In this study, we experimentally investigate QURs constructed with three coherence measures, relative entropy of coherence, l_1 norm of coherence, and coherence of formation, on a family of single-photon states. The lower bound of the QURs is indicated with classical shadow (CS) algorithm [29]. We show that the tightness of coherence lower bounds depends on the reference bases and the purity of quantum state.

This article is organized as follows: In **Section 2**, we introduce the basic idea of QUR using quantum coherence measures. In **Section 3**, we briefly introduce the CS algorithm to detect the purity of a quantum state. In Sections 4 and 5, we present the experimental demonstration and results. Finally, we draw the conclusion in **Section 6**.

2 QUANTUM UNCERTAINTY RELATIONS

A functional C can be regarded as a coherence measure if it satisfies four postulates: nonnegativity, monotonicity, strong monotonicity, and convexity [25]. The different coherence measure plays different roles in quantum information processing. For instance, the relative entropy of coherence plays a crucial role in coherence distillation [30], coherence freezing [31, 32], and the secret key rate in quantum key distribution [33]. The coherence of formation represents the coherence cost, that is, the minimum rate of a maximally coherent pure state consumed to prepare the given state under incoherent and strictly incoherent operations [30]. The l_1-norm of coherence is closely related to quantum multi-slit interference experiments [34] and is used to explore the superiority of quantum algorithms [35–37]. We refer to Ref. [38] for the review of resource theory of quantum coherence. In the following, we give a brief review of QURs constructed with coherence measures of relative entropy of coherence, l_1-norm of coherence, and coherence of formation [26].

2.1 Quantum Uncertainty Relations Using Relative Entropy of Coherence

The relative entropy of coherence of state ρ is defined as [25]:

$$C_{\mathrm{RE}}^{\mathbb{J}}(\rho) = S_{\mathrm{VN}}^{\mathbb{J}}(\rho_d) - S_{\mathrm{VN}}(\rho), \tag{1}$$

where $\mathbb{J} = \{|j\rangle\}$ denotes the measurement basis of observable J, $S_{\mathrm{VN}}(\rho) = -\mathrm{Tr}[\rho\log_2\rho]$ is the von Neumann entropy, and ρ_d is the diagonal part of ρ in measurement basis $\mathbb{J}$. Note that $H(J) = S_{\mathrm{VN}}^{\mathbb{J}}(\rho_d)$. The QUR using relative entropy of coherence [26] is

$$C_{\mathrm{RE}}^{\mathbb{A}}(\rho) + C_{\mathrm{RE}}^{\mathbb{B}}(\rho) \geq h\left(\frac{\sqrt{2\mathcal{P}-1}\left(2\sqrt{c}-1\right)+1}{2}\right) - S_{\mathrm{VN}}(\rho), \tag{2}$$

where $h(x) = -x\log_2 x - (1-x)\log_2(1-x)$ is the binary entropy and $\mathcal{P} = \mathrm{Tr}[\rho^2]$ is the purity of state ρ. Similarly, the entropic uncertainty relations proposed by Sánches-Ruiz [39], Berta et al. [3], and Korzekwa et al. [22] can be expressed in terms of relative entropy of coherence by (see **Supplementary Material** for detailed derivations)

$$C_{\mathrm{RE}}^{\mathbb{A}}(\rho) + C_{\mathrm{RE}}^{\mathbb{B}}(\rho) \geq h\left(\frac{1+\sqrt{2c-1}}{2}\right) - 2S_{\mathrm{VN}}(\rho), \tag{3}$$

$$C_{\mathrm{RE}}^{\mathbb{A}}(\rho) + C_{\mathrm{RE}}^{\mathbb{B}}(\rho) \geq -\log_2 c - S_{\mathrm{VN}}(\rho), \tag{4}$$

$$C_{\mathrm{RE}}^{\mathbb{A}}(\rho) + C_{\mathrm{RE}}^{\mathbb{B}}(\rho) \geq -\left[1 - S_{\mathrm{VN}}(\rho)\right]\log_2 c. \tag{5}$$

Consider a qubit state ρ in spectral decomposition $\rho = \lambda|\psi\rangle\langle\psi| + (1-\lambda)|\psi_\perp\rangle\langle\psi_\perp|$ with $\lambda(1-\lambda)$ being the eigenvalue associated with eigenvector $|\psi\rangle(|\psi_\perp\rangle)$; we have $S_{\mathrm{VN}}(\rho) = -\lambda\log_2\lambda - (1-\lambda)\log_2(1-\lambda)$ where the purity $\mathcal{P}$ is related to λ by $\mathcal{P} = 2\lambda^2 - 2\lambda + 1$.

2.2 Quantum Uncertainty Relations of the l_1 Norm of Coherence Norm of Coherence

The l_1 norm of coherence in fixed measurement bases $\mathbb{J}$ is defined in the form of

$$C_{l_1}^{\mathbb{J}}(\rho) = \sum_{k\neq l}|\langle j_k|\rho|j_l\rangle|, \tag{6}$$

where the QUR using l_1 norm of coherence is [26]

$$C_{l_1}^{\mathbb{A}}(\rho) + C_{l_1}^{\mathbb{B}}(\rho) \geq 2\sqrt{(2\mathcal{P}-1)c(1-c)}. \tag{7}$$

2.3 Quantum Uncertainty Relations Using Coherence of Formation

The coherence of formation in fixed measurement bases $\mathbb{J}$ is defined in the form of

$$C_f^{\mathbb{J}}(\rho) = \inf_{\{p_i,|\varphi_i\rangle\}} \sum_i p_i C_{\mathrm{RE}}^{\mathbb{J}}(|\varphi_i\rangle\langle\varphi_i|), \tag{8}$$

where the infimum is taken over all state decomposition of $\rho = \sum_i p_i|\varphi_i\rangle\langle\varphi_i|$. The QUR using coherence of formation is [26]

$$C_f^{\mathbb{A}}(\rho) + C_f^{\mathbb{B}}(\rho) \geq h\left(\frac{1+\sqrt{1-2(2\mathcal{P}-1)\sqrt{c}\,(1-\sqrt{c}\,)}}{2}\right). \tag{9}$$

3 CLASSICAL SHADOW

From **Section 2**, it is obvious that the purity $\mathcal{P}$ of ρ is the key ingredient in the experimental testing of various QURs. The purity $\mathcal{P}$ can be calculated by reconstructing the density matrix of ρ with QST, which is very costly as the Hilbert space of ρ increases. Another protocol employs two copies of ρ for the detection of $\mathcal{P}$, that is, $\mathcal{P} = \mathrm{Tr}[\Pi\rho\otimes\rho]$, with Π being the local swap operator of two copies of the state [40, 41].

Very recently, the CS algorithm has been theoretically proposed for efficient quantum state detection [29], and has been experimentally realized in the detection of purity of unknown quantum states [42, 43]. In CS algorithm, a randomly selected single-qubit Clifford unitary U is applied on ρ, and then the rotated state $U\rho U^\dagger$ is measured in the Pauli-Z basis, that is, $\mathbb{Z} = \{|z_0\rangle = |0\rangle, |z_1\rangle = |1\rangle\}$. With the outcome of $|z_i\rangle$, the estimator $\hat{\rho}$ is constructed by $\hat{\rho} = 3U^\dagger|z_i\rangle\langle z_i|U - I$. It is equivalent to measure $J = U^\dagger Z U$ ($\mathbb{J} = \{U|0\rangle, U|1\rangle\}$) on ρ, and the measurement basis J is randomly selected from the Pauli observable basis set $\mathbb{J} \in \{\mathbb{X}, \mathbb{Y}, \mathbb{Z}\}$, with a uniform probability $\mathcal{K}(\mathbb{J}) = 1/3$. The estimator $\hat{\rho}$ can be rewritten as $\hat{\rho} = 3|k\rangle\langle k| - I$, where $|k\rangle \in \{|x_0\rangle, |x_1\rangle, |y_0\rangle, |y_1\rangle, |z_0\rangle, |z_1\rangle\}$. In particular, $|x_0\rangle = |+\rangle = (|0\rangle + |1\rangle)/\sqrt{2}$ and $|x_1\rangle = |-\rangle = (|0\rangle - |1\rangle)/\sqrt{2}$ are the eigenvectors of Pauli observable X and $|y_0\rangle = |L\rangle = (|0\rangle + i|1\rangle)/\sqrt{2}$ and $|y_1\rangle = |R\rangle = (|0\rangle - i|1\rangle)/\sqrt{2}$ are the eigenvectors of Pauli observable Y. It is worth noting that the construction of estimator $\hat{\rho}$ only requires one sample. In our demonstrations, one sample is one two-photon coincidence. For a set of estimators $\{\hat{\rho}_i\}$ constructed with N_s samples, the purity of state ρ can be estimated by two randomly selected independent $\hat{\rho}_i$ and $\hat{\rho}_j$, that is, $\hat{\mathcal{P}} = \sum_{i\neq j}\mathrm{Tr}[\Pi\hat{\rho}_i\otimes\hat{\rho}_j]/N_s(N_s-1)$.

4 EXPERIMENT REALIZATIONS

To test the aforementioned QURs of various coherence measures, we consider the following single-qubit state:

$$\rho(\tau) = \tau|+\rangle\langle+| + (1-\tau)\frac{I}{2}, \tag{10}$$

with $0 \leq \tau \leq 1$. Note that $\tau = 1$ corresponds to the pure state $|+\rangle$ and $\tau = 0$ corresponds to the maximally mixed state $I/2$. The experimental setup to generate state in **Eq. 10** is shown in **Figure 1A**. Two photons are generated on a periodically poled potassium titanyl phosphate (PPKTP) crystal pumped by an ultraviolet CW laser diode. The generated two photons are with orthogonal polarization denoted as $|HV\rangle$, where $|H\rangle$ and $|V\rangle$ denote the horizontal and vertical polarization, respectively. Two photons are separated on a polarizing beam splitter (PBS), which transmits $|H\rangle$ and reflects $|V\rangle$. The reflected photon is detected to herald the existence of transmitted photon in state $|H\rangle$, which is then converted to $|+\rangle = (|H\rangle + |V\rangle)/\sqrt{2}$ by a half-wave plate (HWP) set at 22.5°. We sent the heralded photon into a 50:50 beam splitter (BS_1), which transmits (reflects) the single photon with a probability of 50%. The photons in transmitted and reflected mode are denoted as $|t\rangle$ and $|r\rangle$, respectively. Two tunable attenuators are set at modes $|t\rangle$ and $|r\rangle$ to realize the ratio of transmission probability in $|t\rangle$ and $|r\rangle$ of $\frac{\tau}{1-\tau}$. The photon in $|r\rangle$ passes through an unbalanced Mach–Zehnder interferometer (MZI) consisting of two PBS and two mirrors, which acts as a completely dephasing channel in polarization degree of freedom (DOF), that is, $|+\rangle\langle+| \to \mathbb{I}/2$. Finally, the two beams are incoherently mixed on BS_2 to erase the information of path DOF, which leads to the state $\rho(\tau)$ in both output ports. A step-by-step calculation detailing the evolution of the single-photon state through this setup is given in **Eq. 11**:

$$\begin{aligned}
|H\rangle &\xrightarrow{\text{HWP@22.5°}} |+\rangle = \frac{1}{\sqrt{2}}(|H\rangle + |V\rangle)\\
&\xrightarrow{\mathrm{BS}_1} |+\rangle\otimes\frac{1}{\sqrt{2}}(|t\rangle + |r\rangle)\\
&\xrightarrow[\text{at } |t\rangle \text{ and } |r\rangle]{\text{two attenuators}} |+\rangle\otimes\left(\sqrt{\tau}\,|t\rangle + \sqrt{1-\tau}\,|r\rangle\right)\\
&\xrightarrow[\text{at } |r\rangle]{\text{unbalanced MZI}} \tau|+\rangle\langle+|\otimes|t\rangle\langle t| + (1-\tau)I\Big/2\otimes|r\rangle\langle r|\\
&\xrightarrow[\text{incoherently combined}]{\mathrm{BS}_2} \tau|+\rangle\langle+| + (1-\tau)I\Big/2.
\end{aligned} \tag{11}$$

In our experiment, we set the parameter $\tau = 0$ to $\tau = 1$, with an increment of 0.1, and totally generated 11 states. For each generated state, we detect the QURs with the setup shown in **Figure 1B**. The lower bound in QURs related to purity $\mathcal{P}^{\mathrm{CS}}$ is measured with CS algorithm. $C_{\mathrm{RE}}^{\mathbb{J}}$ is detected with projective measurement on basis $\mathbb{J}$, along with the measured purity. $C_{l_1}^{\mathbb{J}}$ ($C_f^{\mathbb{J}}$) is calculated with reconstructed $\rho(\tau)$. All the measurement bases are realized with a HWP, a quarter-wave plate (QWP), and a PBS.

5 EXPERIMENTAL RESULTS

To investigate the accuracy of estimated purity $\mathcal{P}^{\mathrm{CS}}$ with CS algorithms, we also calculate the purity $\mathcal{P}^{\mathrm{QST}}$ with reconstructed density matrix of $\rho(\tau)$ from QST with $N_S = 2000$. The results of $|\mathcal{P}^{\mathrm{QST}} - \mathcal{P}^{\mathrm{CS}}|$ are shown in **Figure 2A**. The more the samples used

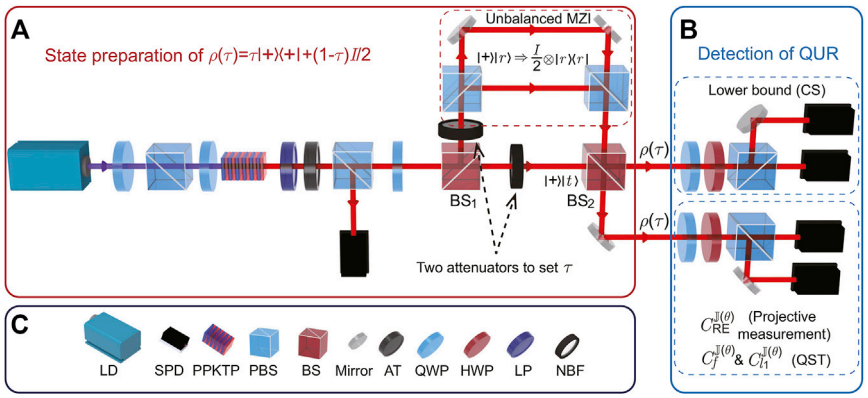

FIGURE 1 | Schematic illustration of the experimental setup. **(A)** The setup to generate the family of states $\rho(\tau) = \tau|+\rangle\langle+| + (1-\tau)\frac{I}{2}$. **(B)** Experimental setup to implement the measurements with CS algorithm and QST. **(C)** Symbols used in **(A)** and **(B)**. Laser diode (LD); single-photon detector (SPD); attenuator (AT); long-wave pass filter (LP); narrow-band filter (NBF).

in CS algorithm, the smaller $|\mathcal{P}^{QST} - \mathcal{P}^{CS}|$ is. We observe $|\mathcal{P}^{QST} - \mathcal{P}^{CS}| < 0.1$ when $N_s \geq 600$. Especially, $|\mathcal{P}^{QST} - \mathcal{P}^{CS}| = 0.0036$ when $N_s = 2000$. In **Figure 2B**, we show the results of $\mathcal{P}^{CS}$ and $\mathcal{P}^{QST}$ with $N_S = 2000$ on 11 prepared $\rho(\tau)$, in which the experimental results of $\mathcal{P}^{CS}$ and $\mathcal{P}^{QST}$ have good agreements with the theoretical predictions. In the following, all the results with CS algorithm are obtained with 2000 samples. We also compare the accuracy of estimated purity $\mathcal{P}$ from CS algorithm and QST with the same N_s (see **Supplementary Material** for the results).

We first focus on the lower bounds in QURs using relative entropy of coherence, that is, **Eqs 2–5**. We calculate the lower bounds in **Eqs 2–5** with the estimated $\mathcal{P}^{CS}$ on $\rho(\tau = 1)$, $\rho(\tau = 0.894)$, $\rho(\tau = 0.688)$, and $\rho(\tau = 0.291)$, respectively. As shown in **Figure 3A**, we observe that the lower bounds in **Eqs 4**, **5** have the same value and outperform others when $\mathbb{A}$ and $\mathbb{B}$ are mutually unbiased ($c = 0.5$). When c becomes larger, lower bounds in **Eqs 2**, **3** are stricter than those in 4 and **Eq. 5**. However, the situation is quite different when the purity becomes smaller. As shown in **Figure 3B–D**, the values of lower bounds in **Eqs 3**, **4** are negative (we denote them as 0) when c is larger than certain values, which means that the lower bounds are loosened as $C_{RE}^{\mathbb{A}}(\rho) + C_{RE}^{\mathbb{B}}(\rho) > 0$ for all ρ.

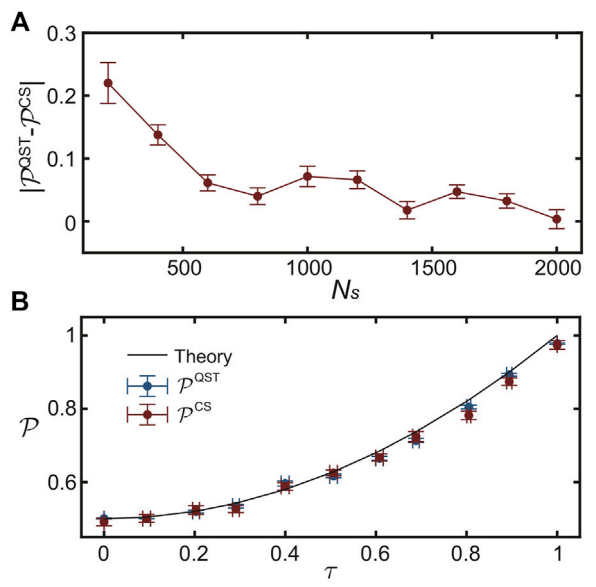

FIGURE 2 | (A) Average estimated $\mathcal{P}^{CS}$ of 11 prepared states with different N_s. **(B)** The results of $\mathcal{P}^{CS}$ (blue dots) and $\mathcal{P}^{QST}$ (red dots). The black line is the theoretical prediction of purity of ideal $\rho(\tau)$.

To investigate the tightness of various lower bounds, we measure $C_{RE}^{\mathbb{A}}(\rho) + C_{RE}^{\mathbb{B}}(\rho)$ in different reference bases. We select observables A and B from set $J(\theta) = \cos\theta Z + \sin\theta X$. Specifically, we fix $A = J(0^\circ)$ and choose $B = J(90^\circ)$, $J(66.42^\circ)$, and $J(36.86^\circ)$, which correspond to $c = 0.5$, 0.7, and 0.9. For each observable $J(\theta)$, we perform the projective measurement on basis $\mathbb{J}(\theta)$, and calculate the Shannon entropy of measurement outcomes $H(J(\theta))$. Thus, we obtain $C_{RE}^{\mathbb{J}(\theta)}(\rho(\tau)) = H(J(\theta)) - S_{VN}(\rho(\tau))$, where $S_{VN}(\rho(\tau))$ can be calculated from $\mathcal{P}^{CS}$. The results of QURs using relative entropy of coherence are shown in **Figure 4**. As shown in **Figure 4A**, the lower bounds in **Eqs 4**, **5** have the same values as $C_{RE}^{\mathbb{A}}(\rho) + C_{RE}^{\mathbb{B}}(\rho)$ is lower bounded by $1 - S_{VN}(\rho)$, when $c = 0.5$ according to the definitions in **Eqs 4**, **5**. When c is larger, the lower bound in **Eq. 2** is stricter than others as reflected in **Figure 4B** and **Figure 4C**.

Next, we investigate the QURs using l_1-norm of coherence and coherence of formation as described in **Eqs 7–9**. We choose observables $A = J(0^\circ) = Z$ and $B = J(90^\circ) = X$ in the coherence measure, which corresponds to $c = 0.5$. The $C_{l_1}^{\mathbb{Z}}(\rho)$ and $C_{l_1}^{\mathbb{X}}(\rho)$ are calculated according to **Eq. 7** with the reconstructed density matrix of $\rho(\tau)$. Thus, $C_f^{\mathbb{Z}}(\rho)$ and $C_f^{\mathbb{X}}(\rho)$ can be calculated with $C_{l_1}^{\mathbb{Z}}(\rho)$ and $C_{l_1}^{\mathbb{X}}(\rho)$ as $C_f(\rho) = h\left(\frac{1+\sqrt{1-C_{l_1}(\rho)}}{2}\right)$ [26]. The results of QURs using l_1 norm of coherence and coherence of formation are shown in **Figure 5A** and **Figure 5B**, respectively, in which the measured coherence is well bounded by the measured lower bounds.

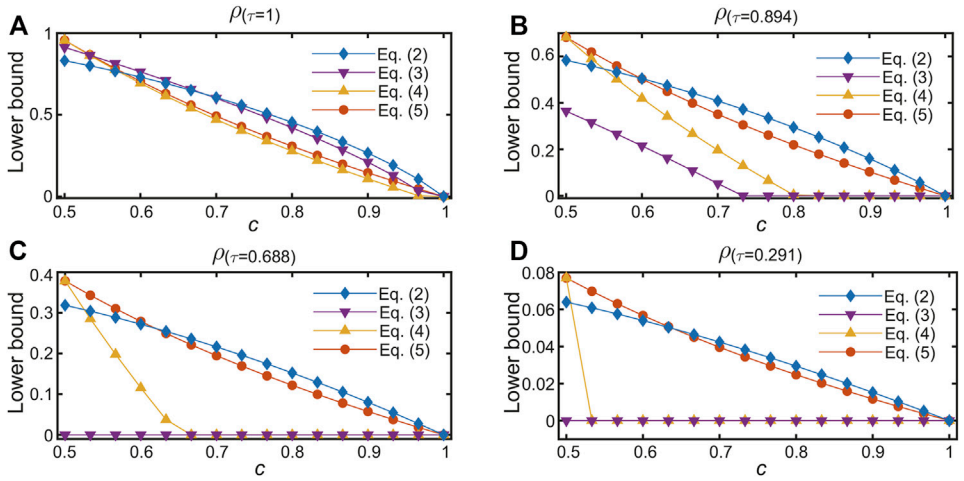

FIGURE 3 | Results of estimated lower bounds in **Eqs 2–5** with different c on state **(A)** $\rho(\tau = 1)$, **(B)** $\rho(\tau = 0.894)$, **(C)** $\rho(\tau = 0.688)$, and **(D)** $\rho(\tau = 0.291)$, respectively.

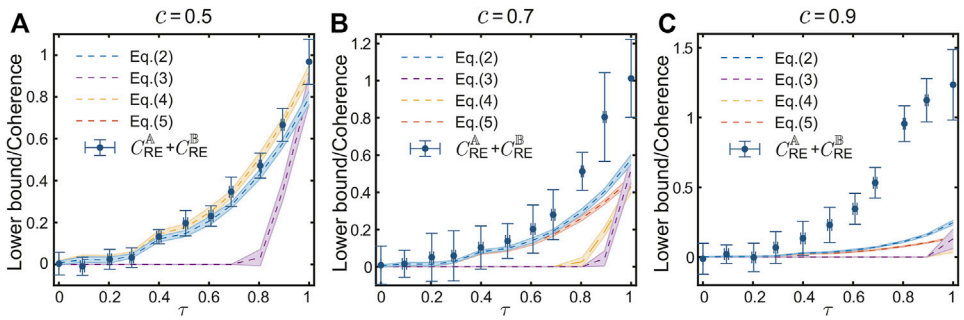

FIGURE 4 | Results of QURs in **Eqs 2–5** on 11 prepared states with **(A)** $c = 0.5$, **(B)** $c = 0.7$, and **(C)** $c = 0.9$. The dashed lines are the measured lower bounds and the shadow area represents the statistical error by repeating CS measurement for 20 times.

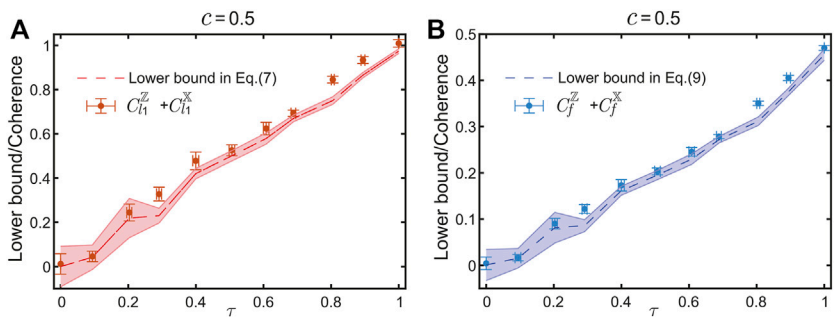

FIGURE 5 | Results of **(A)** QUR with l_1 norm of coherence and **(B)** QUR with coherence of formation with $c = 0.5$.

6 CONCLUSION

In this study, we experimentally investigate quantum uncertainty relations using various coherence measures. The lower bounds in quantum uncertainty relations are detected with the classical shadow algorithm, in which the measurement cost is quite small and independent of the dimension of quantum states. For the quantum uncertainty relation using relative entropy of coherence, we show that the tightness of lower bounds is highly related to the reference basis and purity of quantum state. Moreover, we test the quantum uncertainty relation using l_1 norm of coherence and coherence of formation.

Our results confirm that the tightness of lower bound in quantum uncertainty relations is related to the purity of quantum states and the reference bases, which can benefit the choice of quantum uncertainty relations when considering the experimental imperfections in practice. For instance, the imperfections in state preparation and measurement apparatus correspond to the purity and reference bases in the lower bound, respectively. More importantly, our method can be generalized to multipartite states while it keeps its efficiency. The multipartite coherence could be efficiently estimated using the stabilizer theory [44, 45] and the classical shadow algorithm to detect that the purity of multipartite state is efficient as well [43].

DATA AVAILABILITY STATEMENT

The raw data supporting the conclusions of this article will be made available by the authors, without undue reservation.

AUTHOR CONTRIBUTIONS

XY and HL conceived the idea. TZ and HL designed the experiment. LL and TZ performed the experiment and analyzed the data. HL supervised the project. XY and HL wrote the manuscript with contributions from all authors.

FUNDING

This work is supported by the National Natural Science Foundation of China (Grant No. 11974213, No. 92065112, and No. 12175003), National Key R&D Program of China (Grant No. 2019YFA0308200), Shandong Provincial Natural Science Foundation (Grant No. ZR2019MA001 and No. ZR2020JQ05), Taishan Scholar of Shandong Province (Grant No. tsqn202103013), and Shandong University Multidisciplinary Research and Innovation Team of Young Scholars (Grant No. 2020QNQT).

SUPPLEMENTARY MATERIAL

The Supplementary Material for this article can be found online at: https://www.frontiersin.org/articles/10.3389/fphy.2022.873810/full#supplementary-material

REFERENCES

1. Koashi M. Unconditional Security of Quantum Key Distribution and the Uncertainty Principle. *J Phys Conf Ser* (2006) 36:98–102. doi:10.1088/1742-6596/36/1/016
2. Koashi M. Simple Security Proof of Quantum Key Distribution Based on Complementarity. *New J Phys* (2009) 11:045018. doi:10.1088/1367-2630/11/4/045018
3. Berta M, Christandl M, Colbeck R, Renes JM, Renner R. The Uncertainty Principle in the Presence of Quantum Memory. *Nat Phys* (2010) 6:659–62. doi:10.1038/nphys1734
4. Tomamichel M, Renner R. Uncertainty Relation for Smooth Entropies. *Phys Rev Lett* (2011) 106:110506. doi:10.1103/PhysRevLett.106.110506
5. Vallone G, Marangon DG, Tomasin M, Villoresi P. Quantum Randomness Certified by the Uncertainty Principle. *Phys Rev A* (2014) 90:052327. doi:10.1103/PhysRevA.90.052327
6. Cao Z, Zhou H, Yuan X, Ma X. Source-independent Quantum Random Number Generation. *Phys Rev X* (2016) 6:011020. doi:10.1103/PhysRevX.6.011020
7. Prevedel R, Hamel DR, Colbeck R, Fisher K, Resch KJ. Experimental Investigation of the Uncertainty Principle in the Presence of Quantum Memory and its Application to Witnessing Entanglement. *Nat Phys* (2011) 7:757–61. doi:10.1038/nphys2048
8. Li C-F, Xu J-S, Xu X-Y, Li K, Guo G-C. Experimental Investigation of the Entanglement-Assisted Entropic Uncertainty Principle. *Nat Phys* (2011) 7:752–6. doi:10.1038/nphys2047
9. Berta M, Coles PJ, Wehner S. Entanglement-assisted Guessing of Complementary Measurement Outcomes. *Phys Rev A* (2014) 90:062127. doi:10.1103/PhysRevA.90.062127
10. Walborn SP, Salles A, Gomes RM, Toscano F, Souto Ribeiro PH. Revealing Hidden Einstein-Podolsky-Rosen Nonlocality. *Phys Rev Lett* (2011) 106:130402. doi:10.1103/PhysRevLett.106.130402
11. Schneeloch J, Broadbent CJ, Walborn SP, Cavalcanti EG, Howell JC. Einstein-podolsky-rosen Steering Inequalities from Entropic Uncertainty Relations. *Phys Rev A* (2013) 87:062103. doi:10.1103/PhysRevA.87.062103
12. Giovannetti V, Lloyd S, Maccone L. Advances in Quantum Metrology. *Nat Photon* (2011) 5:222–9. doi:10.1038/nphoton.2011.35
13. Hall MJW, Wiseman HM. Heisenberg-style Bounds for Arbitrary Estimates of Shift Parameters Including Prior Information. *New J Phys* (2012) 14:033040. doi:10.1088/1367-2630/14/3/033040
14. Coles PJ, Berta M, Tomamichel M, Wehner S. Entropic Uncertainty Relations and Their Applications. *Rev Mod Phys* (2017) 89:015002. doi:10.1103/RevModPhys.89.015002
15. Heisenberg W. Über den anschaulichen Inhalt der quantentheoretischen Kinematik und Mechanik. *Z Physik* (1927) 43:172–98. doi:10.1007/BF01397280
16. Robertson HP. The Uncertainty Principle. *Phys Rev* (1929) 34:163–4. doi:10.1103/PhysRev.34.163
17. Deutsch D. Uncertainty in Quantum Measurements. *Phys Rev Lett* (1983) 50:631–3. doi:10.1103/PhysRevLett.50.631
18. Kraus K. Complementary Observables and Uncertainty Relations. *Phys Rev D* (1987) 35:3070–5. doi:10.1103/PhysRevD.35.3070
19. Maassen H, Uffink JBM. Generalized Entropic Uncertainty Relations. *Phys Rev Lett* (1988) 60:1103–6. doi:10.1103/PhysRevLett.60.1103
20. Coles PJ, Yu L, Gheorghiu V, Griffiths RB. Information-theoretic Treatment of Tripartite Systems and Quantum Channels. *Phys Rev A* (2011) 83:062338. doi:10.1103/PhysRevA.83.062338
21. Coles PJ. Unification of Different Views of Decoherence and Discord. *Phys Rev A* (2012) 85:042103. doi:10.1103/PhysRevA.85.042103
22. Korzekwa K, Lostaglio M, Jennings D, Rudolph T. Quantum and Classical Entropic Uncertainty Relations. *Phys Rev A* (2014) 89:042122. doi:10.1103/PhysRevA.89.042122
23. Yuan X, Zhou H, Cao Z, Ma X. Intrinsic Randomness as a Measure of Quantum Coherence. *Phys Rev A* (2015) 92:022124. doi:10.1103/PhysRevA.92.022124
24. Yuan X, Zhao Q, Girolami D, Ma X. Quantum Coherence and Intrinsic Randomness. *Adv Quan Tech* (2019) 2:1900053. doi:10.1002/qute.201900053
25. Baumgratz T, Cramer M, Plenio MB. Quantifying Coherence. *Phys Rev Lett* (2014) 113:140401. doi:10.1103/PhysRevLett.113.140401
26. Yuan X, Bai G, Peng T, Ma X. Quantum Uncertainty Relation Using Coherence. *Phys Rev A* (2017) 96:032313. doi:10.1103/PhysRevA.96.032313
27. Lv W-M, Zhang C, Hu X-M, Cao H, Wang J, Huang Y-F, et al. Experimental Test of the Trade-Off Relation for Quantum Coherence. *Phys Rev A* (2018) 98:062337. doi:10.1103/PhysRevA.98.062337
28. Ding Z-Y, Yang H, Wang D, Yuan H, Yang J, Ye L. Experimental Investigation of Entropic Uncertainty Relations and Coherence Uncertainty Relations. *Phys Rev A* (2020) 101:032101. doi:10.1103/PhysRevA.101.032101

29. Huang H-Y, Kueng R, Preskill J. Predicting many Properties of a Quantum System from Very Few Measurements. *Nat Phys* (2020) 16:1050–7. doi:10.1038/s41567-020-0932-7
30. Winter A, Yang D. Operational Resource Theory of Coherence. *Phys Rev Lett* (2016) 116:120404. doi:10.1103/PhysRevLett.116.120404
31. Bromley TR, Cianciaruso M, Adesso G. Frozen Quantum Coherence. *Phys Rev Lett* (2015) 114:210401. doi:10.1103/PhysRevLett.114.210401
32. Yu X-D, Zhang D-J, Liu CL, Tong DM. Measure-independent Freezing of Quantum Coherence. *Phys Rev A* (2016) 93:060303. doi:10.1103/PhysRevA.93.060303
33. Ma J, Zhou Y, Yuan X, Ma X. Operational Interpretation of Coherence in Quantum Key Distribution. *Phys Rev A* (2019) 99:062325. doi:10.1103/PhysRevA.99.062325
34. Bera MN, Qureshi T, Siddiqui MA, Pati AK. Duality of Quantum Coherence and Path Distinguishability. *Phys Rev A* (2015) 92:012118. doi:10.1103/PhysRevA.92.012118
35. Hillery M. Coherence as a Resource in Decision Problems: The Deutsch-Jozsa Algorithm and a Variation. *Phys Rev A* (2016) 93:012111. doi:10.1103/PhysRevA.93.012111
36. Shi H-L, Liu S-Y, Wang X-H, Yang W-L, Yang Z-Y, Fan H. Coherence Depletion in the Grover Quantum Search Algorithm. *Phys Rev A* (2017) 95:032307. doi:10.1103/PhysRevA.95.032307
37. Liu Y-C, Shang J, Zhang X. Coherence Depletion in Quantum Algorithms. *Entropy* (2019) 21:260. doi:10.3390/e21030260
38. Streltsov A, Adesso G, Plenio MB. Colloquium : Quantum Coherence as a Resource. *Rev Mod Phys* (2017) 89:041003. doi:10.1103/RevModPhys.89.041003
39. Sánches-Ruiz J. Optimal Entropic Uncertainty Relation in Two-Dimensional hilbert Space. *Phys Lett A* (1998) 244:189–95. doi:10.1016/S0375-9601(98)00292-8
40. Horodecki R, Horodecki P, Horodecki M, Horodecki K. Quantum Entanglement. *Rev Mod Phys* (2009) 81:865–942. doi:10.1103/RevModPhys.81.865
41. Brydges T, Elben A, Jurcevic P, Vermersch B, Maier C, Lanyon BP, et al. Probing Rényi Entanglement Entropy via Randomized Measurements. *Science* (2019) 364:260–3. doi:10.1126/science.aau4963
42. Elben A, Kueng R, Huang H-Y, van Bijnen R, Kokail C, Dalmonte M, et al. Mixed-state Entanglement from Local Randomized Measurements. *Phys Rev Lett* (2020) 125:200501. doi:10.1103/PhysRevLett.125.200501
43. Zhang T, Sun J, Fang X-X, Zhang X-M, Yuan X, Lu H. Experimental Quantum State Measurement with Classical Shadows. *Phys Rev Lett* (2021) 127:200501. doi:10.1103/PhysRevLett.127.200501
44. Ding Q-M, Fang X-X, Yuan X, Zhang T, Lu H. Efficient Estimation of Multipartite Quantum Coherence. *Phys Rev Res* (2021) 3:023228. doi:10.1103/PhysRevResearch.3.023228
45. Ding Q-M, Fang X-X, Lu H. The Tightness of Multipartite Coherence from Spectrum Estimation. *Entropy* (2021) 23:1519. doi:10.3390/e23111519

Conflict of Interest: The authors declare that the research was conducted in the absence of any commercial or financial relationships that could be construed as a potential conflict of interest.

frontiers | Frontiers in Physics

ORIGINAL RESEARCH
published: 19 April 2022
doi: 10.3389/fphy.2022.862868

Uncertainty Relations of Non-Hermitian Operators: Theory and Experimental Scheme

*Xinzhi Zhao and Chengjie Zhang**

School of Physical Science and Technology, Ningbo University, Ningbo, China

The theoretical framework for the uncertainty relation of Hermitian operators is perfect and has been applied in many fields. At the same time, non-Hermitian operators are also widely used in some other fields. However, the uncertainty relation of non-Hermitian operators remains to be explored. K.W. Bong and his co-workers proposed the theory of unitary uncertainty relation and verified it in the experiment [Phys. Rev. Lett. 120, 230402 (2018)]. In this work, we generalized this unitary uncertainty relation theory and proposed uncertainty relations of non-Hermitian operators. Due to the difficulties in the direct measurement of non-Hermitian operators in the uncertainty relations, we simplified the uncertainty relation of two non-Hermitian operators with pure states and proposed a realizable experimental measurement scheme by using the Mach–Zehnder interferometer. When the two non-Hermitian operators are unitary, our result can reduce to Bong et al.'s result. Furthermore, for two non-Hermitian operators but not unitary, we obtained a generalized and analogous result of theirs.

Keywords: uncertainty relations, non-Hermitian operators, Mach–Zehnder interferometer, Robertson–Schrödinger uncertainty relations, Heisenberg uncertainty relations

OPEN ACCESS

Edited by:
Ming-Liang Hu,
Xi'an University of Posts and Telecommunications, China

Reviewed by:
Ming Li,
China University of Petroleum, China
Juan He,
Fuyang Normal University, China
Jin-Ming Liu,
East China Normal University, China
Ali Asadian,
Institute for Advanced Studies in Basic Sciences (IASBS), Iran

****Correspondence:***
Chengjie Zhang
chengjie.zhang@gmail.com

Specialty section:
This article was submitted to Quantum Engineering and Technology, a section of the journal Frontiers in Physics

Received: *26 January 2022*
Accepted: *16 March 2022*
Published: *19 April 2022*

Citation:
Zhao X and Zhang C (2022) Uncertainty Relations of Non-Hermitian Operators: Theory and Experimental Scheme. Front. Phys. 10:862868. doi: 10.3389/fphy.2022.862868

1 INTRODUCTION

Uncertainty relations are the basis of quantum theory. It was first proposed by Heisenberg [1] and was rewritten by Kennard [2] and Weyl [3] as the uncertainty relation between position and momentum. Robertson generalized this to any two observables [4]. Schrödinger strengthened the inequality and put forward the Schrödinger uncertainty relation [5] as

$$\langle(\Delta A)^2\rangle\langle(\Delta B)^2\rangle \geq \left|\frac{1}{2}\langle\{A,B\}\rangle - \langle A\rangle\langle B\rangle\right|^2 + \frac{1}{4}|\langle[A,B]\rangle|^2, \tag{1}$$

where $\langle(\Delta O)^2\rangle$ stands for the variance of observable O, $\{A, B\}$ represents the anticommutator of observables A and B, and $[A, B]$ is their commutator. Uncertainty relations have been used in many quantum information tasks, including quantum key distribution [6, 7], deeply quantum systems [8–10], quantum random number generation [11, 12], entanglement witness [13], Einstein–Podolsky–Rosen (EPR) steering [14, 15], quantum metrology [16], and so on.

In quantum theory, we know that those observable measurements of physics are represented by Hermitian operators and can be faithfully represented on measuring instruments. In fact, there are non-Hermitian operators that are not Hermitian conjugated, and these non-Hermitian operators can be observed by weak measurements [17]. Certainly, the measurement of non-Hermitian operators is

not limited to this; weak values of non-Hermitian operators can also be derived from bound state scattering [18]. The problem of eigenvalues of non-Hermitian operators can also be solved by introducing generalized ladder operators [19]. In reality, non-Hermitian operators can be used in many ways such as quantum open systems [20], quantum optics [21], quantum cosmology [22], and many other fields. Furthermore, pseudo-Hermitian operators belong to non-Hermitian operators, which have many applications [23, 24].

The uncertainty relation of unitary operators can reflect the basic characteristics of the quantum world to some extent. In Ref. [25], the authors proposed the uncertainty relation of the unitary operator, satisfying the certain commutative condition in finite dimensions. However, it is not applicable in high dimensions, so Bagchi and Pati put forward the uncertainty relation of general unitary operators, which can be applied to high dimensions [26]. In order to get a more general case, the uncertainty relation of general unitary operators has been experimentally tested [27]. Furthermore, Bong and his co-workers put forward an uncertainty relation: strong unitary and overlap relation, and demonstrated their theory in the experiment [28]. The subtlety of this theory lies in that it greatly simplifies the measurement of the experiment and provides a very valuable experimental idea for reference. In addition, the theory of the strong unitary uncertainty relation has also been discussed in Ref. [29] and has been experimentally realized in Ref. [30].

Unitary operators are a kind of non-Hermitian operators, and the theory about the uncertainty relation of unitary operators has been relatively mature. But what about the uncertainty relations of more general non-Hermitian operators? For non-Hermitian operators, their eigenvalues are complex and cannot be directly observed in experiments. Therefore, we made corresponding changes to the measurement method of non-Hermitian operators. The general derivation of the uncertainty relation of general non-Hermitian operators is given in Ref. [17], but this form lacks experimental protocols to measure this uncertainty relation.

In this study, we proposed uncertainty relations of non-Hermitian operators and designed an experimental scheme to facilitate measurement for two non-Hermitian operators with pure states. The article is organized as follows: First, we briefly proved the uncertainty relation of non-Hermitian operators. Second, we provided an example of the uncertainty relation of two non-Hermitian operators in a pure state, explained how to measure the uncertainty relation of two non-Hermitian operators in an experiment, and proposed a measurement scheme by using the Mach–Zehnder interferometer. Finally, we discussed and summarized the content of the article.

2 UNCERTAINTY RELATIONS FOR NON-HERMITIAN OPERATORS

To propose the uncertainty relation for non-Hermitian operators, we first need to define the variance of a non-Hermitian operator. In Refs. [17, 31], the variance of a non-Hermitian operator O under a state ρ is defined as $\langle(\Delta O)^2\rangle \coloneqq \langle(O^\dagger - \langle O^\dagger\rangle)(O - \langle O\rangle)\rangle = \langle O^\dagger O\rangle - \langle O^\dagger\rangle\langle O\rangle$, where $\langle O\rangle = \mathrm{Tr}(\rho O)$. Based on this definition, we can prove the following uncertainty relation for non-Hermitian operators:

Proposition 1. Two non-Hermitian operators A and B are considered in a d-dimensional Hilbert space; the uncertainty relations for two non-Hermitian operators are

$$\langle(\Delta A)^2\rangle\langle(\Delta B)^2\rangle \geq |\langle A^\dagger B\rangle - \langle A^\dagger\rangle\langle B\rangle|^2, \tag{2}$$

where $\langle(\Delta A)^2\rangle \coloneqq \langle A^\dagger A\rangle - \langle A^\dagger\rangle\langle A\rangle$ and $\langle(\Delta B)^2\rangle \coloneqq \langle B^\dagger B\rangle - \langle B^\dagger\rangle\langle B\rangle$.

Proof. Let us define a 2×2 matrix M as

$$M = \begin{pmatrix} \langle(\Delta A)^2\rangle & \langle A^\dagger B\rangle - \langle A^\dagger\rangle\langle B\rangle \\ \langle B^\dagger A\rangle - \langle B^\dagger\rangle\langle A\rangle & \langle(\Delta B)^2\rangle \end{pmatrix}. \tag{3}$$

Now, let us prove that M is a semi-definite positive matrix. An arbitrary vector $(a,b)^T$ is considered, where a and b are two arbitrary complex numbers; of both numbers, one has

$$\begin{aligned} &(a^\star, b^\star)M\begin{pmatrix} a \\ b \end{pmatrix} \\ &= (a^\star, b^\star)\langle\begin{pmatrix} A^\dagger - \langle A^\dagger\rangle \\ B^\dagger - \langle B^\dagger\rangle \end{pmatrix}(A - \langle A\rangle, B - \langle B\rangle)\rangle\begin{pmatrix} a \\ b \end{pmatrix} \\ &= \langle(a^\star, b^\star)\begin{pmatrix} A^\dagger - \langle A^\dagger\rangle \\ B^\dagger - \langle B^\dagger\rangle \end{pmatrix}(A - \langle A\rangle, B - \langle B\rangle)\begin{pmatrix} a \\ b \end{pmatrix}\rangle \\ &= \langle C^\dagger C\rangle \\ &\geq 0, \end{aligned} \tag{4}$$

where the operator C is defined as

$$C \coloneqq a(A - \langle A\rangle) + b(B - \langle B\rangle). \tag{5}$$

Since for an arbitrary vector $(a,b)^T$, the result $\langle C^\dagger C\rangle$ is always non-negative, and M is semi-definite positive.

If a matrix is semi-definite positive, then its determinant is non-negative. Thus, we have

$$\det(M) \geq 0, \tag{6}$$

with

$$\det(M) = \langle(\Delta A)^2\rangle\langle(\Delta B)^2\rangle - |\langle A^\dagger B\rangle - \langle A^\dagger\rangle\langle B\rangle|^2. \tag{7}$$

Therefore, the uncertainty relations for two non-Hermitian operators (2) have been proved. □

Remark. The uncertainty relation (2) has also been proved in Ref. [17]. When A and B are Hermitian operators, the uncertainty relation (2) reduces to the Schrödinger uncertainty relation (1) since

$$|\langle AB\rangle - \langle A\rangle\langle B\rangle|^2 = \left|\frac{1}{2}\langle\{A,B\}\rangle - \langle A\rangle\langle B\rangle\right|^2 + \frac{1}{4}|\langle[A,B]\rangle|^2$$

holds. Moreover, we generalized proposition 1 to the case of n non-Hermitian operators.

Proposition 2. Consider n non-Hermitian operators $\{A_i\}_{i=1}^n$ in a d-dimensional Hilbert space; the uncertainty relations for n non-Hermitian operators are

$$\det(M) \geq 0, \tag{8}$$

where the matrix M is defined as

$$M_{ij} \coloneqq \langle A_i^\dagger A_j\rangle - \langle A_i^\dagger\rangle\langle A_j\rangle. \tag{9}$$

Proof. The proof is similar to proposition 1. Let us prove that M is a semi-definite positive matrix. An arbitrary vector $(a_1, a_2, \ldots, a_n)^T$ is considered with $\{a_i\}_{i=1}^n$ as arbitrary complex numbers, of which one has

$$(a_1^*, a_2^*, \ldots, a_n^*)M\begin{pmatrix} a_1 \\ a_2 \\ \cdots \\ a_n \end{pmatrix} = (a_1^*, a_2^*, \ldots, a_n^*)$$

$$\left\langle \begin{pmatrix} A_1^\dagger - \langle A_1^\dagger\rangle \\ A_2^\dagger - \langle A_2^\dagger\rangle \\ \cdots \\ A_n^\dagger - \langle A_n^\dagger\rangle \end{pmatrix}(A_1 - \langle A_1\rangle, A_2 - \langle A_2\rangle, \ldots, A_n - \langle A_n\rangle)\right\rangle \begin{pmatrix} a_1 \\ a_2 \\ \cdots \\ a_n \end{pmatrix}$$

$$= \langle (a_1^*, a_2^*, \ldots, a_n^*)\begin{pmatrix} A_1^\dagger - \langle A_1^\dagger\rangle \\ A_2^\dagger - \langle A_2^\dagger\rangle \\ \cdots \\ A_n^\dagger - \langle A_n^\dagger\rangle \end{pmatrix}(A_1 - \langle A_1\rangle, A_2 - \langle A_2\rangle, \ldots, A_n$$

$$-\langle A_n\rangle)\begin{pmatrix} a_1 \\ a_2 \\ \cdots \\ a_n \end{pmatrix}\rangle = \langle C^\dagger C\rangle \geq 0, \tag{10}$$

where the operator C is defined as $C \coloneqq \sum_{i=1}^n a_i(A_i - \langle A_i\rangle)$. Thus, M is semi-definite positive, and $\det(M) \geq 0$ holds. The uncertainty relation still holds for such cases. □

3 UNCERTAINTY RELATIONS FOR TWO NON-HERMITIAN OPERATORS IN PURE STATES

Now, we focused on the uncertainty relations for two non-Hermitian operators (2) in pure states. Two non-Hermitian operators A and B are considered in a d-dimensional Hilbert space; if the state is a pure state $|\phi\rangle$, then

$$\begin{aligned}\langle(\Delta A)^2\rangle &= \langle\phi|A^\dagger A|\phi\rangle - \langle\phi|A^\dagger|\phi\rangle\langle\phi|A|\phi\rangle \\ &= \langle\phi|A^\dagger PA|\phi\rangle,\end{aligned} \tag{11}$$

where P is a project operator defined as $P \coloneqq 1 - |\phi\rangle\langle\phi|$. Similarly, we observed

$$\begin{aligned}\langle(\Delta B)^2\rangle &= \langle\phi|B^\dagger B|\phi\rangle - \langle\phi|B^\dagger|\phi\rangle\langle\phi|B|\phi\rangle \\ &= \langle\phi|B^\dagger PB|\phi\rangle,\end{aligned} \tag{12}$$

and

$$\begin{aligned}|\langle A^\dagger B\rangle - \langle A^\dagger\rangle\langle B\rangle|^2 &= |\langle\phi|A^\dagger B|\phi\rangle - \langle\phi|A^\dagger|\phi\rangle\langle\phi|B|\phi\rangle|^2 \\ &= |\langle\phi|A^\dagger PB|\phi\rangle|^2.\end{aligned} \tag{13}$$

Therefore, the uncertainty relations for two non-Hermitian operators (2) with a pure state $|\phi\rangle$ become

$$\langle\phi|A^\dagger PA|\phi\rangle\langle\phi|B^\dagger PB|\phi\rangle \geq |\langle\phi|A^\dagger PB|\phi\rangle|^2. \tag{14}$$

Moreover, if the dimension of the Hilbert space $d = 2$ (a single qubit system), the rank of P is 1. Thus, P can be rewritten as $P = |\phi_\perp\rangle\langle\phi_\perp|$, where $|\phi_\perp\rangle$ is the orthogonal state of $|\phi\rangle$ in the single qubit system. Thus, the uncertainty relation (14) becomes

$$\begin{aligned}&\langle\phi|A^\dagger|\phi_\perp\rangle\langle\phi_\perp|A|\phi\rangle\langle\phi|B^\dagger|\phi_\perp\rangle\langle\phi_\perp|B|\phi\rangle \\ =\ &|\langle\phi|A^\dagger|\phi_\perp\rangle|^2|\langle\phi|B^\dagger|\phi_\perp\rangle|^2 \\ \geq\ &|\langle\phi|A^\dagger|\phi_\perp\rangle\langle\phi_\perp|B|\phi\rangle|^2.\end{aligned} \tag{15}$$

It is obvious that the " = " always holds in **(15)**.

Based on the aforementioned proof, one can conclude that we can always obtain equality in **(2)** when we only consider pure states in a one-qubit system.

4 TEST UNCERTAINTY RELATION FOR TWO NON-HERMITIAN OPERATORS

The uncertainty relation for two non-Hermitian operators in a one-qubit system is discussed, and the uncertainty relation is experimentally tested *via* weak measurements. Since the variance of a non-Hermitian operator in a state is a concave function of the state, we focused on the uncertainty relation in pure states.

4.1 Theory

Two non-Hermitian operators A and B are considered in a single-qubit system. Suppose the polar decompositions of the non-Hermitian operators A and B are

$$A = S_A U_A, \tag{16}$$

$$B = S_B U_B, \tag{17}$$

where S_A and S_B are two positive semi-definite operators and U_A and U_B are unitary operators. Thus, the variances of A and B in a pure state $|\phi\rangle$ are

$$\begin{aligned}\langle(\Delta A)^2\rangle &= \langle\phi|A^\dagger A|\phi\rangle - \langle\phi|A^\dagger|\phi\rangle\langle\phi|A|\phi\rangle \\ &= \langle\psi|S_A^2|\psi\rangle - \langle\psi|S_A|\phi\rangle\langle\phi|S_A|\psi\rangle,\end{aligned} \tag{18}$$

$$\begin{aligned}\langle(\Delta B)^2\rangle &= \langle\phi|B^\dagger B|\phi\rangle - \langle\phi|B^\dagger|\phi\rangle\langle\phi|B|\phi\rangle \\ &= \langle\chi|S_B^2|\chi\rangle - \langle\chi|S_B|\phi\rangle\langle\phi|S_B|\chi\rangle,\end{aligned} \tag{19}$$

where $|\psi\rangle \coloneqq U_A|\phi\rangle$ and $|\chi\rangle \coloneqq U_B|\phi\rangle$. Moreover, the right hand side of **(2)** becomes

$$\begin{aligned}&|\langle A^\dagger B\rangle - \langle A^\dagger\rangle\langle B\rangle|^2 \\ =\ &|\langle\psi|S_A S_B|\chi\rangle - \langle\psi|S_A|\phi\rangle\langle\phi|S_B|\chi\rangle|^2.\end{aligned} \tag{20}$$

In the following, for the simplicity of experiments, we chose the non-Hermitian operators A and B as

$$A = \sigma_z U_A, \tag{21}$$

$$B = \sigma_x U_B. \tag{22}$$

Thus,

$$\langle(\Delta A)^2\rangle = 1 - \langle\psi|\sigma_z|\phi\rangle\langle\phi|\sigma_z|\psi\rangle, \tag{23}$$

$$\langle(\Delta B)^2\rangle = 1 - \langle\chi|\sigma_x|\phi\rangle\langle\phi|\sigma_x|\chi\rangle, \tag{24}$$

$$\begin{aligned}|\langle A^\dagger B\rangle - \langle A^\dagger\rangle\langle B\rangle|^2 = |&\langle\psi|\sigma_z\sigma_x|\chi\rangle \\ &-\langle\psi|\sigma_z|\phi\rangle\langle\phi|\sigma_x|\chi\rangle|^2.\end{aligned} \tag{25}$$

Now the left hand side of the uncertainty relation (2) becomes

$$\begin{aligned}&\langle(\Delta A)^2\rangle\langle(\Delta B)^2\rangle\\ &= \left(1-\langle\psi|\sigma_z|\phi\rangle\langle\phi|\sigma_z|\psi\rangle\right)\left(1-\langle\chi|\sigma_x|\phi\rangle\langle\phi|\sigma_x|\chi\rangle\right)\\ &= 1-\langle\psi|\sigma_z|\phi\rangle\langle\phi|\sigma_z|\psi\rangle-\langle\chi|\sigma_x|\phi\rangle\langle\phi|\sigma_x|\chi\rangle\\ &\quad+\langle\psi|\sigma_z|\phi\rangle\langle\phi|\sigma_z|\psi\rangle\langle\chi|\sigma_x|\phi\rangle\langle\phi|\sigma_x|\chi\rangle.\end{aligned} \tag{26}$$

Meanwhile, the right hand side of the uncertainty relation (2) becomes

$$\begin{aligned}&|\langle A^\dagger B\rangle-\langle A^\dagger\rangle\langle B\rangle|^2\\ &= |\langle\psi|\sigma_z\sigma_x|\chi\rangle-\langle\psi|\sigma_z|\phi\rangle\langle\phi|\sigma_x|\chi\rangle|^2\\ &= \left(\langle\psi|\sigma_z\sigma_x|\chi\rangle-\langle\psi|\sigma_z|\phi\rangle\langle\phi|\sigma_x|\chi\rangle\right)\left(\langle\chi|\sigma_x\sigma_z|\psi\rangle\right.\\ &\quad\left.-\langle\phi|\sigma_z|\psi\rangle\langle\chi|\sigma_x|\phi\rangle\right)\\ &= \langle\psi|\sigma_z\sigma_x|\chi\rangle\langle\chi|\sigma_x\sigma_z|\psi\rangle-\langle\psi|\sigma_z\sigma_x|\chi\rangle\langle\phi|\sigma_z|\psi\rangle\langle\chi|\sigma_x|\phi\rangle\\ &\quad-\langle\chi|\sigma_x\sigma_z|\psi\rangle\langle\psi|\sigma_z|\phi\rangle\langle\phi|\sigma_x|\chi\rangle\\ &\quad+\langle\psi|\sigma_z|\phi\rangle\langle\phi|\sigma_x|\chi\rangle\langle\phi|\sigma_z|\psi\rangle\langle\chi|\sigma_x|\phi\rangle.\end{aligned} \tag{27}$$

Therefore, the uncertainty relation (2) reduces to

$$\begin{aligned}&\langle\psi|\sigma_z|\phi\rangle\langle\phi|\sigma_z|\psi\rangle+\langle\chi|\sigma_x|\phi\rangle\langle\phi|\sigma_x|\chi\rangle\\ &+\langle\psi|\sigma_z\sigma_x|\chi\rangle\langle\chi|\sigma_x\sigma_z|\psi\rangle-\langle\psi|\sigma_z\sigma_x|\chi\rangle\langle\phi|\sigma_z|\psi\rangle\langle\chi|\sigma_x|\phi\rangle\\ &-\langle\chi|\sigma_x\sigma_z|\psi\rangle\langle\psi|\sigma_z|\phi\rangle\langle\phi|\sigma_x|\chi\rangle\le 1.\end{aligned} \tag{28}$$

Let us define $|\varphi_1\rangle\coloneqq|\phi\rangle$, $|\varphi_2\rangle\coloneqq A|\phi\rangle = \sigma_z|\psi\rangle$, $|\varphi_3\rangle\coloneqq B|\phi\rangle = \sigma_x|\chi\rangle$, and $T_{jk} = \langle\varphi_j|\varphi_k\rangle$; the uncertainty relation (2) becomes

$$|T_{12}|^2+|T_{13}|^2+|T_{23}|^2-T_{23}T_{12}T_{31}-T_{32}T_{21}T_{13}\le 1. \tag{29}$$

Since $T_{32}T_{21}T_{13} = (T_{23}T_{12}T_{31})^*$, we have

$$T_{23}T_{12}T_{31} \coloneqq |T_{23}T_{12}T_{31}|e^{i\Phi}, \tag{30}$$

$$\begin{aligned}\mathrm{Re}\,(T_{23}T_{12}T_{31}) &= \frac{T_{23}T_{12}T_{31}+T_{32}T_{21}T_{13}}{2}\\ &= |T_{23}T_{12}T_{31}|\cos\Phi,\end{aligned} \tag{31}$$

where Φ is the phase of $T_{23}T_{12}T_{31}$, and Re $(T_{23}T_{12}T_{31})$ is the real part of $T_{23}T_{12}T_{31}$. Thus, **Eq. 29** is equivalent to

$$\cos\Phi\ge\frac{|T_{12}|^2+|T_{13}|^2+|T_{23}|^2-1}{2|T_{23}T_{12}T_{31}|}. \tag{32}$$

From $\cos\Phi\le 1$, one has a weaker uncertainty relation of **(32)**,

$$|T_{12}|^2+|T_{13}|^2+|T_{23}|^2-2|T_{23}T_{12}T_{31}|\le 1. \tag{33}$$

Remark. If $A = U_A$ and $B = U_B$, then the uncertainty relations (32) and (33) reduce to the case of unitary operators discussed in Ref. [28]. This theory has a much broader scope and can deal with a wide variety of situations.

4.2 Scheme

Now we discussed how to test the uncertainty relation (32) and its weaker form **(33)** by using the Mach–Zehnder interferometer. According to the theory and measurement ideas proposed by Bong [28] and Nirala [32], the uncertainty relation of non-Hermitian operators can also be expressed by calculating the interference visibility.

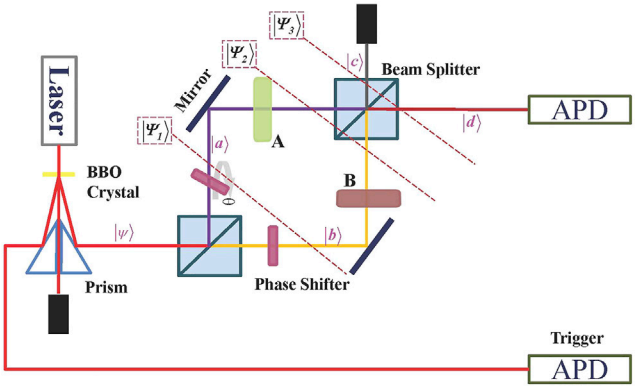

FIGURE 1 | This scheme can test the uncertainty relation for two non-Hermitian operators (*A* and *B*) by using the Mach–Zehnder interferometer. Pairs of single photons are generated using a BBO crystal. The signal single-photon state is prepared in $|\psi\rangle$. After entering a displaced Mach–Zehnder interferometer at a 5050 beam splitter, the photon traverses the interferometer. *B* in the transmitted arm is represented in (*yellow*), and *A* in the reflected arm is represented in (*purple*).

In principle, we can test the uncertainty relation of non-Hermitian operators for any n. Here, we chose a special case of $n = 2$, which requires preparation of a strictly pure state $|\psi\rangle$ and tomographic reconstruction of $|\psi\rangle$, $A|\psi\rangle$, and $B|\psi\rangle$.

Non-Hermitian operators A and B are considered for example. As shown in **Figure 1**, the main component of our setup is the Mach–Zehnder interferometer. For the single-photon source, we have a choice to use a continuous-wave diode laser to pump an optically nonlinear beta barium borate (BBO) crystal. Then, photon pairs are generated by noncollinear type-I spontaneous parametric down-conversion (SPDC). The idler photon (Trigger) heralds the presence of a signal photon. The A and B operators can be implemented by using combinations of optical components in the laboratory such as half-wave plates (HWPs) and quarter-wave plates (QWPs). We used phase shifters on two branches to adjust the optical path difference with a certain angle θ.

It is considered that $|\psi\rangle$ is the input state of the first beam splitter, which is further changed as

$$|\Psi_1\rangle = \frac{1}{\sqrt{2}}\left(ie^{i\theta}|a\rangle+|b\rangle\right)|\psi\rangle, \tag{34}$$

where $|a\rangle$ and $|b\rangle$ are path states corresponding to reflection and transmission, respectively. We placed the optical elements of the operators A and B on the corresponding arms. Before passing through the second beam splitter, the state changes into

$$|\Psi_2\rangle = \frac{1}{\sqrt{2}}\left(ie^{i\theta}A|\psi\rangle|a\rangle+B|\psi\rangle|b\rangle\right). \tag{35}$$

After passing through the second beam splitter, the ports are denoted by $|c\rangle$ and $|d\rangle$. Here, when the two beams finally meet at the beam splitter, there is a phase difference ϵ between the two arms due to propagation. The formation of ϵ is independent of A and B operations.

$$|\Psi_3\rangle = \frac{1}{2}\left(-e^{i\theta}A|\psi\rangle + e^{i\epsilon}B|\psi\rangle\right)|c\rangle + \frac{1}{2}\left(ie^{i\theta}A|\psi\rangle + ie^{i\epsilon}B|\psi\rangle\right)|d\rangle. \tag{36}$$

The detection device is at port $|d\rangle$, which means that what we detected is the component of the total state. This can be carried out by applying the projector $\Pi_d = |d\rangle\langle d|$ to the entire state, so the component of the detection arm state is

$$|\Psi_d\rangle = \Pi_d|\Psi_3\rangle = \frac{1}{2}\left(ie^{i\theta}A|\psi\rangle + ie^{i\epsilon}B|\psi\rangle\right)|d\rangle. \tag{37}$$

Finally, the strength of the detector port is determined by

$$\begin{aligned} N_d &= |\langle d|\Psi_3\rangle|^2 \\ &= \frac{1}{4}\left(\langle A^\dagger A\rangle + \langle B^\dagger B\rangle + e^{i(\epsilon-\theta)}\langle A^\dagger B\rangle + e^{-i(\epsilon-\theta)}\langle B^\dagger A\rangle\right) \\ &= \frac{1}{4}\left(\langle A^\dagger A\rangle + \langle B^\dagger B\rangle + 2|\langle A^\dagger B\rangle|\cos\left(\epsilon-\theta+\varphi_0\right)\right), \end{aligned} \tag{38}$$

where we suppose that $\langle A^\dagger B\rangle = |\langle A^\dagger B\rangle|e^{i\varphi_0}$ and thus $\langle B^\dagger A\rangle = |\langle A^\dagger B\rangle|e^{-i\varphi_0}$.

Hence, we can obtain the interference visibility γ. Based on **Eq. 38**, the maximal and minimal values of N_d can be obtained by varying θ,

$$(N_d)_{max} = \frac{1}{4}\left(\langle A^\dagger A\rangle + \langle B^\dagger B\rangle + 2|\langle A^\dagger B\rangle|\right), \tag{39}$$

$$(N_d)_{min} = \frac{1}{4}\left(\langle A^\dagger A\rangle + \langle B^\dagger B\rangle - 2|\langle A^\dagger B\rangle|\right). \tag{40}$$

The interference visibility γ is defined as

$$\gamma(A,B) \coloneqq \frac{(N_d)_{max} - (N_d)_{min}}{(N_d)_{max} + (N_d)_{min}} = \frac{2|\langle A^\dagger B\rangle|}{\langle A^\dagger A\rangle + \langle B^\dagger B\rangle}. \tag{41}$$

Since $A^\dagger A$ and $B^\dagger B$ are Hermitian operators, these two Hermitian operators can be directly measured by von Neumann measurements. The values of $\langle A^\dagger\rangle$ and $\langle B\rangle$ are similarly determined from the corresponding interference visibilities $\gamma(A, I)$, $\gamma(I, B)$, where I denotes the identity operator. Moreover, when $A = \sigma_z U_A$, $B = \sigma_x U_B$, the interference visibility is given by $\gamma(A, B) = |\langle A^\dagger B\rangle|$. Generally speaking, the expected value that we need to measure is a complex number, it is necessary to measure its real part and imaginary part separately, but it is not usually possible to measure both of them simultaneously. However, our method is to directly measure the modulus of a complex number, and the uncertainty relations (29) and (33) are required to measure the modulus.

5 DISCUSSION AND CONCLUSION

As shown in **Figure 1**, we tested the uncertainty relation of non-Hermitian operators very conveniently. However, this is only a theoretical diagram of the experimental design. If the experimental design scheme is to be applied in real experiments, the Mach–Zehnder interferometer can be displaced by a Sagnac interferometer, which can reduce the influence of the external environment on the experiment.

In conclusion, the uncertainty relation of non-Hermitian operators in any quantum state can be measured. This broadens the practical scope of uncertainty relations, and non-Hermitian operators also have experimentally observable uncertainty relations. The theory would be less restrictive and could be applied to other open systems. In addition, it can be used to solve scattering problems and entanglement problems.

DATA AVAILABILITY STATEMENT

The original contributions presented in the study are included in the article/Supplementary Material; further inquiries can be directed to the corresponding author.

AUTHOR CONTRIBUTIONS

XZ and CZ contributed to the conception and design of the study. XZ wrote the first draft of the manuscript. CZ wrote sections of the manuscript. All authors contributed to manuscript revision, read, and approved the submitted version.

FUNDING

This work is supported by the National Natural Science Foundation of China (Grant No. 11734015) and the K. C. Wong Magna Fund in Ningbo University.

REFERENCES

1. Heisenberg W. Über den anschaulichen Inhalt der quantentheoretischen Kinematik und Mechanik. *Z Physik* (1927) 43:172–98. doi:10.1007/bf01397280
2. Kennard EH. Zur Quantenmechanik Einfacher Bewegungstypen. *Z Physik* (1927) 44:326–52. doi:10.1007/bf01391200
3. Weyl H. *Gruppentheorie und Quantenmechanik*. Leipzig: Hirzel (1928).
4. Robertson HP. The Uncertainty Principle. *Phys Rev* (1929) 34:163–4. doi:10.1103/physrev.34.163
5. Schrödinger E. *Phys Math Kl* (1930) 19:296.
6. Koashi M. Simple Security Proof of Quantum Key Distribution Based on Complementarity. *New J Phys* (2009) 11:045018. doi:10.1088/1367-2630/11/4/045018
7. Berta M, Christandl M, Colbeck R, Renes JM, Renner R. The Uncertainty Principle in the Presence of Quantum Memory. *Nat Phys* (2010) 6:659–62. doi:10.1038/nphys1734
8. Tomamichel M, Renner R. Uncertainty Relation for Smooth Entropies. *Phys Rev Lett* (2011) 106:110506. doi:10.1103/physrevlett.106.110506
9. Wollman EE, Lei CU, Weinstein AJ, Suh J, Kronwald A, Marquardt F, et al. Quantum Squeezing of Motion in a Mechanical Resonator. *Science* (2015) 349:952–5. doi:10.1126/science.aac5138

10. Ding ZY, Huan Y, Dong W, Hao Y, Jie Y, Liu Y. Experimental Investigation of Entropic Uncertainty Relations and Coherence Uncertainty Relations. *Phys Rev A* (2020) 101:032101. doi:10.1103/physreva.101.032101
11. Vallone G, Marangon DG, Tomasin M, Villoresi P. Quantum Randomness Certified by the Uncertainty Principle. *Phys Rev A* (2014) 90:052327. doi:10.1103/physreva.90.052327
12. Zhu C, Hongyi Z, Xiao Y, Xiongfeng M. Source-Independent Quantum Random Number Generation. *Phys Rev X* (2016) 6:011020.
13. Mario B, Patrick JC, Stephanie W. Entanglement-assisted Guessing of Complementary Measurement Outcomes. *Phys Rev A* (2014) 90:062127.
14. Walborn SP, Salles A, Gomes RM, Toscano F, Souto Ribeiro PH. Revealing Hidden Einstein-Podolsky-Rosen Nonlocality. *Phys Rev Lett* (2011) 106:130402. doi:10.1103/physrevlett.106.130402
15. James S, Curtis JB, Stephen PW, Eric GC, John CH. Einstein-Podolsky-Rosen Steering Inequalities from Entropic Uncertainty Relations. *Phys Rev A* (2013) 87:062103.
16. Giovannetti V, Lloyd S, Maccone L. Advances in Quantum Metrology. *Nat Photon* (2011) 5:222–9. doi:10.1038/nphoton.2011.35
17. Pati AK, Singh U, Sinha U. Measuring Non-hermitian Operators via Weak Values. *Phys Rev A* (2015) 92:052120. doi:10.1103/physreva.92.052120
18. Matzkin A. Weak Measurements in Non-hermitian Systems. *J Phys A: Math Theor* (2012) 45:444023. doi:10.1088/1751-8113/45/44/444023
19. l'Yi WS. Non-Hermitian Quantum Canonical Variables and the Generalized Ladder Operators. *Phys Rev A* (1996) 53:1251–6. doi:10.1103/physreva.53.1251
20. Feshbach H. Unified Theory of Nuclear Reactions. *Ann Phys* (1958) 5:357–90. doi:10.1016/0003-4916(58)90007-1
21. Aharonov Y, Massar S, Popescu S, Tollaksen J, Vaidman L. Adiabatic Measurements on Metastable Systems. *Phys Rev Lett* (1996) 77:983–7. doi:10.1103/physrevlett.77.983
22. Rostami T, Jalalzadeh S, Moniz PV. Quantum Cosmological Intertwining: Factor Ordering and Boundary Conditions from Hidden Symmetries. *Phys Rev D* (2015) 92:023526. doi:10.1103/physrevd.92.023526
23. Zhan X, Wang K, Xiao L, Bian Z, Zhang Y, Sanders BC, et al. Experimental Quantum Cloning in a Pseudo-unitary System. *Phys Rev A* (2020) 101:010302. doi:10.1103/physreva.101.010302
24. Chen YC, Gong M, Xue P, Yuan HD, Zhang CJ. Quantum Deleting and Cloning in a Pseudo-unitary System. *Front Phys* (2021) 16:53601. doi:10.1007/s11467-021-1063-z
25. Massar S, Spindel P. Uncertainty Relation for the Discrete Fourier Transform. *Phys Rev Lett* (2008) 100:190401. doi:10.1103/physrevlett.100.190401
26. Bagchi S, Pati AK. Uncertainty Relations for General Unitary Operators. *Phys Rev A* (2016) 94:042104. doi:10.1103/physreva.94.042104
27. Xiao L, Wang K, Zhan X, Bian Z, Li J, Zhang Y, et al. Experimental Test of Uncertainty Relations for General Unitary Operators. *Opt Express* (2017) 25:17904. doi:10.1364/oe.25.017904
28. Bong K-W, Tischler N, Patel RB, Wollmann S, Pryde GJ, Hall MJW. Strong Unitary and Overlap Uncertainty Relations: Theory and Experiment. *Phys Rev Lett* (2018) 120:230402. doi:10.1103/physrevlett.120.230402
29. Bing Y, Naihuan J, Xianqing LJ. Strong Unitary Uncertainty Relations. *Phys Rev A* (2019) 100:022116.
30. Qu D, Wang K, Xiao L, Zhan X, Xue P. Experimental Demonstration of strong Unitary Uncertainty Relations. *Opt Express* (2021) 29:29567. doi:10.1364/oe.438774
31. Anandan J. Geometric Phase for Cyclic Motions and the Quantum State Space Metric. *Phys Lett A* (1990) 147:3–8. doi:10.1016/0375-9601(90)90003-7
32. Nirala G, Sahoo SN, Pati AK, Sinha U. Measuring Average of Non-hermitian Operator with Weak Value in a Mach-Zehnder Interferometer. *Phys Rev A* (2019) 99:022111. doi:10.1103/physreva.99.022111

Conflict of Interest: The authors declare that the research was conducted in the absence of any commercial or financial relationships that could be construed as a potential conflict of interest.

frontiers | Frontiers in Physics

ORIGINAL RESEARCH
published: 27 May 2022
doi: 10.3389/fphy.2022.915863

Finite-Size Scaling on a Digital Quantum Simulator Using Quantum Restricted Boltzmann Machine

Bilal Khalid[1], *Shree Hari Sureshbabu*[2], *Arnab Banerjee*[1] *and Sabre Kais*[3]*

[1]*Department of Physics and Astronomy, Purdue University, West Lafayette, IN, United States,* [2]*Elmore Family School of Electrical and Computer Engineering, Purdue University, West Lafayette, IN, United States,* [3]*Department of Chemistry, Department of Physics and Astronomy and Purdue Quantum Science and Engineering Institute, Purdue University, West Lafayette, IN, United States*

The critical point and the critical exponents for a phase transition can be determined using the Finite-Size Scaling (FSS) analysis. This method assumes that the phase transition occurs only in the infinite size limit. However, there has been a lot of interest recently in quantum phase transitions occurring in finite size systems such as a single two-level system interacting with a single bosonic mode e.g., in the Quantum Rabi Model (QRM). Since these phase transitions occur at a finite system size, the traditional FSS method is rendered inapplicable for these cases. For cases like this, we propose an alternative FSS method in which the truncation of the system is done in the Hilbert space instead of the physical space. This approach has previously been used to calculate the critical parameters for stability and symmetry breaking of electronic structure configurations of atomic and molecular systems. We calculate the critical point for the quantum phase transition of the QRM using this approach. We also provide a protocol to implement this method on a digital quantum simulator using the Quantum Restricted Boltzmann Machine algorithm. Our work opens up a new direction in the study of quantum phase transitions on quantum devices.

Keywords: finite-size scaling, quantum phase transition, quantum simulator, quantum restricted Boltzmann machine, quantum rabi model

OPEN ACCESS

Edited by:
Jun Feng,
Xi'an Jiaotong University, China

Reviewed by:
Shihao Ru,
Xi'an Jiaotong University, China
Xin Wang,
Xi'an Jiaotong University, China
Liming Zhao,
Southwest Jiaotong University, China

***Correspondence:**
Sabre Kais
kais@purdue.edu

Specialty section:
This article was submitted to Quantum Engineering and Technology, a section of the journal Frontiers in Physics

Received: *08 April 2022*
Accepted: *02 May 2022*
Published: *27 May 2022*

Citation:
Khalid B, Sureshbabu SH, Banerjee A and Kais S (2022) Finite-Size Scaling on a Digital Quantum Simulator Using Quantum Restricted Boltzmann Machine. Front. Phys. 10:915863. doi: 10.3389/fphy.2022.915863

1 INTRODUCTION

A phase transition occurs whenever the thermodynamic functions of a system become non-analytic e.g. as a liquid changes into a gas, the density of the system changes discontinuously. If the phase transition occurs at a finite temperature $T \neq 0$, the transition is called a classical phase transition (CPT) as it is dominated by thermal fluctuations. On the other hand, if the transition occurs by tuning some parameter in the system's Hamiltonian as $T \to 0$, it is called a quantum phase transition (QPT) since it is dominated by quantum fluctuations. A CPT appears only when the system is infinite i.e., in the thermodynamic limit [1]. On the other hand, a QPT doesn't necessarily require the thermodynamic limit. Recently there has been a lot of interest in QPTs occurring in finite size light-matter interaction systems [2–7].

Quantum Rabi Model (QRM) describes the interaction of a two-level system with a bosonic field mode (see **Eq. 1** for the Hamiltonian.) This model has gained a lot of significance in the study of ultrastrong light-matter coupling regimes where the so-called counterrotating terms can not be

ignored [8]. Quantum Rabi Model has been shown to exhibit a QPT [2]. Namely, when the energy separation of the two levels in the system Ω becomes infinitely large compared to the frequency of the bosonic mode ω_0, the ground state of the Hamiltonian undergoes a phase transition from a normal phase to a superradiant phase as the light-matter coupling exceeds the critical value. Moreover, the ground state of the Jaynes-Cummings model (JCM) which can be obtained from the QRM by performing the rotating-wave approximation has also been shown to exhibit the normal-superradiant phase transition [3]. Later on, a more general anisotropic QRM in which the rotating and counter-rotating terms can have different coupling strengths was also considered [4]. The QRM and JCM are limiting cases of this model. It was shown that the ground state for this more general case also undergoes the normal-superradiant phase transition. The phase transition in QRM has also been demonstrated experimentally using a $^{171}Yb^{+}$ ion in a Paul trap [7]. This experimental demonstration of a phase transition in a single two-level system has incited a lot of interest since this opens up an avenue for studying critical phenomena in controlled, small quantum systems.

In CPTs and some QPTs (which require $N \to \infty$), a finite-size scaling (FSS) analysis can be done to extract the critical point and the critical exponents of the transition [1, 9]. While this procedure is inapplicable to the QPTs discussed above since these phase transitions occur at a finite system size, the phase transitions in these paradigmatic light-matter interaction models occur only in the limit $\Omega/\omega_0 \to \infty$ and FSS analysis can be done in Ω/ω_0 [2–4] instead. In this paper, however, we propose a different approach to study such phase transitions. We apply the FSS in Hilbert space method [10–15] to the QPT in Quantum Rabi Model. In this approach, the truncation of the system is done not in the physical space but in the Hilbert space. The set of basis states spanning the infinite dimensional Hilbert space is truncated to a finite set and the scaling ansatz is employed in terms of the size of this set. This approach has previously been developed and applied to a single particle in Yukawa potential [11, 13] and the problem of finding electronic structure critical parameters for atomic and molecular systems [10, 12, 14–16].

In recent years, digital and analog quantum simulators have emerged as a promising platform for the simulation of quantum phenomena. Quantum simulators have already been used to study phase transitions using the method of partition function zeros [17] and the Kibble-Zurek mechanism [18, 19]. In this paper, we present a protocol to implement the finite-size scaling method on a digital quantum simulator. We use the Quantum Restricted Boltzmann Machine (QRBM) algorithm to find the critical point of the Quantum Rabi model.

This paper is organized as follows. In **Section 2**, we explain the theory of Quantum Rabi Model, Finite-Size Scaling and the Quantum Restricted Boltzmann Machine. In **Section 3**, we present our results obtained using the exact diagonalization method and QRBM. Finally in **Section 4**, we discuss our results and future prospects of studying quantum phase transitions on quantum devices.

2 THEORY

2.1 Quantum Rabi Model

The QRM describes a two-level system interacting with a bosonic field mode. The Hamiltonian is [2],

$$H_{Rabi} = \frac{\Omega}{2}\sigma_z + \omega_0 a^\dagger a - \lambda\sigma_x\left(a + a^\dagger\right) \tag{1}$$

where we've chosen $\hbar = 1$. Here, σ_z and σ_x are the Pauli Z and X matrices respectively, Ω is the energy separation between the two levels in the system, ω_0 is the frequency of the bosonic mode and λ is the system-environment coupling strength. The parity operator $\Pi = e^{i\pi(a^\dagger a + |\uparrow\rangle\langle\uparrow|)}$ commutes with H_{Rabi}. So, H_{Rabi} has a Z_2 symmetry.

This model has a critical point at $g = 2\lambda/\sqrt{\omega_0\Omega} = g_c = 1$ in the limit $\Omega/\omega_0 \to \infty$ [2]. $\Omega/\omega_0 \to \infty$ is analogous to the thermodynamic limit for this case, and in experiments where Ω/ω_0 has to be finite, we'll observe finite-size effects like in any other phase transition [2]. For $g < 1$, the system is in the *normal phase* and the ground state is $|\phi^0_{np}(g)\rangle = \mathcal{S}[r_{np}(g)]|0\rangle|\downarrow\rangle$ where $\mathcal{S}[x] = \exp[\frac{x}{2}(a^{\dagger 2} - a^2)]$ and $r_{np}(g) = -\frac{1}{4}\ln(1 - g^2)$. The rescaled ground state energy and photon number are $e_G(g) = \frac{\omega_0}{\Omega}\langle H_{Rabi}\rangle = -\omega_0/2$ and $n_G(g) = \frac{\omega_0}{\Omega}\langle a^\dagger a\rangle = 0$ respectively. For $g > 1$, the system is in a *superradiant phase* and the ground state is two-fold degenerate, $|\phi^0_{sp}(g)\rangle = \mathcal{D}[\pm\alpha_g]\mathcal{S}[r_{sp}(g)]|0\rangle|\downarrow^{\pm}\rangle$ here $r_{sp}(g) = -\frac{1}{4}\ln(1 - g^{-4})$ and $\mathcal{D}[\alpha] = \exp[\alpha(a^\dagger - a)]$. $|\downarrow^{\pm}\rangle$ is the negative eigenvalue eigenstate of $\frac{1}{2g^2}\sigma_z \pm \frac{2\lambda\alpha_g}{g^2\Omega}\sigma_x$ where $\alpha_g = \sqrt{\frac{\Omega}{4g^2\omega_0}}(g^4 - 1)$. The rescaled ground state energy and photon number are $e_G(g) = \frac{\omega_0}{\Omega}\langle H_{Rabi}\rangle = -\omega_0(g^2 + g^{-2})/4$ and $n_G(g) = \frac{\omega_0}{\Omega}\langle a^\dagger a\rangle = (g^2 - g^{-2})/4$ respectively.

As shown in **Figures 1A,B**, d^2e_G/dg^2 is discontinuous at $g = g_c = 1$, indicating a continuous phase transition and $n_G = \frac{\omega_0}{\Omega}\langle a^\dagger a\rangle$ is an order parameter for this phase transition. In the *normal phase*, n_G is zero whereas in the *superradiant phase*, Z_2 symmetry is spontaneously broken and n_G becomes non-zero.

We can also write effective low-energy Hamiltonians in both the *normal* and the *superradiant phases*. For $g < 1$, H_{Rabi} can be reduced to the following effective Hamiltonian [2],

$$H_{np} = \omega_0 a^\dagger a - \frac{\omega_0 g^2}{4}\left(a + a^\dagger\right)^2 - \frac{\Omega}{2}. \tag{2}$$

The system's degrees of freedom have been removed by projecting to $|\downarrow\rangle\langle\downarrow|$, since this is a low energy description. Similarly, for $g > 1$ the effective Hamiltonian can be written as [2],

$$H_{sp} = \omega_0 a^\dagger a - \frac{\omega_0}{4g^4}\left(a + a^\dagger\right)^2 - \frac{\Omega}{2}\left(g^2 + g^{-2}\right), \tag{3}$$

where this time around the Hamiltonian has been projected along $|\downarrow^{\pm}\rangle\langle\downarrow^{\pm}|$. In **Section 3**, we'll use H_{np} and H_{sp} to find the critical point of the model.

2.2 Finite-Size Scaling

The FSS method is widely used to determine the critical points and the critical exponents in phase transitions [1]. To demonstrate the method, consider that we have an infinite $2d$ system that undergoes a classical phase transition at a critical temperature $T = T_c$ [9]. Suppose Q is a quantity that becomes singular at $T = T_c$ with some power law behavior

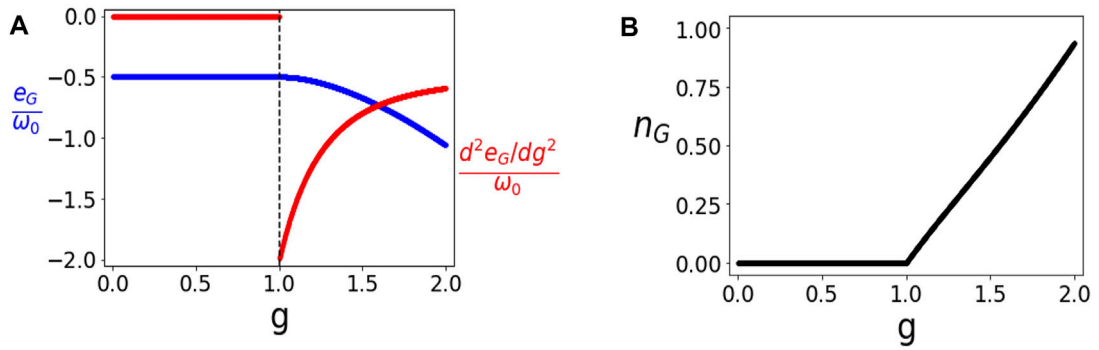

FIGURE 1 | Phase Transition in Quantum Rabi Model. **(A)** The rescaled ground state energy $e_G/\omega_0 = \langle H_{Rabi}\rangle/\Omega$ and $(d^2e_G/dg^2)/\omega_0$ as functions of g. The discontinuity in $(d^2e_G/dg^2)/\omega_0$ at $g = g_c = 1$ indicates a countinuous phase transition. **(B)** The order parameter $n_G = \frac{\omega_0}{\Omega}\langle a^\dagger a\rangle$ as a function of g. n_G becomes non-zero when the Z_2 symmetry is spontaneously broken at $g > g_c = 1$.

$$Q_\infty(T) \sim |T - T_c|^{-\omega}. \tag{4}$$

We can also think of this system as an infinite collection of infinite stripes, where the stripes are infinitely extended along one direction and stacked along the perpendicular direction. Now suppose there are only an N number of stripes. If N is finite, Q should be regular at $T = T_c$ since finite systems cannot have non-analyticities at $T \neq 0$. The singularity at $T = T_c$ should appear only when $N \to \infty$. The finite size scaling hypothesis assumes the existence of a scaling function F_Q such that

$$Q_N(T) \simeq Q_\infty(T) F_Q\left(N/\xi_\infty(T)\right), \tag{5}$$

where Q_N is the observable Q for a system with N stripes and Q_∞ corresponds to the system in the thermodynamic limit. ξ_∞ is the correlation length for the infinite system. **Eq. 5** is valid when N is large. The correlation length also diverges as a power law near the critical point,

$$\xi_\infty(T) \sim |T - T_c|^{-\nu}. \tag{6}$$

Substituting **Eqs 4**, **6** in **Eq. 5**,

$$Q_N(T) \simeq |T - T_c|^{-\omega} F_Q\left(N|T - T_c|^{\nu}\right). \tag{7}$$

Since $Q_N(T)$ should be regular at $T = T_c$, the scaling function should cancel the divergence due to $|T - T_c|^{-\omega}$. Therefore, the scaling function should be of the form $F_Q(x) \sim x^{\omega/\nu}$ as $x \to 0$. We should then have,

$$Q_N(T_c) \sim N^{\omega/\nu}. \tag{8}$$

If we define a function $\Delta_Q(T; N, N')$ such that

$$\Delta_Q(T; N, N') = \frac{\log\left(Q_N(T)/Q_{N'}(T)\right)}{\log\left(N/N'\right)}, \tag{9}$$

then the value of this function at $T = T_c$, $\Delta_Q(T_c; N, N') \simeq \omega/\nu$ is independent of N and N'. Therefore, for three different values N, N' and N'', the curves $\Delta_Q(T; N, N')$ and $\Delta_Q(T; N', N'')$ will intersect at the critical point $T = T_c$. This is how we can locate the critical point using the finite size scaling hypothesis.

We can also find the critical exponents ω and ν. Noting from **Eq. 4** that

$$\frac{\partial Q_\infty(T)}{\partial T} \sim |T - T_c|^{-(\omega+1)}. \tag{10}$$

Therefore, we should have $\Delta_{\partial Q/\partial T}(T_c; N, N') \simeq (\omega + 1)/\nu$. Define a new function $\Gamma_\omega(T; N, N')$ such that

$$\Gamma_\omega(T; N, N') = \frac{\Delta_Q(T; N, N')}{\Delta_{\partial Q/\partial T}(T; N, N') - \Delta_Q(T; N, N')}. \tag{11}$$

The value of this function at the critical point $\Gamma_\omega(T_c; N, N') \simeq \omega$ is independent of N and N' and gives us the critical exponent ω. Then ν can be determined using

$$\nu \simeq \frac{\omega}{\Delta_Q(T_c; N, N')}. \tag{12}$$

As we've already stated in the *Introduction*, this method cannot be used for the kinds of phase transitions we are interested in which occur at a finite system size. However, for such cases we can consider an extension of the approach discussed above [10–16]. In this extended approach, instead of truncating the system in the physical space, the system is truncated in the Hilbert space [16]. The FSS ansatz looks exactly the same except that N now represents the size of the set of basis states which spans the truncated Hilbert space [16]. Moreover, the temperature T will be replaced by the parameter g which is being tuned across the critical point. This approach has been shown by Kais and co-workers to work in the case of a particle in Yukawa potential [11, 13] and the calculation of electronic structure critical parameters for atomic and molecular systems [10, 12, 14–16].

2.3 Quantum Restricted Boltzmann Machine

Solving quantum many-body problems accurately has been a taxing numerical problem since the size of the wavefunction

scales exponentially. The idea of taking advantage of the aspects of Machine Learning (ML) related to dimensionality reduction and feature extraction to capture the most relevant information came from the work by Carleo and Troyer [20], which introduced the idea of representing the many-body wavefunction in terms of an Artificial Neural Network (ANN) to solve for the ground states and time evolution for spin models, with a Restricted Boltzmann Machine (RBM) as the chosen architecture for this ANN. More recently, the critical behavior of the quantum Hall plateau transition based on wavefunctions has been studied in a 2D disordered electron system with the usage of a Convolutional Neural Network (CNN) [21]. However, we focus on using an RBM architecture in this work. An RBM consists of a visible layer and a hidden layer with each neuron in the visible layer connected to all neurons in the hidden layer but the neurons within a layer are not connected to each other. The quantum state is ψ expanded in the basis $|x\rangle$:

$$|\psi\rangle = \sum \psi(x)|x\rangle \tag{13}$$

The Neural Network Quantum State (NQS) [20] describes the wavefunction $\psi(x)$ to be written as $\psi(x;\ \theta)$, where θ represents the parameters of the RBM. $\psi(x;\ \theta)$ is now written in terms of the probability distribution that is obtained from the RBM as follows:

$$\psi(x;\theta) \propto \sum_{\{h\}} e^{\frac{1}{2}\sum_i a_i\sigma_i^z + \sum_j b_j h_j + \sum_{ij} w_{ij}\sigma_i^z h_j} \tag{14}$$

where, σ_i^z is the Pauli z operator at i^{th} site, σ_i^z and h_j take values $\{+1, -1\}$, $\theta = \{a_i, b_j, w_{ij}\}$ are the trainable bias and weight parameters of the RBM. Using stochastic optimization, the energy $E(\theta)$ is minimized.

This work was extended to obtain the ground states of the Bose-Hubbard model [22] and for the application of quantum state tomography [23].

With the rapid developments in the domains of ML and Quantum Computing (QC), the appetite for integrating ideas in both of these areas has been growing considerably. The last decade has seen a surge in the application of classical ML for quantum matter, wherein these methods have been adopted to benchmark, estimate and study the properties of quantum matter [24–27], with recently showing provable classification efficiency in classifying quantum states of matter [28]. RBM based ansätzes have been shown to capture entanglement transitions [29] and using an RBM with local sparse connectivity achieves higher accuracy compared to its dense counterpart when applied to disordered quantum Ising chains [30]. The protocols and algorithms related to ML implementable on a quantum system so-called Quantum machine Learning [31] is expected to have the potential of changing the course of fundamental scientific research [32] along with industrial pursuit.

In lieu of today's Noisy Intermediate Scale Quantum (NISQ) devices, the ideas which utilize both classical and quantum resources, such that the part of the problem which has an exponential scaling is implemented on the quantum platform while the rest are dealt with classically, are being carefully investigated for various applications. Such algorithms are known as classical-quantum hybrid algorithms. In the work by Xia and Kais [33], a modified RBM with three layers was introduced, the third layer to account for the sign of the wavefunction, to solve for the ground state energies of molecules (see **Figure 2**). Now, the parametrized wavefunction $\psi(x;\ \theta)$ is written as a function of $P(x)$ along with a sign function $s(x)$:

$$P(\mathbf{x}) = \frac{\sum_{\{h\}} e^{\sum_i a_i\sigma_i^z + \sum_j b_j h_j + \sum_{ij} w_{ij}\sigma_i^z h_j}}{\sum_{\mathbf{x}'}\sum_{\{h\}} e^{\sum_i a_i\sigma_i^{z'} + \sum_j b_j h_j + \sum_{ij} w_{ij}\sigma_i^{z'} h_j}} \tag{15}$$

$$s(\mathbf{x}) = \tanh\left[\left(c + \sum_i d_i\sigma_i\right)\right] \tag{16}$$

The wavefunction ansatz in terms of the RBM can be expressed as [33]:

$$|\psi\rangle = \sum_x \sqrt{P(x)}s(x)|x\rangle \tag{17}$$

A quantum circuit comprising of a single-qubit (R_y) and multi-qubit y-rotation gates ($C1 - C2 - R_y$) is employed, to sample the Gibbs distribution. The utilization of R_y gates caters to the bias parameter of visible and hidden layers part of the distribution, while $C1 - C2 - R_y$ gates tend to the weights part of the distribution. In the work by Sureshbabu et al. [34], the implementation of such a circuit on IBM-Q devices was shown, wherein a new ancillary qubit is introduced to store the value corresponding to every $C1 - C2 - R_y$ gate (**Figure 3**). The term n denotes the number of visible qubits and m denotes the number of hidden units. In this formalism, the number of ancillary qubits required is $n \times m$. Starting all the qubits from a $|0\rangle$, the R_y and $C1 - C2 - R_y$ rotations are performed, and a measurement is performed on all the qubits. If all the ancillary qubits are in $|1\rangle$, then the sampling is deemed successful and the states corresponding to the first $m + n$ qubits provide the distribution $P(x)$. The joint probability distribution defined over the parameters of the circuit $\theta = \{a, b, w\}$ and a set of $y = \{\sigma^z, h\}$ is given by:

$$P(y,\theta) = \frac{e^{\sum_i a_i\sigma_i^z + \sum_j b_j h_j + \sum_{ij} w_{ij}\sigma_i^z h_j}}{\sum_{\{y\}} e^{\sum_i a_i\sigma_i^{z'} + \sum_j b_j h_j + \sum_{ij} w_{ij}\sigma_i^{z'} h_j}} \tag{18}$$

The probability of successful sampling can be improved by rewriting the distribution $P(y,\ \theta)$ as $Q(y,\ \theta)$ and setting $k = max\left(1, \frac{|w_{ij}|}{2}\right)$[33, 35]:

$$Q(y,\theta) = \frac{e^{\frac{1}{k}\left(\sum_i a_i\sigma_i^z + \sum_j b_j h_j + \sum_{ij} w_{ij}\sigma_i^z h_j\right)}}{\sum_{\{y\}} e^{\frac{1}{k}\left(\sum_i a_i\sigma_i^{z'} + \sum_j b_j h_j + \sum_{ij} w_{ij}\sigma_i^{z'} h_j\right)}} \tag{19}$$

Firstly, the QRBM is implemented classically, i.e., the quantum circuit is simulated on a classical computer. This execution caters to the ideal results that can be obtained through the QRBM algorithm. Then, the quantum circuit is implemented on the Digital Quantum Simulator, the *qasm*

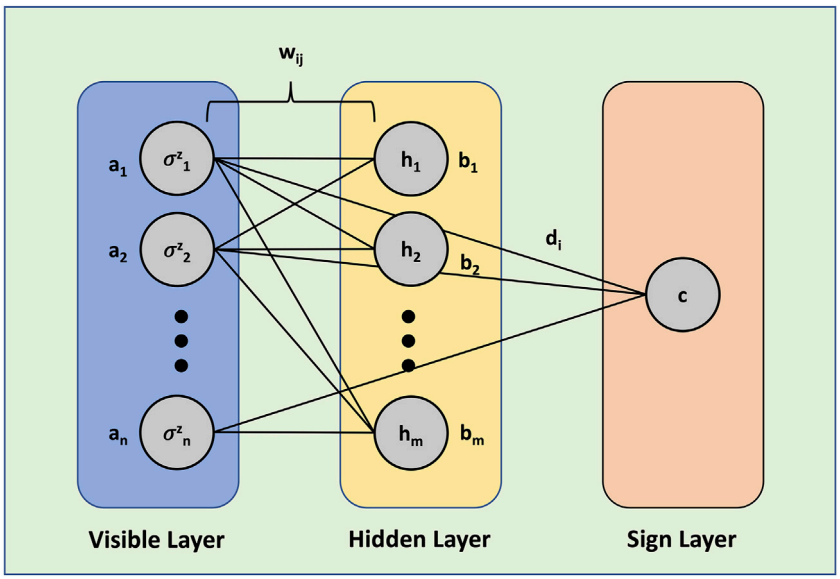

FIGURE 2 | Restricted Boltzmann Machine architecture. The first layer is the visible layer with bias parameters denoted by a_i. The second layer is the hidden layer with bias parameters denoted by b_j. The third layer is the sign layer with bias parameters denoted by c. The weights associated with the connections between the visible neurons and the hidden neurons are designated by w_{ij}. The weights associated with the connections between the visible neurons and the neuron of the sign layer are designated by d_i.

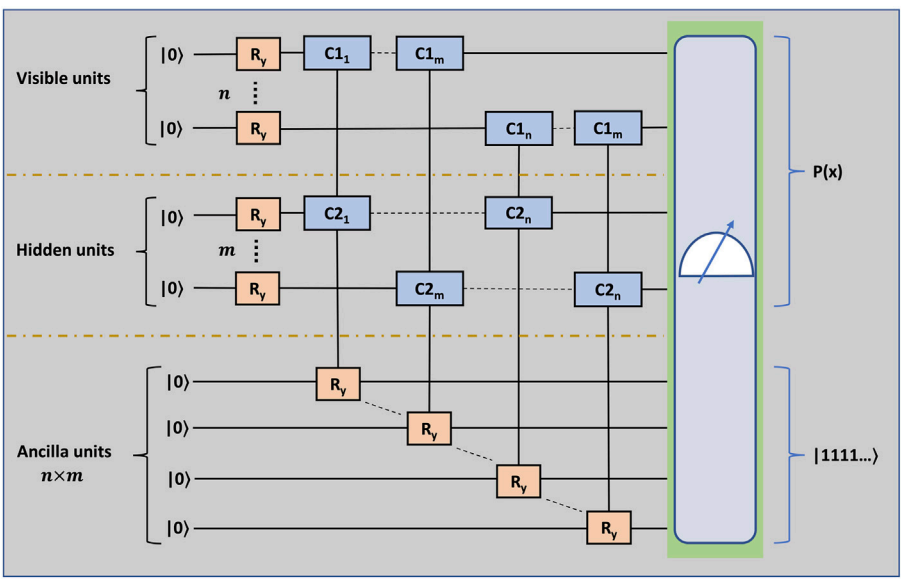

FIGURE 3 | The quantum circuit to sample the Gibbs distribution. n is the number of qubits belonging to the visible layer and m is the number of qubits belonging to the hidden layer. There are $m \times n$ ancillary qubits.

simulation backend. This simulator is part of the high-performance simulators from IBM-Q. The circuit is realized using IBM's Quantum Information Software Toolkit titled Qiskit [36]. Though no noise model was utilized, as a result of finite sampling, statistical fluctuations in the values of probabilities in observing the circuit in the measurement basis, are present in the obtained results.

Having obtained the distribution $Q(y, \theta)$, the probabilities are raised to the power of k, to get $P(y, \theta)$. Following this, the sign function is computed classically, thereby calculating $|\psi\rangle$. Then,

the expectation value for the Hamiltonian H $[\langle\Psi|H|\Psi\rangle]$ is computed to get the energy, which is minimized using gradient descent to obtain the ground state eigenenergy of H.

The resource requirements demanded by this algorithm are quadratic. The number of qubits required are $(m + n)$ to encode the visible and hidden nodes, and $(m \times n)$ to account for the ancillary qubits. Hence, the number of qubits scales as $O(mn)$. The number of R_y gates required are $(m + n)$ and the number of $C1 - C2 - R_y$ gates required are $(m \times n)$. In addition, each $C1 - C2 - R_y$ gate requires $6n$ X-gates to account for all the states spanned by the control qubits. Therefore, the number of gates required also scales as $O(mn)$. Obtaining the ground states or minimum eigenvalues of a given matrix using exact diagonalization has a complexity of $\approx j^3$, with j being the dimension of the column space for the given matrix [37].

3 RESULTS

3.1 Exact Diagonalization

In this section, we demonstrate the calculation of the critical point of the Quantum Rabi model using the Finite-Size Scaling method. As discussed before, the phase transition in QRM occurs only in the limit $\Omega/\omega_0 \to \infty$. This limit is not straightforward to implement in H_{Rabi} given in **Eq. 1**. Instead, we have considered the effective low-energy Hamiltonians H_{np} and H_{sp} given in **Eqs 2**, **3** respectively. In H_{np} and H_{sp}, Ω is involved only in a constant term which can be removed from the Hamiltonians and the limit $\Omega/\omega_0 \to \infty$ can then be easily imposed.

In H_{np} and H_{sp}, the degrees of freedom of the two-level system have been traced out and the only degrees of freedom we have are those of the bosonic mode. Let's first consider the *normal phase* Hamiltonian H_{np}. The Hilbert space for this Hamiltonian is spanned by the familiar harmonic oscillator number states $\{|0\rangle, |1\rangle, |2\rangle, \ldots\}$. We can truncate the full Hilbert space to an N-dimensional Hilbert space spanned by $\{|0\rangle, |1\rangle, \ldots, |N-1\rangle\}$ to apply the finite-size scaling analysis. In this restricted Hilbert space, the matrix form of $H_{np}^{(N)}$ can be found by using $a|m\rangle = \sqrt{m}|m-1\rangle$ and $a^\dagger|m\rangle = \sqrt{m+1}|m+1\rangle$. Once we have the matrix form, we can then use the exact diagonalization method to find the ground state of $H_{np}^{(N)}$ with energy $E_{np}^{(N)}$.

Consider the scaling law for the ground state energy in the vicinity of the critical point $g = g_c$,

$$E(g) \sim |g - g_c|^{\alpha}. \tag{20}$$

Here E is the ground state energy. We slightly modify the formula in **Eq. 9** to take into account the difference in the signs of the exponents in **Eqs 4**, **20**. The new formula with $Q = E$ is,

$$\Delta_{H_{np}}(g; N, N') = \frac{\log\left(E_{np}^{(N)}(g) \Big/ E_{np}^{(N')}(g)\right)}{\log(N'/N)}, \tag{21}$$

We plot the curves $\Delta_{H_{np}}(g; N, N+2)$ for $N = 8, 10, \ldots, 30$ in **Figure 4A**. We then plot the intersection points $g_{np}^{(N)}$ of the curves $\Delta_{H_{np}}(g; N-4, N-2)$ and $\Delta_{H_{np}}(g; N-2, N)$ as a function of N as shown in **Figure 4B**. To find the limit of $g_{np}^{(N)}$ as $N \to \infty$, we used the Bulirsch-Stoer algorithm [44, 45]. The limit was calculated to be $g_{np}^{(N)} \to 0.999996$. So $g_c^{(np)} = 0.999996$.

In a similar way, we then consider H_{sp}. The curves $\Delta_{H_{sp}}(g; N, N+2)$ are plotted in **Figure 4C** for $N = 8, 10, \ldots, 30$ and the intersection points $g_{sp}^{(N)}$ are plotted in **Figure 4D** as a function of N. In this case, the extrapolation to $N \to \infty$ gives the critical value $g_c^{(sp)} = 0.999987$. Both the calculated values of $g_c^{(np)}$ and $g_c^{(sp)}$ are very close to the exact value $g_c = 1$.

3.2 Quantum Restricted Boltzmann Machine

Now we illustrate the implementation of the FSS method using the QRBM algorithm. The results are shown in **Figure 5**. **Figure 5A,C** show the results for H_{np} and H_{sp} using the classical implementation of the algorithm respectively. Whereas, **Figure 5B,D** correspond to the results for H_{np} and H_{sp} when the algorithm is implemented using the *qasm* simulator from IBM-Q respectively. The QRBM algorithm is run for $N = 8$, 10, 12, 14, 16.

For the case of N = 8, the number of qubits associated with the visible nodes equals 3, the number of qubits associated with the hidden nodes equals 3, and 9 ancillary qubits were used. The quantum circuit consists of 6 R_y gates associated with the bias parameters, 9 $C1 - C2 - R_y$ gates associated with the weights. Since, each $C1 - C2 - R_y$ gate requires 6 X-gates, a total of 54 X-gates were used. For the case of N = 10,..,16, the number of qubits associated with the visible nodes equals 4, the number of qubits associated with the hidden nodes equals 4, and 16 ancillary qubits were used. The quantum circuit consists of 8 R_y gates associated with the bias parameters, 16 $C1 - C2 - R_y$ gates associated with the weights. Since, each $C1 - C2 - R_y$ gate requires 6 X-gates, a total of 96 X-gates were used.

Starting from random initialization, all parameters are updated via gradient descent. A learning rate of 0.01 was chosen and the algorithm is run for around 30,000 iterations. In order to assist with the convergence to the minimum eigenenergies, warm starting is employed. The method of warm starting is essentially initializing the parameters of the current point with the parameters of a previously converged point of calculation, which helps in avoiding the convergence to a local minima.

The black curves plotted in the insets in **Figure 5** represent the deviation of the QRBM results (black dashed curves) from the exact diagonalization results (blue solid curves). They were calculated using the average of the quantity $|\Delta^{(ED)}(g) - \Delta^{(QRBM)}(g)/\Delta^{(ED)}(g)| \times 100$ over all the four curves. An enlarged version of the error plots is shown in **Figure 6** can be found in the *Supporting Information* section. For each case the overall error close to $g = 1.000$ is not more than ~ 5% which implies convergence to the right result. Moreover, for the case of H_{sp}, we notice that the error is very small for the classical implementation i.e., ~ < 1% throughout the range of the graph.

The critical point using H_{np} was found to be $g_c^{(np)} = 1.008$ for both the classical and *qasm* implementations. Similarly, the

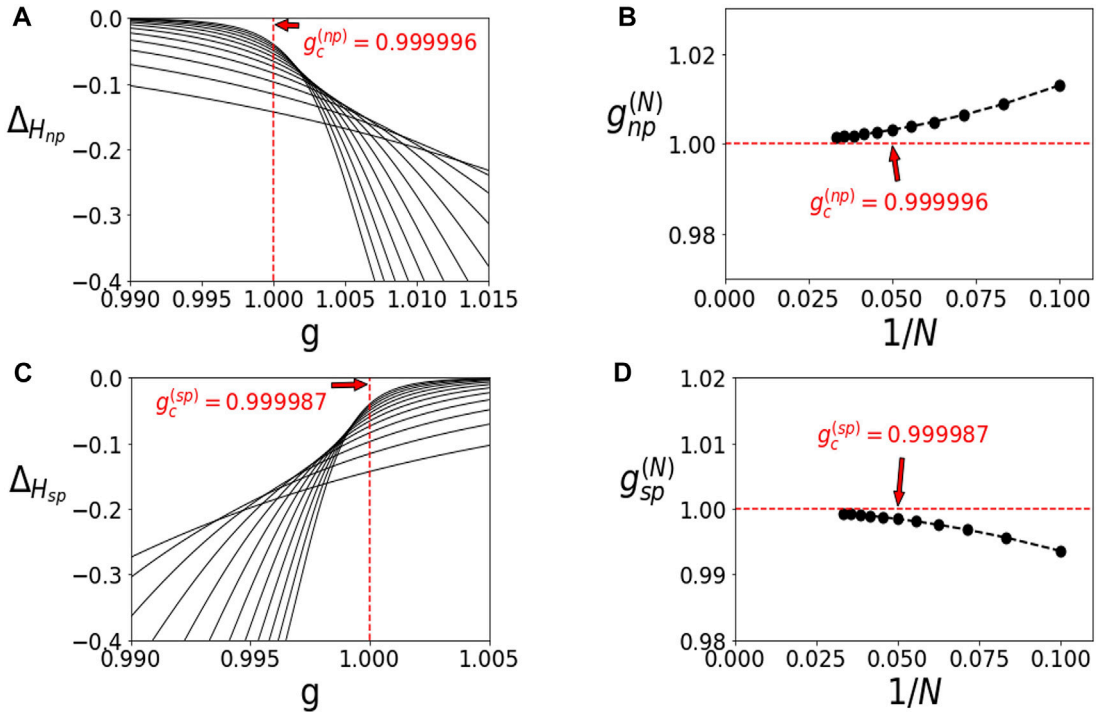

FIGURE 4 | Finite-Size Scaling for Quantum Rabi model**.** We used $N = 8, 10, \ldots, 32$. **(A)** Graphs of $\Delta_{H_{np}}(g; 8, 10)$, $\Delta_{H_{np}}(g; 10, 12), \ldots,$ $\Delta_{H_{np}}(g; 30, 32)$ as a function of g. **(B)** Intersection points $g_{np}^{(N)}$ where $\Delta_{H_{np}}(g_{np}^{(N)}; N-4, N-2) = \Delta_{H_{np}}(g_{np}^{(N)}; N-2, N)$, as a function of $1/N$. As $N \to \infty$, $g_{np}^{(N)} \to 0.999996$. So, $g_c^{(np)} = 0.999996$. **(C)** Graphs of $\Delta_{H_{sp}}(g; 8, 10)$, $\Delta_{H_{sp}}(g; 10, 12), \ldots,$ $\Delta_{H_{sp}}(g; 30, 32)$ as a function of g. **(D)** Intersection points $g_{sp}^{(N)}$ where $\Delta_{H_{sp}}(g_{sp}^{(N)}; N-4, N-2) = \Delta_{H_{sp}}(g_{sp}^{(N)}; N-2, N)$, as a function of $1/N$. As $N \to \infty$, $g_{sp}^{(N)} \to 0.999987$. So, $g_c^{(sp)} = 0.999987$.

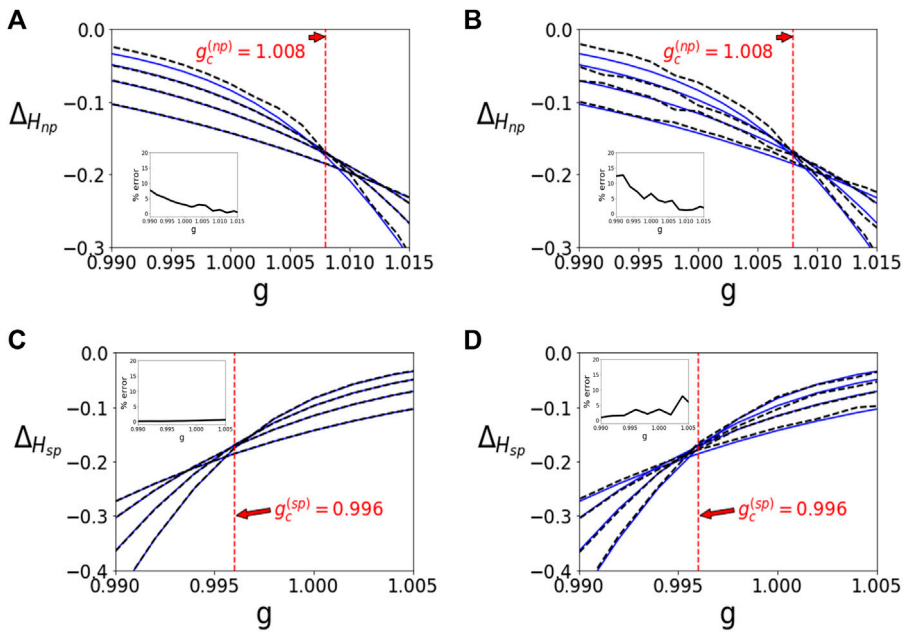

FIGURE 5 | QRBM Implementation of FSS for QRM. The light blue line represents results obtained from exact diagonalization and dashed black line represents QRBM results. **(A)** Classical implementation of QRBM corresponding to normal phase, graphs of $\Delta_{H_{np}}(g; 8, 10)$, $\Delta_{H_{np}}(g; 10, 12), \ldots,$ $\Delta_{H_{np}}(g; 14, 16)$ as a function of g. **(B)** QRBM implemented on *qasm* simulator corresponding to normal phase, graphs of $\Delta_{H_{np}}(g; 8, 10)$, $\Delta_{H_{np}}(g; 10, 12), \ldots,$ $\Delta_{H_{np}}(g; 14, 16)$ as a function of g. The $g_c^{(np)}$ in both the cases is calculated to be 1.008. **(C)** Classical implementation of QRBM corresponding to superradiant phase, graphs of $\Delta_{H_{sp}}(g; 8, 10)$, $\Delta_{H_{sp}}(g; 10, 12), \ldots,$ $\Delta_{H_{sp}}(g; 14, 16)$ as a function of g. **(D)** QRBM implemented on *qasm* simulator corresponding to superradiant phase, graphs of $\Delta_{H_{sp}}(g; 8, 10)$, $\Delta_{H_{sp}}(g; 10, 12), \ldots,$ $\Delta_{H_{sp}}(g; 14, 16)$ as a function of g. The $g_c^{(sp)}$ in both the cases is calculated to be 0.996. The inset plots display the mean percentage error between the exact diagonalization results and QRBM results.

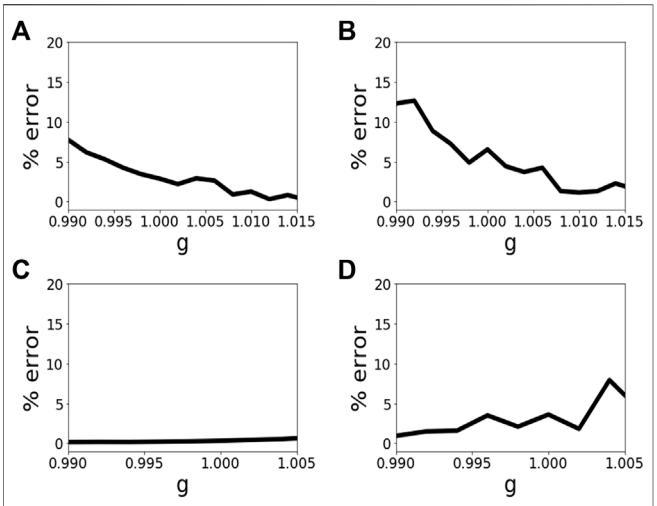

FIGURE 6 | Error plots from the insets of **Figure 5**. **(A–D)** are the insets shown in **Figures 5A–D** respectively.

critical point for the case of H_{sp} was found to be $g_c^{(sp)} = 0.996$ for both the classical and *qasm* implementations. Here we notice that although, the convergence for the data obtained from both the classical and *qasm* implementations turns out to be the same for both H_{np} and H_{sp}, such a perfect match appears to be somewhat coincidental. Here, again the Bulirsch-Stoer algorithm [44, 45] which sets the criteria used to deduce these convergence results. The convergence plots are shown in **Figure 7** have been added to the *Supporting Information* section.

4 DISCUSSION AND OUTLOOK

In this paper, we have used the Finite-Size Scaling in Hilbert Space approach to calculate the critical point of the Quantum Rabi Model. We used the low-energy effective Hamiltonians for both the normal and superradiant phases respectively to show that the critical point is $g_c \approx 1$. The original FSS approach in which the truncation is done in the physical space has been widely used to calculate critical points and critical exponents since its inception. However, that approach was not applicable to Quantum Phase Transitions which occur at a finite system size. With the rise in interest in QPTs occurring in these finite size systems, our approach provides a natural extension of the original FSS method to study such phase transitions. To our knowledge, this is the first time this approach has been used to study a QPT in a light-matter interaction system.

We have also provided a recipe for the implementation of this method on a universal quantum computer using the Quantum Restricted Boltzmann Machine algorithm. It was shown that results obtained from the classical gate simulation match those obtained from the IBM-Q's *qasm* simulator. Such an implementation scales quadratically while the exact diagonalization scales cubically in the best case and exponentially in the worst case. Looking forward, we are interested in applying this approach to other QPTs such as the QPT in anisotropic QRM. We would also like to use our method to calculate the critical exponents in addition to the critical points in these phase transitions. It would also be interesting to see if this approach can be used to predict any new phase transition for some other non-integrable model.

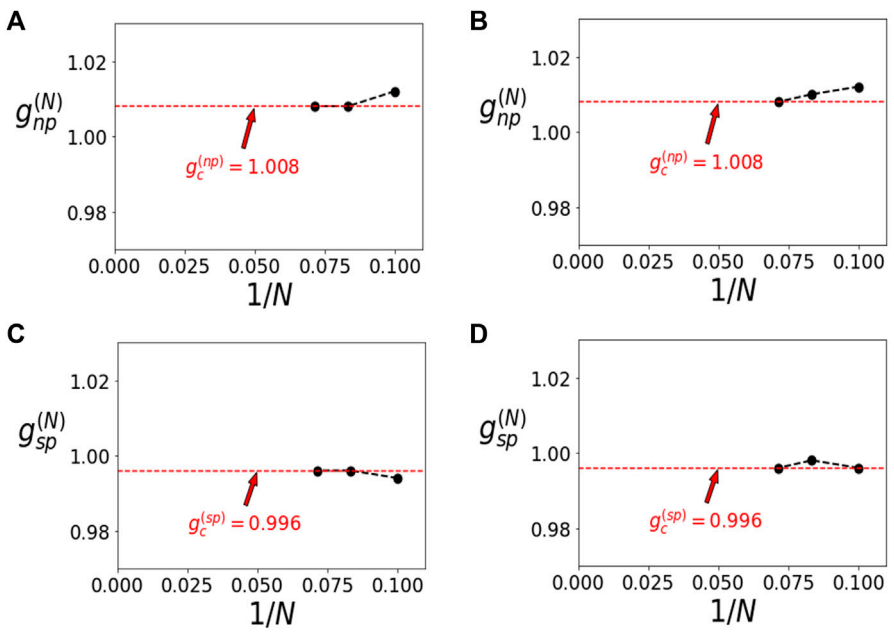

FIGURE 7 | Convergence diagrams for results in **Figure 5**. **(A–D)** correspond to convergence results for data in **Figures 5A–D** respectively. The same procedure was used as the one shown in **Figures 4B,D**.

Another very promising research direction is to implement the FSS method for phase transitions in classically intractable many-body models such as exotic electronic and magnetic systems. These include general quantum materials, for example where Coulomb potential leads to a gapped spectrum in energy, including in direct band-gap semiconductors in the thermodynamic limit. Conventionally speaking, it might be necessary to resort to the original finite-size scaling in the physical space approach for these systems since they exhibit criticality only in the limit $N \to \infty$. However, the ground state of an appropriately truncated Hamiltonian could be deduced using the QRBM algorithm as shown in the paper towards efficient implementation on a digital quantum simulator. A simile can also be drawn between a many-body bulk gap separating a continuum of excited states from the ground state manifold to the gapped Rabi model discussed in this paper. Such an approach can be useful in emergent topological systems, such as in Weyl semimetals, 1-D Kitaev spin chains, quantum spin liquids, and others, on which there is a tremendous explosion of interest [38–43]. Topological phase transitions are devoid of any conventional order parameter and a quantum solution deriving from the approach outlined in this paper can help us bypass resource and scaling limitations of DMRG and exact diagonalization approaches to calculate the critical point and the critical exponents.

DATA AVAILABILITY STATEMENT

The original contributions presented in the study are included in the article/Supplementary Material, further inquiries can be directed to the corresponding author.

AUTHOR CONTRIBUTIONS

SK and AB designed the research problem, BK and SS performed the calculations, all authors discussed the results and wrote the paper.

ACKNOWLEDGMENTS

We acknowledge funding by the US Department of Energy, Office of Science, National Quantum Information Science Research Centers, Quantum Science Center.

REFERENCES

1. Goldenfeld N. *Lectures on Phase Transitions and the Renormalization Group; Frontiers in Physics*. Addison-Wesley Publishing Company (1992).
2. Hwang M-J, Puebla R, Plenio MB. Quantum Phase Transition and Universal Dynamics in the Rabi Model. *Phys Rev Lett* (2015) 115:180404. doi:10.1103/physrevlett.115.180404
3. Hwang M-J, Plenio MB. Quantum Phase Transition in the Finite Jaynes-Cummings Lattice Systems. *Phys Rev Lett* (2016) 117:123602. doi:10.1103/physrevlett.117.123602
4. Liu M, Chesi S, Ying Z-J, Chen X, Luo H-G, Lin H-Q. Universal Scaling and Critical Exponents of the Anisotropic Quantum Rabi Model. *Phys Rev Lett* (2017) 119:220601. doi:10.1103/physrevlett.119.220601
5. Hwang M-J, Rabl P, Plenio MB. Dissipative Phase Transition in the Open Quantum Rabi Model. *Phys Rev A* (2018) 97:013825. doi:10.1103/physreva.97.013825
6. Xie Y-F, Chen X-Y, Dong X-F, Chen Q-H. First-order and Continuous Quantum Phase Transitions in the Anisotropic Quantum Rabi-Stark Model. *Phys Rev A* (2020) 101:053803. doi:10.1103/physreva.101.053803
7. Cai M-L, Liu Z-D, Zhao W-D, Wu Y-K, Mei Q-X, Jiang Y, et al. Observation of a Quantum Phase Transition in the Quantum Rabi Model with a Single Trapped Ion. *Nat Commun* (2021) 12:1126. doi:10.1038/s41467-021-21425-8
8. Forn-Díaz P, Lamata L, Rico E, Kono J, Solano E. Ultrastrong Coupling Regimes of Light-Matter Interaction. *Rev Mod Phys* (2019) 91:025005. doi:10.1103/revmodphys.91.025005
9. Derrida B, Seze LD. In Application of the Phenomenological Renormalization to Percolation and Lattice Animals in Dimension 2. In: JL CARDY, editor. *Current Physics–Sources and Comments*, 2. Elsevier (1988). p. 275–83. doi:10.1016/b978-0-444-87109-1.50024-8
10. Neirotti JP, Serra P, Kais S. Electronic Structure Critical Parameters from Finite-Size Scaling. *Phys Rev Lett* (1997) 79:3142–5. doi:10.1103/physrevlett.79.3142
11. Serra P, Neirotti JP, Kais S. Finite-size Scaling Approach for the Schrödinger Equation. *Phys Rev A* (1998) 57:R1481–R1484. doi:10.1103/physreva.57.r1481
12. Serra P, Neirotti JP, Kais S. Electronic Structure Critical Parameters for the Lithium Isoelectronic Series. *Phys Rev Lett* (1998) 80:5293–6. doi:10.1103/physrevlett.80.5293
13. Serra P, Neirotti JP, Kais S. Finite Size Scaling in Quantum Mechanics. *J Phys Chem A* (1998) 102:9518–22. doi:10.1021/jp9820572
14. Kais S, Serra P. Quantum Critical Phenomena and Stability of Atomic and Molecular Ions. *Int Rev Phys Chem* (2000) 19:97–121. doi:10.1080/014423500229873
15. Shi Q, Kais S. Finite Size Scaling for Critical Parameters of Simple Diatomic Molecules. *Mol Phys* (2000) 98:1485–93. doi:10.1080/00268970009483354
16. Kais S, Serra P. Finite-Size Scaling for Atomic and Molecular Systems. *Adv Chem Phys* (2003) 125:1–99. doi:10.1002/0471428027.ch1
17. Francis A, Zhu D, Huerta Alderete C, Johri S, Xiao X, Freericks JK, et al. Many-body Thermodynamics on Quantum Computers via Partition Function Zeros. *Sci Adv* (2021) 7:eabf2447. doi:10.1126/sciadv.abf2447
18. Keesling A, Omran A, Levine H, Bernien H, Pichler H, Choi S, et al. Quantum Kibble–Zurek Mechanism and Critical Dynamics on a Programmable Rydberg Simulator. *Nature* (2019) 568:207–11. doi:10.1038/s41586-019-1070-1
19. Dupont M, Moore JE. *Quantum Criticality Using a Superconducting Quantum Processor* (2021). *arXiv:2109.10909*.
20. Carleo G, Troyer M. Solving the Quantum many-body Problem with Artificial Neural Networks. *Science* (2017) 355:602–6. doi:10.1126/science.aag2302
21. Li Z, Luo M, Wan X. Extracting Critical Exponents by Finite-Size Scaling with Convolutional Neural Networks. *Phys Rev B* (2019) 99:075418. doi:10.1103/physrevb.99.075418
22. Saito H. Solving the Bose-Hubbard Model with Machine Learning. *J Phys Soc Jpn* (2017) 86:093001. doi:10.7566/jpsj.86.093001
23. Torlai G, Mazzola G, Carrasquilla J, Troyer M, Melko R, Carleo G. Neural-network Quantum State Tomography. *Nat Phys* (2018) 14:447–50. doi:10.1038/s41567-018-0048-5
24. Carrasquilla J, Melko RG. Machine Learning Phases of Matter. *Nat Phys* (2017) 13:431–4. doi:10.1038/nphys4035
25. Deng D-L, Li X, Das Sarma S. Machine Learning Topological States. *Phys Rev B* (2017) 96:195145. doi:10.1103/physrevb.96.195145
26. Butler KT, Davies DW, Cartwright H, Isayev O, Walsh A. Machine Learning for Molecular and Materials Science. *Nature* (2018) 559:547–55. doi:10.1103/physrevb.96.195145
27. Carleo G, Cirac I, Cranmer K, Daudet L, Schuld M, Tishby N, et al. Machine Learning and the Physical Sciences. *Rev Mod Phys* (2019) 91:045002. doi:10.1103/revmodphys.91.045002

28. Huang H-Y, Kueng R, Torlai G, Albert VV, Preskill J. *Provably Efficient Machine Learning for Quantum many-body Problems* (2021). *arXiv preprint arXiv:2106.12627*.
29. Medina R, Vasseur R, Serbyn M. Entanglement Transitions from Restricted Boltzmann Machines. *Phys Rev B* (2021) 104:104205. doi:10.1103/physrevb.104.104205
30. Pilati S, Pieri P. Simulating Disordered Quantum Ising Chains via Dense and Sparse Restricted Boltzmann Machines. *Phys Rev E* (2020) 101:063308. doi:10.1103/PhysRevE.101.063308
31. Biamonte J, Wittek P, Pancotti N, Rebentrost P, Wiebe N, Lloyd S. Quantum Machine Learning. *Nature* (2017) 549:195–202. doi:10.1038/nature23474
32. Sajjan M, Li J, Selvarajan R, Sureshbabu SH, Kale SS, Gupta R, et al. *Quantum Computing Enhanced Machine Learning for Physico-Chemical Applications* (2021). *arXiv preprint arXiv:2111.00851*.
33. Xia R, Kais S. Quantum Machine Learning for Electronic Structure Calculations. *Nat Commun* (2018) 9:4195–6. doi:10.1038/s41467-018-06598-z
34. Sureshbabu SH, Sajjan M, Oh S, Kais S. Implementation of Quantum Machine Learning for Electronic Structure Calculations of Periodic Systems on Quantum Computing Devices. *J Chem Inf Model* (2021) 61(6):2667–2674. doi:10.1021/acs.jcim.1c00294
35. Sajjan M, Sureshbabu SH, Kais S. Quantum Machine-Learning for Eigenstate Filtration in Two-Dimensional Materials. *J Am Chem Soc* (2021) 143:18426–45. doi:10.1021/jacs.1c06246
36. Aleksandrowicz G, Alexander T, Barkoutsos P, Bello L, Ben-Haim Y, Bucher D, et al. Qiskit: An Open-Source Framework for Quantum Computing. *Zenodo* (2019) 16:11. doi:10.5281/zenodo.2562111
37. Harris CR, Millman KJ, van der Walt S, Gommers R, Virtanen P, Cournapeau D, et al. Array Programming with NumPy. *Nature* (2020) 585:357–62. doi:10.1038/s41586-020-2649-2
38. Satzinger KJ, Liu YJ, Smith A, Knapp C, Newman M, Jones C, et al. Realizing Topologically Ordered States on a Quantum Processor. *Science* (2021) 374:1237–41. doi:10.1126/science.abi8378
39. Kitaev A. Anyons in an Exactly Solved Model and beyond. *Ann Phys* (2006) 321:2–111. January Special Issue. doi:10.1016/j.aop.2005.10.005
40. Liu Y-J, Shtengel K, Smith A, Pollmann F. *Methods for Simulating String-Net States and Anyons on a Digital Quantum Computer*. *arXiv:2110.02020* 2021.
41. Xiao X, Freericks JK, Kemper AF. Determining Quantum Phase Diagrams of Topological Kitaev-Inspired Models on NISQ Quantum Hardware. *Quantum* (2021) 5:553. doi:10.22331/q-2021-09-28-553
42. Wen X-G. Colloquium: Zoo of Quantum-Topological Phases of Matter. *Rev Mod Phys* (2017) 89:041004. doi:10.1103/revmodphys.89.041004
43. Hasan MZ, Kane CL. Colloquium: Topological Insulators. *Rev Mod Phys* (2010) 82:3045–67. doi:10.1103/revmodphys.82.3045
44. Bulirsch R, Stoer J. Numerical Treatment of Ordinary Differential Equations by Extrapolation Methods. *Numer Math* (1966) 8:1–13. doi:10.1007/bf02165234
45. Henkel M, Schutz G. Finite-lattice Extrapolation Algorithms. *J Phys A: Math Gen* (1988) 21:2617–33. doi:10.1088/0305-4470/21/11/019

Conflict of Interest: The authors declare that the research was conducted in the absence of any commercial or financial relationships that could be construed as a potential conflict of interest.

Publisher's Note: All claims expressed in this article are solely those of the authors and do not necessarily represent those of their affiliated organizations, or those of the publisher, the editors and the reviewers. Any product that may be evaluated in this article, or claim that may be made by its manufacturer, is not guaranteed or endorsed by the publisher.

APPENDIX A:

Bulirsch-Stoer Algorithm

For $h_N = 1/N$ where $N = 0, 1, 2, \ldots$, the Bulirsch-Stoer algorithm can be used to find the limit of a function $T(h_N)$ as $N \to \infty$[44,45]. For demonstration, consider that we only have $T(h_N)$ for $N = 0, 1, 2, 3$, then the following rows are computed successively,

0	$T_0^{(0)}$		$T_0^{(1)}$		$T_0^{(2)}$	$T_0^{(3)}$
1		$T_1^{(0)}$		$T_1^{(1)}$	$T_1^{(2)}$	
2			$T_2^{(0)}$		$T_2^{(1)}$	
3				$T_3^{(0)}$		

using the following rules

$$T_{-1}^{(N)} = 0 \tag{22}$$

$$T_0^{(N)} = T(h_N) \tag{23}$$

$$T_{m\geq 1}^{(N)} = T_{m-1}^{(N+1)} + \left(T_{m-1}^{(N+1)} - T_{m-1}^{(N)}\right)\left[\left(\frac{h_N}{h_{N+m}}\right)^{\omega}\left(1 - \frac{T_{m-1}^{(N+1)} - T_{m-1}^{(N)}}{T_{m-1}^{(N+1)} - T_{m-2}^{(N+1)}}\right) - 1\right]^{-1} \tag{24}$$

where ω is a free parameter determined by minimizing $\varepsilon_m^{(i)} = |T_m^{(i+1)} - T_m^{(i)}|$. The final answer is $T_3^{(0)}$.

frontiers | Frontiers in Physics

ORIGINAL RESEARCH
published: 08 June 2022
doi: 10.3389/fphy.2022.896164

Unextendible Entangled Bases With a Fixed Schmidt Number Based on Generalized Weighing Matrices

Yuan-Hong Tao[1,2], *Xin-Lei Yong*[2], *Ya-Ru Bai*[1], *Dan-Ni Xu*[1] *and Shu-Hui Wu*[1]*

[1]Department of Big Data, School of Science, Zhejiang University of Science and Technology, Hangzhou, China, [2]Department of Mathematics, College of Sciences, Yanbian University, Yanji, China

We systematically study the constructions of unextendible entangled bases with a fixed Schmidt number k (UEB*k*) in a bipartite system $\mathbb{C}^d \otimes \mathbb{C}^{d'}$. Motivated by the methods of [J. Phys. A 52 : 375,303, 2019], we construct (*dd*' – *v*)-member UEB*k*s in $\mathbb{C}^d \otimes \mathbb{C}^{d'}$ by using generalized weighing matrices and thus generalize the results of [arXiv: 1909.10043, 2020]. We also present the corresponding expressions of our constructions and graphically illustrate UEB3s in $\mathbb{C}^5 \otimes \mathbb{C}^6$ and $\mathbb{C}^6 \otimes \mathbb{C}^6$.

Keywords: unextendible entangled bases with a fixed schmidt number k, quantum entanglement, Schmidt number, generalized weighing matrix, entangled bases with a fixed Schmidt number

OPEN ACCESS

Edited by:
Ming-Liang Hu,
Xi'an University of Posts and Telecommunications, China

Reviewed by:
Bin Chen,
Tianjin Normal University, China
Yu Guo,
Shanxi Datong University, China
Mao-Sheng Li,
South China University of Technology, China

****Correspondence:***
Shu-Hui Wu
wushuhui12@126.com

Specialty section:
This article was submitted to Quantum Engineering and Technology, a section of the journal Frontiers in Physics

Received: *14 March 2022*
Accepted: *19 April 2022*
Published: *08 June 2022*

Citation:
Tao Y-H, Yong X-L, Bai Y-R, Xu D-N and Wu S-H (2022) Unextendible Entangled Bases With a Fixed Schmidt Number Based on Generalized Weighing Matrices. Front. Phys. 10:896164. doi: 10.3389/fphy.2022.896164

1 INTRODUCTION

Entanglement is an essential resource of quantum information processing, and it presents the nature of quantum mechanics [1, 2]. It is also related to some fundamental problems in quantum mechanics such as reality and non-locality [3, 4]. Quantum entanglement has significant applications in many fields such as quantum teleportation [5], quantum dense coding [6], quantum tomography [7], and the mean kings problem [8].

In order to characterize quantum entanglement, the analysis of various bases in the state space has attracted extensive attention in recent years. The notion of unextendible product basis (UPB) in multipartite quantum systems has been deeply studied. The member of a UPB is not perfectly distinguishable by local positive-operator-valued measurements and classical communication, which shows the non-locality without entanglement [9]. As the generalization of UPB, the notion of unextendible maximally entangled basis (UMEB) has been proposed [10]. Since then, many results of UMEBs in arbitrary bipartite spaces are established: no UMEB in $\mathbb{C}^2 \otimes \mathbb{C}^2$, 6-member UMEB in $\mathbb{C}^3 \otimes \mathbb{C}^3$, 12-member UMEB in $\mathbb{C}^4 \otimes \mathbb{C}^4$ [10], 30-member UMEB in $\mathbb{C}^6 \otimes \mathbb{C}^6$ [11], d^2-member UMEB in $\mathbb{C}^d \otimes \mathbb{C}^{d'}$ $(d'/2 < d < d')$, and qd^2-member UMEB in $\mathbb{C}^d \otimes \mathbb{C}^{d'}$ $(d' = qd + r, 0 < r < d)$ [12–14] and different members of UMEBs in $\mathbb{C}^{pd} \otimes \mathbb{C}^{qd'}$ $(p \le q)$ [15–18].

In [19], Guo first proposed the unextendible entangled basis with a fixed Schmidt number k (UEB*k*) in $\mathbb{C}^d \otimes \mathbb{C}^{d'}$ $(2 \le k < d < d')$; thereafter, the concepts and constructions of entangled basis with Schmidt number k (EB*k*) and special entangled basis with Schmidt number k (SEB*k*) have been presented successively [20]. Later, Guo also generalized the construction of UEB*k* from bipartite systems to multipartite quantum systems [21].

Li *et al* [22] first constructed the SEB*k*s in $\mathbb{C}^d \otimes \mathbb{C}^{d'}$ via some generalized weighing matrices, which is a breakthrough structure for *dd*' is not the multiple of *k*. Furthermore, Wang [23] combines the decomposition of the whole matrix space and generalized weighing matrices to consrtuct the SUEB*k*s, which provides a useful way to construct different members of UEB*k*s in $\mathbb{C}^d \otimes \mathbb{C}^{d'}$, but it still has some imperfections and unmentioned issues, such as the bounds of the space dimension, the order, and the concrete mathematical expression of the UEB*k*s.

In this paper, we mainly focus on the construction of UEB*k*s in bipartite systems. Motivatied by the method of [22, 23], using generalized weighing matrices, we provide flexible and diverse constructions of different members of UEB*k*s. We first introduce some related notions and terminologies; then, we propose three different ways to construct $(dd' - v)$-member UEB*k*s in $\mathbb{C}^d \otimes \mathbb{C}^{d'}$ and present the corresponding mathematical expressions. We also give some examples of UEB3 in $\mathbb{C}^5 \otimes \mathbb{C}^6$ and $\mathbb{C}^6 \otimes \mathbb{C}^6$.

2 PRELIMINARIES

In order to better comprehend the notion of UEB*k* in $\mathbb{C}^d \otimes \mathbb{C}^{d'}$, we first introduce the concept of EB*k* and SEB*k* in $\mathbb{C}^d \otimes \mathbb{C}^{d'}$. In the sequel, we always assume that $d \le d'$.

The Schmidt number of a bipartite pure state $|\phi\rangle \in \mathbb{C}^d \otimes \mathbb{C}^{d'}$, denoted by $Sr(|\phi\rangle)$, is defined as the length of its Schmidt decomposition: if its Schmidt decomposition is $|\phi\rangle = \sum_{n=0}^{k-1} \lambda_n |e_n\rangle |e_n'\rangle$, then its Schmidt number is k, that is, $Sr(|\phi\rangle) = k$. It is clear that $Sr(|\phi\rangle) = rank(\rho_1) = rank(\rho_2)$, where ρ_i denotes the reduced state of the ith part of $\rho = |\phi\rangle\langle\phi|$. If an orthonormal basis is constructed by such $|\phi_i\rangle$s, then it is called an entangled basis with Schmidt number k (EBk) [20]. Particularly, if it is an EBk and all the Schmidt coefficients of $\{|\phi_i\rangle\}$s equal to $\frac{1}{\sqrt{k}}$, then it is called a special entangled basis with Schmidt number k (SEBk). It is obvious that SEBk becomes a product basis (PB) when $k = 1$ and a maximally entangled basis (MEB) when $k = d$.

A set of states $\{|\phi_i\rangle \in \mathbb{C}^d \otimes \mathbb{C}^{d'} : i = 1, 2, \ldots, m, m < dd'\}$ is called an m-number unextendible entangled bases with Schmidt number k (UEBk) [19] if and only if

(i) $Sr(|\phi_i\rangle) = k$ and $|\phi_i\rangle$, $i = 1, 2, \ldots, m$ are all entangled states;
(ii) $\langle\phi_i|\phi_j\rangle = \delta_{ij}$;
(iii) if $\langle\phi_i|\psi\rangle = 0$ for all $i = 1, 2, \ldots, m$, then $Sr(|\phi_i\rangle) \ne k$.

Actually, there is a similar concept in matrix spaces [20]. Let $\{|k\rangle\}$ and $\{|\ell'\rangle\}$ be the standard computational bases of $\mathbb{C}^d$ and $\mathbb{C}^{d'}$, respectively, and $\{|\phi_i\rangle\}_{i=1}^{dd'}$ be an orthonormal basis of $\mathbb{C}^d \otimes \mathbb{C}^{d'}$. Let $M_{d\times d'}$ be the Hilbert space of all $d \times d'$ complex matrices equipped with the inner product defined by $\langle A|B\rangle = \mathrm{Tr}(A^\dagger B)$ for any $A, B \in M_{d\times d'}$. If $\{A_i\}_{i=1}^{dd'}$ constitutes a Hilbert–Schmidt basis of $M_{d\times d'}$, where $\langle A_i|A_j\rangle = d\delta_{ij}$, then there is a one-to-one correspondence between $\{|\phi_i\rangle\}$ and $\{A_i\}$ as follows [20]:

$$|\phi_i\rangle = \sum_{k,\ell} a_{kl}^{(i)} |k\rangle|\ell'\rangle \in \mathbb{C}^d \otimes \mathbb{C}^{d'} \quad \Leftrightarrow \quad A_i = \left[\sqrt{d}\, a_{k\ell}^{(i)}\right] \in \mathcal{M}_{d\times d'},$$
$$Sr(|\phi_i\rangle) = rank(A_i), \qquad \langle\phi_i|\phi_j\rangle = \frac{1}{d}\mathrm{Tr}\left(A_i^\dagger A_j\right), \tag{1}$$

A set of $d \times d'$ complex matrices $\{A_i : i = 1, 2, \ldots, n, n \le dd'\}$ is called an unextendible rank-k Hilbert–Schmidt basis of $M_{d\times d'}$ [24] if and only if

(*i*) rank $(A_i) = k$ for any i;
(*ii*) $\mathrm{Tr}(A_i^\dagger A_j) = \delta_{i,j}$;
(*iii*) if $\mathrm{Tr}(A_i^\dagger B) = 0$, $i = 1, 2, \ldots, n$, then $rank(B) \ne k$.

It turns out that $\{A_i : rank(A_i) = k\}$ is an unextendible Hilbert–Schmidt basis of $M_{d\times d'}$ if and only if $\{\phi_i\}$ is a UEBk of $\mathbb{C}^d \otimes \mathbb{C}^{d'}$. Therefore, the UEB$k$ problem is equivalent to the unextendible rank-k Hilbert–Schmidt basis of the associated matrix space.

We next introduce the definition and properties of a generalized weighing matrix, which has been effectively used to construct SEBks in $\mathbb{C}^d \otimes \mathbb{C}^{d'}$ [22]. As a continuation, we will use it to construct UEBks in $\mathbb{C}^d \otimes \mathbb{C}^{d'}$ in this paper.

Definition 1: [22] A generalized weighing matrix is a square $a \times a$ matrix A all of whose non-zero entries are nth roots of unity such that $AA^\dagger = kI_a$. It follows that $1/\sqrt{k}\ A$ is a unitary matrix so that $AA^\dagger = kI_a$ and every row and column of A has exactly k non-zero entries. k is called the weight, and n is called the order of A. Denoting the set of all such generalized weighing matrices by $W(n, k, a)$.

It is worth noting that the generalized weight matrix does not always exist; for the existence and detailed discussion of the generalized weight matrix, we can refer to Ref. [22].

Lemma 1: [22] Let a, b be two positive integers with a great common divisor being g. For any integers d, $d' \ge \max\{a, b\}$, if $g|dd'$, then dd' can be written as $dd' = sa + pb$, where $s, p \in \mathbb{N}$.

3 THREE KINDS OF ($DD' - V$)-MEMBER UEB*KS*

Let $M_{d\times d'}$ be the Hilbert space of all $d \times d'$ complex matrices, V be a subspace of $M_{d\times d'}$ such that each matrix in V is a $d \times d'$ matrix ignoring v elements, depending on the position occupied by the ignored v elements: 1) all the ignored elements occupy N columns, 2) all the ignored elements occupy N rows, and 3) all the ignored elements occupy rows and columns; we construct three kinds of $(dd' - v)$-member UEBks.

3.1 All the Ignored Elements Occupy *N* Columns

In this section, we first construct the $(dd' - v)$-member UEBk in $\mathbb{C}^d \otimes \mathbb{C}^{d'}$, in which all the v ignored elements occupied N columns in the matrix, and then present some examples of UEB3s in $\mathbb{C}^5 \otimes \mathbb{C}^6$.

Theorem 1: Let k be a positive integer, $b, n \in \mathbb{N}$ such that $W(n, k, b)$ is non-empty, and $\gcd(k, b) = 1$ (the greatest common divisor of k and b). Let V be a subspace of $M_{d\times d'}$ such that each matrix in V is a $d \times d'$ matrix ignoring v elements which occupied N rows with $N = 1, \ldots, k-1$ and $d - N \ge b$ and $dd' - v = s \cdot k + p \cdot b$ with $1 \le v \le d'N$. If $\min\{d, d'\} \ge \max\{k, b\}$, then there exists $dd' - v$ member UEBk in $\mathbb{C}^d \otimes \mathbb{C}^{d'}$.

Proof. First, for different values of p and s, we construct different pure states as follows: when $p \ge 1$ and $s \ge 1$, set

$$|\phi_{m,l}\rangle = \begin{cases} \frac{1}{\sqrt{k}}\sum_{u=0}^{k-1}\xi_k^{mu}|r_{lk+u}\rangle, & 0\leqslant l\leqslant s-1, \\ \frac{1}{\sqrt{k}}\sum_{u=1}^{b}x_{ij}^{(t)}|r_{sk-1+(l-s)b+u}\rangle, & s\leqslant l\leqslant s+p-1, \end{cases} \tag{2}$$

when $s = 0$, $p \geq 1$, set

$$|\phi_{m,l}\rangle = \frac{1}{\sqrt{k}}\sum_{u=1}^{b}x_{ij}^{(t)}|r_{sk-1+(l-s)b+u}\rangle, \quad 0\leqslant l\leqslant p-1, \tag{3}$$

when $p = 0$, $s \geq 1$, set

$$|\phi_{m,l}\rangle = \frac{1}{\sqrt{k}}\sum_{u=0}^{k-1}\xi_k^{mu}|r_{lk+u}\rangle, \quad 0\leqslant l\leqslant s-1, \tag{4}$$

where $\xi_k = e^{\frac{2\pi\sqrt{-1}}{k}}$, $m = 0, 1, \ldots, k-1$; $x_{i,j}^{(t)}$ means the t ($0 \leq t \leq b-1$) row of the generalized weights matrix $W(n, k, b)$, and $sk-1+(l-s)b+u = c\cdot(d-N+1)+e = f\cdot d'+g$; $l\cdot k+u = c\cdot(d-N+1)+e = f\cdot d'+g$ with $0 \leq e < d$, $0 \leq g < d'$. Also,

$$|r_{lk+u}\rangle = |e\oplus_{(d-N+1)}\sum_{i=0}^{\alpha}C_i\oplus_{(d-N+1)}C\left(e\oplus_{(d-N+1)}\sum_{i=0}^{\alpha}C_i, g\right)\rangle|g'\rangle, \quad 0\leq\alpha\leq\nu, \tag{5}$$

with

$$C\left(e\oplus_{(d-N+1)}\sum_{i=0}^{\alpha}C_i, g\right) = \begin{cases} 1, & C\left(e\oplus_{(d-N+1)}\sum_{i=0}^{\alpha}C_i, g\right) = C_\alpha, \\ 0, & otherwise, \end{cases} \tag{6}$$

where $C_0 = 0$, $C_\alpha = 1$ denotes the ignored elements.

We next prove that all the above $\{|\phi_{m,l}\rangle\}$ constitute a $dd' - \nu$ ($1 \leq \nu \leq d'N$)-member UEBk in $\mathbb{C}^d \otimes \mathbb{C}^{d'}$:

(i) It is clear that $Sr(|\phi_l\rangle) = k$ for any l, m, t.
(ii) Orthogonality.

According to the construction given by the above expression, the elements of each state lie in different rows and columns, so the proof of the orthogonality is as follows:

$$\langle\phi_{\tilde{m},l}|\phi_{m,l}\rangle = \frac{1}{k}\sum_{\tilde{u}=0}^{k-1}\sum_{u=0}^{k-1}\xi_k^{ml}\xi_k^{\widetilde{-m\tilde{l}}}\langle r_{\tilde{l}k+u}|r_{lk+u}\rangle = \frac{1}{k}\sum_{u=0}^{k-1}\xi_k^{ml-m\tilde{l}}\delta_{l\tilde{l}} = \delta_{m\tilde{m}}\delta_{l\tilde{l}},$$

$$\langle\phi_{\tilde{t},l}|\phi_{t,l}\rangle = \frac{1}{k}\sum_{\tilde{u}=0}^{p-1}\sum_{u=0}^{p-1}x_{ij}^{(\tilde{t})}x_{ij}^{(t)}\langle r_{sk-1+(\tilde{l}-s)b+u}|r_{sk-1+(l-s)b+u}\rangle = \frac{1}{k}\sum_{u=0}^{p-1}\delta_{t\tilde{t}}\delta_{l\tilde{l}} = \delta_{t\tilde{t}}\delta_{l\tilde{l}},$$

$$\langle\phi_{\tilde{m},l}|\phi_{t,l}\rangle = \frac{1}{k}\sum_{\tilde{u}=0}^{k-1}\sum_{u=0}^{p-1}\xi_k^{\widetilde{-m\tilde{l}}}x_{ij}^{(t)}\langle r_{\tilde{l}k+u}|r_{sk-1+(l-s)b+u}\rangle = \frac{1}{k}\sum_{\tilde{u}=0}^{k-1}\sum_{u=0}^{p-1}\delta_{\tilde{\xi},x}\delta_{l\tilde{l}} = \delta_{\tilde{\xi},x}\delta_{l\tilde{l}}.$$

(iii) Unextendibility.

It is obvious that there are no UEBk in $V^{\perp}$ since $N < k$.

In order to understand the above structure more intuitively, we give the following examples to illustrate it.

Example 1: Constructing 26-member UEB3 in $\mathbb{C}^5 \otimes \mathbb{C}^6$.

As $d = 5$, $d' = 6$, $k = 3$, $n = 2$, $b = \nu = 4$, and $5\times 6-4 = 26 = 6\times 3+2\times 4$, $s = 6$, $p = 2$, $0 \leq l \leq 7$ and

$$W(2,3,4) = \begin{pmatrix} 0 & 1 & 1 & 1 \\ 1 & 0 & -1 & 1 \\ 1 & 1 & 0 & -1 \\ 1 & -1 & 1 & 0 \end{pmatrix} \tag{7}$$

According to the proof of Theorem 1, we have the following pure states:

$$\begin{aligned} &|\phi_{m,0}\rangle = \tfrac{1}{\sqrt{3}}(\xi_3^0|r_0\rangle + \xi_3^m|r_1\rangle + \xi_3^{2m}|r_2\rangle); \\ &\vdots \\ &|\phi_{m,5}\rangle = \tfrac{1}{\sqrt{3}}(\xi_3^0|r_{15}\rangle + \xi_3^m|r_{16}\rangle + \xi_3^{2m}|r_{17}\rangle); \\ &|\phi_{t,6}\rangle = \tfrac{1}{\sqrt{3}}(x_{t,0}^{(t)}|r_{18}\rangle + x_{t,1}^{(t)}|r_{19}\rangle + x_{t,2}^{(t)}|r_{20}\rangle) + x_{t,3}^{(t)}|r_{21}\rangle; \\ &|\phi_{t,7}\rangle = \tfrac{1}{\sqrt{3}}(x_{t,0}^{(t)}|r_{22}\rangle + x_{t,1}^{(t)}|r_{23}\rangle + x_{t,2}^{(t)}|r_{24}\rangle) + x_{t,3}^{(t)}|r_{25}\rangle; \end{aligned}$$

where $m = 0, 1, 2$, $t = 0, 1, 2, 3$.

As $C_0 = 0$, $C_1 = C(4,4) = 1$, $C_2 = C(4,2) = 1$, $C_3 = C(4,4) = 1$, $C_4 = C(4,3) = 1$,

$\alpha = 0$, $|r_i\rangle = |e\oplus_5 C(e, g)|g'\rangle$;

$\alpha = 1$, $|r_i\rangle = |e\oplus_5 C_1\oplus_5 C(e\oplus_5 C_1, g)|g'\rangle$;

$\alpha = 2$, $|r_i\rangle = |e\oplus_5(C_1+C_2)\oplus_5 C(e\oplus_5(C_1+C_2), g)|g'\rangle$;

$\alpha = 3$, $|r_i\rangle = |e\oplus_5(C_1+C_2+C_3)\oplus_5 C(e\oplus_5(C_1+C_2+C_3), g)|g'\rangle$;

$\alpha = 4$, $|r_i\rangle = |e\oplus_5(C_1+C_2+C_3+C_4)\oplus_5 C(e\oplus_5(C_1+C_2+C_3+C_3), g)|g'\rangle$;

Taking specific values into the above formula, the 26-member UEB3 in $\mathbb{C}^5 \otimes \mathbb{C}^6$ can be expressed as follows:

$$\begin{cases} |\phi_{0,1,2}\rangle = \frac{1}{\sqrt{3}}(|00'\rangle + \alpha|11'\rangle + \alpha^2|22'\rangle), \\ |\phi_{3,4,5}\rangle = \frac{1}{\sqrt{3}}(|33'\rangle + \alpha|04'\rangle + \alpha^2|15'\rangle), \\ |\phi_{6,7,8}\rangle = \frac{1}{\sqrt{3}}(|20'\rangle + \alpha|31'\rangle + \alpha^2|02'\rangle), \\ |\phi_{9,10,11}\rangle = \frac{1}{\sqrt{3}}(|13'\rangle + \alpha|24'\rangle + \alpha^2|35'\rangle), \\ |\phi_{12,13,14}\rangle = \frac{1}{\sqrt{3}}(|40'\rangle + \alpha|01'\rangle + \alpha^2|12'\rangle), \\ |\phi_{15,16,17}\rangle = \frac{1}{\sqrt{3}}(|23'\rangle + \alpha|34'\rangle + \alpha^2|05'\rangle), \end{cases} \quad \begin{cases} |\phi_{18}\rangle = \frac{1}{\sqrt{3}}(|21'\rangle + |32'\rangle + |03'\rangle), \\ |\phi_{19}\rangle = \frac{1}{\sqrt{3}}(|10'\rangle - |32'\rangle + |03\rangle), \\ |\phi_{20}\rangle = \frac{1}{\sqrt{3}}(|10'\rangle + |21'\rangle - |03'\rangle), \\ |\phi_{21}\rangle = \frac{1}{\sqrt{3}}(|10'\rangle - |21'\rangle + |32'\rangle), \\ |\phi_{22}\rangle = \frac{1}{\sqrt{3}}(|25'\rangle + |30'\rangle + |41'\rangle), \\ |\phi_{23}\rangle = \frac{1}{\sqrt{3}}(|14'\rangle - |30'\rangle + |41'\rangle), \\ |\phi_{24}\rangle = \frac{1}{\sqrt{3}}(|14'\rangle + |25'\rangle - |41'\rangle), \\ |\phi_{25}\rangle = \frac{1}{\sqrt{3}}(|14'\rangle - |25'\rangle + |30\rangle), \end{cases} \tag{8}$$

where $\alpha = 1$, ω, ω^2 and $\omega = e^{\frac{2\pi\sqrt{-1}}{3}}$.

The following chart is indeed the space decomposition of the space of the coefficient matrices, whose first column and first row represent the bases of the previous space and latter space, respectively. The stars represent the ignored elements, and the same number or alphabet in **Table 1** together constitutes a state in UEB3.

Example 2: Constructing 29,28,25,24-member UEB3s in $\mathbb{C}^5 \otimes \mathbb{C}^6$.

Similar to the analysis in Example 1, we only present the chart of corresponding matrix to represent the structure of UEB3s.

Considering the following matrices,

$$V_1 = \begin{pmatrix} 0&0&0&0&0&0 \\ 0&0&0&0&0&0 \\ 0&0&0&0&0&0 \\ 0&0&0&0&0&0 \\ 0&0&0&0&0&\star \end{pmatrix}, \quad V_2 = \begin{pmatrix} 0&0&0&0&0&0 \\ 0&0&0&0&0&0 \\ 0&0&0&0&0&0 \\ 0&0&0&0&0&0 \\ 0&0&0&0&\star&\star \end{pmatrix}. \tag{9}$$

$$V_3 = \begin{pmatrix} 0&0&0&0&0&0\\ 0&0&0&0&0&0\\ 0&0&0&0&0&0\\ 0&0&0&0&0&0\\ 0&\star&\star&\star&\star&\star \end{pmatrix}. \quad V_4 = \begin{pmatrix} 0&0&0&0&0&0\\ 0&0&0&0&0&0\\ 0&0&0&0&0&0\\ 0&0&0&0&0&0\\ \star&\star&\star&\star&\star&\star \end{pmatrix}. \quad (10a)$$

the specific UEB3s of V_1, V_2, V_3, V_4 are shown in **Table 2-5** respectively.

3.2 All the Ignored Elements Occupy *N* Rows

In this section, we first construct the $(dd' - v)$-member UEBk in $\mathbb{C}^d \otimes \mathbb{C}^{d'}$, in which all the v ignored elements occupied N rows in the matrix, and then present some examples of UEB3s also in $\mathbb{C}^5 \otimes \mathbb{C}^6$.

Theorem 2: Let k be a positive integer, $b, n \in \mathbb{N}$ such that $W(n, k, b)$ is non-empty, and $\gcd(k, b) = 1$. Let V be a subspace of $M_{d\times d'}$ such that each matrix in V is a $d \times d'$ matrix ignoring v elements which occupied N rows with $N = 1, \ldots, k-1$, $d' - N \geq b$ and $dd' - v = s \cdot k + p \cdot b$ with $1 \leq v \leq dN$. If $\min\{d, d'\} \geq \max\{k, b\}$, then there exists $dd' - v$ $(1 \leq v \leq dN)$-member UEBk in $\mathbb{C}^d \otimes \mathbb{C}^{d'}$.

Proof. First, for different values of p and s, we construct different pure states as follows: if $p \geq 1$ and $s \geq 1$, let

$$|\phi_{m,l}\rangle = \begin{cases} \frac{1}{\sqrt{k}}\sum_{u=0}^{k-1}\xi_k^{mu}|r_{lk+u}\rangle, & 0 \leqslant l \leqslant s-1, \\ \frac{1}{\sqrt{k}}\sum_{u=1}^{b}x_{ij}^{(t)}|r_{sk-1+(l-s)b+u}\rangle, & s \leqslant l \leqslant s+p-1. \end{cases} \quad (10b)$$

if $s = 0$, $p \geq 1$, let

$$|\phi_{m,l}\rangle = \frac{1}{\sqrt{k}}\sum_{u=1}^{b}x_{ij}^{(t)}|r_{sk-1+(l-s)b+u}\rangle, \quad 0 \leqslant l \leqslant p-1, \quad (11)$$

if $p = 0$, $s \geq 1$, let

$$|\phi_{m,l}\rangle = \frac{1}{\sqrt{k}}\sum_{u=0}^{k-1}\xi_k^{mu}|r_{lk+u}\rangle, \quad 0 \leqslant l \leqslant s-1. \quad (12)$$

where $\xi_k = e^{\frac{2\pi\sqrt{-1}}{k}}$; $m = 0, 1, \ldots, k-1$; $x_{i,j}^{(t)}$ means the t $(0 \leq t \leq b-1)$ row in the generalized weights matrix $W(n, k, b)$, and $sk - 1 + (l-s)b + u = c \cdot d + e$; $l \cdot k + u = c \cdot d + e$ with $0 \leq e < d$,

$$|r_{lk+u}\rangle = |e\rangle|\left(c \oplus_{(d'-N+1)} e \oplus_{(d'-N+1)} C\left(e, c \oplus_{(d'-N+1)} e\right) + \beta\right)'\rangle, \quad (13)$$

with

$$C\left(e, c \oplus_{(d'-N+1)} e\right) = \begin{cases} 1, & C(e, c \oplus_{(d'-N+1)} e = C_\alpha, \\ 0, & otherwise, \end{cases} \quad (14)$$

where $C_0 = 0$, $C_\alpha = 1$ denotes the ignored elements. It is worthy of note that β in **formula (13)** is a regulating term, $\beta = 0$ in the common cases, $\beta = 1$ if $|e\rangle|c \oplus_{(d'-N+1)} e\rangle$ coincides with the previous answer of **formula (13)**.

Similiar to Theorem 1, we can prove that $\{|\phi_{m,l}\rangle\}$ constitute $dd' - v$ $(1 \leq v \leq dN)$-member UEBks in $\mathbb{C}^d \otimes \mathbb{C}^{d'}$.

Example 3: Constructing 29,26,25,23-member UEB3 in $\mathbb{C}^5 \otimes \mathbb{C}^6$.

Considering the following matrices,

$$V_1 = \begin{pmatrix} 0&0&0&0&0&0\\ 0&0&0&0&0&0\\ 0&0&0&0&0&0\\ 0&0&0&0&0&0\\ 0&0&0&0&0&\star \end{pmatrix}, \quad V_2 = \begin{pmatrix} 0&0&0&0&0&0\\ 0&0&0&0&0&\star\\ 0&0&0&0&0&\star\\ 0&0&0&0&0&\star\\ 0&0&0&0&0&\star \end{pmatrix}, \quad (15)$$

$$V_3 = \begin{pmatrix} 0&0&0&0&0&\star\\ 0&0&0&0&0&\star\\ 0&0&0&0&0&\star\\ 0&0&0&0&0&\star\\ 0&0&0&0&0&\star \end{pmatrix}, \quad V_4 = \begin{pmatrix} 0&0&0&0&0&\star\\ 0&0&0&0&0&\star\\ 0&0&0&0&0&\star\\ 0&0&0&0&\star&\star\\ 0&0&0&0&\star&\star \end{pmatrix}. \quad (16a)$$

the specific UEB3s of V_1, V_2, V_3, V_4 are shown in **Table 6-9** respectively.

3.3 All the Ignored Elements Occupy Both *x* Rows and *y* Columns

In this section, we will construct $(dd' - v)$-member UEBk in a bipartite system $\mathbb{C}^d \otimes \mathbb{C}^{d'}$ with all the v ignored elements occupying both x rows and y columns in the matrix, and we will also present some different examples of UEB3s in $\mathbb{C}^5 \otimes \mathbb{C}^6$.

Theorem 3: Let k be a positive integer, $b, n \in \mathbb{N}$ such that $W(n, k, b)$ is non-empty, and $\gcd(k, b) = 1$ (the greatest common divisor of k and b). Let V be a subspace of $M_{d\times d'}$ such that each matrix in V is a $d \times d'$ matrix ignoring v elements which occupied x rows and y columns with $x + y < k$, $d - x \geq b$ and $d' - y \geq b$; $dd' - v = s \cdot k + p \cdot b$ with $1 \leq v \leq d'x + dy$. If $\min\{d, d'\} \geq \max\{k, b\}$, then there exists $(dd' - v)$, $(1 \leq v \leq d'x + dy)$-member UEBk in $\mathbb{C}^d \otimes \mathbb{C}^{d'}$.

Proof. First, for different values of p and s, we construct different pure states as follows: if $p \geq 1$ and $s \geq 1$, set

$$|\phi_{m,l}\rangle = \begin{cases} \frac{1}{\sqrt{k}}\sum_{u=0}^{k-1}\xi_k^{mu}|r_{lk+u}\rangle, & 0 \leqslant l \leqslant s-1, \\ \frac{1}{\sqrt{k}}\sum_{u=1}^{b}x_{ij}^{(t)}|r_{sk-1+(l-s)b+u}\rangle, & s \leqslant l \leqslant s+p-1. \end{cases} \quad (16b)$$

if $s = 0$, $p \geq 1$, set

$$|\phi_{m,l}\rangle = \frac{1}{\sqrt{k}}\sum_{u=1}^{b}x_{ij}^{(t)}|r_{sk-1+(l-s)b+u}\rangle, \quad 0 \leqslant l \leqslant p-1, \quad (17)$$

if $p = 0$, $s \geq 1$, set

$$|\phi_{m,l}\rangle = \frac{1}{\sqrt{k}}\sum_{u=0}^{k-1}\xi_k^{mu}|r_{lk+u}\rangle, \quad 0 \leqslant l \leqslant s-1. \quad (18)$$

where $\xi_k = e^{\frac{2\pi\sqrt{-1}}{k}}$, $m = 0, 1, \ldots, k-1$; $x_{i,j}^{(t)}$ means the t $(0 \leq t \leq b-1)$ row in the generalized weights matrix $W(n, k, b)$, and $sk - 1 + (l-s)b + u = f \cdot (d' - N + 1) + g$; $l \cdot k + u = c \cdot (d - N + 1) + e = f \cdot (d' - N + 1) + g$ with $0 \leq e < d$, $0 \leq g < d'$. Denoting $A = e \oplus_d \sum_{i=0}^{\alpha} C_i$, $B = g \oplus_{d'} \sum_{i=0}^{\alpha} C_i$, then

TABLE 1 | 6×3+2×4=30,–,4=26-member UEB3.

	$\|0'\rangle$	$\|1'\rangle$	$\|2'\rangle$	$\|3'\rangle$	$\|4'\rangle$	$\|5'\rangle$
$\|0\rangle$	1	5	3	a	2	6
$\|1\rangle$	a	1	5	4	b	2
$\|2\rangle$	3	A	1	6	4	b
$\|3\rangle$	b	3	A	2	6	4
$\|4\rangle$	5	B	*	*	*	*

TABLE 2 | 7×3+2×4=29-member.

–	$\|0'\rangle$	$\|1'\rangle$	$\|2'\rangle$	$\|3'\rangle$	$\|4'\rangle$	$\|5'\rangle$
$\|0\rangle$	1	b	7	6	4	2
$\|1\rangle$	3	1	b	a	6	4
$\|2\rangle$	5	3	1	b	a	6
$\|3\rangle$	7	5	3	2	b	a
$\|4\rangle$	a	7	5	4	2	*

TABLE 3 | 8×3+1×4=28-member.

–	$\|0'\rangle$	$\|1'\rangle$	$\|2'\rangle$	$\|3'\rangle$	$\|4'\rangle$	$\|5'\rangle$
$\|0\rangle$	1	a	5	4	2	7
$\|1\rangle$	7	1	a	6	4	2
$\|2\rangle$	3	8	1	a	6	4
$\|3\rangle$	5	3	8	2	a	6
$\|4\rangle$	7	5	3	a	*	*

TABLE 4 | 7×3+1×4=25-member.

–	$\|0'\rangle$	$\|1'\rangle$	$\|2'\rangle$	$\|3'\rangle$	$\|4'\rangle$	$\|5'\rangle$
$\|0\rangle$	1	5	3	a	2	6
$\|1\rangle$	7	1	5	4	a	2
$\|2\rangle$	3	7	1	6	4	a
$\|3\rangle$	a	3	7	2	6	4
$\|4\rangle$	5	*	*	*	*	*

TABLE 5 | 8×3+0,×,4=24-member.

–	$\|0'\rangle$	$\|1'\rangle$	$\|2'\rangle$	$\|3'\rangle$	$\|4'\rangle$	$\|5'\rangle$
$\|0\rangle$	1	5	3	8	2	6
$\|1\rangle$	7	1	5	4	8	2
$\|2\rangle$	3	7	1	6	4	8
$\|3\rangle$	5	3	7	2	6	4
$\|4\rangle$	*	*	*	*	*	*

TABLE 6 | 7×3+2×4=29-member.

–	$\|0'\rangle$	$\|1'\rangle$	$\|2'\rangle$	$\|3'\rangle$	$\|4'\rangle$	$\|5'\rangle$
$\|0\rangle$	1	2	4	6	7	b
$\|1\rangle$	b	1	3	4	6	a
$\|2\rangle$	a	b	1	3	5	6
$\|3\rangle$	7	a	b	2	3	5
$\|4\rangle$	4	5	7	a	2	*

$$|r_{lk+u}\rangle = |A \oplus_d C(A,B)\rangle|B \oplus_{d'} C(A,B)'\rangle, \tag{19}$$

with

$$C(A,B) = \begin{cases} 1, & C(A,B) = C_\alpha, \\ 0, & otherwise, \end{cases} \tag{20}$$

where $C_0 = 0$, $C_\alpha = 1$ denotes the ignored elements.

Similar to Theorem 1, we can prove that $\{|\phi_{m,l}\rangle\}$ constitute $dd' - v$ $(1 \le v \le d'x + dy)$-member UEB*k*s in $\mathbb{C}^d \otimes \mathbb{C}^{d'}$.

Example 4: Constructing 26,25,24,23-member UEB3 in $\mathbb{C}^5 \otimes \mathbb{C}^6$.

Considering the following matrices,

$$V_1 = \begin{pmatrix} 0&0&0&0&0&0 \\ 0&0&0&0&0&0 \\ 0&0&0&0&0&0 \\ 0&0&0&0&0&\star \\ 0&0&0&\star&\star&\star \end{pmatrix}, \quad V_2 = \begin{pmatrix} 0&0&0&0&0&0 \\ 0&0&0&0&0&\star \\ 0&0&0&0&0&\star \\ 0&0&0&0&0&\star \\ 0&0&0&0&\star&\star \end{pmatrix}, \tag{21}$$

$$V_3 = \begin{pmatrix} 0&0&0&0&0&0 \\ 0&0&0&0&0&0 \\ 0&0&0&0&0&\star \\ 0&0&0&0&0&\star \\ 0&0&\star&\star&\star&\star \end{pmatrix}, \quad V_4 = \begin{pmatrix} 0&0&0&0&0&0 \\ 0&0&0&0&0&\star \\ 0&0&0&0&0&\star \\ 0&0&0&0&0&\star \\ 0&0&\star&\star&\star&\star \end{pmatrix}. \tag{22a}$$

TABLE 7 | 6×3+2×4=26-member.

–	$\|0'\rangle$	$\|1'\rangle$	$\|2'\rangle$	$\|3'\rangle$	$\|4'\rangle$	$\|5'\rangle$
$\|0\rangle$	1	2	4	6	a	b
$\|1\rangle$	a	1	3	4	6	*
$\|2\rangle$	6	b	1	3	5	*
$\|3\rangle$	5	a	b	2	3	*
$\|4\rangle$	4	5	a	b	2	*

the specific UEB3s of V_1, V_2, V_3, V_4 are shown in **Table 10-13**, respectively.

Comparing **Tables 4**, **8**, **11**, we can find that they are all 25-member UEB3s in $\mathbb{C}^5 \otimes \mathbb{C}^6$, but they are different since the ignored elements occupy different positions. The above structure has given the location of the elements in each state, but the expressions are not always applicable when $d = d'$. For the case of $d = d'$, Ref. [23] provided a good method to construct the UEB*k*; now, we give some concrete examples to illustrate it.

Example 5: Constructing 26,25,24,23-member UEB3 in $\mathbb{C}^6 \otimes \mathbb{C}^6$.

Considering the following matrices,

TABLE 8 | 7×3+1×4=25-member.

—	$\|0'\rangle$	$\|1'\rangle$	$\|2'\rangle$	$\|3'\rangle$	$\|4'\rangle$	$\|5'\rangle$
$\|0\rangle$	1	2	4	6	7	*
$\|1\rangle$	a	1	3	4	6	*
$\|2\rangle$	6	a	1	3	5	*
$\|3\rangle$	5	7	a	2	3	*
$\|4\rangle$	4	5	7	a	2	*

TABLE 9 | 5×3+2×4=23-member.

—	$\|0'\rangle$	$\|1'\rangle$	$\|2'\rangle$	$\|3'\rangle$	$\|4'\rangle$	$\|5'\rangle$
$\|0\rangle$	1	2	4	a	b	*
$\|1\rangle$	b	1	3	4	a	*
$\|2\rangle$	a	b	1	3	5	*
$\|3\rangle$	3	5	a	2	*	*
$\|4\rangle$	2	4	5	b	*	*

TABLE 10 | 2×3+5×4=26-member.

—	$\|0'\rangle$	$\|1'\rangle$	$\|2'\rangle$	$\|3'\rangle$	$\|4'\rangle$	$\|5'\rangle$
$\|0\rangle$	1	e	d	b	a	2
$\|1\rangle$	2	1	e	d	c	a
$\|2\rangle$	b	a	1	e	d	c
$\|3\rangle$	c	b	a	2	e	*
$\|4\rangle$	d	c	b	*	*	*

TABLE 11 | 7×3+1×4=25-member.

—	$\|0'\rangle$	$\|1'\rangle$	$\|2'\rangle$	$\|3'\rangle$	$\|4'\rangle$	$\|5'\rangle$
$\|0\rangle$	1	a	6	5	4	2
$\|1\rangle$	2	1	a	7	5	*
$\|2\rangle$	4	3	1	a	7	*
$\|3\rangle$	6	4	3	2	a	*
$\|4\rangle$	7	6	5	3	*	*

TABLE 12 | 8×3+0,×,4=24-member.

—	$\|0'\rangle$	$\|1'\rangle$	$\|2'\rangle$	$\|3'\rangle$	$\|4'\rangle$	$\|5'\rangle$
$\|0\rangle$	1	7	6	5	3	2
$\|1\rangle$	2	1	8	6	5	4
$\|2\rangle$	4	3	1	8	7	*
$\|3\rangle$	5	4	3	2	8	*
$\|4\rangle$	7	6	*	*	*	*

TABLE 13 | 5×3+2×4=23-member.

—	$\|0'\rangle$	$\|1'\rangle$	$\|2'\rangle$	$\|3'\rangle$	$\|4'\rangle$	$\|5'\rangle$
$\|0\rangle$	1	b	a	4	3	2
$\|1\rangle$	2	1	b	a	5	*
$\|2\rangle$	4	3	1	b	a	*
$\|3\rangle$	5	4	3	2	b	*
$\|4\rangle$	a	5	*	*	*	*

TABLE 14 | 9,×,3+2×4=35-member.

—	$\|0'\rangle$	$\|1'\rangle$	$\|2'\rangle$	$\|3'\rangle$	$\|4'\rangle$	$\|5'\rangle$
$\|0\rangle$	1	2	4	6	8	a
$\|1\rangle$	a	1	3	5	7	9
$\|2\rangle$	9	b	1	3	5	7
$\|3\rangle$	7	9	b	2	3	5
$\|4\rangle$	6	8	a	b	2	4
$\|5\rangle$	4	6	8	a	b	*

TABLE 15 | 8×3+2×4=32-member.

—	$\|0'\rangle$	$\|1'\rangle$	$\|2'\rangle$	$\|3'\rangle$	$\|4'\rangle$	$\|5'\rangle$
$\|0\rangle$	1	2	4	6	8	a
$\|1\rangle$	b	1	3	5	7	8
$\|2\rangle$	a	b	1	3	5	7
$\|3\rangle$	7	a	b	2	3	5
$\|4\rangle$	6	8	a	b	2	4
$\|5\rangle$	4	6	*	*	*	*

TABLE 16 | 8×3+2×4=32-member.

—	$\|0'\rangle$	$\|1'\rangle$	$\|2'\rangle$	$\|3'\rangle$	$\|4'\rangle$	$\|5'\rangle$
$\|0\rangle$	1	2	4	6	7	a
$\|1\rangle$	a	1	3	4	6	8
$\|2\rangle$	8	6	1	3	5	*
$\|3\rangle$	6	8	b	2	3	*
$\|4\rangle$	5	7	a	b	2	*
$\|5\rangle$	4	5	7	a	b	*

TABLE 17 | 8×3+2×4=23-member.

—	$\|0'\rangle$	$\|1'\rangle$	$\|2'\rangle$	$\|3'\rangle$	$\|4'\rangle$	$\|5'\rangle$
$\|0\rangle$	1	2	4	6	8	a
$\|1\rangle$	b	1	3	4	6	8
$\|2\rangle$	8	b	1	3	5	6
$\|3\rangle$	7	a	b	2	3	*
$\|4\rangle$	5	7	a	b	2	*
$\|5\rangle$	4	5	7	a	*	*

TABLE 18 | construction in [23].

	$\|0'\rangle$	$\|1'\rangle$	$\|2'\rangle$	$\|3'\rangle$	$\|4'\rangle$	$\|5'\rangle$	$\|6'\rangle$
$\|0\rangle$	1	2	3	4	5	a	b
$\|1\rangle$	b	1	2	3	4	5	a
$\|2\rangle$	a	b	1	2	3	4	5
$\|3\rangle$	a	b	*	*	*	*	*
$\|4\rangle$	*	*	*	*	*	*	*

TABLE 19 | Our construction.

—	$\|0'\rangle$	$\|1'\rangle$	$\|2'\rangle$	$\|3'\rangle$	$\|4'\rangle$	$\|5'\rangle$	$\|6'\rangle$
$\|0\rangle$	1	b	4	2	a	5	3
$\|1\rangle$	3	1	a	4	2	b	5
$\|2\rangle$	5	3	1	a	4	2	b
$\|3\rangle$	b	a	*	*	*	*	*
$\|4\rangle$	*	*	*	*	*	*	*

$$V_1 = \begin{pmatrix} 0&0&0&0&0&0\\ 0&0&0&0&0&0\\ 0&0&0&0&0&0\\ 0&0&0&0&0&0\\ 0&0&0&0&0&0\\ 0&0&0&0&0&\star \end{pmatrix}, \quad V_2 = \begin{pmatrix} 0&0&0&0&0&0\\ 0&0&0&0&0&0\\ 0&0&0&0&0&0\\ 0&0&0&0&0&0\\ 0&0&0&0&0&0\\ 0&0&\star&\star&\star&\star \end{pmatrix}, \quad (22b)$$

$$V_3 = \begin{pmatrix} 0&0&0&0&0&0\\ 0&0&0&0&0&0\\ 0&0&0&0&0&\star\\ 0&0&0&0&0&\star\\ 0&0&0&0&0&\star\\ 0&0&0&0&0&\star \end{pmatrix}, \quad V_4 = \begin{pmatrix} 0&0&0&0&0&0\\ 0&0&0&0&0&0\\ 0&0&0&0&0&0\\ 0&0&0&0&0&\star\\ 0&0&0&0&0&\star\\ 0&0&0&0&\star&\star \end{pmatrix}. \quad (23)$$

the specific UEB3s of V_1, V_2, V_3, V_4 are shown in **Table 14-17**, respectively.

Remark 1: We systematically show three methods (or orders) to construct the UEB*k*s in different cases and present the corresponding mathematical expressions, which is better than that in [23] since it only provide one limited order. For example, we can construct 23-member SUEB3 in $\mathbb{C}^5 \otimes \mathbb{C}^7$ when $a = 3$, $b = 4$, which cannot be constructed by the order in [23], see **Table 18**, **19**.

Remark 2: Our results cover wider spaces than that of Ref. [23]. The smallest space we can discuss is $\mathbb{C}^4 \otimes \mathbb{C}^5$ when $a = 3$, $b = 4$, while the smallest space [23] can discuss is $\mathbb{C}^5 \otimes \mathbb{C}^7$ when $a = 3$, $b = 4$, $k = 3$. Futhermore, even in $\mathbb{C}^5 \otimes \mathbb{C}^6$, we also present different members of UEB3s.

4 CONCLUSION

We have proposed three ways to construct different members of UEB*k*s in $\mathbb{C}^d \otimes \mathbb{C}^{d'}$ and have shown their concrete expressions. As an example of each method, we have presented different members of UEB3s in $\mathbb{C}^5 \otimes \mathbb{C}^6$ and $\mathbb{C}^6 \otimes \mathbb{C}^6$. It is noteworthy that our result is based on the existence of generalized weighing matrices, so it is also of significance for us to find more generalized weighing matrices, such as skew Hadamard matrices.

By using our constructions, one can get at most $(dd' - v)$ members of UEB*k* in $\mathbb{C}^d \otimes \mathbb{C}^{d'}$, which has not specifically mentioned in the previous literature studies.

DATA AVAILABILITY STATEMENT

The original contributions presented in the study are included in the article/supplementary material; further inquiries can be directed to the corresponding author.

AUTHOR CONTRIBUTIONS

Y-HT, X-LY, and S-HW write the paper together; others review and check the paper.

FUNDING

This work was supported by the Natural Science Foundation of China under Number 11761073.

REFERENCES

1. Nielsen MA, Chuang IL. *Quantum Computation and Quantum Information*. Cambridge, U.K.: Cambridge University Press (2004).
2. Einstein A, Podolsky B, Rosen N. Can Quantum-Mechanical Description of Physical Reality Be Considered Complete? *Phys Rev* (1935) 47:777–80. doi:10.1103/physrev.47.777
3. Nikolopoulos GM, Alber G. Security Bound of Two-Basis Quantum-Key-Distribution Protocols Usingqudits. *Phys Rev A* (2005) 72:032320. doi:10.1103/physreva.72.032320
4. Mafu M, Dudley A, Goyal S, Giovannini D, McLaren MJ, Konrad T, et al. High-dimensional Orbital-Angular-Momentum-Based Quantum Key Distribution with Mutually Unbiased Bases. *Phy Rev A* (2013) 88:032305. doi:10.1103/physreva.88.032305
5. Paw lowski M, Zukowski M. Optimal Bounds for Parity-Oblivious Random Access Codes. *Phy Rev A* (2010) 81:042326.
6. Wootters WK, Fields BD. Optimal State-Determination by Mutually Unbiased Measurements. *Ann Phys* (1989) 191:363–81. doi:10.1016/0003-4916(89)90322-9
7. Fernnadez-Parez A, Klimov AB, Saavedra C. Quantum Proces Reconstruction Baed on Mutually Unbiased Basis. *Phys Rev A* (2011) 83:052332.
8. Englert BG, Aharonov Y. The Mean king's Problem: Prime Degrees of freedom. *Phys Lett A* (2011) 84:042306.
9. Bennett CH, Divincenzo DP, Mor T, Shor PW, Smolin JA, Terhal BM, et al. Unextendible Product Bases and Bound Entanglement. *Phys Rev Lett* (1999) 82:5385–8. doi:10.1103/physrevlett.82.5385
10. Bravyi S, Smolin JA. Unextendible Maximally Entangled Bases. *Phys Rev A* (2011) 84:042306. doi:10.1103/physreva.84.042306
11. Wang Y-L, Li M-S, Fei S-M, Zheng Z-J. Connecting Unextendible Maximally Entangled Base with Partial Hadamard Matrices. *Quan Inf Process* (2017) 16(3):84. doi:10.1007/s11128-017-1537-7
12. Chen B, Fei SM. Unextendible Maximally Entangled Bases and Mutually Unbiased Bases. *Phys Rev A* (2013) 88:034301. doi:10.1103/physreva.88.034301
13. Nan H, Tao Y-H, Li L-S, Zhang J. Unextendible Maximally Entangled Bases and Mutually Unbiased Bases in $\mathbb{C}^d \otimes \mathbb{C}^{d'}$. *Int J Theor Phys* (2015) 54:927–32. doi:10.1007/s10773-014-2288-1
14. Li MS, Wang YL, Fei SM, Zheng ZJ. Unextendible Maximally Entangled Bases in $\mathbb{C}^d \otimes \mathbb{C}^{d'}$. *Phys Rev A* (2014) 89:062313.
15. Wang YL, Li MS, Fei SM. Unextendible Maximally Entangled Bases in $\mathbb{C}^d \otimes \mathbb{C}^{d'}$. *Phys Rev A* (2014) 90:034301.
16. Guo Y. Constructing the Unextendible Maximally Entangled Bases from the Maximally Entangled Bases. *Phys Rev A* (2016) 94:052302. doi:10.1103/physreva.94.052302
17. Zhang G-J, Tao Y-H, Han Y-F, Yong X-L, Fei S-M. Unextendible Maximally Entangled Bases in $\mathbb{C}^{pd} \otimes \mathbb{C}^{qd}$. *Quan Inf Process* (2018) 17:318. doi:10.1007/s11128-018-2094-4

18. Shi F, Zhang X, Guo Y. Constructions of Unextendible Entangled Bases. *Quan Inf Process* (2019) 18:324. doi:10.1007/s11128-019-2435-y
19. Guo Y, Wu S. Unextendible Entangled Bases with Fixed Schmidt Number. *Phys Rev A* (2014) 90:054303. doi:10.1103/physreva.90.054303
20. Guo Y, Du S, Li X, Wu S. Entangled Bases with Fixed Schmidt Number. *J Phys A: Math Theor* (2015) 48:245301. doi:10.1088/1751-8113/48/24/245301
21. Guo Y, Jia Y, Li XL. Multipartite Unextendible Entangled Basis. *Quan Inf Process* (2015) 14:3553–68. doi:10.1007/s11128-015-1058-1
22. Li M-S, Wang Y-L. Construction of Special Entangled Basis Based on Generalized Weighing Matrices. *J Phys A: Math Theor* (2019) 52:375303. doi:10.1088/1751-8121/ab331b
23. Wang YL. Special Unextendible Entangled Bases with Continuous Integer Cardinality. *arXiv:1909.10043v1* (2019).
24. Zhang GJ, Tao YH, Han YF, Yong XL, Fei SM. Constructions of Unextendible Maximally Entangled Bases in $\mathbb{C}^d \otimes \mathbb{C}^{d'}$. *Sci Rep* (2018) 8(1):3193. doi:10.1038/s41598-018-21561-0

Conflict of Interest: The authors declare that the research was conducted in the absence of any commercial or financial relationships that could be construed as a potential conflict of interest.

frontiers | Frontiers in Physics

ORIGINAL RESEARCH
published: 08 July 2022
doi: 10.3389/fphy.2022.955786

On Non-Convexity of the Nonclassicality Measure *via* Operator Ordering Sensitivity

Shuangshuang Fu[1], *Shunlong Luo*[2,3] *and Yue Zhang*[4,5]*

[1]School of Mathematics and Physics, University of Science and Technology Beijing, Beijing, China, [2]Academy of Mathematics and Systems Science, Chinese Academy of Sciences, Beijing, China, [3]School of Mathematical Sciences, University of Chinese Academy of Sciences, Beijing, China, [4]State Key Laboratory of Mesoscopic Physics, School of Physics, Frontiers Science Center for Nano-optoelectronics, Peking University, Beijing, China, [5]Beijing Academy of Quantum Information Sciences, Beijing, China

In quantum optics, nonclassicality in the sense of Glauber-Sudarshan is a valuable resource related to the quantum aspect of photons. A desirable and intuitive requirement for a consistent measure of nonclassicality is convexity: Classical mixing should not increase nonclassicality. We show that the recently introduced nonclassicality measure [Phys. Rev. Lett. **122**, 080402 (2019)] is not convex. This nonclassicality measure is defined via operator ordering sensitivity, which is an interesting and significant probe (witness) of nonclassicality without convexity but can be intrinsically connected to the convex Wigner-Yanase skew information [Proc. Nat. Acad. Sci. United States **49**, 910 (1963)] *via* the square root operation on quantum states. Motivated by the Wigner-Yanase skew information, we also propose a faithful measure of nonclassicality, although it cannot be readily computed, it is convex.

Keywords: coherent states, nonclassicality, operator ordering sensitivity, convexity, Wigner-Yanase skew information

OPEN ACCESS

Edited by:
Dong Wang,
Anhui University, China

Reviewed by:
Shao-Ming Fei,
Capital Normal University, China
Zhaoqi Wu,
Nanchang University, China

****Correspondence:***
Yue Zhang
zhangyue@baqis.ac.cn

Specialty section:
This article was submitted to Quantum Engineering and Technology, a section of the journal Frontiers in Physics

Received: *29 May 2022*
Accepted: *13 June 2022*
Published: *08 July 2022*

Citation:
Fu S, Luo S and Zhang Y (2022) On Non-Convexity of the Nonclassicality Measure via Operator Ordering Sensitivity. Front. Phys. 10:955786. doi: 10.3389/fphy.2022.955786

1 INTRODUCTION

In the conventional scheme of Glauber-Sudarshan, nonclassicality of light refers to quantum optical states that cannot be expressed as classical (probabilistic) mixtures of Glauber coherent states [1–7]. Its detection and quantification are of both theoretical and experimental importance in quantum optics [8–17]. Recently, a remarkable and interesting nonclassicality measure is introduced in Ref. [18]. This measure is well motivated and has operational significance stemmed from operator ordering sensitivity [18], which is also known as squared quadrature coherence scale in measuring quadrature coherence [19], and proved to be closely related to the entanglement [20]. Here we demonstrate that this nonclassicality measure, as well as the operator ordering sensitivity, are not convex. This means that classical (probabilistic) mixing of states can increase nonclassicality, as quantified by this nonclassicality measure via the operator ordering sensitivity. Our result complements the key contribution in Ref. [18].

By the way, we show that the operator ordering sensitivity, though not convex, can be connected to a convex quantity via the very simple and straightforward operation of square root. The modified quantity has both physical and information-theoretic significance, and is actually rooted in an amazing quantity of Wigner and Yanase, introduced in 1963 [21]. Motivated by the Wigner-Yanase skew information, we also propose a faithful measure of nonclassicality which is convex.

To be precise, let us first recall the basic idea and the key quantities in Ref. [18]. Consider a single-mode bosonic field with annihilation operator a and creation operator $a^\dagger$ satisfying the commutation relation

$$[a, a^\dagger] = \mathbf{1}.$$

Let $D(\alpha) = e^{\alpha a^\dagger - \alpha^* a}$ be the Weyl displacement operators with amplitudes $\alpha \in \mathbb{C}$, then $|\alpha\rangle = D(\alpha)|0\rangle$ are the coherent states [1–3]. For a bosonic field state ρ, consider the parameterized phase space distributions [18]

$$W_s(z) = \frac{1}{\pi^2}\int_{\mathbb{C}} e^{s|z|^2/2+\alpha z^* - \alpha^* z}\mathrm{tr}\left(\rho D(\alpha)\right)d^2\alpha$$

on the phase space $\mathbb{C}$, where $s \in [-1, 1]$, $d^2\alpha = dxdy$ with $\alpha = x + iy, x, y \in \mathbb{R}$, and tr denotes operator trace. In particular, for $s = 1, 0, -1$, the corresponding phase space distributions are the Glauber-Sudarshan P functions, the Wigner functions, and the Husimi functions, respectively.

Motivated by operator ordering due to noncommutativity and in terms of the Hilbert-Schmidt norm, the quantity

$$S_o(\rho) = -\frac{d}{ds}\ln\left(\pi\|W_s\|^2\right)|_{s=0}$$

is introduced as a probe of nonclassicality of ρ in Ref. [18], and is called operator ordering sensitivity. Here

$$\|W_s\|^2 = \int_{\mathbb{C}} |W_s(z)|^2 d^2 z.$$

It turns out that.

$$S_o(\rho) = -\frac{1}{2\mathrm{tr}\left(\rho^2\right)}\left(\mathrm{tr}\left([\rho, Q]^2\right) + \mathrm{tr}\left([\rho, P]^2\right)\right), \tag{1}$$

where $[X, Y] = XY - YX$ denotes operator commutator, and

$$Q = \frac{a + a^\dagger}{\sqrt{2}}, \qquad P = \frac{a - a^\dagger}{\sqrt{2}i}$$

are the conjugate quadrature operators. Simple manipulation shows that

$$S_o(\rho) = \frac{1}{\mathrm{tr}\left(\rho^2\right)}\mathrm{tr}\left([\rho, a][\rho, a]^\dagger\right). \tag{2}$$

Moreover, the following nonclassicality measure

$$\mathcal{N}(\rho) = \inf_{\sigma\in\mathcal{C}} |||\tilde{\rho} - \tilde{\sigma}||| \tag{3}$$

is introduced as a key result [18]. Here $\mathcal{C}$ is the set of classical states (i.e., mixtures of coherent states), $\tilde{\rho} = \rho/\sqrt{\mathrm{tr}\left(\rho^2\right)}$, $\tilde{\sigma} = \sigma/\sqrt{\mathrm{tr}\left(\sigma^2\right)}$, and the norm $|||\cdot|||$ is defined as

$$|||X|||^2 = \frac{1}{2}\mathrm{tr}\left([X^\dagger, Q][Q, X] + [X^\dagger, P][P, X]\right).$$

In particular,

$$|||\tilde{\rho}|||^2 = S_o(\rho)$$

is precisely the operator ordering sensitivity.

The purpose of this work is to demonstrate that the nonclassicality measure $\mathcal{N}(\cdot)$ defined by **Eq. 3** is not convex. Consequently, this quantity cannot be a consistent measure of nonclassicality if one imposes the fundamental rationale that classical mixing of quantum states should not increase nonclassicality, which resembles the idea that classical mixing of quantum states should not increase entanglement. By the way, we also demonstrate that the operator ordering sensitivity $S_o(\cdot)$ defined by **Eq. 2** is not convex either.

The structure of the remainder of the paper is as follows. In **Section 2**, we demonstrate that the nonclassicality measure $\mathcal{N}(\cdot)$ is not convex through counterexamples. In **Section 3**, we show that although the operator ordering sensitivity $S_o(\cdot)$ is not convex, it can be directly connected to a convex quantity related to the celebrated Wigner-Yanase skew information. By the way, we also present a simple proof of the fact that $S_o(\rho) \le 1$ for any classical state. In **Section 4**, we bring up a convex measure of nonclassicality based on the Wigner-Yanase skew information. Finally, a summary is presented in **Section 5**.

2 NON-CONVEXITY OF THE NONCLASSICALITY MEASURE $\mathcal{N}(\rho)$

In this section, we show that $\mathcal{N}(\rho)$ defined by **Eq. 3**, the nonclassicality measure introduced in Ref. [18], is not convex. First recall that by the triangle inequality for norm and the fact that the set $\tilde{\mathcal{C}}$, the image of $\mathcal{C}$ under the map $\rho \to \tilde{\rho} = \rho/\sqrt{\mathrm{tr}\left(\rho^2\right)}$, is contained inside the unit ball, it is shown that [18]

$$|||\tilde{\rho}||| - 1 \le \mathcal{N}(\rho) \le |||\tilde{\rho}||| \tag{4}$$

with $|||\tilde{\rho}||| = \sqrt{S_o(\rho)}$.

Now we give a family of counterexamples to show that $\mathcal{N}(\rho)$ is not convex with respect to ρ. Considering the mixture

$$\rho = \frac{1}{2}\rho_1 + \frac{1}{2}\rho_2$$

of the vacuum state $\rho_1 = |0\rangle\langle 0|$ (which is classical) and the Fock state $\rho_2 = |n\rangle\langle n|$ with $n > 1$, then by direct calculation, we have

$$S_o(\rho_1) = 1, \qquad S_o(\rho_2) = 1 + 2n.$$

To evaluate $S_o(\rho)$, noting that

$$S_o(\rho) = 1 + \frac{2}{\mathrm{tr}\left(\rho^2\right)}\left(\mathrm{tr}\left(a\rho^2 a^\dagger\right) - \mathrm{tr}\left(\rho a^\dagger \rho a\right)\right),$$

we have, by direct calculation, that

$$\mathrm{tr}\left(\rho^2\right) = \frac{1}{2}, \qquad \mathrm{tr}\left(a\rho^2 a^\dagger\right) = \frac{n}{4}, \qquad \mathrm{tr}\left(\rho a^\dagger \rho a\right) = 0,$$

from which we obtain

$$S_o(\rho) = 1 + n.$$

It follows from the inequality chain (4) that

$$\mathcal{N}(\rho_1) \le \sqrt{S_o(\rho_1)} = 1,$$
$$\mathcal{N}(\rho_2) \le \sqrt{S_o(\rho_2)} = \sqrt{1 + 2n},$$

while

$$\mathcal{N}(\rho) \ge \sqrt{S_o(\rho)} - 1 = \sqrt{1 + n} - 1.$$

Consequently,

$$\frac{1}{2}\mathcal{N}(\rho_1)+\frac{1}{2}\mathcal{N}(\rho_2)\leq\frac{1+\sqrt{1+2n}}{2}.$$

Since when $n > 24$, the following inequality holds

$$\sqrt{1+n}-1>\frac{1+\sqrt{1+2n}}{2},$$

it follows that

$$\mathcal{N}(\rho)\geq\sqrt{1+n}-1>\frac{1+\sqrt{1+2n}}{2}\geq\frac{1}{2}\mathcal{N}(\rho_1)+\frac{1}{2}\mathcal{N}(\rho_2).$$

This implies that $\mathcal{N}(\cdot)$ is not convex. In this sense, $\mathcal{N}(\cdot)$ cannot be a consistent measure of nonclassicality because classical mixing should not increase nonclassicality. Of course, $\mathcal{N}(\cdot)$ still captures certain features of nonclassicality and can be used as a probe of nonclassicality.

3 RELATING THE OPERATOR ORDERING SENSITIVITY $S_o(\rho)$ TO THE WIGNER-YANASE SKEW INFORMATION

As a side issue, in this section, we show that although the operator ordering sensitivity $S_o(\rho)$ is not convex either with respect to ρ, it can be intrinsically related to the celebrated Wigner-Yanase skew information, which is convex.

First, we illustrate non-convexity of $S_o(\rho)$ through the following counterexamples. Take

$$\rho_1=\frac{1}{2}(|0\rangle\langle 0|+|1\rangle\langle 1|),\qquad \rho_2=|2\rangle\langle 2|,\qquad p_1=\frac{1}{4},\qquad p_2=\frac{3}{4},$$

where $|n\rangle$ are the Fock (number) states with

$$a|0\rangle=0,\qquad a|n\rangle=\sqrt{n}|n-1\rangle,\qquad n=1,2,\ldots,$$

and

$$a^\dagger|n\rangle=\sqrt{n+1}|n+1\rangle,\qquad n=0,1,\cdots.$$

Now direct evaluation yields

$$[\rho_1,a]=\frac{1}{\sqrt{2}}|1\rangle\langle 2|,\qquad [\rho_2,a]=\sqrt{3}|2\rangle\langle 3|-\sqrt{2}|1\rangle\langle 2|,$$

and

$$[p_1\rho_1+p_2\rho_2,a]=-\frac{5\sqrt{2}}{8}|1\rangle\langle 2|+\frac{3\sqrt{3}}{4}|2\rangle\langle 3|.$$

Substituting the above into **Eq. 2**, we obtain

$$S_o(\rho_1)=1,\qquad S_o(\rho_2)=5,$$

and

$$S_o(p_1\rho_1+p_2\rho_2)=\frac{79}{19}>p_1S_o(\rho_1)+p_2S_o(\rho_2)=4.$$

This implies that $S_o(\rho)$ is not convex.

In the above counterexamples showing non-convexity of $S_o(\rho)$, both the constituent states ρ_1 and ρ_2 are nonclassical in the sense that they cannot be represented as probabilistic mixtures of coherent states [1–3]. The following counterexamples illustrates that even the mixture of a classical thermal state and a nonclassical state can demonstrate non-convexity. Considering the thermal state

$$\tau_1=(1-\lambda)\sum_{n=0}^{\infty}\lambda^n|n\rangle\langle n|,\qquad \lambda\in(0,1),\tag{5}$$

which is classical and the Fock state $\tau_2=|1\rangle\langle 1|$, and their mixture

$$\tau=\frac{1}{2}(\tau_1+\tau_2),$$

then by direct calculation, we have

$$S_o(\tau_1)=\frac{1-\lambda}{1+\lambda},\qquad S_o(\tau_2)=3.$$

To evaluate $S_o(\tau)$, noting that from **Eq. 2**, we have

$$S_o(\tau)=1+\frac{2}{\mathrm{tr}(\tau^2)}\left(\mathrm{tr}(a\tau^2a^\dagger)-\mathrm{tr}(a\tau a^\dagger\tau)\right).$$

Now direct calculation leads to

$$\mathrm{tr}(\tau^2)=\frac{1+\lambda(1-\lambda^2)}{2(1+\lambda)},$$
$$\mathrm{tr}(a\tau^2a^\dagger)=\frac{1+4\lambda+4\lambda^2-2\lambda^3-2\lambda^4}{4(1+\lambda)^2},$$
$$\mathrm{tr}(a\tau a^\dagger\tau)=\frac{\lambda+(1-\lambda)(1+2\lambda^2)(1+\lambda)^2}{4(1+\lambda)^2},$$

from which we obtain

$$S_o(\tau)=1+\frac{\lambda(2+3\lambda-3\lambda^2+2\lambda^4)}{(1+\lambda-\lambda^3)(1+\lambda)},\qquad \lambda\in(0,1).$$

Clearly

$$\lim_{\lambda\to 1}S_o(\tau)=3>\frac{1}{2}\lim_{\lambda\to 1}S_o(\tau_1)+\frac{1}{2}\lim_{\lambda\to 1}S_o(\tau_2)=\frac{3}{2}.$$

By continuity, this implies that $S_o(\cdot)$ is not convex for λ close to 1. More explicitly, for $\lambda = 0.9$, we have

$$S_o(\tau)\approx 2.45>\frac{1}{2}(S_o(\tau_1)+S_o(\tau_2))\approx 1.53,$$

which explicitly shows that $S_o(\cdot)$ is not convex.

The non-convex quantity $S_o(\rho)$ can be modified to a convex one if we formally replace ρ by the square root $\sqrt{\rho}$ in **Eq. 1** and define

$$\hat{S}_o(\rho)=-\frac{1}{2}\left(\mathrm{tr}\left(\left[\sqrt{\rho},Q\right]^2\right)+\mathrm{tr}\left(\left[\sqrt{\rho},P\right]^2\right)\right),\tag{6}$$

which is precisely the sum of the Wigner-Yanase skew information [21]

$$I(\rho,Q)=-\frac{1}{2}\mathrm{tr}\left(\left[\sqrt{\rho},Q\right]^2\right),\qquad I(\rho,P)=-\frac{1}{2}\mathrm{tr}\left(\left[\sqrt{\rho},P\right]^2\right).$$

Remarkably, $\hat{S}_o(\rho)$ defined by **Eq. 6** can be more succinctly expressed as

$$\hat{S}_o(\rho)=\mathrm{tr}\left(\left[\sqrt{\rho},a\right]\left[\sqrt{\rho},a\right]^\dagger\right),\tag{7}$$

which is essentially (up to a constant factor 1/2) an extension of the Wigner-Yanase skew information, as can be readily

seen if we recast the original Wigner-Yanase skew information [21]

$$I(\rho,K)=-\frac{1}{2}\mathrm{tr}\Big(\big[\sqrt{\rho},K\big]^2\Big)$$

of the quantum state ρ with respect to (skew to) the observable (Hermitian operator) K as

$$I(\rho,K)=\frac{1}{2}\mathrm{tr}\Big(\big[\sqrt{\rho},K\big]\big[\sqrt{\rho},K\big]^{\dagger}\Big),$$

and formally replace the Hermitian operator K by the non-Hermitian annihilation operator a. An apparent interpretation of $\hat{S}_o(\rho)$ is the quantum uncertainty of the conjugate pair (Q, P) in the state ρ [22–24].

Due to the convexity of the Wigner-Yanase skew information [21], $\hat{S}_o(\rho)$ is convex with respect to ρ, in sharp contrast to $S_o(\rho)$. Moreover, $\hat{S}_o(\rho)$ has many nice features as guaranteed by the fundamental properties of the Wigner-Yanase skew information and its various physical and information-theoretic interpretations [24].

It is amusing to note the analogy between the passing from classical probability distributions to quantum mechanical amplitudes and that from $S_o(\rho)$ to $\hat{S}_o(\rho)$: Both involve the square root of states.

By the way, we present an alternative and simple proof of the interesting fact that [18]

$$S_o(\rho)\le 1$$

for any classical state ρ, which implies that $S_o(\cdot)$ is convex when the component states are restricted to coherent states (noting that $S_o(|\alpha\rangle\langle\alpha|)=1$ for any coherent state $|\alpha\rangle$), though it is not convex in the whole state space. To this end, let the Glauber-Sudarhsan P representation of ρ be

$$\rho=\int P(\alpha)|\alpha\rangle\langle\alpha|d^2\alpha,$$

then

$$\mathrm{tr}\left(a\rho^2a^{\dagger}\right)=\int P(\alpha)P(\beta)\alpha*\beta e^{-|\alpha-\beta|^2}d^2\alpha d^2\beta=\int P(\alpha)P(\beta)\beta*\alpha e^{-|\alpha-\beta|^2}d^2\alpha d^2\beta,$$
$$\mathrm{tr}\left(a\rho a^{\dagger}\rho\right)=\int P(\alpha)P(\beta)|\alpha|^2e^{-|\alpha-\beta|^2}d^2\alpha d^2\beta=\int P(\alpha)P(\beta)|\beta|^2e^{-|\alpha-\beta|^2}d^2\alpha d^2\beta,$$

from which we obtain

$$\begin{aligned}S_o(\rho)&=1+\frac{2}{\mathrm{tr}\left(\rho^2\right)}\left(\mathrm{tr}\left(a\rho^2a^{\dagger}\right)-\mathrm{tr}\left(a\rho a^{\dagger}\rho\right)\right)\\&=1-\frac{2}{\mathrm{tr}\left(\rho^2\right)}\int P(\alpha)P(\beta)|\alpha-\beta|^2e^{-|\alpha-\beta|^2}d^2\alpha d^2\beta.\end{aligned}$$

In particular, if ρ is a classical state, then $P(\alpha)\ge 0$, and this implies that $S_o(\rho)\le 1$ for any classical state ρ. In contrast, the fact that

$$\hat{S}_o(\rho)\le 1 \tag{8}$$

for any classical state follows readily from the convexity of $\hat{S}_o(\rho)$ and $\hat{S}_o(|\alpha\rangle\langle\alpha|)=1$ for any coherent state $|\alpha\rangle$.

4 A CONVEX MEASURE OF NONCLASSICALITY

Motivated by the Wigner-Yanase skew information, we propose a measure of nonclassicality defined as

$$\begin{aligned}\hat{\mathcal{N}}(\rho)&=\inf_{\sigma\in\mathcal{C}}\left|\!\left|\!\left|\sqrt{|\rho-\sigma|}\right|\!\right|\!\right|^2\\&=\inf_{\sigma\in\mathcal{C}}\mathrm{tr}\Big(\big[\sqrt{|\rho-\sigma|},a\big]\big[\sqrt{|\rho-\sigma|},a\big]^{\dagger}\Big).\end{aligned}$$

Here $|A|=\sqrt{A^{\dagger}A}$ is the square root of $A^{\dagger}A$, and $\mathcal{C}$ is the set of classical states.

It is clear that $\hat{\mathcal{N}}(\rho)$ is a faithful measure of nonclassicality, $\hat{\mathcal{N}}(\rho)>0$ for all nonclassical states and $\hat{\mathcal{N}}(\rho)=0$ for all classical states. Compared with the nonclassicality measure $\mathcal{N}(\rho)$ which is not convex, we prove below that $\hat{\mathcal{N}}(\rho)$ is convex.

Considering the convex combination of quantum states ρ_1 and ρ_2 with probabilities $p_1=p$ and $p_2=1-p$ respectively, the mixed state is denoted by

$$\rho=p_1\rho_1+p_2\rho_2.$$

Supposing that

$$\hat{\mathcal{N}}(\rho_1)=\inf_{\sigma\in\mathcal{C}}\left|\!\left|\!\left|\sqrt{|\rho_1-\sigma|}\right|\!\right|\!\right|^2=\left|\!\left|\!\left|\sqrt{|\rho_1-\sigma_1|}\right|\!\right|\!\right|^2,$$
$$\hat{\mathcal{N}}(\rho_2)=\inf_{\sigma\in\mathcal{C}}\left|\!\left|\!\left|\sqrt{|\rho_2-\sigma|}\right|\!\right|\!\right|^2=\left|\!\left|\!\left|\sqrt{|\rho_2-\sigma_2|}\right|\!\right|\!\right|^2,$$

due to the fact that the convex combination of classical states is also a classical state, we have $\sigma_c=p_1\sigma_1+p_2\sigma_2\in\mathcal{C}$, therefore

$$\begin{aligned}\hat{\mathcal{N}}(\rho)&=\inf_{\sigma\in\mathcal{C}}\left|\!\left|\!\left|\sqrt{|\rho-\sigma|}\right|\!\right|\!\right|^2\\&\le\left|\!\left|\!\left|\sqrt{|p_1\rho_1+p_2\rho_2-\sigma_c|}\right|\!\right|\!\right|^2=\left|\!\left|\!\left|\sqrt{|p_1(\rho_1-\sigma_1)+p_2(\rho_2-\sigma_2)|}\right|\!\right|\!\right|^2\\&\le\left|\!\left|\!\left|\sqrt{p_1|\rho_1-\sigma|+p_2|\rho_2-\sigma|}\right|\!\right|\!\right|^2\\&\le p_1\left|\!\left|\!\left|\sqrt{|\rho_1-\sigma_1|}\right|\!\right|\!\right|^2+p_2\left|\!\left|\!\left|\sqrt{|\rho_2-\sigma_2|}\right|\!\right|\!\right|^2=p_1\hat{\mathcal{N}}(\rho_1)+p_2\hat{\mathcal{N}}(\rho_2).\end{aligned}$$

Here the second inequality holds due to

$$|A+B|\le|A|+|B|, \tag{10}$$

which can be obtained from the fact that $|A+\lambda B|^2\ge 0$ for all real λ. While the third inequality follows from the convexity of the celebrated Wigner-Yanase skew information, the convexity of the measure $\hat{\mathcal{N}}(\rho)$ is easily proved. We point out here that similar to other measures involving optimization, this nonclassicality measure $\hat{\mathcal{N}}(\rho)$ can not be readily computed. It would be desirable if tight bounds of this quantity can be given.

Similarly from inequality (10) and the convexity of the Wigner-Yanase skew information, we have

$$\begin{aligned}\hat{\mathcal{N}}(\rho)&=\inf_{\sigma\in\mathcal{C}}\left|\!\left|\!\left|\sqrt{|\rho-\sigma|}\right|\!\right|\!\right|^2\le\inf_{\tau_1\in\mathcal{T}}\left|\!\left|\!\left|\sqrt{|\rho-\tau_1|}\right|\!\right|\!\right|^2\\&\le\inf_{\tau_1\in\mathcal{T}}\left|\!\left|\!\left|\sqrt{|\rho|+|\tau_1|}\right|\!\right|\!\right|^2=2\inf_{\tau_1\in\mathcal{T}}\left|\!\left|\!\left|\sqrt{\frac{1}{2}|\rho|+\frac{1}{2}|\tau_1|}\right|\!\right|\!\right|^2\\&\le\left|\!\left|\!\left|\sqrt{|\rho|}\right|\!\right|\!\right|^2+\inf_{\tau_1\in\mathcal{T}}\left|\!\left|\!\left|\sqrt{|\tau_1|}\right|\!\right|\!\right|^2=\left|\!\left|\!\left|\sqrt{|\rho|}\right|\!\right|\!\right|^2=\hat{S}_o(\rho),\end{aligned}$$

where $\mathcal{T}$ is the set of thermal states as defined in **Eq. 5**, the first inequality follows from the fact that thermal states are classical states (that is, $\mathcal{T}\subseteq\mathcal{C}$), and the last inequality holds since $\inf_{\tau_1}\left|\!\left|\!\left|\sqrt{|\tau_1|}\right|\!\right|\!\right|^2=\inf_{\tau_1\in\mathcal{T}}\hat{S}_o(\tau_1)=\inf_{\lambda\in(0,1)}(1-\sqrt{\lambda})/(2+2\sqrt{\lambda})=0$, as shown in Ref. [24]. Analogously, we notice that

$$\begin{aligned}\hat{S}_o(\rho) &= \left|\!\left|\!\left| \sqrt{|\rho|} \right|\!\right|\!\right|^2 \\ &\le \left|\!\left|\!\left| \sqrt{|\rho-\sigma|+|\sigma|} \right|\!\right|\!\right|^2 = 2\left|\!\left|\!\left| \sqrt{\frac{1}{2}|\rho-\sigma|+\frac{1}{2}|\sigma|} \right|\!\right|\!\right|^2 \\ &\le \left|\!\left|\!\left| \sqrt{|\rho-\sigma|} \right|\!\right|\!\right|^2 + \left|\!\left|\!\left| \sqrt{|\sigma|} \right|\!\right|\!\right|^2 \\ &\le \left|\!\left|\!\left| \sqrt{|\rho-\sigma|} \right|\!\right|\!\right|^2 + 1,\end{aligned}$$

where σ is a classical state, and the last inequality can be directly obtained from inequality (8). So we have

$$\hat{S}_o(\rho) - 1 \le \hat{\mathcal{N}}(\rho) \le \hat{S}_o(\rho).$$

In other words, $\hat{\mathcal{N}}(\rho)$ may be well estimated by the convex nonclassicality quantifier $\hat{S}_o(\rho)$ for highly nonclassical states.

5. CONCLUSION

We have demonstrated that $\mathcal{N}(\cdot)$, a recently introduced significant nonclassicality measure based on the operator ordering sensitivity, is not convex, and thus cannot be a consistent measure of the conventional nonclassicality of light in the sense of Glauber-Sudarshan. This non-convexity should be borne in mind whenever one wants to employ $\mathcal{N}(\cdot)$ to quantify nonclassicality in quantum optics in the customary fashion. We have proposed a faithful measure of nonclassicality $\hat{\mathcal{N}}(\cdot)$ which is convex. One obstacle of applying this measure is that it can not be readily computed due to the optimization over the set of classical states.

By the way, we have also demonstrated that although the important operator ordering sensitivity $S_o(\cdot)$ is not convex either, it can be simply connected to the convex Wigner-Yanase skew information via the square root operation on quantum states, which is reminiscent of the passing from probabilities to amplitudes via square roots, so fundamental in going from classical to quantum.

Due to the remarkable properties and information-theoretic significance of the Wigner-Yanase skew information, it is desirable to employ this quantity to study nonclassicality of light in particular, and nonclassicality of arbitrary quantum states in general.

DATA AVAILABILITY STATEMENT

The original contributions presented in the study are included in the article/supplementary material further inquiries can be directed to the corresponding author.

AUTHOR CONTRIBUTIONS

All authors listed have made a substantial, direct, and intellectual contribution to the work and approved it for publication.

FUNDING

This work was supported by the Fundamental Research Funds for the Central Universities (Grant No. FRF-TP-19-012A3), the National Natural Science Foundation of China (Grant No. 11875317), the China Postdoctoral Science Foundation (Grant No. 2021M690414), the Beijing Postdoctoral Research Foundation (Grant No. 2021ZZ091), and the National Key R&D Program of China (Grant No. 2020YFA0712700).

REFERENCES

1. Glauber RJ. Coherent and Incoherent States of the Radiation Field. *Phys Rev* (2013) 131:2766–88.
2. Sudarshan ECG. Equivalence of Semiclassical and Quantum Mechanical Descriptions of Statistical Light Beams. *Phys Rev Lett* (1963) 10:277–9. doi:10.1103/physrevlett.10.277
3. Titulaer UM, Glauber RJ. Correlation Functions for Coherent Fields. *Phys Rev* (1965) 140:B676–B682. doi:10.1103/physrev.140.b676
4. Walls DF, Milburn GJ. *Quantum Optics*. Berlin: Springer-Verlag (1994).
5. Mandel L, Wolf E. *Optical Coherence and Quantum Optics*. Cambridge: Cambridge Univ. Press (1995).
6. Scully MO, Zubairy MS. *Quantum Optics*. Cambridge: Cambridge Univ. Press (1997).
7. Dodonov VV, Man'ko VI. *Theory of Nonclassical States of Light*. London: Taylor & Francis (2003).
8. Mandel L. Sub-poissonian Photon Statistics in Resonance Fluorescence. *Opt Lett* (1979) 4:205–97. doi:10.1364/ol.4.000205
9. Hillery M. Nonclassical Distance in Quantum Optics. *Phys Rev A* (1987) 35: 725–32. doi:10.1103/physreva.35.725
10. Marian P, Marian TA, Scutaru H. Quantifying Nonclassicality of One-Mode Gaussian States of the Radiation Field. *Phys Rev Lett* (2002) 88:153601. doi:10.1103/physrevlett.88.153601
11. Lemos HCF, Almeida ACL, Amaral B, Oliveira AC. Roughness as Classicality Indicator of a Quantum State. *Phys Lett A* (2018) 382:823–36. doi:10.1016/j.physleta.2018.01.023
12. Lee CT. Measure of the Nonclassicality of Nonclassical States. *Phys Rev A* (1991) 44:R2775–R2778. doi:10.1103/physreva.44.r2775
13. Richter T, Vogel W. Nonclassicality of Quantum States: a Hierarchy of Observable Conditions. *Phys Rev Lett* (2002) 89:283601. doi:10.1103/physrevlett.89.283601
14. Gehrke C, Sperling J, Vogel W. Quantification of Nonclassicality. *Phys Rev A* (2012) 86:052118. doi:10.1103/physreva.86.052118
15. Ryl S, Sperling J, Agudelo E, Mraz M, Köhnke S, Hage B, et al. Unified Nonclassicality Criteria. *Phys Rev A* (2015) 92:011801. doi:10.1103/physreva.92.011801
16. Asbóth JK, Calsamiglia J, Ritsch H. Computable Measure of Nonclassicality for Light. *Phys Rev Lett* (2005) 94:173602. doi:10.1103/physrevlett.94.173602
17. Yadin B, Binder FC, Thompson J, Narasimhachar V, Gu M, Kim MS. Operational Resource Theory of Continuous-Variable Nonclassicality. *Phys Rev X* (2018) 8:041038. doi:10.1103/physrevx.8.041038
18. De Bièvre S, Horoshko DB, Patera G, Kolobov MI. Measuring Nonclassicality of Bosonic Field Quantum States via Operator Ordering Sensitivity. *Phys Rev Lett* (2019) 122:080402. doi:10.1103/PhysRevLett.122.080402
19. Hertz A, De Bièvre S. Quadrature Coherence Scale Driven Fast Decoherence of Bosonic Quantum Field States. *Phys Rev Lett* (2020) 124:090402. doi:10.1103/PhysRevLett.124.090402
20. Hertz A, Cerf NJ, Bièvre SD. Relating the Entanglement and Optical Nonclassicality of Multimode States of a Bosonic Quantum Field. *Phys Rev A* (2020) 102:032413. doi:10.1103/physreva.102.032413
21. Wigner EP, Yanase MM. Information Contents of Distributions. *Proc Natl Acad Sci U.S.A* (1963) 49:910–8. doi:10.1073/pnas.49.6.910

22. Luo S. Quantum versus Classical Uncertainty. *Theor Math Phys* (2005) 143: 681–8. doi:10.1007/s11232-005-0098-6
23. Luo S, Sun Y. Quantum Coherence versus Quantum Uncertainty. *Phys Rev A* (2017) 96:022130. doi:10.1103/physreva.96.022130
24. Luo S, Zhang Y. Quantifying Nonclassicality via Wigner-Yanase Skew Information. *Phys Rev A* (2019) 100:032116. doi:10.1103/physreva.100.032116

Conflict of Interest: The authors declare that the research was conducted in the absence of any commercial or financial relationships that could be construed as a potential conflict of interest.

Publisher's Note: All claims expressed in this article are solely those of the authors and do not necessarily represent those of their affiliated organizations, or those of the publisher, the editors and the reviewers. Any product that may be evaluated in this article, or claim that may be made by its manufacturer, is not guaranteed or endorsed by the publisher.

frontiers | Frontiers in Physics

ORIGINAL RESEARCH
published: 19 July 2022
doi: 10.3389/fphy.2022.941159

Probing Genuine Multipartite Einstein–Podolsky–Rosen Steering and Entanglement Under an Open Tripartite System

Wen-Yang Sun[1,2,3]*, *Amin Ding*[1], *Haitao Gao*[1], *Le Wang*[1], *Juan He*[2] and *Liu Ye*[3]

[1]School of Electrical and Electronic Engineering, Anhui Science and Technology University, Bengbu, China, [2]Key Laboratory of Functional Materials and Devices for Informatics of Anhui Higher Education Institutes, Fuyang Normal University, Fuyang, China, [3]School of Physics and Optoelectronics Engineering, Anhui University, Hefei, China

Einstein–Podolsky–Rosen steering is a peculiar quantum nonlocal correlation and has unique physical characteristics and a wide application prospect. Even more importantly, multipartite steerable states have more vital applications in the future quantum information field. Thus, in this work, we explored the dynamics characteristics of both genuine multipartite steering (GMS) and genuine multipartite entanglement (GME) and the relations of both under an open tripartite system. Specifically, the tripartite decoherence system may be modeled by the three parties of a tripartite state that undergo the noisy channels. The conditions for genuine entangled and steerable states can be acquired for the initial tripartite state. The results showed that decoherence noises can degrade the genuine multipartite entanglement and genuine multipartite steering and even induce its death. Explicitly, GME and GMS disappear with the increase in the decoherence strength under the phase damping channel. However, GME and GMS rapidly decay to death with the increase in the channel-noise factor and then come back to life soon after in the bit flip channel. Additionally, the results indicate that GMS is born of GME, but GME does not imply GMS, which means that the set of genuine multipartite steerable states is a strict subset of the set of genuine multipartite entangled states. These conclusions may be useful for discussing the relationship of quantum nonlocal correlations (GME and GMS) in the decoherence systems.

Keywords: open system, genuine multipartite steering, genuine multipartite entanglement, noise channel, uncertainty relation

OPEN ACCESS

Edited by:
Jun Feng,
Xi'an Jiaotong University, China

Reviewed by:
Rui Qu,
Xi'an Jiaotong University, China
Liming Zhao,
Southwest Jiaotong University, China

***Correspondence:**
Wen-Yang Sun
swy_3299@163.com

Specialty section:
This article was submitted to Quantum Engineering and Technology, a section of the journal Frontiers in Physics

Received: *11 May 2022*
Accepted: *16 June 2022*
Published: *19 July 2022*

Citation:
Sun W-Y, Ding A, Gao H, Wang L, He J and Ye L (2022) Probing Genuine Multipartite Einstein–Podolsky–Rosen Steering and Entanglement Under an Open Tripartite System. Front. Phys. 10:941159. doi: 10.3389/fphy.2022.941159

INTRODUCTION

EPR steering and entanglement are two fundamental characteristics of quantum mechanics and that are inextricably linked. For the moment, the researchers believe that EPR steering stems from entanglement, but entanglement does not imply EPR steering [1, 2]. EPR entanglement characterizes quantum nonlocal correlations among remote parties that are totally forbidden within the classical regime. Moreover, multipartite entangled states have important applications in the field of quantum information. Utilizing and characterizing such quantum resources stemming from multipartite nonlocal correlations [3] are rather crucial for the applications of the information theory [4–10] and from foundational perspectives. A multipartite state is deemed to be genuinely multipartite entangled

[11] if and only if the state may not be written as a convex linear combination of states, each of which is disentangled with reference to some partition.

One the other hand, the concept of EPR steering was first introduced by Schrödinger [12, 13] in the context of the EPR argument [14]. Conceptually, EPR steering describes a nontrivial trait of quantum mechanics that an observer can immediately "steer" a distant party by employing the local quantum measures. EPR steering can be detected by utilizing EPR steering inequalities [15–22]; the violation of EPR steering inequalities can indicate that EPR steering occurs. At first, Reid [23] derived an inequality for EPR steering based on Heisenberg uncertainty relation in 1989. Then, EPR steering was formally defined in 2007 [24]. Numerous EPR steering inequalities have since been given; however, most respect was given to detecting bipartite EPR steering [25]. Additionally, multipartite steerable states have vital applications in the future quantum information field. Consequently, the detection and investigation of multipartite EPR steering is more important and challenging. The concept of multipartite EPR steering was first introduced by He and Reid [26] and developed for Gaussian states by Kogias et al. [27]. Experiments were followed [28–32], which motivated research studies of the monogamy relationship of EPR steering [33, 34]. Moreover, Wang et al. [35] have optimized the collective EPR steering for the tripartite state within a particular optics-based system in 2014.

In a realistic world, a quantum system ineluctably suffers from the influence of the decoherence attributed to the mutual effect between the system and its external noises. Typically, noisy environments usually can be classified into two species, namely, non-Markovian and Markovian environments [36–40]. In detail, the Markovian noisy environment is featured by leading to the degeneration of quantum nonlocal correlations [40]. By contrast, as a normative non-Markovian noisy environment [41, 42], a dynamic characteristic of quantum nonlocal correlations can be discovered, which is the renewal of quantum nonlocal correlations after a finite time period of the entire disappearance [43]. As a consequence, in the course of quantum information processing, considering the external noisy environments is indispensable and significant under a realistic regime. However, in the past years, there have been only a few authors to examine the steerability of multipartite states in the local noisy environments [44–46]. Hence, we will concentrate on exploring the genuine multipartite steering (GMS) and genuine multipartite entanglement (GME) under the noise channels. We here mainly probed the dynamic characteristics of GME and GMS and the relationship between them under the noise channels.

The remainder of this article is organized as follows. In Section II, we introduced the measuring method of GME and GMS within the multi-body systems, respectively. Then, we investigated the dynamic behaviors of GMS for the initial tripartite state under two kinds of different noises in Section 3. In Section 4, we probed the characteristic of GME and compared it with GMS as the tripartite state under the two kinds of different noises. Finally, we ended up our article with a brief conclusion.

2 MEASUREMENTS OF GME AND GMS

2.1 Measurement of GME

In the first place, a method to measure multi-body entanglement is introduced, viz., GME. *N*-partite entanglement is defined by its opposite, bi-separability. An *N*-partite state that cannot be written as an ensemble of bi-separable states is an *N*-partite entangled state. Employing the results of Ref. [47], for a multi-body quantum state $|\psi\rangle$, if the state's density matrix ρ is an *X*-structured matrix form

$$\rho = \begin{pmatrix} a_1 & & & & & & c_1 \\ & a_2 & & & & c_2 & \\ & & \ddots & & \iddots & & \\ & & & a_n & c_n & & \\ & & & c_n^* & b_n & & \\ & & \iddots & & & \ddots & \\ & c_2^* & & & & b_2 & \\ c_1^* & & & & & & b_1 \end{pmatrix}, \quad (1)$$

where $n = 2^{N-1}$, and N is the number of qubits in a quantum state. For example, if the quantum state is a three-qubit state, N is equal to three, and $n = 4$. In addition, we require $|c_i| \le \sqrt{a_i b_i}$ and $\sum_i (a_i + b_i) = 1$ to ensure that ρ is positive and normalized. In the circumstances, one can give the expression of GME for the *X*-structured matrix ρ [47].

$$GME = 2\max\left\{0, |c_i| - \sum_{j\neq i}^{n}\sqrt{a_j b_j}\right\}, \quad i, j = 0, 1, 2, \ldots, n, \quad (2)$$

where **Eq. 2** is a quantified expression for multi-body entanglement, and the range is zero to one. If the value of the GME is equal to zero, which means that the tripartite state does not have genuine multipartite entanglement, then the tripartite state is not a genuine tripartite entangled state. Furthermore, if the value of the GME is greater than zero and less than or equal to one, which means that the tripartite state does have genuine multipartite entanglement, the tripartite state is a genuine tripartite entangled state. Moreover, the value of the GME is equal to one, which means that the tripartite state is the maximal genuine entangled state.

2.2 Measurement of GMS

According to the method proposed by He and Reid [26], if the tripartite system is a three-qubit system, with the usual Pauli operators defined for each site, the uncertainty relation for spin implies $(\Delta\sigma_x^{(k)})^2 + (\Delta\sigma_y^{(k)})^2 \ge 1$, $(\Delta\sigma_z^{(k)})^2 + (\Delta\sigma_y^{(k)})^2 \ge 1$ and for each site $k = 1, 2, 3$. The approach given by He and Reid [26] will be used; the conditions for steering can be given by

$$\begin{aligned} S_I:&= \left\langle\left[\Delta\left(\sigma_z^{(1)} - \sigma_z^{(2)}\right)\right]^2\right\rangle + \left\langle\left[\Delta\left(\sigma_x^{(1)} + \sigma_y^{(2)}\sigma_y^{(3)}\right)\right]^2\right\rangle \ge 1, \\ S_{II}:&= \left\langle\left[\Delta\left(\sigma_z^{(2)} - \sigma_z^{(3)}\right)\right]^2\right\rangle + \left\langle\left[\Delta\left(\sigma_x^{(2)} + \sigma_y^{(1)}\sigma_y^{(3)}\right)\right]^2\right\rangle \ge 1, \\ S_{III}:&= \left\langle\left[\Delta\left(\sigma_z^{(3)} - \sigma_z^{(1)}\right)\right]^2\right\rangle + \left\langle\left[\Delta\left(\sigma_x^{(3)} + \sigma_y^{(2)}\sigma_y^{(1)}\right)\right]^2\right\rangle \ge 1. \end{aligned} \quad (3)$$

where $\langle(\Delta\sigma_i)^2\rangle$ denotes the variance of the quantum observable σ_i, and $i = x, y, z$. Then, let us introduce the set of all bipartitions of N parties. Each bipartition is a division of

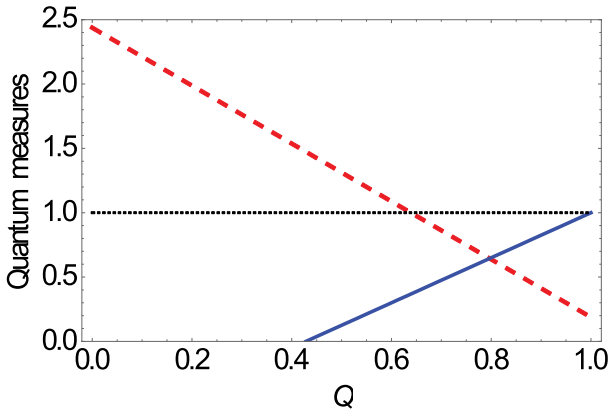

FIGURE 1 | (Color online) Quantum measures {GME (blue solid line) and GMS inequality (red dashed line)} as a function of the state parameter Q, when α is equal to $\sqrt{2}/2$. Here, the value of the black dashed line is equal to 1.

the set $\{1, 2, \ldots, N\}$ into two non-overlapping and non-empty subsets $\{A_s, B_s\}$. The set of all such bipartitions is denoted by $J = \{J_1, J_2, \ldots J_{2^{N-1}-1}\}$. For example, for a three-qubit state, there are three bipartitions $\{A_s, B_s\}$ that are $\{23, 1\}_s$, $\{13, 2\}_s$, and $\{12, 3\}_s$. As a matter of fact, inequalities S_I, S_{II}, and S_{III} are implied by bipartitions $\{23, 1\}_s$, $\{13, 2\}_s$, and $\{12, 3\}_s$, respectively. Consequently, the expression of GMS inequality for the tripartite qubit-state can be written as

$$GMS(\rho): = \{S_I + S_{II} + S_{III} \geq 1\}. \tag{4}$$

If the GMS inequality in **Eq. 4** is violated, which is sufficient to show GMS, and the value of GMS inequality is smaller, it means that the steerability is stronger.

3 DYNAMIC PROPERTIES OF GMS FOR THE INITIAL TRIPARTITE STATE WITHIN THE TWO KINDS OF THE DIFFERENT NOISES

In this section, we assume that there are three parties and they share an initial three-qubit state in the form of [48, 49].

$$\rho = Q(|cGHZ\rangle\langle cGHZ|) + \frac{1-Q}{8} I_8, \quad 0 \leq Q \leq 1, \tag{5}$$

where $|cGHZ\rangle = \alpha|000\rangle + \sqrt{1-\alpha^2}|111\rangle$, $0 \leq \alpha \leq 1$, and I_8 is the 8×8 identity matrix. Based on **Eqs 2**, **4**, we can obtain the three-qubit states of GME $2\alpha Q\sqrt{(1-\alpha^2)} - 3/4(1-Q)$ and GMS inequality $39/16 - 3/2Q(1 + \alpha\sqrt{1-\alpha^2}) \geq 1$, respectively. In **Figure 1**, the red dashed line is below the black dashed line, which means the tripartite state is a genuine tripartite steerable state. On the contrary, if the red dashed line is above the black dashed line, which means the tripartite state is not a genuine tripartite steerable state. Thus, when α is equal to $\sqrt{2}/2$, one can obtain that the tripartite state is a genuine steerable state in the case of $23/36 < Q \leq 1$, while it is a genuine unsteerable state for $0 \leq Q \leq 23/36$ in **Figure 1**. Moreover, the tripartite state is entangled for $1 \geq Q > 3/7$ and is separable for $3/7 \geq Q \geq 0$. The maximally entangled state ($Q = 1, \alpha = \sqrt{2}/2$) is a maximally genuine tripartite steerable state. Hence, we can draw a conclusion that for the whole set of the three-qubit states, it holds that $GMS \Rightarrow GME$, suggesting a hierarchy according to which all GMS's states are genuinely entangled, while GME does not imply GMS, which means that the set of genuine tripartite steerable states is a strict subset of the set of genuine tripartite entangled states.

Next, we considered that the tripartite states each independently and locally interacts with a zero-temperature reservoir. Herein, the two kinds of different noisy channels were considered: the bit flip (BF) channel and phase damping (PD) channel, respectively. In this context, the system–environment interaction *via* the operator-sum representation formalism is utilized. Following the approach of the Kraus operators, the time-evolution of the initial three-qubit states under the local noisy environment can be expressed by the trace-preserving quantum operation $\xi(\rho)$, which is $\xi(\rho) = \sum_i K_i \rho K_i^\dagger$ with the Kraus operators satisfying the trace-preserving condition $\sum_i K_i K_i^\dagger = I$. The influence of the flip noises is to damage the correlations contained in the phase relations without the exchange of energy. The Kraus operators for the BF noise channel can be given by

$$K_0 = \sqrt{d} I, K_1 = \sqrt{1-d}\sigma_x, \tag{6}$$

where one can call that d is the channel-noise factor and $0 \leq d \leq 1$, and I is the 2×2 unit density matrix. The set is interpreted as corresponding to a probability d of remaining in the same state and a probability $1 - d$ of having an error $0 \leftrightarrow 1$. The factor K_1 in **Eq. 6** ensures that at $d = 1/2$ has maximal ignorance about the occurrence of an error and thereby has minimum information about the state [50].Furthermore, the PD noise channel depicts the losing correlations without the loss of energy. It leads to decoherence without relaxation. The Kraus operators can be given as

$$K_2 = \begin{pmatrix} 1 & 0 \\ 0 & \sqrt{1-d} \end{pmatrix}, K_3 = \begin{pmatrix} 0 & 0 \\ 0 & \sqrt{d} \end{pmatrix}, \tag{7}$$

where d is the decoherence strength, and $0 \leq d \leq 1$. For convenience, here, we collectively call that d is the channel-noise factor in the BF and PD noise channels.

As a consequence, when three parties (all subsystem) of the three-qubit states suffer from the two different noisy environments, we then can obtain the non-zero elements of two kinds of the different final states, ρ_{BF} and ρ_{PD}, respectively.

To be precise, as three parties of the three-qubit states undergo the BF channel, the final state can be written as

$$\begin{aligned} \rho_{BF} = {} & K_0 \otimes K_0 . \rho . (K_0 \otimes K_0)^\dagger + K_1 \otimes K_1 . \rho . (K_1 \otimes K_1)^\dagger \\ & + K_0 \otimes K_1 . \rho . (K_0 \otimes K_1)^\dagger + K_1 \otimes K_0 . \rho . (K_1 \otimes K_0)^\dagger, \end{aligned} \tag{8}$$

Hence, we can obtain the non-zero elements of the final states ρ_{BF} as follows:

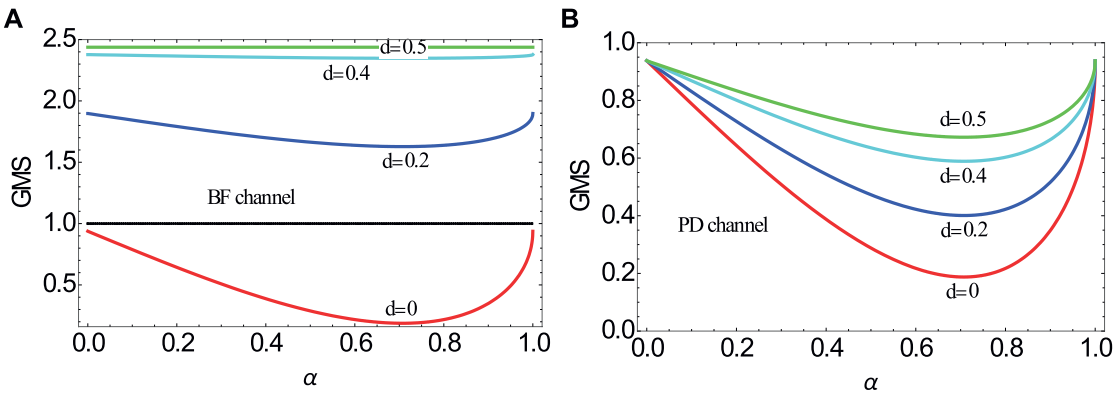

FIGURE 2 | (Color online) GMS-inequality as a function of the state parameter α in terms of different channel-noise factors d for $Q = 1$, when the initial three-qubit state is under the different noisy channels. **(A)** BF channel. **(B)** PD channel.

$$\begin{aligned}
&\rho_{BF}18 = \rho_{BF}81 = \alpha\sqrt{1-\alpha^2}[1+3(d-1)d]Q,\\
&\rho_{BF}27 = \rho_{BF}72 = \rho_{BF}36 = \rho_{BF}63 = \rho_{BF}45 = \rho_{BF}54 = \alpha\sqrt{1-\alpha^2}(1-d)dQ,\\
&\rho_{BF}11 = \frac{1}{8}\{1+(2d-1)[2(5-2d)d-7+8\alpha^2(1+(d-1)d)]Q\},\\
&\rho_{BF}22 = \rho_{BF}33 = \rho_{BF}55 = \frac{1}{8}-\frac{1}{8}(2d-1)\{-1+2[3+4\alpha^2(d-1)-2d]d\}Q,\\
&\rho_{BF}44 = \rho_{BF}66 = \rho_{BF}77 = \frac{1}{8}\{1+(2d-1)[1+2(1+4\alpha^2(d-1)-2d)d]Q\},\\
&\rho_{BF}88 = \frac{1}{8}+\left\{d^3-\frac{1}{8}+\alpha^2[1+d((3-2d)d-3)]\right\}Q.
\end{aligned} \tag{9}$$

Then, as three parties of the three-qubit states, **Eq. 5** suffers from the PD channel; the final state can be written as

$$\begin{aligned}
\rho_{PD} = {} & K_2\otimes K_2.\rho.(K_2\otimes K_2)^\dagger + K_3\otimes K_3.\rho.(K_3\otimes K_3)^\dagger\\
& + K_3\otimes K_2.\rho.(K_3\otimes K_2)^\dagger + K_2\otimes K_3.\rho.(K_2\otimes K_3)^\dagger,
\end{aligned} \tag{10}$$

and the non-zero elements of final states ρ_{PD} are

$$\begin{aligned}
&\rho_{PD}11 = \frac{1}{8}+\left(\alpha^2-\frac{1}{8}\right)Q,\\
&\rho_{PD}88 = \frac{1}{8}[1+(7-8\alpha^2)Q],\\
&\rho_{PD}18 = \rho_{PD}81 = \alpha\sqrt{1-\alpha^2}(1-d)^{3/2}Q,\\
&\rho_{PD}27 = \rho_{PD}72 = \rho_{PD}36 = \rho_{PD}63 = \rho_{PD}45 = \rho_{PD}54 = 0,\\
&\rho_{PD}22 = \rho_{PD}33 = \rho_{PD}44 = \rho_{PD}55 = \rho_{PD}66 = \rho_{PD}77 = \frac{1-Q}{8}.
\end{aligned} \tag{11}$$

Herein, by using **Eqs 3**, **4**, one can gain an analytical expression of the GMS inequality for the initial state within the two kinds of different noisy channels, respectively. In accordance with the abovementioned analysis, one can draw the GMS inequality of the states ρ_{BF} and ρ_{PD} as a function of the state parameters α in terms of the different channel-noise factor d for $Q = 1$ in **Figure 2**. From these figures, one can see that the overall trend of the GMS inequality first decreases and then increases with the increase in the state parameter α for a fixed d, whatever the initial state is under the BF channel or PD channel. The value of α is equal to $\sqrt{2}/2$, which corresponds to the position of the maximal genuine steerability for the tripartite state. As the channel-noise factor grows, it does not change. It turns out that the noisy environments cannot destroy the symmetry of GMS for the inertial state. Moreover, we observed that GMS will rapidly disappear with the increasing channel-noise factor d in the BF channel. However, GMS will not fleetly disappear with the increasing channel-noise factor d in the PD channel. It means that the BF and PD noises can seriously influence and damage the GMS. However, the impact of the PD noise on GMS is weaker than that of the BF noise.

Then, in order to explore the influence of the state parameters Q on the GMS inequality in terms of different channel-noise factors d for $\alpha = \sqrt{2}/2$, **Figure 3** is drawn. As shown in **Figure 3**, one can see that GMS inequality rapidly decreases to zero with the increase in the state parameters Q, when there is no effect of the decoherence noise, namely, $d = 0$. This demonstrates that the steerability of the state is stronger. We also found that the GMS occurs only when the state parameters Q increases to a fixed value. However, the properties of the GMS are different in the BF and PD noises, when the channel-noise factor is nonzero. In the BF channel, when the channel-noise factor is equal to 0.2, 0.4, and 0.5, respectively, GMS disappears whatever the state parameter Q is. Particularly, for the channel-noise factor $d = 0.5$, the tripartite state has minimum information. In addition, GMS can appear with the increase in the state parameter Q, while the channel-noise factor is equal to 0.2, 0.4, and 0.5 in **Figure 3** (2), respectively.

Next, we considered the effects of the state parameters Q and the channel-noise factor d on the GMS inequality, for which **Figures 4**,**5** were drawn. As shown in **Figures 4**, **5**, it can be concluded that the GMS inequality first increases and then decreases with the increase in the channel-noise factor d within the BF channel, whatever the value of the state parameter Q is; however, the GMS inequality increases with the increase in the channel-noise factor d in the PD channel.

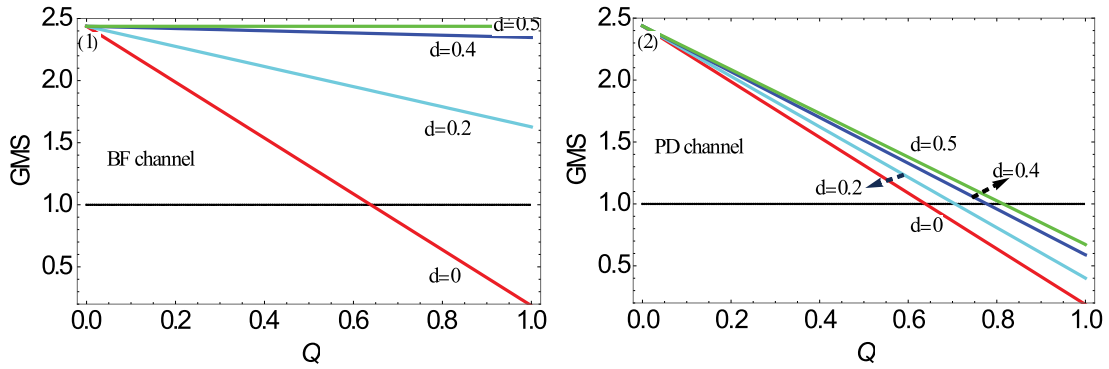

FIGURE 3 | (Color online) GMS inequality as a function of the state parameter Q in terms of different channel-noise factors d for $\alpha = \sqrt{2}/2$ in the different noisy channels. **(1)** BF channel. **(2)** PD channel.

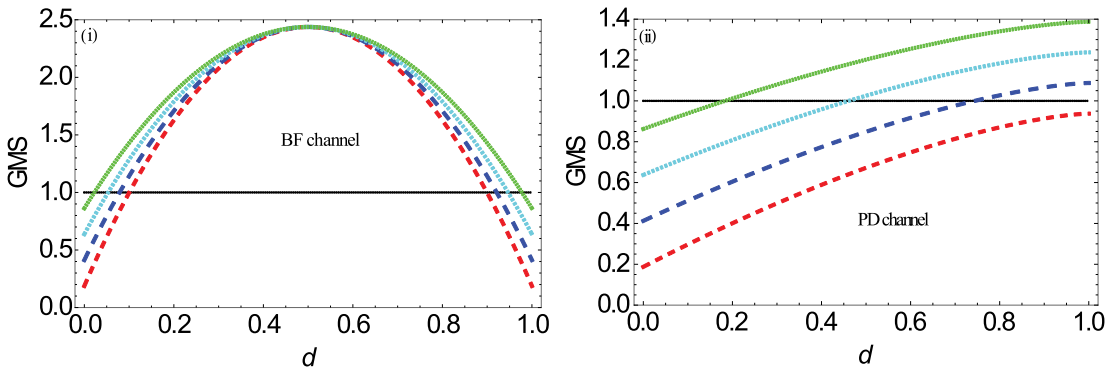

FIGURE 4 | (Color online) GMS inequality as a function of the channel-noise factor d in terms of different state parameters Q for $\alpha = \sqrt{2}/2$ within the different noisy channels. **(i)** BF channel. **(ii)** PD channel. Here, $Q = 1$ (red dashed lines), $Q = 0.9$ (blue dashed lines), $Q = 0.8$ (cyan dashed lines), and $Q = 0.7$ (green dashed lines).

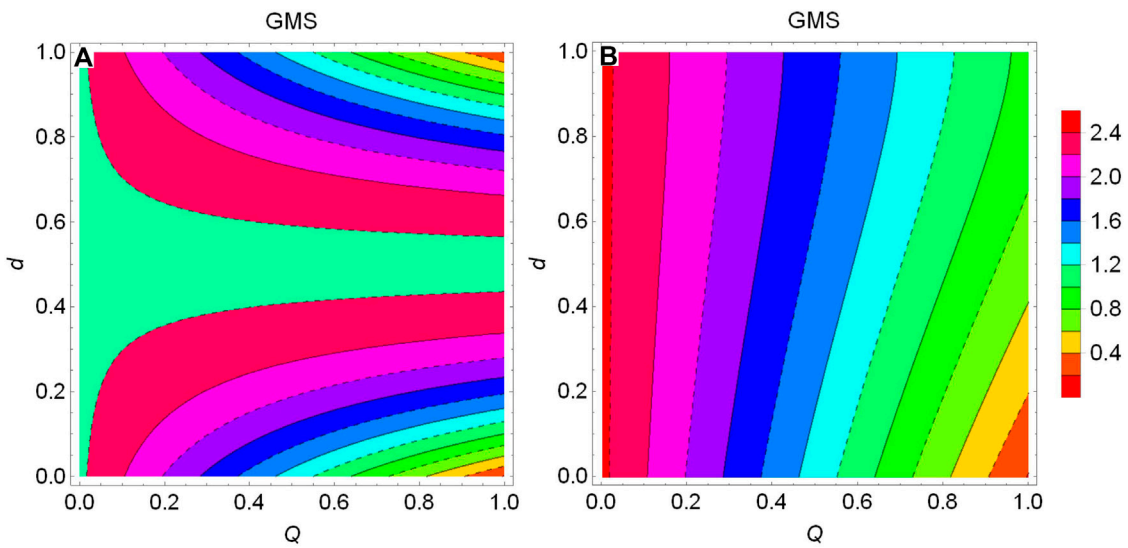

FIGURE 5 | (Color online) Contour plot of GMS inequality versus the state parameter Q and the channel-noise factor d with $\alpha = \sqrt{2}/2$ under the different noisy channels. **(A)** BF channel. **(B)** PD channel.

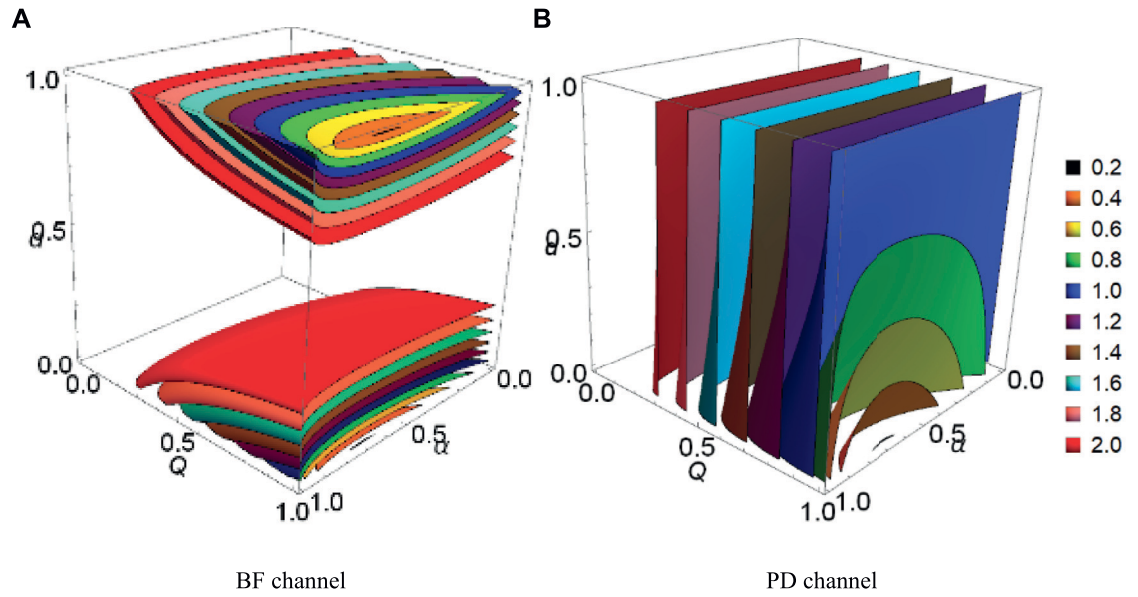

FIGURE 6 | (Color online) 3D contour plot of GMS inequality versus the state parameters Q and α and the channel-noise factor d under the different noisy channels. **(A)** BF channel. **(B)** PD channel.

We discovered that the GMS can be detected if and only if the channel-noise factor d is larger than $(6-\sqrt{23})/12$ and less than $(6+\sqrt{23})/12$ under the BF channel in **Figure 4(i)** and **Figure 5A**. Moreover, when the channel-noise factor d is equal to 0.5, the values of the GMS inequality are invariable in the BF channel. At the moment, the tripartite state has minimum information and no quantum correlation.

Hence, we can conclude that the decoherence effect can destroy the steerability of quantum states or even completely disable the steerability. In order to more intuitively observe the influence of the three parameters (the channel-noise factor d and the state parameters Q and α) on GMS, we drew a three-dimensional contour map of the GMS inequality in **Figure 6**. We can draw the same conclusions as mentioned earlier, and we will not go into them here.

4 DYNAMIC CHARACTERISTICS OF GME AND ITS COMPARISON WITH THE GMS UNDER THE TWO KINDS OF THE DIFFERENT NOISES

It is generally acknowledged that quantum steering originates from quantum entanglement; however, entanglement does not imply steering, which means that the set of steerable states is a strict subset of the set of entangled states. In this section, we probed the dynamic characteristics of GME and then discussed the relationship between GMS and the GME under the two kinds of the noisy channels.

By employing **Eq. 2**, we can give the expressions of the GME as

$$GME(BF) = 2\max\Big[0, |\rho_{BF}18| - 3\sqrt{\rho_{BF}22\cdot\rho_{BF}77}, |\rho_{BF}27| - \big(\sqrt{\rho_{BF}11\cdot\rho_{BF}88} + 2\sqrt{\rho_{BF}33\cdot\rho_{BF}66}\big)\Big], \tag{12}$$

and

$$GME(PD) = 2\max\Big[0, \alpha\sqrt{1-\alpha^2}\,(1-d)^{3/2}Q - \frac{3}{8}(1-Q)\Big], \tag{13}$$

under the BF and PD channels, respectively.

To begin with, we considered the influence of the state parameters Q and α on GME, when d is a constant value. As shown in **Figure 7**, the GME first increases and then reduces with the increasing state parameter α, as Q is a constant value. Additionally, the tripartite state is a product state with no GME, when the state parameter α is equal to zero or one. We also obtained that GME increases with the increase in the state parameter Q. Thus, we think that Q is a purity parameter for the tripartite state. The bigger the Q, the bigger the GME is. The tripartite state is a maximal entangled state, when $\alpha = \sqrt{2}/2$, $Q = 1$, and there is no decoherence.

Next, for comparing GME with GMS and the relationship between GMS and GME, we investigated the influence between the state parameters α and the channel-noise factor d on the GME and the GMS for $Q = 0.9$. In the BF channel, both GME and GMS first rapidly decay to death with the increasing channel-noise factor d and then come back to life (see **Figure 8A**). However, both GME and GMS tardily decay to death with the increasing channel-noise factor d within the PD channel. Meanwhile, as shown in **Figure 8B**, when GMS and GME just disappear, the channel-noise factor d has a critical value, and the critical values are $d \approx 0.744$ and $d \approx 0.809$, respectively. In other words, as the channel-noise factor is approximately smaller than 0.744, the tripartite state is both genuine steerable and entangled. If the channel-noise factor is

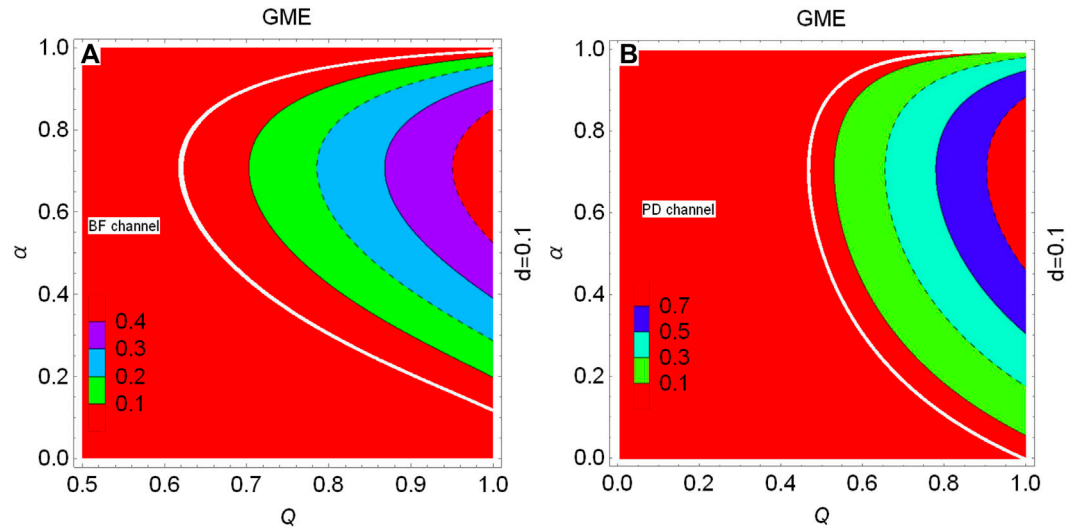

FIGURE 7 | (Color online) Contour plot of GME versus the state parameters Q and α for $d = 0.1$ in the different noisy channels. **(A)** BF channel. **(B)** PD channel.

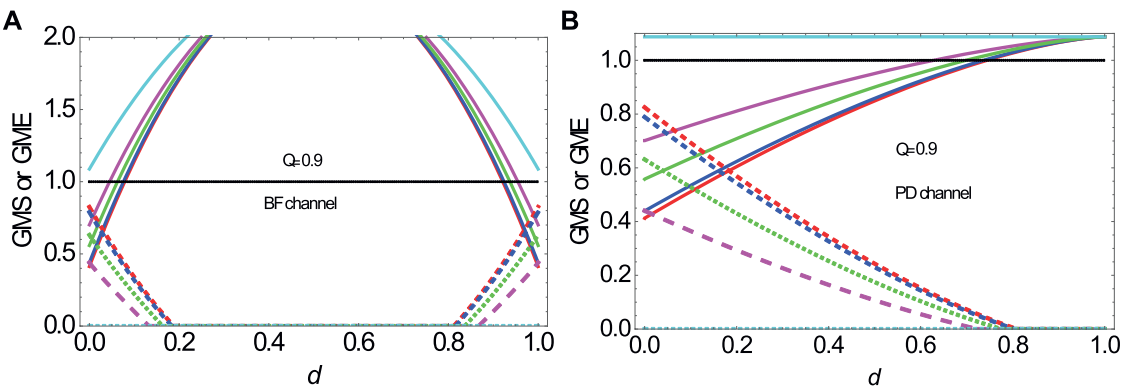

FIGURE 8 | (Color online) Variety of quantum measures (GME (dashed line) and GMS (solid line)) as a function of channel-noise factor d in terms of different state parameters α for $Q = 0.9$. **(A)** shows the BF channel, and **(B)** shows the PD channel. Here, $\alpha = \sqrt{2}/2$ (red lines), $\alpha = 0.3$ (pink lines), $\alpha = 0.6$ (blue lines), $\alpha = 0.9$ (green lines), and $\alpha = 1$ (cyan lines).

larger than 0.744 but less than 0.809, the tripartite state is unsteerable and only genuinely entangled. The channel-noise factor is larger than 0.809, and the tripartite state is both unsteerable and disentangled. It is indicated that GMS originates from GME, but GME does not imply to GMS, which means that the set of genuine multipartite steerable states is a strict subset of the set of genuine multipartite entangled states. This result is also true in the BF channel (see **Figure 8A**). These conclusions may be useful for analyzing the relationship of quantum nonlocal correlations (GME and GMS) in the decoherence noise.

5 CONCLUSION

In this article, we mainly investigated the physical characteristic of GME and GMS within the two kinds of the different noisy channels. In contrast with our previous work [49], we used different initial states, and this state (see **Eq. 5**) is more general. In addition, here, we utilized different measurement methods for the multipartite quantum nonlocal correlation (GME) in this work. The anti-decoherence ability of GME is stronger than that of GMN. In the next place, a tripartite state is subjected to different decoherence noisy environments, but one is under curved spacetime (non-inertial frame) and one is without (this work). Consequently, in this study, we first discussed that the dynamic properties of GMS and GME for the initial tripartite state and the conditions for entangled and steerable states can be given. Then, the effect of BF and PD noises on the GMS is discussed, respectively. The results indicated that GMS is very flimsy under the influence of the decoherence. Specifically, GMS will perish with the increase in

the channel-noise factor under the PD channel. However, GMS rapidly decays to death with the increase in the channel-noise factor and then come back to life soon in the BF channel. At the end, we studied the dynamic characteristics of GME and discussed the relationship between GME and GMS under decoherence noises. The decoherence noises can also degrade the GME and even induce its death. In addition, we can draw a conclusion that GMS originates from GME, but the GME does not imply GMS, which means that the set of genuine multipartite steerable states is a strict subset of the set of genuine multipartite entangled states. These conclusions may be useful for analyzing the relationship of quantum nonlocal correlations in the decoherence noises.

DATA AVAILABILITY STATEMENT

The original contributions presented in the study are included in the article/Supplementary Material; further inquiries can be directed to the corresponding author.

AUTHOR CONTRIBUTIONS

W-YS contributed to the conception and design of the study. W-YS wrote the first draft of the manuscript. A Ding, H-TG, and JH wrote sections of the manuscript. All authors revised, read, and approved the submitted manuscript.

FUNDING

This work was supported by the Anhui Provincial Natural Science Foundation under the Grant No. 2008085QF328, and the Open Project Program of Key Laboratory of Functional Materials and Devices for Informatics of Anhui Higher Education Institutes (Fuyang Normal University) under Grant No. FSKFKT003, and the Talent Introduction Project of Anhui Science and Technology University under Grant Nos. DQYJ202005 and DQYJ202004, and also the Natural Science Foundation of Education Department of Anhui Province under Grant Nos. KJ2021A0865, KJ2021ZD0071 and KJ2021A0867.

REFERENCES

1. Jones SJ, Wiseman HM, Doherty AC. Entanglement, Einstein-Podolsky-Rosen Correlations, Bell Nonlocality, and Steering. *Phys Rev A* (2007) 76:052116. doi:10.1103/physreva.76.052116
2. Wu S-M, Zeng H-S. Genuine Tripartite Nonlocality and Entanglement in Curved Spacetime. *Eur Phys J C* (2022) 82:4. doi:10.1140/epjc/s10052-021-09954-4
3. Bengtsson I, Zyczkowski K. A Brief Introduction to Multipartite Entanglement. arXiv preprint arXiv: 1612.07747 (2016). doi:10.48550/arXiv.1612.07747
4. Hillery M, Bužek V, Berthiaume A. Quantum Secret Sharing. *Phys Rev A* (1999) 59:1829–34. doi:10.1103/physreva.59.1829
5. Sørensen AS, Mølmer K. Entanglement and Extreme Spin Squeezing. *Phys Rev Lett* (2001) 86:4431. doi:10.1103/physrevlett.86.4431
6. Raussendorf R, Briegel HJ. A One-Way Quantum Computer. *Phys Rev Lett* (2001) 86:5188–91. doi:10.1103/physrevlett.86.5188
7. Chen K, Lo H-K. Multi-partite Quantum Cryptographic Protocols with Noisy GHZ States. *Quan Inf. Comput* (2007) 7:689–715. doi:10.26421/qic7.8-1
8. Briegel HJ, Browne DE, Dür W, Raussendorf R, Van den Nest M. Measurement-based Quantum Computation. *Nat Phys* (2009) 5:19–26. doi:10.1038/nphys1157
9. Toth G. Multipartite Entanglement and High-Precision Metrology. *Phys Rev A* (2012) 85:022322. doi:10.1103/physreva.85.022322
10. Dai TZ, Fan Y, Qiu L. Complementary Relation between Tripartite Entanglement and the Maximum Steering Inequality Violation. *Phys Rev A* (2022) 105:022425. doi:10.1103/physreva.105.022425
11. Gühne O, Seevinck M. Separability Criteria for Genuine Multiparticle Entanglement. *New J Phys* (2010) 12:053002. doi:10.1088/1367-2630/12/5/053002
12. Schrödinger E. Discussion of Probability Relations between Separated Systems. *Proc Cambridge Philos Soc* (1935) 31:555. doi:10.1017/s0305004100013554
13. Schrödinger E. Probability Relations between Separated Systems. *Proc Cambridge Philos Soc* (1936) 32:446. doi:10.1017/s0305004100019137
14. Einstein A, Podolsky B, Rosen N. Can Quantum-Mechanical Description of Physical Reality Be Considered Complete? *Phys Rev* (1935) 47:777–80. doi:10.1103/physrev.47.777
15. Cavalcanti EG, Jones SJ, Wiseman HM, Reid MD. Experimental Criteria for Steering and the Einstein-Podolsky-Rosen Paradox. *Phys Rev A* (2009) 80:032112. doi:10.1103/physreva.80.032112
16. Cavalcanti EG, Foster CJ, Fuwa M, Wiseman HM. Analog of the Clauser-Horne-Shimony-Holt Inequality for Steering. *J Opt Soc Am B* (2015) 32:A74. doi:10.1364/josab.32.000a74
17. Schneeloch J, Broadbent CJ, Walborn SP, Cavalcanti EG, Howell JC. Einstein-Podolsky-Rosen Steering Inequalities from Entropic Uncertainty Relations. *Phys Rev A* (2013) 87:062103. doi:10.1103/physreva.87.062103
18. Chen J-L, Ye X-J, Wu C, Su H-Y, Cabello A, Kwek LC, et al. All-versus-nothing Proof of Einstein-Podolsky-Rosen Steering. *Sci Rep* (2013) 3:2143. doi:10.1038/srep02143
19. Jevtic S, Hall MJW, Anderson MR, Zwierz M, Wiseman HM. Einstein-Podolsky-Rosen Steering and the Steering Ellipsoid. *J Opt Soc Am B* (2015) 32:A40. doi:10.1364/josab.32.000a40
20. Costa ACS, Angelo RM. Quantification of Einstein-Podolski-Rosen Steering for Two-Qubit States. *Phys Rev A* (2016) 93:020103. doi:10.1103/physreva.93.020103
21. Kogias I, Skrzypczyk P, Cavalcanti D, Acín A, Adesso G. Hierarchy of Steering Criteria Based on Moments for All Bipartite Quantum Systems. *Phys Rev Lett* (2015) 115:210401. doi:10.1103/physrevlett.115.210401
22. Zukowski M, Dutta A, Yin Z. Geometric Bell-like Inequalities for Steering. *Phys Rev A* (2015) 91:032107. doi:10.1103/physreva.91.049902
23. Reid MD. Demonstration of the Einstein-Podolsky-Rosen Paradox Using Nondegenerate Parametric Amplification. *Phys Rev A* (1989) 40:913–23. doi:10.1103/physreva.40.913
24. Wiseman HM, Jones SJ, Doherty AC. Steering, Entanglement, Nonlocality, and the Einstein-Podolsky-Rosen Paradox. *Phys Rev Lett* (2007) 98:140402. doi:10.1103/physrevlett.98.140402
25. Uola R, Costa ACS, Nguyen HC, Gühne O. Quantum Steering. *Rev Mod Phys* (2020) 92:015001. doi:10.1103/revmodphys.92.015001
26. He QY, Reid MD. Genuine Multipartite Einstein-Podolsky-Rosen Steering. *Phys Rev Lett* (2013) 111:250403. doi:10.1103/physrevlett.111.250403
27. Kogias I, Lee AR, Ragy S, Adesso G. Quantification of Gaussian Quantum Steering. *Phys Rev Lett* (2015) 114:060403. doi:10.1103/PhysRevLett.114.060403
28. Cavalcanti D, Skrzypczyk P, Aguilar GH, Nery RV, Ribeiro PHS, Walborn SP. Detection of Entanglement in Asymmetric Quantum Networks and Multipartite Quantum Steering. *Nat Commun* (2015) 6:7941. doi:10.1038/ncomms8941
29. Armstrong S, Wang M, Teh RY, Gong Q, He Q, Janousek J, et al. Multipartite Einstein-Podolsky-Rosen Steering and Genuine Tripartite Entanglement with Optical Networks. *Nat Phys* (2015) 11:167–72. doi:10.1038/nphys3202
30. Kunkel P, Prüfer M, Strobel H, Linnemann D, Frölian A, Gasenzer T, et al. Spatially Distributed Multipartite Entanglement Enables EPR Steering of Atomic Clouds. *Science* (2018) 360:413–6. doi:10.1126/science.aao2254

31. Fadel M, Zibold T, Décamps B, Treutlein P. Spatial Entanglement Patterns and Einstein-Podolsky-Rosen Steering in Bose-Einstein Condensates. *Science* (2018) 360:409–13. doi:10.1126/science.aao1850
32. Opanchuk B, Rosales-Zárate L, Teh RY, Dalton BJ, Sidorov A, Drummond PD, et al. Mesoscopic Two-Mode Entangled and Steerable States of 40 000 Atoms in a Bose-Einstein-Condensate Interferometer. *Phys Rev A* (2019) 100:060102. doi:10.1103/physreva.100.060102
33. Deng X, Xiang Y, Tian C, Adesso G, He Q, Gong Q, et al. Demonstration of Monogamy Relations for Einstein-Podolsky-Rosen Steering in Gaussian Cluster States. *Phys Rev Lett* (2017) 118:230501. doi:10.1103/physrevlett.118.230501
34. Cheng S, Milne A, Hall MJW, Wiseman HM. Volume Monogamy of Quantum Steering Ellipsoids for Multiqubit Systems. *Phys Rev A* (2016) 94:042105. doi:10.1103/physreva.94.042105
35. Wang M, Gong Q, He Q. Collective Multipartite Einstein-Podolsky-Rosen Steering: More Secure Optical Networks. *Opt Lett* (2014) 39:6703. doi:10.1364/ol.39.006703
36. Zhang W-M, Lo P-Y, Xiong H-N, Tu MW-Y, Nori F. General Non-markovian Dynamics of Open Quantum Systems. *Phys Rev Lett* (2012) 109:170402. doi:10.1103/physrevlett.109.170402
37. Yin XL, Ma J, Wang XG, Nori F. Spin Squeezing under Non-markovian Channels by the Hierarchy Equation Method. *Phys Rev A* (2012) 86:012308. doi:10.1103/physreva.86.012308
38. Zhang J, Liu Y-X, Wu R-B, Jacobs K, Nori F. Non-Markovian Quantum Input-Output Networks. *Phys Rev A* (2013) 87:032117. doi:10.1103/physreva.87.032117
39. Xiong H-N, Lo P-Y, Zhang W-M, Feng DH, Nori F. Non-Markovian Complexity in the Quantum-To-Classical Transition. *Sci Rep* (2015) 5:13353. doi:10.1038/srep13353
40. Myatt CJ, King BE, Turchette QA, Sackett CA, Kielpinski D, Itano WM, et al. Decoherence of Quantum Superpositions through Coupling to Engineered Reservoirs. *Nature* (2000) 403:269–73. doi:10.1038/35002001
41. Lo Franco R, Bellomo B, Andersson E, Compagno G. Revival of Quantum Correlations without System-Environment Back-Action. *Phys Rev A* (2012) 85:032318. doi:10.1103/physreva.85.032318
42. Xu J-S, Sun K, Li C-F, Xu X-Y, Guo G-C, Andersson E, et al. Experimental Recovery of Quantum Correlations in Absence of System-Environment Back-Action. *Nat Commun* (2013) 4:2851. doi:10.1038/ncomms3851
43. Mazzola L, Maniscalco S, Piilo J, Suominen K-A, Garraway BM. Sudden Death and Sudden Birth of Entanglement in Common Structured Reservoirs. *Phys Rev A* (2009) 79:042302. doi:10.1103/physreva.79.042302
44. Wang M, Gong QH, Ficek Z, He QY. Role of thermal Noise in Tripartite Quantum Steering. *Phys Rev A* (2014) 90:023801. doi:10.1103/physreva.90.023801
45. Wang M, Xiang Y, He Q, Gong Q. Asymmetric Quantum Network Based on Multipartite Einstein-Podolsky-Rosen Steering. *J Opt Soc Am B* (2015) 32:A20. doi:10.1364/josab.32.000a20
46. Wang M, Xiang Y, He QY, Gong QH. Detection of Quantum Steering in Multipartite Continuous-Variable Greenberger-horne-zeilinger-like States. *Phys Rev A* (2015) 91:012112. doi:10.1103/physreva.91.012112
47. Rafsanjani SMH, Huber M, Broadbent CJ, Eberly JH. Genuinely Multipartite Concurrence of *N*-Qubit *X* Matrices. *Phys Rev A* (2012) 86:062303. doi:10.1103/physreva.86.062303
48. Ma XS, Wang AM, Cao Y. Entanglement Evolution of Three-Qubit States in a Quantum-Critical Environment. *Phys Rev B* (2007) 76:155327. doi:10.1103/physrevb.76.155327
49. Sun W-Y, Wang D, Ye L. Dynamics and Recovery of Genuine Multipartite Einstein-Podolsky-Rosen Steering and Genuine Multipartite Nonlocality for a Dissipative Dirac System via the Unruh Effect. *Annalen Der Physik* (2018) 530:1700442. doi:10.1002/andp.201700442
50. Salles A, de Melo F, Almeida MP, Hor-Meyll M, Walborn SP, Souto Ribeiro PH, et al. Experimental Investigation of the Dynamics of Entanglement: Sudden Death, Complementarity, and Continuous Monitoring of the Environment. *Phys Rev A* (2008) 78:022322. doi:10.1103/physreva.78.022322

Conflict of Interest: The authors declare that the research was conducted in the absence of any commercial or financial relationships that could be construed as a potential conflict of interest.

Advantages of publishing in Frontiers

OPEN ACCESS
Articles are free to read for greatest visibility and readership

FAST PUBLICATION
Around 90 days from submission to decision

HIGH QUALITY PEER-REVIEW
Rigorous, collaborative, and constructive peer-review

TRANSPARENT PEER-REVIEW
Editors and reviewers acknowledged by name on published articles

Frontiers
Avenue du Tribunal-Fédéral 34
1005 Lausanne | Switzerland

Visit us: www.frontiersin.org
Contact us: frontiersin.org/about/contact

REPRODUCIBILITY OF RESEARCH
Support open data and methods to enhance research reproducibility

DIGITAL PUBLISHING
Articles designed for optimal readership across devices

FOLLOW US
@frontiersin

IMPACT METRICS
Advanced article metrics track visibility across digital media

EXTENSIVE PROMOTION
Marketing and promotion of impactful research

LOOP RESEARCH NETWORK
Our network increases your article's readership